EVALUATION OF STRUCTURE-PROPERTY RELATIONSHIPS WITHIN INSECT CUTICLE TO IDENTIFY MOTIFS FOR BIOMATERIAL DESIGN

BY

Patricia Sprouse

Submitted to the graduate degree program in Bioengineering and the Graduate Faculty of the University of Kansas School of Engineering in partial fulfillment of the requirements for the degree of Doctor of Philosophy

Committee members

Dr. Stevin Gehrke, Committee Chair

Dr. Michael Detamore

Dr. Prajnaparamita Dhar

Dr. Elizabeth Friis

Dr. Paulette Spencer

Date defended

ACCEPTANCE PAGE

The Dissertation Committee for Patricia Sprouse certifies
that this is the approved version of the following dissertation:

Evaluation of Structure-Property Relationships within Insect Cuticle to Identify Motifs for Biomaterial Design

Committee members

Dr. Stevin Gehrke, Committee Chair

Dr. Michael Detamore

Dr. Prajnaparamita Dhar

Dr. Elizabeth Friis

Dr. Paulette Spencer

Date defended

ABSTRACT

Biological materials have mechanical properties that have been highly tuned for specific functions. The properties are governed by combinations of molecular interactions that are incorporated at multiple length scales in hierarchical structures. Establishing the links between molecular interactions and physical properties in biological materials has the potential to improve the design of structural biomaterials by offering effective design strategies. Insect cuticle, in particular, is an interesting model for studying structure-property relationships because it can have a wide range of mechanical properties despite a limited compositional makeup. The elytron, or outer wing cover, of the beetle is a strong and tough biomaterial made mostly of proteins, chitin, catechols and water. The objective of this thesis was to investigate molecular interactions among the components of elytral cuticle to both understand their role in governing *in vivo* properties as well as their future potential as biomaterial design motifs. The objective was addressed using two approaches. First, the intact elytron was studied to identify material design concepts that contribute to the strong and tough physical properties of the structure. Second, simplified systems of cuticular components were examined *in vitro* to help understand the *in vivo* roles of specific interactions with the future goal of providing new biomaterial design motifs.

Studies on the intact elytron from the yellow mealworm beetle, *Tenebrio molitor*, determined that the cuticle is not compositionally uniform throughout development. Instead, new material is continuously secreted from the epidermal cells. The color change and the frequency dependence of the cuticle plateaued after 48 hours, indicating that the initially secreted material matures within 48 hours of eclosion. The mature cuticle bears the tensile load while additional material is subsequently deposited and matured over a week of development.

Important contributions of both covalent and non-covalent interactions were identified in cuticle using dynamic mechanical analysis over a broad range of frequency, temperature and by treatments with non-covalent bond breaking-solvents. Indirect evidence pointed to the dominant role of covalent interactions in stabilizing the cuticle shortly after secretion from the epidermal cells. Dynamic mechanical analysis showed that the storage modulus of fully tanned and dried elytra was less frequency dependent ($n = 0.013 \pm 0.004$) than the modulus of untanned and dried elytra ($n = 0.05 \pm 0.024$), even at frequencies as low as 0.01 rad/s. Additionally, increasing the temperature from 25 to 150°C, up to the point of degradation, resulted in only a 3.5 fold decrease in the storage modulus and modest rise in the tan δ curve for fully tanned elytra. To further separate the role of covalent and non-covalent interactions in elytral cuticle, solvents were used to disrupt non-covalent interactions. More material could be extracted from partially tanned elytra than from fully tanned elytra, most likely reflecting the lower degree of covalent crosslinking in the immature layers of cuticle within partially tanned elytra. Soaking fully tanned elytra in formic acid, which disrupts hydrogen bonding, caused the static mechanical properties to resemble those of partially tanned elytra, which is consistent with the view that covalent crosslinks within the load bearing layers of cuticle are established within 48 hours. The role of non-covalent interactions was also highlighted by mechanical tests after treating with formic acid. The solvent caused a 5-fold decrease in the Young's modulus of fully tanned elytra, suggesting that a significant portion of the stiffness (which increases 20-fold with maturation) is provided by non-covalent interactions. The added stiffness provided by non-covalent interactions appears to have been provided without compromising toughness; that is, apparent hydrogen bonding caused a proportional increase in fracture stress and decrease in fracture strain, thus leaving toughness unchanged. Despite uncovering important contributions from

covalent and non-covalent interactions within the network as a whole, the complexity of the biological structure makes it difficult to identify the exact interactions contributing to the physical properties. Thus, simplified systems were used to study specific molecular interactions *in vitro*.

The hypothesized interactions that were studied *in vitro*, namely protein-chitin complexation, protein-catechol and protein-protein crosslinks, and protein-Ni^{2+} complexation, were studied using two abundant cuticle proteins in the elytra of the red flour beetle, *Tribolium castaneum*, CPR27 and CP30. CPR27 has a conserved sequence of amino acids that has been hypothesized to bind chitin. Results from active microrheology showed that addition of CPR27 to fluorescently-labeled aqueous chitosan solutions caused a 2-fold decrease in viscosity. Since this microrheology technique allows for the simultaneous visualization of microstructure, the appearance of bright fluorescent spots was observed along with the drop in viscosity. Together the results indicated that CPR27 complexation with chitosan caused aggregation that effectively removed material from the vicinity of the microrheology probes. CP30, which does not contain the conserved chitin-binding sequence, did not display similar evidence of complexation. The role of quinone crosslinking of both proteins with the catechol, N-β-alanyldopamine, was examined using passive microrheology. Microparticle formation was observed in solutions containing protein and laccase, catechol and laccase, and protein, catechol and laccase. However, elasticity was observed only when the protein was present, consistent with the hypothesis that quinone crosslinking has a mechanical role in cuticle, as concluded by the studies on elytra. However, further tests are needed to reproduce the data and verify the origin of elasticity. The highly unusual sequence of highly repetitive short blocks of positive and negative residues in CP30 suggested that it may self-assemble or interact with multivalent metal ions.

The protein was found to aggregate or adsorb to surfaces, preventing analysis, near the isoelectric point of 5.82. However, spectroscopic studies suggested the protein had an extended α-helical conformation at other pH conditions. CP30 was also shown to interact with nickel ions to form microparticles that induced elasticity in the fluid. The interactions involving these two cuticle proteins suggest new motifs that could be used in the design of tunable biomaterials. The rational design of proteins with specific covalent and non-covalent interactions with polysaccharides or ions, inspired by insect cuticle, may lead to biomaterials with enhanced mechanical properties.

Acknowledgements

I gratefully acknowledge funding from the Madison and Lila Self Graduate Fellowship and the National Science Foundation grant IOS 0726425. I also acknowledge my advisor, Dr. Stevin Gehrke and other mentors, Drs. Michael Detamore, Prajnaparamita Dhar, Lisa Friis, and Paulette Spencer for serving on my dissertation committee and for their valuable guidance and support with regard to my research project and my development as a scientist. I would also like to acknowledge Drs. Neal Dittmer, Michael Kanost and Karl Kramer from Kansas State University, who are indispensable to the insect cuticle project and have provided me with valuable insights and suggestions, not to mention beetles and proteins, for this work. Also I would like to thank those that assisted in the research methods required for this work: Dr. Joseph Lomakin for introducing me to the project and dynamic mechanical testing, Dr. Lisa Friis and Dr. Anil Misra for advice on mechanical testing methods, Dr. Paulette Spencer for the use of laboratory equipment, Dr. Qiang Ye for help with μ-Raman spectroscopy, Viraj Singh for his help with microXCT tomography, Heather Shinogle for her assistance with SEM, Dr. Russ Middaugh for the use of laboratory equipment, Dr. Christopher Olsen for his assistance with CP30 characterization techniques and Xia Hong for her analysis of my passive microrheology data.

Thanks to other members of Dr. Gehrke's lab who provided constant support both scientifically and personally: Anahita Khanlari, Linda Steele, Tiffany Suekama, and Erik van Kampen and thanks to the undergraduates Jessica Ettsity and Russell Thomas for their work on the project for several summers.

I am especially thankful to my mentor, Dr. Stevin Gehrke, for his constant and sincere guidance both professionally and personally. His passion for his work and his commitment to high quality research is inspirational and his positive and encouraging attitude make an incredible impact on the lives of many students. I will always admire his character as both a person and professor.

I want to give a special thanks to my husband, Charles, for his unconditional love and support and my son, John-Paul, and the baby girl within me for being my motivations to complete this work. And a deep thanks to my parents, Randy and Debbie, my siblings, and my in-laws, Chuck and Sonia, for their countless babysitting hours and their love and encouragement through everything. None of this would have been possible without the generosity of my family. Finally, thanks most of all to the Sacred Heart of Jesus and the Blessed Virgin Mary for providing the strength to persevere in the face of challenges.

TABLE OF CONTENTS

Chapter 1: Introduction

The overall objective of this thesis was to identify important molecular interactions within insect cuticle, both to deepen the understanding of structure-property relationships in the native tissue as well as to inspire new design motifs for structural biomaterials. Insect cuticle has a wide range of mechanical properties even though the main structural components are proteins and polysaccharides. The complex organization and interactions among the macromolecules produce multifunctional tissues that have impressive mechanical performance. However, many of the molecular interactions, especially the covalent and non-covalent links between proteins and between proteins and chitin, are poorly understood. Uncovering the nature of these interactions and their role in mechanical performance is an important goal in biomimetic material design.

Therefore, the work in this thesis addressed two major aims: 1) the study of structure-property relationships in an intact cuticle structure, the beetle elytron and 2) the examination of hypothesized molecular interactions *in vitro*. For the first aim, the conventional biomimetic approach was applied to the insect cuticle; that is, detailed studies of cuticle properties, especially the mechanics, were performed to illuminate key features that could inspire new design principles for biomaterials. The second aim, on the other hand, used a reverse biomimetic approach, in which a hypothesized biological feature was mimicked *in vitro* in order to learn about the function of that feature *in vivo* and the usefulness of that feature in biomaterial design. This approach is based on the realization that the structure and properties of individual cuticle components and interactions among those components must be studied in well-defined conditions *in vitro*, apart from the complexity of the biological organism, in order to better understand their role *in vivo* and to learn how they could be useful in technological applications.

In vitro, factors that are fixed *in vivo,* such as the relative amounts of different components, can be varied, thus allowing a systematic exploration of how each component contributes to physical properties.

The thesis is organized into three parts. Part 1 consists of Chapter 2, which provides background material on biomimetic material research. It reviews some of the most useful design principles discovered within nature, highlighting the importance of hierarchical structural organization and precisely controlled chemical interactions. It then discusses how current research methods are being used to uncover unknown design features within natural materials. Finally, the application of these natural material design principles is discussed by reviewing emerging approaches to biomimetic material design. Many examples of nature inspired material design strategies are given with an emphasis on protein, polysaccharide and catechol based materials since they are the main constituents of insect cuticle and the subject of the experimental chapters that follow.

Part 2 addresses the first major aim. It presents two major studies on the beetle elytron that shed light on the molecular interactions and how they develop throughout maturation of the insect. Chapter 3 and 4 are studies that stemmed from the work of my predecessors at KU, Chris Eichler and Joseph Lomakin. They developed the dynamic mechanical analysis methods that led to results which supported the view that the macromolecules in cuticle become more crosslinked with maturation. The influence of microstructural changes and relative influence of covalent and non-covalent crosslinks on the mechanical properties, however, was still unclear. Chapter 3, therefore, goes into a more detailed study on the temporal development of the elytron to better understand how chemical interactions and microstructural features influence the physical properties of the material. Results supported a model of cuticle development in which epidermal

cells continuously secrete cuticular material that becomes stabilized by crosslinking and pigmentation within 48 hours. The initially secreted material bears the bulk of the mechanical load while subsequent material is deposited and tanned. Imaging of the microstructure revealed that much of the dehydration occurred within the cavities between the two cuticular laminations, thus emphasizing the dominant role of protein crosslinking over dehydration in stabilizing the structure. The crosslinking and layered architecture represent important design features for mechanically robust biomaterials.

Chapter 4 aimed to clarify the roles of covalent and non-covalent interactions by extending the dynamic mechanical tests previously performed on elytral cuticle to lower frequencies and higher temperatures and by studying the properties of elytra after soaking in solvents that disrupt non-covalent bonds. The results emphasized the importance of both types of crosslinks for the high strength and stiffness of the elytral cuticle. The process of generating and interpreting the data for these studies motivated the transition to the third part of this thesis. Given the complexity of the biological structure, it seemed logical to isolate certain interactions within well-defined model systems and examine their usefulness as biomaterial design motifs.

Part 3, therefore, addresses the second major aim, using a reverse biomimetics approach in which *in vitro* molecular interactions are examined to elucidate their *in vivo* function and to evaluate their potential as a design concept for new biomaterials. It describes several hypothesized interactions between cuticle proteins and other cuticle components that were examined *in vitro* using microrheology, microscopy and spectroscopy to infer the mechanical role of those interactions *in vivo.* Microrheology is a useful tool for studying rare or expensive materials, which is often the case for recombinant proteins. It can measure the viscoelastic properties of complex fluids and can therefore detect changes in the macromolecular

connectivity within those solutions. Thus, it is a useful tool for understanding both the nature and mechanical effects of macromolecular interactions and associations.

Chapter 5 describes a study that used microrheology and fluorescence imaging to provide direct evidence of chitosan complexation with a cuticle protein that contains a sequence domain hypothesized to be involved in chitin binding. The results indicate that the binding motif has an important role in governing the mechanical properties of cuticle and may inspire the design of improved biomaterials.

Chapter 6 describes microrheological tests on *in vitro* model reactions involving the key molecules hypothesized to be involved in quinone crosslinking of cuticle proteins. Results showed that the hypothesized reactions led to the formation of microparticles and the viscoelastic behavior of the solutions appeared to change. Further work is needed to achieve more reliable results, but the usefulness of microrheology for the study of such systems was demonstrated.

Chapter 7 explains the structural characterization of a unique cuticle protein that was hypothesized to self-assemble via electrostatics or metal-ion coordination bonds. The results showed that the protein had an extended helical structure under the conditions tested, but aggregated close to the isoelectric point of the protein. Thus, the electrostatic self-assembly hypothesis was not directly supported but was not ruled out. The hypothesized interaction with metal ions was supported by the formation of microparticles and the development of elasticity within solutions of the protein and nickel ions. The findings support the view that the protein has a role in stabilizing mechanical properties of cuticle and its unique sequence may be useful as a motif for generating materials with controlled structures and properties.

Finally, Chapter 8 summarizes the key findings as well as the limitations of the experimental work described in this thesis. It then provides recommendations for future

experiments that would address the limitations of this work as well as extend it to new scientific questions and potential applications.

The long term goal of the work described in this thesis is to develop biomimetic materials with highly tuned mechanical properties for applications such as tissue engineering, drug delivery and wound healing. Materials that will be placed in the human body must be capable of responding to a variety of loads over a range of time scales. With a clear understanding of how molecular structures and interactions govern dynamic mechanical properties, biomedical materials can be rationally designed to have ideal, even multifunctional, properties for the particular application. Biomimetics is a privileged strategy for developing improved materials because it begins with a material that has already been optimized to perform a function. The experiments in this thesis advance the understanding of structure-property relationships within insect cuticle, making this type of biomimetic material design a less-distant reality.

List of Symbols and Abbreviations

RR: Rebers and Riddiford
E': storage modulus
E'': loss modulus
tan δ: loss tangent (=E''/E')
n: frequency power law exponent
RNAi: RNA interference
NBAD: N-β-alanyldopamine
NADA: N-acetyldopamine
DOPA: 3,4-dihydroxyphenylalanine
TFA: trifluoracetic acid
HFIP: hexafluoroisopropanol
LiBr: lithium bromide
GuHCl: guanidine hydrochloride
FA: formic acid
KITO-3: Low molecular weight, FITC-labelled chitosan from Akina, Inc.
η: viscosity
MSD: mean squared displacement

Part 1: Background

Chapter 2: Inspiration from Biology for the Design of Structural Biomaterials

2.1 Introduction

Biomimetic research aims to apply the designs of nature to solving problems in very diverse areas such as medicine [1], architecture [2, 3], materials science [4], nanotechnology [5], catalysis [6] and optics [7]. Natural materials are a rich source of inspiration for engineers seeking to improve the performance of synthetic materials. In particular, the mechanical properties of natural materials are closely tailored to the material function [8]. The remarkable and diverse properties stem from complex hierarchical structures and precisely assembled chemical interactions. Understanding the nature of structure-function relationships is an important step in mimicking certain properties of natural materials.

Naturally occurring polymers have a history of utility in structural applications, such as natural textiles made from silk, cotton, wool and leather. Silk has even been used as a biomedical suture material for centuries [9]. However, in the 20th century, the use of biological materials was largely replaced by synthetic polymers because they were versatile, inexpensive and easier to process [1]. The precise control over conformation and organization of biopolymers, though, is unsurpassed by synthetic materials [10]. Biological materials have diverse, multi-functional properties, making them attractive sources of inspiration for designing biomaterials [11]. With expanding capabilities in biochemistry and microfabrication, biomimetic material design has the potential to approach the multi-scale control over material properties achieved in natural materials.

In order to successfully produce synthetic bioinspired materials, the design principles responsible for the ideal properties of natural materials must first be identified. This review will cover some of the major structural and chemical design principles discovered in natural materials, the approaches to discovering additional design principles, and some strategies for applying those principles in the development of biomedical materials.

2.2 Biological Material Design Principles

2.2.1 Hierarchical structure

The biological synthesis of materials must use a limited set of chemical elements (mostly C, N, O, H, Ca, P, S, Si) in an aqueous environment with minimal energy expenditure to construct materials with a wide range of mechanical properties [1, 4, 12-14]. Natural materials rely on a hierarchical design, in which the structures are precisely controlled from the macroscale down to the nanoscale, to control the material properties. The final structure is often superior to the individual parts because the organization exploits the best features of each component. For example, the mollusk shell has a fracture toughness that is an order of magnitude greater than the main building block, calcium carbonate, that constitutes 95% of its makeup [4]. Several examples are given below, illustrating how hierarchical organizations in biological materials lead to enhanced properties.

2.2.1.1 Insect cuticle

Insect cuticle is a hierarchical structure composed mainly of proteins, chitin, catechols, enzymes, lipids and water [15]. It covers the body of insects and functions as a barrier to the surroundings and defense against predators [16]. Cuticle is often classified into soft and hard

cuticle; soft cuticle, which makes up structures such as joints, are flexible and allow for locomotion while hard cuticle, found in structures such as the outer wing covers (elytra), provides structure and protection [17-20]. Both hard and soft cuticle materials are made of the same components, but a small difference in structure can translate to a large difference in mechanical properties [1]. The stiffness can vary from kilopascals to tens of gigapascals [21]. However, the nature of the microstructural interactions allowing for the diverse properties is not fully understood.

An illustration of cuticle architecture is shown in Figure 1.1 [22]. Although this depicts lobster cuticle, the general organization is the same as insect cuticle, except that insect cuticles are not mineralized. On the molecular level, antiparallel chitin chains are bundled into nanofibrils that are about 3 nm in diameter and a few hundred nm long [21]. The chains are highly connected through hydrogen bonds, making the fibrils very stiff; the modulus likely exceeds 150 GPa [21]. The size of the fibrils is probably at a minimum in order to allow the highest surface area for interfacial interactions while maintaining stability of the fibril. However, fibrils with larger diameters have been found in some mandible cuticle, possibly because it must resist large compressive loads [23]. The chitin fibrils are embedded in a protein matrix, possibly wrapped in an organized fashion with specific chitin-protein interactions.

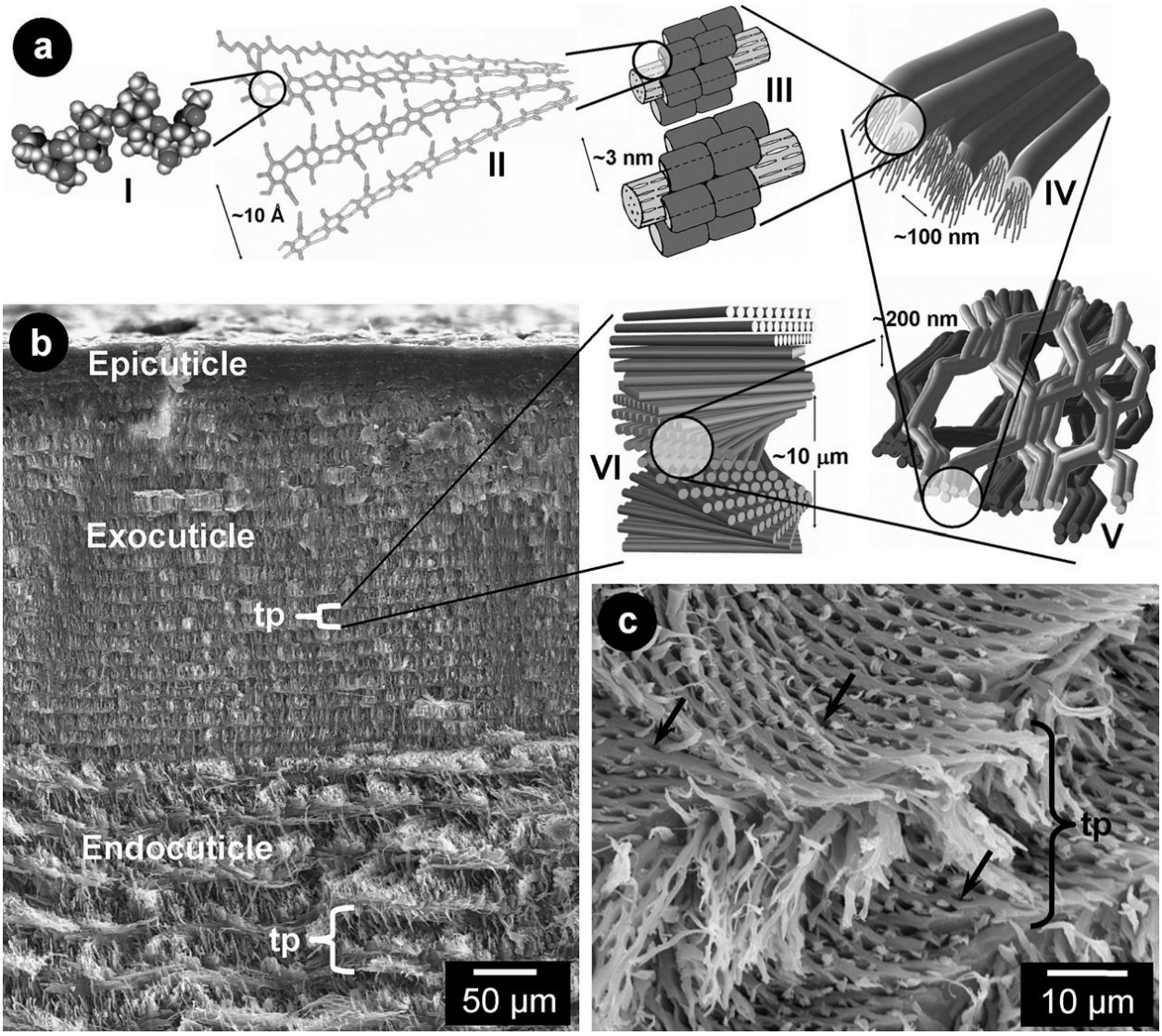

Figure 1.1. Illustration of the hierarchical structure of cuticle. Reprinted from [22] with permission from Elsevier.

Many diverse types of proteins have been identified within insect cuticle, but the structure and properties are not well studied [24, 25]. Among the proteins identified, many have conserved regions of amino acids that may serve a common function in different cuticles [25]. For example, the Rebers-Riddiford (RR) motif is a 28-residue consensus sequence that is hypothesized to be involved in chitin binding [26-29]. Proteins isolated from soft cuticle were classified as RR-1 and proteins from hard cuticle were classified as RR-2 [30, 31]. The RR

motif is discussed in more detail in Chapter 5. The nature of chitin-protein binding is not clear, but some studies have suggested that the RR region folds into β-pleated sheets that interact with chitin chains via hydrogen bonds and aromatic interactions [31, 32].

On the microscale, insect cuticle is a lamellar structure. The cuticle material is secreted by the underlying epidermal cells into an assembly zone [33]. The orientation of the chitin fibers rotates gradually, resulting in planes of parallel chitin-protein fibers with a twisted plywood-like architecture that is stiff in multiple directions (see part VI in Figure 1.1). Furthermore, the cuticle consists of three main groups of layers: an inner, compliant endocuticle, a stiff exocuticle, and an outer, waxy epicuticle [15]. The layered architecture makes the material tougher; with bending forces, the stiff exocuticle is loaded in compression while the compliant endocuticle is loaded in tension, thus allowing for more elastic energy storage in the exocuticle as well as larger deformations in the endocuticle [34]. The toughness is also higher in crack opening and tearing when the inner layer is more compliant [35].

The main processes that are involved, to various extents, in controlling the mechanical properties of cuticle are sclerotization, tanning and dehydration. A more detailed review of these processes is provided in Part 2. Briefly, sclerotization is the process in which the cuticle becomes stiffer, harder, and less flexible and resists extraction and enzymatic degradation [36]. Tanning refers specifically to the color change of cuticle due to development of pigmentation [36]. Dehydration also occurs as the biopolymers become more hydrophobic and water is actively removed by epidermal cells [16]. The relative importance of these processes and the interactions among the structural biopolymers that form as they occur is the main focus of this thesis.

2.2.1.2 Mussel byssus thread

Mussels attach to rocks with the byssus thread, a long filament made of a collagen core surrounded by a protein-rich cuticle matrix [4]. The byssus thread is remarkably hard yet extensible due to the microstructure of the cuticle [4]. The cuticle matrix has localized regions of highly crosslinked protein, or "granules," formed through metal coordination bonds between Fe^{3+} and 3,4-dihydroxyphenylalanine (DOPA), thus conferring hardness [4]. The rest of the matrix material is less crosslinked and more extensible than the granules. Under large strains, the non-covalent metal-DOPA crosslinks can break and reform, allowing the material to stretch up to 100% and subsequently recover the original stiffness [4].

2.2.1.3 Spider silk

Silk is a protein polymer that is produced and spun into fibers by organisms such as silkworms, spiders, scorpions and flies [9]. Depending on the source of the silk, it can vary in the composition and mechanical properties. Spider dragline silk, in particular, displays impressive stiffness and strength as well as extensibility; the fracture strength of silk from *Nephila clavipes* has a tensile strength around 900 MPa, a modulus around 12 GPa and a fracture strain around 18% [37]. The properties arise, in large part, from the hierarchical organization of the proteins, which is illustrated in Figure 1.2 [38]. On the nanoscale, there are protein strands that are highly hydrogen bonded into β-sheet nanocrystals [39-41]. The nanocrystals are embedded in a semi-amorphous protein matrix which confers extensibility to the material [38]. The nanocrystal/protein network is further formed into fibrils [39-41]. The fibrils are then bundled into a larger fiber that has a higher tensile strength per unit mass than steel [4, 39-42]. Computational analysis of the nanocrystals suggested there was a critical size, under which the

hydrogen bonds worked cooperatively to resist stresses, thereby increasing the strength and toughness of the fibers [43].

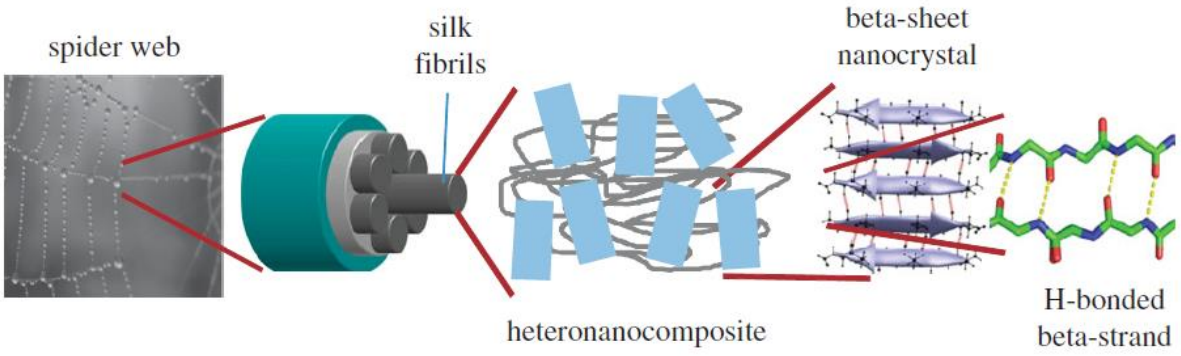

Figure 1.2. Hierarchical structure of spider silk. Reprinted with permission from [38].

2.2.1.4 Nacre

Nacre is the material that forms the inner layer of the mollusk shell [1]. Nacre is composed of 95% calcium carbonate, yet it is 3000 times tougher and 1000 times more resistant to fracture than crystalline calcium carbonate. The remarkable mechanical properties are possible because the brittle calcium carbonate material is embedded in a ductile chitin-protein matrix [1].

Proceeding from the macroscale down to the nanoscale, nacre has 6 different layers of hierarchy. Each layer contributes in some way to the high-performance of the material. The two-layered design consists of a hard and brittle outer layer and a plastically deformable inner layer that can dissipate energy [44]. Further, growth lines exist on the millimeter scale, within which aragonite (a form of calcium carbonate [45]) tablets make up micron-thick layers. The tablet interfaces are nanometers in dimension and promote strain-hardening when the tablets shear past each other. The dove-tail shape of the tablets also encourages locking of the components which similarly resists crack propagation. Thus, as a crack grows, toughness

increases [44]. Pre-stresses within nacre create strain gradients that contribute to the curved shape of the shell and may help to close cracks that are propagating from the outside [46, 47]. Some recent studies have achieved high toughnesses in synthetic materials, such as polymer films and ceramic-based composites, by mimicking the brick and mortar design of nacre [48-54].

2.2.1.5 Bone

Like nacre, bone is a composite of organic and inorganic material whose properties are superior to the main mineral component; it has a significantly higher fracture toughness than hydroxyapatite alone [4]. The properties are a result of the organization of the mineral phase with an organic protein phase. Hydroxyapatite (HAP), which is a form of calcium apatite $Ca_5(PO_4)_3(OH)$, and tropocollagen (TP) interact to form 6-7 levels of hierarchy [44]. Nanocrystals are embedded in collagen fibrils, which are arranged in either woven, plywood or aligned 3-dimensional patterns. These features are further built into lamellae or osteons [44]. Bone has the ability to heal after minor crack formation. Osteoclasts and osteoblasts are specialized cells that respond to mechanical loads by breaking down or building up new bone tissue. In this way, bone density can adapt to the loading requirements. In fact, 25% of the skeleton is completely turned over every year in a healthy person [44].

The interface between the inorganic and organic phases is thought to impart much of the toughness to bone. The large amount of interfacial surface area allows for deflection of cracks [46]. Cracks will propagate preferably along the cement lines of osteons, thus favoring longitudinal bone splitting rather than transverse breaking [55]. Also, the HAP and TP are layered and staggered in a way that maximizes the interfacial contact and thus promotes effective tension-shear load transfer [45]. The chemical attraction between the Ca^{2+}, PO_4^{3-} and OH^- ions

in HAP and the NH^{3+} and COO^{-} groups on TP imparts added toughness by forming sacrificial bonds (i.e. bonds that break and reform under stress) [45, 56, 57]. Water also strengthens the interface due to its polar and hydrogen-bonding nature [45]. It is unclear whether this nanoscale design is introduced primarily for mechanical purposes or whether it is a geometrical result of growth and mineralization [45]. Nevertheless, the structure offers insight into efficient arrangements of minerals and organic matrix.

2.2.1.6 Mammalian Teeth

Teeth are biocomposites made of a hard, stiff and brittle enamel layer covering a soft and compliant dentin interior. Enamel is 96% mineral and doesn't contain living tissue, but does experience chemical exchange [58]. Dentin is only 70% mineral and contains living pulp and nutrient flow [58]. The interface between the two, called the enamel-dentin-junction (EDJ) is microns in thickness. The tooth is anchored to the periodontal ligament via a cementum layer.

Enamel has been described as the "masterpiece of bioceramics" [59]. The hardness and abrasion resistance is due to the nanoscale organization of calcium hydroxyapatite crystallites aligned perpendicular to the surface [59, 60]. Interestingly, a genetically remote organism, the crayfish, has the same type of structural design in its mandible, suggesting that the design evolved in response to the functional demands of chewing food [60].

The hydroxyapatite mineralized rods are connected by a nanometer-thick organic sheath, radiating out from the EDJ. The rods are arranged in bundles in a woven pattern [58]. Enamel also contains organic matter-filled defects called tufts and spindles that extend along the enamel wall [58]. Studies on these defects reveal that tooth structures survive by containing damage rather than avoiding it completely [61]. The cracks are stabilized by stress shielding from

neighboring cracks, they are prevented from propagating by the decussation (or crossover) of rods, and they are healed by the infiltration of organic material [61]. It has also been proposed that enamel can yield via sacrificial bonds in the protein layer that links the HAP crystallites. It may experience creep deformation with some recovery after loading as well [58].

2.2.1.7 Conclusions

The enhancement of mechanical properties through a hierarchical design is key to the successful function of biological materials. Some common features can be seen within hierarchical biomaterials. First, the combination of stiff and flexible phases results in a higher overall toughness. The stiff phase can be composed of minerals, as in the case of nacre, bone and teeth, fibrous components such as silk or chitin fibers, or a crosslinked protein phase as appears in the insect cuticle and mussel byssus thread. The stiff components provide a high resistance to stress, but are often inherently brittle. Thus, the stiff phase is often embedded in a more ductile organic matrix, and small amounts of matrix material can improve the toughness dramatically. Another common feature is the orientation of structures with a specific direction to provide resistance to load in certain directions. The twisted plywood-like architecture of cuticle layers provides multidirectional resistance to stress, nacre has a brittle outer layer and ductile inner layer to enhance resistance in bending, and the calcium hydroxyapatite crystallites in teeth are aligned perpendicular to the surface to enhance the hardness and abrasion resistance. Lastly, biological materials are often built up from the molecular-level to the macroscopic level to incorporate different features at several length-scales. If engineers could replicate the intricate multi-scale structural organization of biological materials from the nanoscale to the macroscale, we would undoubtedly improve the performance and expand the capabilities of biomaterials

2.2.2 Optimized Chemical Interactions

In addition to this precise control of structure, however, it is important to tune the chemical interactions as well. Biological materials incorporate a variety of chemical bonds in a way that confers remarkably diverse properties. Understanding those relationships is also key to successful biomimetic designs.

2.2.2.1 Covalent Crosslinking

The covalent crosslinking of proteins is a way to achieve high strength biomaterials without the need for mineralization. Insect cuticle, described in 2.2.1.1, most likely modulates the level of covalent crosslinking of proteins over time to stabilize the mature structure [20]. The squid modulates the level of covalent crosslinks spatially. The very stiff beak must connect to soft body of the squid, so rather than an abrupt interface, there is a stiffness gradient in which the pigmentation and protein crosslinking gradually decrease and water content increases from the tip to the base of the beak [13]. The highly crosslinked beak is a hard and stiff material despite the lack of any mineral and metal components [62]. The toughness is higher than mineralized tissues such as enamel [13]. The properties of the beak are a function of the densely crosslinked protein network as well as the low water content; the catechol 3,4-dihydroxyphenyl-L-alanine (DOPA) forms crosslinks with the histidine residues on the protein, and is likely responsible for dehydrating the tissue as well [63].

Biological systems often use enzymes to trigger the crosslinking of proteins. For example, transglutaminase is needed for natural wound healing in order to crosslinks the glutamine and lysine groups on fibrin proteins to stabilize blood clots [64-66]. Researchers have

found that enzymatic crosslinking is generally a more gentle and biocompatible (i.e. non-cytotoxic) approach to forming crosslinked materials, compared to photo and thermal initiation, because it does not require toxic chemical initiators and does not cause a large increase in temperature [67]. Messersmith *et al.* have developed hydrogels that mimic the enzymatic crosslinking mechanism involved in the blood coagulation cascade [67]. The gels were synthesized from a solution of 4-armed poly(ethylene glycol) modified with fibrin peptides which were crosslinked by transglutaminase [67]. Since transglutaminase depends on calcium ions as a cofactor [68], the gels could be rapidly formed *in situ* by a thermally-triggered release of calcium from liposomes [67]. Another group also used transglutaminase to crosslink fibrin into gels as well as to covalently incorporate peptides from other proteins that promoted nerve regeneration [69].

Covalent bonds between cysteine residues are important for stabilizing the folded structure of many proteins [70, 71]. Li and Haynie have used a biomimetic approach based on the disulfide bonds within proteins to crosslink polyelectrolyte multilayers and thus increase their structural integrity [72]. The approach was advantageous because the bonds could be formed under mild conditions, the number of bonds could be highly controlled and they were reversible, making the materials promising for films, coatings on biomedical implants and drug delivery devices [72].

2.2.2.2 Non-covalent Interactions

By themselves, non-covalent interactions are generally weaker than covalent interactions. However, they often impart important mechanical properties to natural materials, since strength is not the only important quality of a biological structure. Non-covalent bonds can confer added

toughness, energy dissipation, stimuli responsive and self-healing characteristics to materials in ways that cannot be achieved by covalent interactions. For example, the extreme toughness of nacre relies on intermediate strength non-covalent bonds within the organic matrix [73]. One of the proteins from the matrix was isolated and sequenced, revealing a highly modular conserved sequence. The protein was attached to an atomic force microscope and a flat surface to study the mechanics of breaking the modular structure. The force-extension curves showed a saw-tooth pattern reflecting either the opening of loops or folded domains or the breaking of sacrificial bonds. Whatever the exact mechanism, the non-covalent interactions increased the total energy required to break the molecule [73]. It is important to understand how different types of non-covalent interactions affect the properties of natural materials in order to design effective biomimetic materials. Thus some important contributions of hydrogen bonds, ion-mediated sacrificial bonds, hydrophobic interactions and van der Waals interactions are reviewed below.

Hydrogen bonds

Hydrogen bonds alone are intrinsically weaker than covalent bonds. However, in biological materials they are often grouped together and work cooperatively. In fact, the density of hydrogen bonding can be tuned to confer functionality at different length scales within the same material. For example, in silk, hydrogen bonds are clustered in beta-sheet nanocrystals, making the material extremely strong [12]. At the same time, silk is quite extensible because the stiff nanocrystals are embedded in a more disordered phase of protein with proline-rich segments that prevent aggregation of strands and provide twists with “hidden length” [38]. The concept of hidden length refers to additional extensibility provided by the breaking and reforming of non-covalent interactions that hold a biopolymer in a particular folded or modular configuration. The

ability to self-heal, or reform after the stress is removed, improves the toughness of the material. Besides silk, the clustering of hydrogen bonds is seen in many other biological structures such as muscle and cytoskeletal proteins, suggesting it is an effective design principle within natural materials to confer strength and toughness [12, 74].

The stability of hydrogen bonds depends greatly on water content. For example, the rapid decrease in the elastic modulus of cellulosic materials with wetting has been related to the cooperative dissociation of hydrogen bonds [75]. The mechanical properties of many other natural materials are also extremely sensitive to water content [76-78], suggesting that hydrogen bonds play an important role [34]. However, most natural materials have many other types of molecular interactions that contribute to the mechanical properties, so understanding the relative importance of each requires careful experimental controls. As noted in 2.2.1.1, in the discussion of insect cuticle, the importance of hydrogen bonding and water content vs. covalent bonds has been a debated subject, but recent studies maintain the importance of both [20]. Part 2 of this thesis provides additional clarification on the role of water, non-covalent interactions such as hydrogen bonds, and covalent interactions on the properties of insect cuticle.

Ion-mediated sacrificial bonds

Ion-mediated bonds are another form of non-covalent interaction used widely by biological materials. The advantage of these interactions is that they can break and reform under stress, imparting some self-healing capability to the tissue. They also provide "hidden length" to materials because they must be stretched and ruptured before the stronger bonds are stressed, thus increasing the total energy required to fracture a material [56]. The toughness and strength as well as the self-healing abilities of tendon fibrils were associated with Ca^{2+} ion sacrificial

bonds. The bonds were described as a "nanoscale velcro," capable of binding two surfaces in close proximity but not completely touching [79]. Calcium-mediated sacrificial bonds are also important for the high stiffness of bone as well as its ability to dissipate energy [56, 80, 81]. A model system using atomic force microscopy to simulate the separation of mineralized collagen fibrils showed that energy dissipation was greater if Ca^{2+} ions were present in the buffer rather than Na^{+} ions [56]. The multivalent ions were able to provide a link between negative residues on proteins as well as hydroxyapatite [56].

Multivalent metal ions have been suggested to have a structural role in many other natural materials. For example, protein-metal coordination bonds are thought to be responsible for the self-healing characteristics of mussel byssal threads [82]. Also, the *Nereis* marine worm jaw is almost as hard (defined as the peak load over the area of impression during indentation tests) as dentin even though it is not mineralized [83, 84]. Instead, the hardening is thought to come from extensive zinc coordination crosslinking among the protein matrix [13, 83]. Coordination bonds between proteins and multivalent metal ions have also been linked to increased hardness and stiffness of arthropod cuticle [85-88]. Since many of the hard 'tools' such as jaws, leg claws and mandibles are enriched in transition metals, it is thought that they play a mechanical role. However, direct evidence of the protein-metal interactions is lacking and the precise structural role is not clear [89]. Chapter 7 of this thesis provides evidence of a histidine-rich cuticle protein interacting with nickel ions, thus supporting the view that protein-metal interactions play a role in cuticle properties.

Hydrophobic interactions

Hydrophobic interactions are attractive interactions between non-polar, organic molecules in water [90]. The structure of many biological molecules relies on self-assembly processes driven largely by hydrophobic interactions. Cell membranes, for example, are formed by the self-assembly of phospholipids, which form a bilayer where the hydrophobic ends face the center and the hydrophilic ends face outward. Phospholipids can also self-assemble into vesicles, micelles and tubules [91, 92].

Protein folding is often controlled by hydrophobic interactions. A key structural motif found in proteins involved with DNA transcription as well as in keratins is the leucine zipper [93]. The structure relies on a repeat sequence that has a specific placement of hydrophobic residues (frequently leucine) that align on one face of the helix. Their interaction with water is kept to a minimum by the formation of coiled-coils, which are further stabilized by electrostatic interactions among other residues within the repeat sequence [93]. The combination of specific electrostatic and hydrophobic interactions has been shown to give control over the assembly of designed peptide materials [94].

Hydrophobic interactions are also responsible for the modular unfolding of titin, an important muscle proteins [73, 95, 96]. Single molecule mechanical tests showed that a sawtooth pattern in the force-extension curve of titin corresponded to unfolding of individual immunoglobulin-like domains held together by hydrophobic interactions [73, 95, 96]. Titin is an example of how the molecular structure governs the mechanics, and therefore the function, of a biopolymer.

Van der Waals interactions

Van der Waals interactions, which are the collection of attractive and repulsive forces arising from dipole and induced dipole forces, are weakest of chemical interactions, yet they still play a role in stabilizing biological materials. For example, the gecko toe pad has hundreds of thousands of setae, or hair-like keratin structures, each of which has hundreds of nanometer sized projections that attach to surfaces through van der Waals forces [97, 98]. The sheer number of these weak bonds creates a remarkably effective adhesive system, allowing the gecko to run on almost any surface, even upside down [98]. The system highlights how structure and chemistry are often both crucial to the function of the material. The concept of gecko adhesion is being used to develop biomimetic surgical adhesives [99, 100]. Van der Waals interactions are also important attractive forces that hold organic and inorganic components together in materials such as nacre. Layered composite films made from montromillonite clay platelets and polyelectrolytes were inspired by the strong electrostatic and van der Waals interactions at the organic/inorganic interface of nacre [51].

2.3 Uncovering unknown structure-function relationships

Many structure-function relationships have been established in natural materials, but there are also many more features that have yet to be identified through chemical and structural characterization. It is important to always look for new ways of uncovering structure-function relationships in natural materials. It is equally important not just to observe the properties of natural materials and try to replicate them, but also to understand why that structure has acquired that property. Natural materials go through long adaptation processes to solve problems, but often it is not clear what problems were solved or what constraints or requirements led to those

solutions [14]. Therefore, carefully study the structure-function relationships within natural materials must be used to identify the key features responsible for a function or property of interest.

The most straightforward way to study biological materials is to fully characterize the chemical, structural and mechanical properties of the structures in their native, *in vivo* state using the most advanced techniques available. Certainly, spectroscopic, microscopic and mechanical analysis has uncovered much of what is currently known about natural materials. For example, the structure of silk has been uncovered through years of research using X-ray diffraction [101], NMR [102, 103], IR and Raman spectroscopy [104]. However, many natural materials possess hidden features that remain inaccessible using the standard techniques. For example, the quinone crosslinking hypothesis for insect cuticle was a longstanding debate because the proteins were inextractable and standard biochemical techniques were not able to identify two proteins connected by a single quinone molecule. Therefore, further insight required an unconventional approach which adapted characterization techniques from synthetic polymer science. Lomakin *et al*. used dynamic mechanical analysis to suggest the importance of crosslinks within sclerotized elytral cuticle, and the knock-down of enzymes thought to be involved in the crosslinking pathway provided additional support for the importance of crosslinks in mechanical stabilization [20]. Part 2 of this thesis uses mechanical analysis to further clarify the roles of covalent and non-covalent crosslinks. Future studies on natural materials may also have to creatively apply the methods developed in other fields to gain new information [4].

Another way to learn more about the structural properties of natural materials is to take advantage of the extremely small scale mechanical testing methods currently available, such as atomic force microscopy, nanoindentation and microrheology. Microrheology has emerged as a

technique to measure local, small scale mechanical properties of biological materials [105-110]. Microrheology and macrorheology were used to study the extracellular matrix of the jellyfish and heterogeneity in the viscoelastic properties was found at the microscale and adult jellyfish were locally stiffer than juvenille jellyfish [111]. The multi-scale mechanical analysis, coupled with electron microscopy suggested that aggregations within the fibrous architecture of the mesoglea accounted for the differences in properties [111]. Microrheology is also useful for studying natural materials that exist only in very small quantities. For example, it was used to characterize the viscoelastic properties of extremely small volumes (0.1 nl) of the secretory fluid from attachment hairs on the beetle adhesive pad [109]. Surprisingly, the fluid was found to be purely viscous, but a high viscosity (due to a high molecular weight) ensured robust adhesion as well as limited evaporation [109].

In addition to experimental studies, theoretical models can be used to gain further insight into the role of structural elements in a biological material. Finite element analysis of ammonite shells was used to show that flaw tolerance is enhanced when the number of hierarchical levels increases despite the same makeup of constituent materials [112]. The flaw tolerance was a result of heterogenous interfacial strain distributions spread damage rather than allowing complete failure [112]. A computational model was also used to simulate the hydrogen bonds in β-sheet proteins within silk fibers, revealing that an optimal aspect ratio results in maximum strength and toughness [43].

Despite the advanced techniques and computational models that exist for studying intact biological structures, some features will remain inaccessible due to the structural and compositional complexity. Therefore, a "reverse" biomimetics approach may be helpful. This approach would begin with mimicking some hypothesized biological feature *in vitro* and varying

the parameters associated with that feature in order to learn about the function of that particular feature apart from the complex biological system [4]. For example, atomic force microscopy has been used to study the mechanics of single molecules isolated from complex structural biomaterials [73, 95]. The *in vitro* studies within Part 3 of this thesis follow this approach, where certain hypothesized interactions are studied apart from the complexity of intact insect cuticle in order to learn about their unique contribution to the material properties.

2.4 Emerging Approaches to Biomimetic Material Design

The design principles found within biological materials are increasingly being used to develop improved structural materials for biomedical applications. The ability to tune the structure and interactions of the building blocks is key to the performance of biological structural materials. Several approaches in biomaterial design are making progress toward capturing the control over material properties that have been discovered in natural materials.

2.4.1 Protein-based materials

Proteins are a unique class of polymers that exhibit remarkable versatility in function through highly controlled structures. Despite the limited set of amino acids available as building blocks, extremely diverse proteins are produced in nature, ranging from fibrous structural proteins to globular enzymes [93]. The different functions are a result of the precise, three dimensional control of the structure that is directed by the amino acid sequence of each protein. Proteins are critical in directing the assembly of biological materials as well as controlling the function of the material [5]. Even though progress has been made in the control of synthetic

polymer characteristics [113], they still cannot be controlled to the degree that the is seen in biomacromolecules such as proteins [93].

Protein engineering, therefore, offers a strategy for developing protein-based materials with highly controlled structures [93]. The process involves selecting an amino acid sequence based on what is known about the properties and function of that protein in nature. The DNA fragment coding for that sequence can either be cloned from the organism or made from artificial genes, after which it is transplanted into a host microorganism, usually *E. coli*, and expressed as protein [93]. With this strategy, not only can engineers tune the mechanical properties, but they can also incorporate domains that control cell behavior. Additionally, there is less batch-to-batch variability in protein properties and lower possibility of disease transmission than using mammalian derived proteins [11]. Also, some proteins such as spider dragline silk are desirable as a biomaterial, but cannot be obtained in sufficient quantities because spiders are predators, so protein engineering offers a means for scaling up production of this material [93].

One example of a protein-based biomaterial is a reversible hydrogel made from recombinant artificial proteins. The concept was introduced by Tirrell's research group at the University of Massachusetts, who developed a pH and temperature sensitive hydrogel using recombinant proteins containing self-assembling leucine zipper domains at the ends and a hydrophilic polyelectrolyte domain in the center [114]. Another recent example is an environmentally responsive hydrogel made from a rationally designed peptide consisting of a beta-roll motif that was discovered in bacteria [115]. The conserved sequence was shown to be disordered in the absence of calcium but folds into a highly ordered, compact and stable beta-roll structure upon binding to calcium [116, 117]. The dependence on calcium allowed the motif to

be used in an environmentally responsive hydrogel in which the strength could be precisely tuned by the concentration of calcium [115].

Other recombinant polypeptides have been synthesized based on the elastic properties of elastin and resilin proteins. Elastin-based polypeptides, using the highly repetitive VPGVG sequence, are the most widely used biomaterial of this type [118-122]. Natural polymers made from recombinant expression of elastin-like peptides, for example, were produced for the regeneration of vascular tissue [119]. The material incorporated the elastin-like sequence domains along with domains such as RGD, known to bind endothelial cells, to achieve a matrix that was mechanically and chemically favorable for vascular tissue growth [119]. Another polypeptide with a resilin-like motif was shown to have highly elastic properties as well as cell adhesion properties [123].

Genetic engineering of protein materials also offers more versatility than simply replicating natural proteins. For example, inserting non-natural amino acids like trifluoroleucine into recombinant protein sequences has been studied as a way to control the chemical, physical and biological properties [124]. Additionally, the combination of synthetic and biological polymers has resulted in highly tunable materials with multifunctional properties. A copolymer made of lactic acid and lysine, for example, was shown to have controlled degradation times due to the lactic acid component as well as cell adhesion properties due to coupling of RGD peptides to the lysine component [125]. In another example, poly(ethylene glycol diacrylate) (PEG-DA) was grafted onto engineered peptides to form hydrogels that were suitable for tissue regeneration [126]. The peptides contained sequences from fibrinogen and anti-thrombin III in order to promote cell adhesion, plasmin degradation and heparin binding. The PEG-DA could be photo-crosslinked to obtain a larger Young's modulus [126].

Another emerging strategy in protein-based materials is “molecular biomimetics,” or the formation of materials at the molecular level using the recognition properties of proteins [5]. Since proteins can direct the organization of inorganic materials by binding and controlling the crystal growth, the hope is to create hybrid materials similar to natural protein-inorganic materials such as bone, enamel and nacre [127]. The strategy uses the tools of molecular biology and nanotechnology to engineer at the molecular and nanoscale, thus promising great potential for controlling structure.

While the potential for producing sophisticated protein-based materials is great, there are also several drawbacks. Protein structures are difficult to predict, recombinant proteins synthesis is expensive and difficult to scale-up, and it is difficult to sufficiently purify the proteins to prevent an inflammatory and immune response [93, 122, 128]. Additionally, protein engineering may not be necessary for every case in which one seeks to replicate a protein characteristic. For example, the adhesive properties of the protein glue that holds the mussel byssus thread to the substratum under water were captured to some extent by preparing co-polypeptides of lysine and 3,4-dihydroxyphenyl-L-alanine (DOPA) rather than replicating the entire sequence using gene expression [129]. The methods readily produced large quantities of material. Such an example illustrates the importance of identifying the essential features of a natural material that account for a particular function. Replicating only the essential features will simplify biomimetic strategies and save considerable time and expense. Nevertheless, protein-based materials may lead to a new generation of biomaterials with controlled structures and properties.

2.4.2 Polysaccharide-based materials

Polysaccharides are the most abundant biopolymer and are used to provide energy storage or structural support to biological organisms. Chitin is the second most abundant structural polysaccharide after cellulose in biological materials. The chemical structure, shown in Figure 1.3, is poly-β-(1,4)-N-acetyl-glucosamine [130]. It is generally insoluble, unless partially deacetylated into chitosan, which makes it soluble in acidic conditions. Even though chitin is almost as abundant in nature as cellulose, it is much less utilized for engineering materials because it is difficult to imitate the microstructure of chitinous materials [1].

One area where chitin and chitosan have been used is for biomedical applications; but despite the fact that they have mostly a mechanical role in nature, the choice is often based on the chemical rather than mechanical properties [1]. Since it is cationic, chitosan has a natural antibacterial quality because it binds with anionic polymers on bacterial cell walls and promotes their death [1]. Chitosan also associates with anionic extracellular matrix components such as glycosaminoglycans and proteoglycans, making it a good material for tissue engineering scaffolds [1]. However, the available fabrication methods for chitosan materials, such as freeze drying into porous scaffolds, molding or electrospinning into fibers, do not yet take full advantage of the mechanical potential of the molecule [1]. Such potential will only be realized by directing the material synthesis at much smaller scales. A recent study imitated the phase-separated arrangement of chitosan and protein within insect cuticle to form a material called "shrilk" (made from chitosan and silk fibroin) that was two times stronger than the stronger, chitosan component and ten times stronger than a blend of each [131]. Also, a method for producing chitin nanofibers has recently been developed and has been combined with silk protein to achieve high-strength films [132, 133].

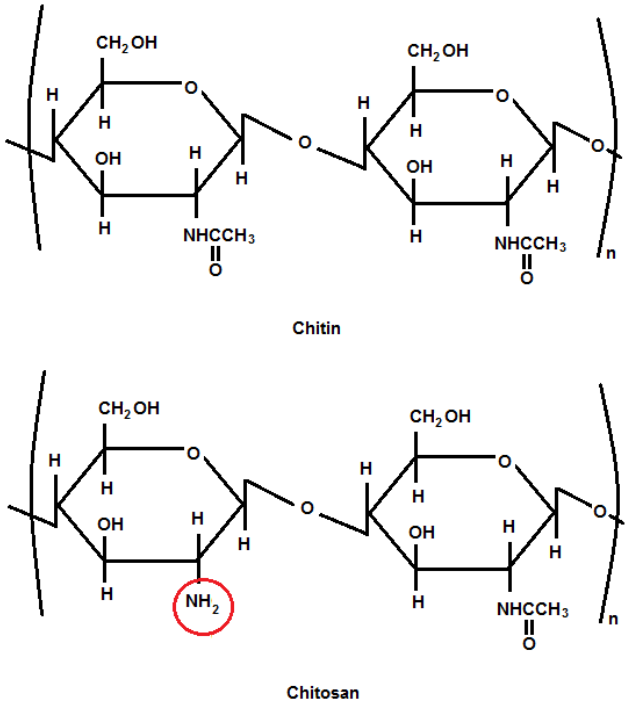

Figure 1.3. Repeat units of chitin and chitosan. Chitosan is formed by partial deacetylation of chitin, as shown by the red circle.

Hyaluronan is a glycosaminoglycan found in biological fluids and tissues such as synovial fluid and extracellular matrix. It is a high molecular weight polymer of alternating (1,4)-β linked D-glucuronic and (1,3)-β linked N-acetyl-D-glucosamine residues [134]. It has unique viscoelastic properties stemming from its high molecular weight, which can reach 10^7 Da [134]. It has been useful in a variety of clinical applications such as filling or augmenting tissues, separating injured tissues to prevent excessive scar tissues or supplementing synovial fluid to relieve arthritis pain [135]. Crosslinking the carboxylate groups of HA can produce a biocompatible hydrogels and microgels with tunable degradation properties for drug delivery and tissue regeneration [136, 137].

Seaweed polysaccharides, such as alginate and agarose, are also an important biopolymers. Alginate comes from brown algae; it is a block copolymer of 1,4-linked β-

D-mannuronic acid (M) and α-L-guluronic acid (G) [130]. The physical properties vary depending on the ratio and distribution of M to G [130]. G-blocks can form stable crosslinks with calcium ions, and therefore gels with tunable properties can be formed by controlling the length of the G-blocks [130]. Alginate can also be mixed with chitosan to form electrostatic complexes to obtain fibers or films [138]. Alginate gels are biocompatible and have been useful for developing tissue engineering scaffolds, drug delivery devices, wound dressings [130]. Several other polysaccharides, such as carrageenans, galactomannans, glucomannans and xanthans are being explored for biomaterial development and their properties can be tuned by chemical modifications to achieve tailored properties.

2.4.3 Catechol-based materials

Catechols, which are benzene derivatives with two *ortho*-hydroxyl groups, occur widely in nature [139]. They have very versatile functions such as adhering to surfaces, binding molecules within complex systems, providing a framework for 2D or 3D structures and reversibly responding to stimuli [139]. The versatile functions are a result of their reactive nature with oxidizing agents and their ability to form hydrogen bonds and metal coordination bonds [139]. The versatility, however, can be a challenge because it can be difficult to control the chemistry and therefore the properties [139]. However, the properties of catechol materials have inspired many biomedical materials.

In particular, the adhesive role of catechols within mussel foot proteins, which strongly adhere even to low-fouling surfaces in wet conditions has inspired the design of biomedical adhesives [140]. Mussel proteins contain the catecholic amino acid, 3,4-dihydroxyphenyl-L-alanine (DOPA), which anchors the structure to surfaces through metal coordination bonds [141-

143] and hydrogen bonds [140, 144-146]. The DOPA can also be oxidized to quinones to serve as covalent crosslinkers [140, 146, 147]. The functions of catechols within mussel proteins have inspired the design of many different adhesives with high interfacial shear strengths [129, 148, 149]. A challenge was to balance the degree of oxidation of the catechols because the oxidation to quinones promoted internal cohesiveness of the material whereas the parent catechols were much more adhesive [148]. Hydrogels have also been developed by incorporating catechols into crosslinked polymer matricies for uses such as surgical adhesives [150, 151], hernia repair [152], and anti-bleeding materials [153]. The coordination crosslinking motif between the DOPA residues of mussel proteins and Fe^{3+} has also been exploited to create self-healing gels [154].

Melanin is a generic term that describes pigment polymers found in natural materials such as hair, skin, eyes and *Sepia* ink [139]. The lack of solubility has made chemical analysis of melanin difficult and led to lack of consensus regarding the structure. However, recent spectroscopic studies suggest it is formed by aggregation of oligomers rather than high-molecular weight polymers [155, 156]. Melanin has been associated with the hardness and stiffness of structures such as the marine worm (*glycera*) jaw [157]. A widely studied synthetic analogue of melanin is polydopamine, which is used as a coating material and adhesive primer [139, 158]. For example, polydopamine has been used to immobilize proteins on surfaces to promote a variety of cell responses [159-162]. Thus, incorporating catechols into synthetic or peptide materials can expand the possible functions of that material. For example, catechols could be used within tissue engineering scaffolds to promote adhesion to the native tissue as well as directed cell responses. Additionally, they can be used to anchor different polymers to biomaterial substrates to provide anti-fouling, antibacterial, anti-corrosion, anti-wear, hydrophobic or hydrophilic coatings [139].

2.4.5 Composite materials

To improve the performance of biomaterials, it is increasingly important to look beyond simple one-component materials. The combination of materials with different, but complementary, properties is routinely seen in nature, as was discussed above where the small amounts of organic material in mineralized tissues offers a mechanism to dissipate energy and therefore increases the toughness [13]. In the same way, biomedical materials must utilize different materials to achieve multifunctional properties that will withstand the loads of the human body. An example of this was seen when elastin was incorporated into collagen-based tissue engineering scaffolds for blood vessel regeneration, which improved the mechanical properties of the material and made them more similar to native tissue [163]. The hybrid design maintained the stiffness provided by the collagen but improved the creep and stress relaxation response by incorporating the elastin, which could support loads over longer periods of time [163]. It is especially important to match the properties of vascular materials to the natural tissue because mismatches can alter the flow of blood which can trigger intimal hyperplasia [164].

Another composite strategy is synthetic-biopolymer hybrid materials [165-167]. For example, temperature sensitive hydrogels were developed by incorporating heparin and heparin binding peptides into poly (ethylene glycol) gels in a way that mimics the protein-polysaccharide interactions within extracellular matrix. Control over viscoelastic properties could be achieved by altering the heparin binding affinity of the peptides [168]. Additionally, domains such as RGD, coiled-coil, β-sheet and α-helical forming peptides, have been incorporated into poly (ethylene glycol) polymers to control properties such as cell adhesion, self-assembly, stimuli responsiveness and degradability [165, 169].

Multicomponent designs are becoming more common for hydrogel materials. Hydrogels, since they are solid materials made of mostly water, are uniquely suited to a variety of biomedical applications. However, hydrogels are generally weak and brittle materials whereas many applications such as tissue engineering scaffolds, wound dressings and drug delivery devices require a material that can withstand substantial mechanical loads and deformations [170]. Therefore, much research is focusing on improving the mechanical properties, especially the modulus and toughness, of hydrogels [170-185]. For example brittle and ductile networks have been combined in a double network design to achieve improved fracture properties [181]. Also, microgels have been incorporated into bulk hydrogels to improve the fracture properties by serving as sacrificial bonds [186]. The examples illustrate the need for combining mechanisms to dissipate mechanical energy with mechanisms to maintain elasticity to achieve high performance hydrogels. The combination of these mechanisms can also be incorporated at multiple length scales, as hierarchical biological materials often do, to improve the properties further [170].

2.5 Conclusions

Natural materials offer a rich source of inspiration for the design of high performance biomaterials. Many features of biological materials have been used to improve the properties of biomedical materials including a hierarchical design and precisely controlled chemical interactions that balance the need for elasticity, stiffness and strength with the need for energy dissipation, deformation and toughness. There are many design features, however, that have yet to be uncovered so it is important to use advanced, small-scale research tools and to collaborate across disciplines to probe structure-function relationships in natural materials even further. The

findings can be incorporated into the design of highly efficient and multifunctional materials such as protein, polysaccharide and catechol based materials, self-healing materials and composite materials. The possibility of improving biomaterial properties by applying the designs of nature is an exciting area of future research.

PART 2: STRUCTURE-PROPERTY RELATIONSHIPS WITHIN INTACT INSECT CUTICLE

ORIGIN OF THE WORK

The following two chapters stem from the work begun by Chris Eichler and Joseph Lomakin at KU. Chris initiated the study for his MS, developing the dynamic mechanical testing methods and analysis. Joe continued the work in his PhD, performing a detailed study of *Tribolium castaneum* and *Tenebrio molitor* in which he used dynamic mechanical analysis and RNA interference to show the importance of crosslinking rather than plasticization for the stabilization of cuticle as an insect matures. This study was submitted to *Biomacromolecules* [20], but there were a number of concerns raised by reviewers. Two of the most notable concerns were 1) the possibility that microstructural changes influence the mechanical development of the structure over time and 2) the possibility of forming non-covalent crosslinks upon dehydration. Thus, I was responsible for addressing these concerns with additional experimental work that strengthened the arguments and an in-depth response to reviewers. The preliminary work I performed was described in the discussion and supplementary information and led to a successful publication of the paper with myself as second author after Joe [20].

Thus, Chapter 3 investigated the hypothesis that microstructural changes, specifically the addition of material post-ecdysis and the non-uniform water loss, affect the changes in mechanical properties of the elytra structure as a whole. The previous work considered the elytron as a uniform material reacting over time, which still provided valuable information about the importance of crosslinking in the structure as a whole. However, a more detailed analysis of the property changes with time and how the property changes relate to microstructural changes

provided important information about the structure-property relationships that may be useful as biomaterial design criteria.

Chapter 4 addressed the reviewer comments that stressed the importance of distinguishing between covalent bonds and hydrogen bonds, which may also play an important role in cuticle as dehydration can induce the formation of strong, cooperative structures such as β-sheets with a high degree of hydrogen bonding. Thus, Chapter 4 examined the hypothesis that non-covalent crosslinks could have a significant contribution to mechanical properties, even if covalent crosslinks dominate. Non-covalent interactions have been shown to have a role in toughening materials [12, 73, 74, 175], so the idea was worth exploring in cuticle. The goal was to more clearly address the role of covalent interactions and non-covalent interactions within insect cuticle. Additionally, the experiments aimed to strengthen the arguments of the previous study, which were not fully accepted by reviewers.

Review of Insect Cuticle Literature

Insect cuticle, one of the most widespread biological materials, can have stiffness values that span 8 orders of magnitude even though it is generally made of chitin, proteins, catechols and some enzymes and lipids [34]. The hierarchical structure of insect cuticle was described in Chapter 2. The processes thought to control the mechanical properties of cuticle, namely tanning (sclerotization and pigmentation) and dehydration, were also introduced but are reviewed in more detail here since they are key to interpreting the results of this thesis.

As an adult insect matures, it may undergo tanning. Tanning refers to both the sclerotization and pigmentation of the cuticle. Sclerotization is the process in which phenolic compounds are incorporated into the cuticle and has been reviewed several times [16, 187-190]. The extent of sclerotization is thought to, in part, explain the diversity of cuticle properties. The

process begins with the secretion of catechols, such as N-acetyldopamine (NADA) and N-β-alanyldopamine (NBAD), from the epidermal cells [16, 191, 192]. The structure of NADA and NBAD are shown in Figure 2-1. The secretion of catechols into the cuticle matrix after ecdysis appears to be regulated by the hormone bursicon [193, 194]. The catechols can be oxidized by enzymes to form *ortho*-quinones or *para*-quinone methides [187]. Laccase is most likely the enzyme responsible involved in sclerotization, but the role of other enzymes such as peroxidases cannot be ruled out [187, 195-198]. The quinones can then be polymerized into pigment molecules to give coloration to the cuticle [187]. Insect cuticles have a variety of colors, from nearly colorless to brownish to completely black, depending on the type of pigment molecules formed [187]. Black cuticles, for example, contain melanin which is polymerized dopamine [199]. The melanin can be in the form of granules or distributed throughout the cuticle [200-202]. The quinones are also reactive toward nucleophilic groups on proteins [187] and histidine and lysine-containing adducts have been shown *in vitro* [203-205]. Additionally, proteins with covalently bound catecholamines were identified *in vivo* [206-212].

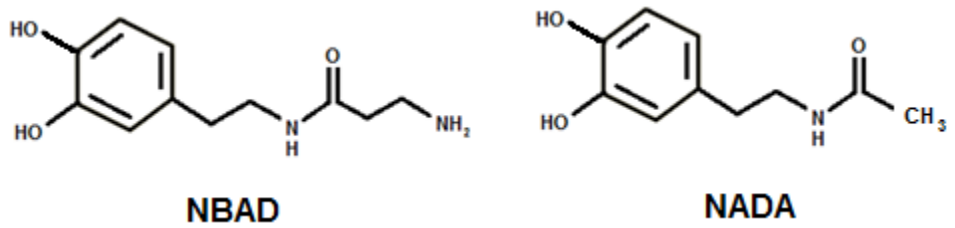

Figure 2-1. Chemical structures of the catechols, N-β-alanyldopamine (NBAD) and N-acetyldopamine (NADA).

The theory of protein crosslinking in insect cuticle was first proposed by Pryor in 1940 [213]. The hypothesis is that a quinone reacts with two amino acids on separate proteins to form a crosslink. The reaction mechanism for quinone crosslinking of proteins is illustrated in Figure 6.1. The crosslinking has been suggested as the major factor leading to the changes in

mechanical properties that occur over time [187, 190]. However, while the reactions are theoretically possible, the existence of quinone crosslinks has not been explicitly proven by chemical analysis due to the intractable nature of the mature cuticle [17, 27, 214].

Some researchers argue that dehydration, not crosslinking, is responsible for the mechanical changes during cuticle development [188, 215]. Controlled dehydration may occur when quinone molecules react with just one protein which increases the hydrophobicity of the matrix without forming a crosslink, when water is displaced by pigment molecules, or when water is actively resorbed through the epidermal cells [16]. The reduced plasticization and increased physical interactions due to water loss undoubtedly affect the mechanical properties of cuticle. For example, *Rhodnius prolixus*, whose nervous system can signal mechanisms to reversibly alter the pH of the abdominal cuticle to increase or decrease the water content, alters the properties to allow significant expansion and contraction while feeding on large volumes of blood [1]. In general, though, dehydration and sclerotization occur simultaneously, so it has been difficult to determine the relative importance of each for the mechanical stability of mature cuticular structures.

Our group has used mechanical analysis to show that the elastic modulus of beetle elytral cuticle becomes less frequency dependent as the insect matures, and dehydration alone does not account for this change [216]. Since a lower frequency dependence corresponds to a higher degree of crosslinking in polymer systems, the result is consistent with the theory of quinone crosslinking. Additionally, when the metabolic pathways thought to be responsible for covalent crosslinking were knocked down by RNA interference, the frequency dependence of elytra increased relative to native cuticle [216]. Thus, crosslinking reactions are important for the

mechanical stabilization of elytral cuticle. Chapters 3 and 4 of this thesis follow up on these studies to further clarify the roles of covalent and non-covalent crosslinking.

CHAPTER 3: TEMPORAL CHANGES IN THE PHYSICAL AND MECHANICAL PROPERTIES OF THE *TENEBRIO MOLITOR* ELYTRON UNDERGOING MATURATION

3.1 ABSTRACT

The changes in physical properties of the *Tenebrio molitor* elytron (modified forewing) were studied to understand how the development of microstructure and chemical interactions are important to biomaterial design. Analysis of the physical and mechanical properties supports a model of elytron maturation in which cuticular material is continuously secreted from epidermal cells to produce an extracellular matrix in which the uppermost layers mature before those underneath. It was hypothesized that enzymatic cross-linking and pigmentation reactions help to stabilize the protein-chitin network within the initial layers of cuticle shortly after eclosion, and that these mature layers bear the bulk of the mechanical loads as subsequent layers are deposited and tanned. Results showed that the frequency dependence of the storage modulus and the tan δ values decreased rapidly during the beginning of maturation, reaching constant values after only 48 hours post-eclosion. The tan δ decreased over 2 times, indicating the importance of cross-linking. Furthermore, the elytron also reached its mature color within the first few days after eclosion. The water content declined from 75% to 31%, with a large part of water lost from within the spaces between cuticular laminations rather than the solid cuticular material itself. Dehydration, therefore, had a less significant influence on the mechanical properties of the elytron during maturation than protein cross-linking, which stabilizes the structure early in the maturation process. The work highlights the importance of microstructure together with covalent and non-covalent interactions for the design of tough biomaterials.

3.2 INTRODUCTION

The hierarchical nature of some biological materials confers remarkable toughness and strength, but the ability to imitate nature's designs is not yet possible [127]. Further understanding of the biofabrication process is needed to suggest techniques for producing equally sophisticated biopolymer composites for technological or medical purposes [127]. Recent studies on insect cuticle suggest that it may be an excellent model for developing biomaterials [20, 78, 217-219]. The structure of beetle wings and wing covers (elytra), in particular, could inspire the design of strong yet lightweight composite materials [219, 220]. Mature elytral cuticle has an ultimate stress of 29 MPa and ultimate strain of 3% [20], approaching the mechanical properties of bone, which has a fracture stress of 120 MPa and fracture strain of 2% when loaded in the longitudinal direction [221]. Dirks and Taylor found that the work of fracture for a fresh locust tibia was 5.56 kJ m^{-2} [218], which makes the tibia even tougher than bone. It is noteworthy that insect cuticle possesses such properties even though it is a purely organic composite material without the reinforcement of a mineral phase. Insect cuticle has recently inspired the development of a chitosan-fibroin laminate in which the interaction between protein and polysaccharide phases accounts for unexpected increases in strength and toughness [222]. The modulus and fracture properties of these laminates are surprisingly comparable to beetle elytral cuticle [20, 222]. A better understanding of the structure-function relationships in cuticle and other natural biomaterials, which often have properties superior to synthetic analogs, is widely recognized to provide new concepts and strategies for the design of new materials for biomedical and other applications [218, 223-225].

The insect cuticle or exoskeleton is a mechanically efficient biocomposite material; it is lightweight, allowing for insect flight, yet it is strong and tough, protecting the insect from injury. Cuticle is primarily made of proteins, chitin, catechols and water, but the molecular

interactions among these components are not well understood. *In vivo*, the temporal development of cuticle is highly regulated and coordinated by complex biosynthetic pathways. The physical properties of cuticle are quite diverse despite being made of a limited set of organic compounds. The stiffness can actually span several orders of magnitude depending on the location or maturity of the cuticle [8, 34]. For example, the beetle elytron or modified forewing transforms from a soft and flexible tissue to a hard and rigid appendage as the adult insect matures [20]. Uncovering structure-function relationships that account for such diverse properties in biomaterials such as the elytron is an important goal in experimental biology [226].

The current understanding of insect elytral cuticle development is that the elytra are not compositionally uniform materials that simply mature over the course of a few days. Rather, the epidermal cells secrete layers of new material according to circadian rhythms into the cuticle structures for several days after eclosion, development regulated by wing selector genes such as *vestigial* [227-229]. Thus, the cuticle is a multi-layered material built up from the cells below [230, 231]. In fact, the epidermal cells closely control the temporal, spatial and quantitative coordination of events needed to synthesize and traffic the organic molecules into the cuticle [232]. The undulations on the apical plasma membrane help to control the architecture of cuticle as material is released. Chitin fibers are secreted from the crests of the plasma membrane, while protein and other molecules are secreted from vesicles that fuse with the grooves between each crest [232]. The coordinated secretion results in layers of cuticle with chitin microfibrils embedded in a protein-rich matrix, possibly arranged in an organized fashion with specific chitin-protein interactions. Each additional layer is secreted with a rotation with respect to the above layer, resulting in a twisted plywood-like architecture.

On another hierarchical level, insect cuticle consists of three groups of layers: an inner, pliant endocuticle, a stiff exocuticle, and an outer, waxy epicuticle [15]. Some types of cuticle have unusual layering involving additional mesocuticle layers with mechanical properties that confer specialized functions [233]. Previous studies have examined the architecture of cuticle from the yellow mealworm beetle, *Tenebrio molitor* Linnaeus (COLEOPTERA: TENEBRIONIDAE), using microscopic and histological methods [234-236]. The exocuticle has very small angles of rotation between each layer, resulting in a helicoidal structure, whereas the endocuticle has only a thin helicoidal region between orthogonal layers [237]. The mechanism of the rotations is unknown, though it is assumed to be self-organizing [232]. On yet another hierarchical level, elytra are composed of two layers of epidermal cells that secrete an upper and lower cuticular lamination. Between the two laminations, there is hemolymph that initially facilitates elytron expansion and also provides nutrients to the cells. By full maturity, the hemolymph has been resorbed and the upper and lower laminations have fused together along lines running parallel to the anterior-posterior axis of the insect, leaving air filled cavities between.

There are two major types of insect cuticle: soft cuticle typically found in the body wall of larval stages of many insects and in joints, which allows for flexibility and locomotion, and hard cuticle which provides structure and protection [17]. Some types of soft cuticle, such as the buckling region of locust hindlegs, are able to stretch and absorb energy because they are made of flexible proteins known as resilin [18]. Hard cuticle, such as the cuticle in the beetle elytron or gula is hard and stiff because it is highly tanned [19, 20]. Tanning (sclerotization and pigmentation) is a process that occurs with maturation, in which the structure becomes stiffer, harder, pigmented, and intractable to extraction and enzymatic degradation [238]. Both sclerotization and pigmentation begin with the secretion of catechols from the epidermal cells.

Enzymatic oxidation of catechols by laccase can form quinones and quinone methides that can either form pigments or react with the nucleophilic groups on cuticular proteins and possibly with the hydroxyl and amino groups of chitin or chitosan [62, 195, 239]. Theoretically, the reactions of catechols with proteins or chitin could form covalent cross-links, thereby modifying the mechanical properties as the cuticle matures. However, the existence of covalent cross-links has not been explicitly proven by chemical analysis due to the intractable nature of the mature cuticle.

In our recent studies using dynamic mechanical analysis and RNA interference, we found evidence supporting the quinone cross-linking theory [20]. While some may argue that dehydration is responsible for mechanical changes during cuticle development due to loss of plasticization and possible physical associations [188, 215], our work indicated that both dehydration and covalent cross-links contribute to the stabilization of cuticle as an insect matures. Our prior work and other prior studies on mechanical properties of cuticle, however, considered the structures as uniform materials without considering how microstructural features influence the final properties [20, 218]. Also, while we established the importance of cross-linking and dehydration by comparing between fresh and dry elytra at the beginning and end of maturation, we did not attempt to understand the kinetics of these processes or the relationship to the microstructural changes as we do in this study.

In addition to sclerotization, pigmentation develops when multiple quinones react to form high molecular weight molecules such as melanin. These large pigment molecules can be expected to increase the stiffness via chain entanglements, but also to increase the viscous damping if they are not covalently bound to the surrounding cuticle network. Distinguishing between the effects of pigmentation, physical and covalent cross-linking as well as dehydration

on the development of cuticle properties is difficult, because most, if not all, of the complex processes occur over the same time frame. Both the degree to which each process occurs, as well as its timing within maturation, are expected to influence the final properties of the cuticle.

Little information is currently available about the temporal changes in the physical and mechanical properties during cuticle formation. In this study, it was hypothesized that both microstructural and molecular interactions influence the changes in cuticle properties during maturation. The material cannot be viewed as simply a uniform material; instead a more refined model that considers the layered microstructure must be considered. To provide a more detailed view of its microstructural development, micro-computed X-ray tomography (microXCT) was used to investigate the elytron of *T. molitor*. Additionally, the temporal changes in mass, water content, pigmentation and dynamic mechanical properties of the elytron as the adult matures were measured. The results are interpreted in light of the hypothesized model of cuticle development, illustrated in Schematic 3.1, in which material is continuously secreted layer-by-layer from the epidermal cells, with initially secreted material maturing first followed by the subsequently deposited material. The importance of microstructure and cross-linking interactions within this hierarchical material are discussed, which may help in the design of advanced composite materials.

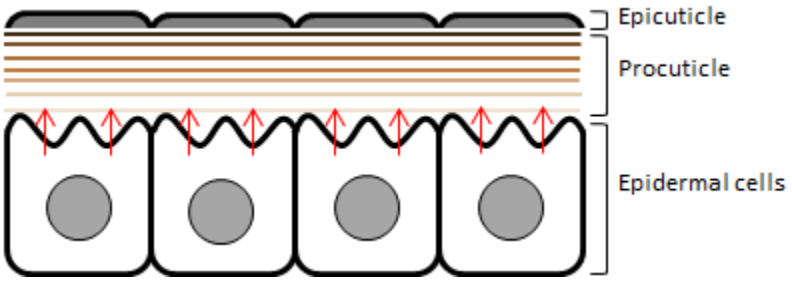

Schematic 3.1. Hypothesized model of cuticle development. The epidermal cells secrete layers of material into the procuticle, which may be further subdivided into a more sclerotized exocuticle and less sclerotized endocuticle. Here, the shading indicates that the layers undergo pigmentation and sclerotization in the order in which they are secreted from the underlying epidermal cells. The model is based on Moussian (2010).

3.3 Materials and Methods

3.3.1 Materials

Tenebrio molitor were reared at the Agricultural Research Service's Center for Grain and Animal Health Research, a part of the U.S. Department of Agriculture in Manhattan, KS. *Tenebrio* is closely related to the red flour beetle, *Tribolium castaneum*, a species that we also have utilized previously (Lomakin et al., 2011). The larger size of *Tenebrio*, however, makes it more suitable for a study involving mechanical measurements. Pupae were transferred to the University of Kansas where they were kept at room temperature on a diet of wheat flour, rolled oats and 5% brewers' yeast. Insects were carefully monitored to note the time of eclosion. At specific time points post-eclosion, the abdomen was separated from the thorax with tweezers, after which the elytra were removed and tested.

3.3.2 Methods

Imaging of microstructure

A MicroXCT tomographic X-Ray microscope from Xradia (Pleasanton, CA, USA) was used to obtain images of dried elytra at two time points, 12 h and 7 d post-eclosion. The 12 h elytra have high water contents, so they were dried using a Tousimus automated critical point dryer to ensure that the structures did not collapse upon drying. The MicroXCT microscope uses phase contrast instead of absorption contrast and offers substantially improved image contrast for soft biological tissues to allow their visualization. A 20x magnification was used, resulting in a pixel size of 0.9 μm.

SOLIDS DEPOSITION AND DEHYDRATION

Elytra were removed from live insects at precise time points post-eclosion and tested quickly to prevent water loss to the atmosphere. Fresh masses were determined on an analytical balance (±0.01 mg) within 1 minute and mechanical tests were performed within 12 minutes. Even for the fully untanned (0 h) elytra, which are approximately 75% water, the water content only decreases by about 1.4% during the first 15 minutes. To test dry samples, elytra were dried over calcium sulfate in a desiccator for at least 24 h, by which time a constant mass was attained.

PIGMENTATION DEVELOPMENT

The time course of the color change was quantified by measuring the mean brightness of dried elytra at different stages of maturity. The elytra were lined up on white paper and photographed from above. The images were converted to grayscale and the brightness value of a rectangular section from the center of each elytron was measured using ImageJ software.

MECHANICAL ANALYSIS

Dynamic mechanical tests were performed on an RSAIII dynamic mechanical analyzer (TA Instruments, New Castle, DE, USA). Samples were mounted lengthwise between tensile grips and dynamic tests were run by procedures established in our previous work [20]. Briefly, frequency sweeps were run from 0.1-100 rad/s at a strain of 0.1%, which was confirmed to be within the linear viscoelastic region by strain sweep measurements. At such small strains, the oscillatory tests can probe the structure and dynamics of the material without causing any nonlinear effects such as strain hardening or irreversible structure changes. The elastic (storage) modulus, E', the viscous (loss) modulus, E", and their ratio (E''/E'), tan δ, were measured over this range of frequencies. The frequency dependence of the storage modulus was fit to a power law model ($r^2>0.95$) between 1 and 100 rad/s, where E' is proportional to ω^n. The thickness

values used to calculate the mechanical properties were determined by interpolating values from the average center-line thicknesses of the dorsal lamination of elytra at 0 h, 24 h, and 7 d maturity determined by scanning electron microscopy (Lomakin et al., 2011).

3.4 RESULTS

To study the temporal development of the cuticle, several different properties of the *Tenebrio* elytron were quantified as a function of the maturation time, from immediately after eclosion until the fully mature state. The goal was to compare the time scales of development of cuticle properties and relate them to the overall material interactions among cuticle components. The structural development was visualized by capturing microXCT images of the elytron at 12 h post-eclosion and full maturity. The microstructural development helped to inform the analysis of the temporal development of several additional properties. The temporal change in color was quantified as a measure of pigmentation, the changes in fresh and dry masses were taken as a measure of solids deposition and dehydration rate, and the changes in dynamic mechanical properties were measured to distinguish among material relationships.

3.4.1 IMAGING OF MICROSTRUCTURE

Arthropod cuticle is a hierarchical structure and it is therefore important to consider cuticular structures at multiple length scales. On the microscale, the elytron is made of two cuticular laminations forming a corrugated shape with cavities that run longitudinally down the structure. The detailed internal structures can be observed in microXCT images. As depicted in Fig. 3.1, the field of view is only a small section (~0.7 mm wide x 0.7 mm long) from the center of the whole elytron (3 mm wide x 11 mm long). The microXCT images are shown in Figs. 3.2-3.4. Movie files of the rotated three-dimensional image can also be viewed in color in the

supplementary information. Figures 3.2 and 3.3 show three-dimensional views of an elytron at 12 h and at 7 days of maturity, respectively. Slices from the cross-section are shown in two-dimensions with scale bars in Fig. 3.4.

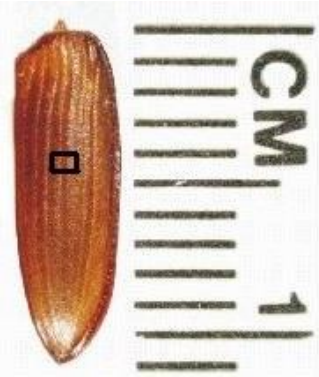

Figure 3.1. The whole elytron, with the field of view for MicroXCT imaging shown within the black square.

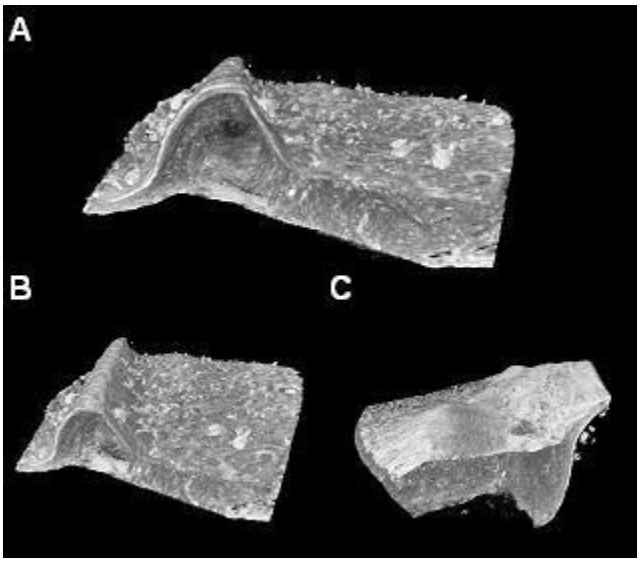

Figure 3.2. 3D MicroXCT images showing the (A) cross-section, (B) dorsal surface and (C) ventral surface of a dry *Tenebrio* elytron at a maturation time of 12 h. See Fig. 3.4 for the scale.

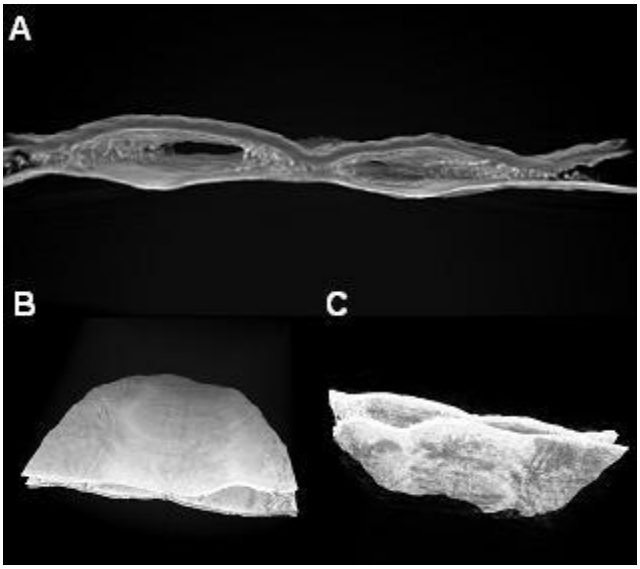

Figure 3.3. 3D MicroXCT images showing the (A) cross-section, (B) dorsal surface and (C) ventral surface of a dry *Tenebrio* elytron at a maturation time of 7 d. See Fig. 3.4 for the scale.

The two-dimensional slices of the cross-sectional views reveal several differences between the 12 h elytron and fully tanned elytron. Most notably, the corrugated shape clearly becomes more defined as the insect matures. In the immature elytron shown in Fig. 3.4A, the two cuticular laminations are separated by a space containing hemolymph. In the fully mature elytron in Fig. 3.4B, the two cuticular laminations have become partially fused together to form a corrugated structure with cavities filled with air because the hemolymph has been resorbed. The points of fusion between the two laminations form parallel rib-like structures (striae) running lengthwise along the elytron. Only the dorsal cuticular lamination undergoes extensive tanning. It is also significant that the dorsal lamination becomes thicker over time, increasing from about 10 μm to 20 μm, while the ventral lamination maintains a nearly constant thickness.

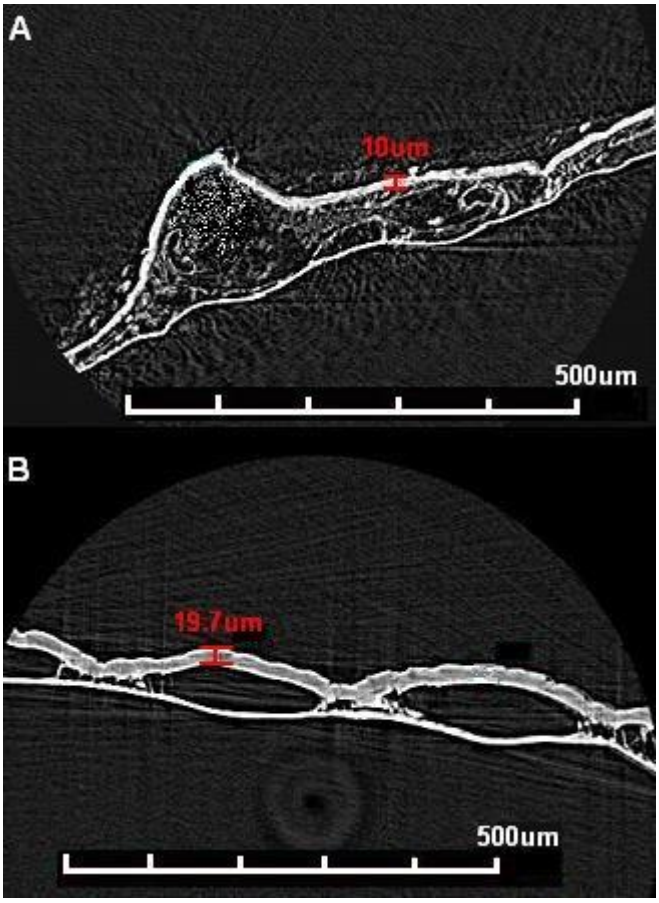

Figure 3.4. 2D Cross-sectional MicroXCT images of an elytron from *Tenebrio* at (A) 12 h maturity and (B) 7 d maturity (Scale bars = 500 μm).

3.4.2 AVERAGE SOLIDS DEPOSITION AND DEHYDRATION

The water contents of *Tenebrio* elytra as a function of time were calculated from the fresh and dry masses. The fresh and dry masses are plotted as a function of maturation time in Fig. 3.5. With the exception of the 0 h time point, the fresh mass increases slightly with maturation, at a rate of 4.7 ± 1.3 μg/h. The 0 h fresh mass is most likely high because of the presence of residual molting fluid and hemolymph associated with the elytron, both of which are being resorbed just prior to and soon after adult eclosion. The dry mass, on the other hand, changes more significantly, increasing more than two-fold at a rate of 7.7 ± 0.6 μg/h. The constant increase in dry mass shows that new material is being secreted continuously from the underlying

epidermal cells. Fig. 3.6 shows that the water content of an elytron declines linearly over time, decreasing from 75% water immediately after adult eclosion to 31% water at full maturity. Beyond 7 days, the water content remains relatively constant (at 16 days, the water content is 28 ± 3%).

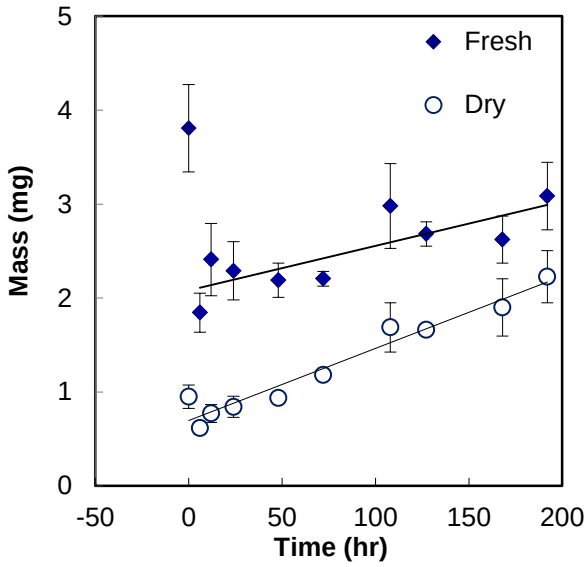

Figure 3.5. Fresh and dry masses of *Tenebrio* elytra as a function of maturation time. The dry mass increases at a rate greater than that of the fresh mass. Error bars are standard deviations with sample size ≥ 4.

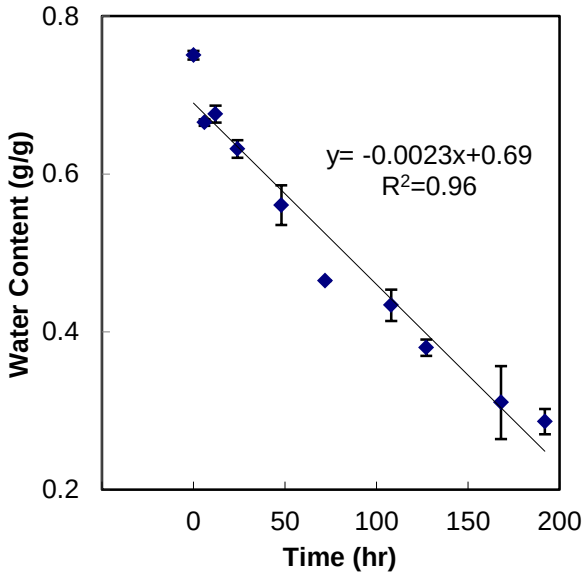

Figure 3.6. Elytral water content declines linearly as the insects develop to full maturity. Beyond 200 hrs, no change is seen. Error bars are standard deviations with sample size ≥ 4.

3.4.3 PIGMENTATION DEVELOPMENT

The color of the *Tenebrio* elytron changes from off-white to dark blackish brown as the insect matures and pigmentation develops, as shown in the inset of Fig. 3.7. The change in color was quantified in terms of brightness, which is plotted in Fig. 3.7. The brightness decreases to about 20% of the original brightness after maturation is complete. After about 24 hours, the brightness has decreased by about half, but the color change is almost complete after only two to three days of development. It is important to note that, since only the uppermost surface is observed, this measurement reflects changes in the initially secreted dorsal cuticular layer.

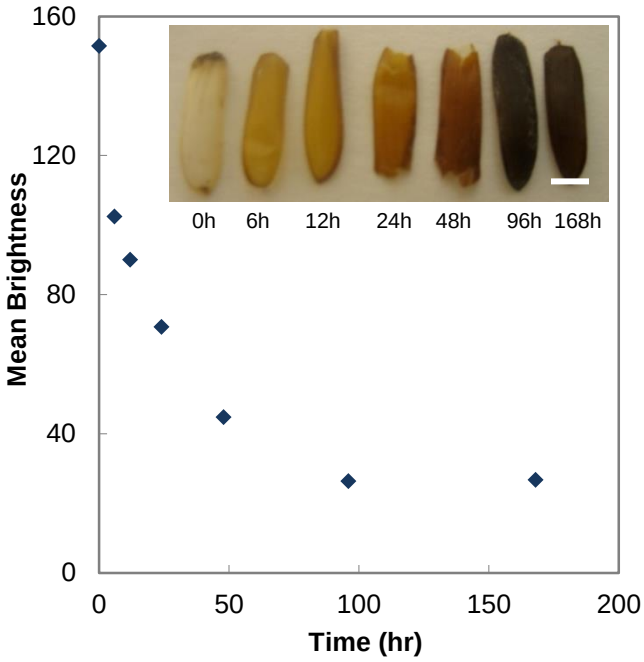

Figure 3.7. Color (scale bar = 3 mm) and brightness changes of *Tenebrio* elytra as the adult matures and tanning takes place.

3.4.4 MECHANICAL PROPERTIES

Dynamic mechanical analysis is a technique used commonly for investigating the structure of polymer networks [240]. It measures the viscoelastic properties of a sample by

applying an oscillatory stress or strain and measuring the material response. The measured stress in a viscoelastic material falls between that of an ideal elastic material, in which stress is perfectly in phase with strain, and an ideal viscous material, in which stress is perfectly out of phase with strain. The property obtained from these experiments is the complex modulus, E*, which is a measure of the material stiffness. E* can be separated into two components: the storage (or elastic) modulus, E', which corresponds to the recoverable energy, and the loss (or viscous) modulus, E'', which corresponds to the energy dissipated as heat. The ratio E''/E' is equal to tan δ, where δ is the phase lag between the stress and strain waves. The value of tan δ can range between 0 (perfectly elastic material) and +∞ (perfectly viscous material). A useful test mode for dynamic mechanical analysis is referred to as frequency sweeps, which measure E', E'' and tan δ as a function of the frequency of the applied strain.

Additionally, the frequency exponent is obtained by fitting the storage modulus to a power law model over the range of 1-100 rad/s. Thus, a lower value of n corresponds to a lower frequency dependence of the storage modulus due to molecular immobility within that frequency range. The frequency exponent and tan δ are measures of the same phenomenon; that is, the relative contribution of the viscous and elastic response of a material to dynamic strain. However, n is extracted from two decades of frequency data, whereas tan δ must be selected at an arbitrary representative frequency to make a direct comparison. Both values will decrease with the formation of interactions that are permanent within the time-scale of the experiment. Examining tan δ and n of dried elytra helps separate the effects of dehydration and cross-linking by eliminating the influence of water. Also, the influence of pigmentation and water loss can be assessed by comparing their rates of change with rate of change in mechanical properties.

Fig. 3.8 shows the average frequency sweep data for a sample set of elytra at 0 h, 24 h and 7d post-eclosion in the fresh and dry states. These data demonstrate the reproducibility of such tests, as they match previously reported data within experimental error [20]. The trends were consistent with the effects expected from the formation of covalent cross-links due to quinone tanning reactions. Briefly, a lower frequency dependence of the storage modulus and a lower tan δ suggested that crosslinks were formed as maturation proceeded.

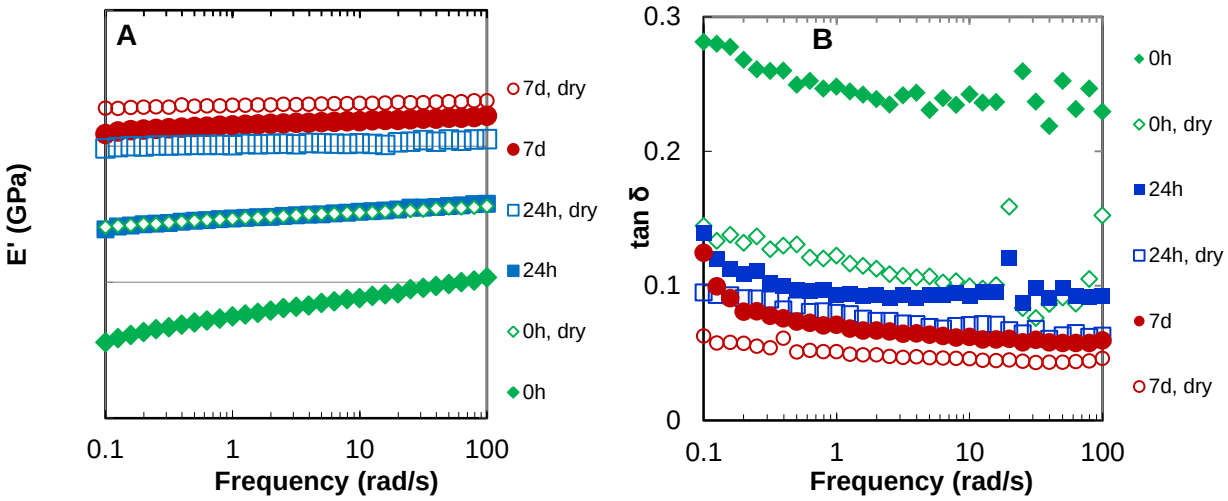

Figure 3.8. A) The storage modulus, E', increases and the frequency dependence decreases with maturation time and dehydration of *Tenebrio* elytra. B) Tan δ (=E''/E') decreases upon maturation and dehydration of the elytra.

Frequency sweeps were performed on elytra at 7 different stages of maturity in order to more closely examine the kinetics of mechanical changes. From the frequency sweep data, the magnitude of E' at 1 rad/s is extracted and plotted as a function of maturation time in Fig. 3.9. For dry elytra, there was a rapid increase in E' initially but not a statistically significant change after 48 hours. For fresh elytra, E' increased linearly until 48 hours and plateaued after 100 hours.

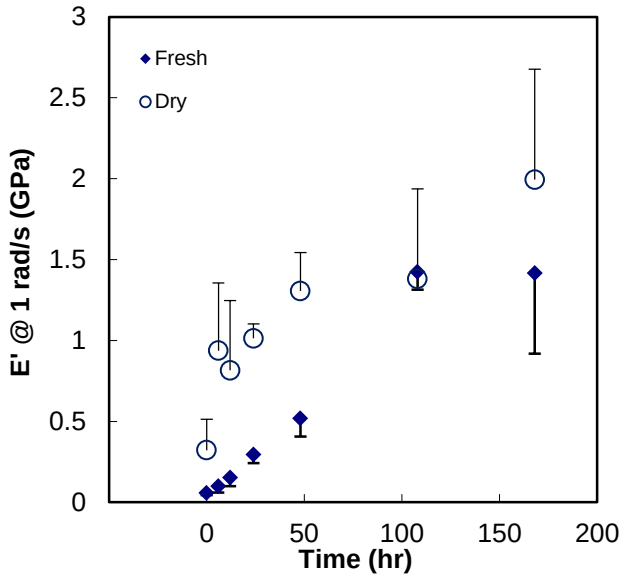

Figure 3.9. Storage modulus, E' measured at 1 rad/s, as a function of maturation time for fresh and dry elytra of *Tenebrio*. The magnitude increases gradually for the fresh elytra and more rapidly for the dry elytra. Error bars are standard deviations with sample size ≥ 3 (shown in one direction only for clarity).

The tan δ and frequency exponent for 7 time-points post-eclosion are summarized in Fig. 3.10. The value of tan δ at 1 rad/s is reported in Fig 3.10A. Most of the change in tan δ happened within the first 48 h of maturation. For fresh elytra, tan δ declined by half within the first 12 h, falling from 0.24 ± 0.07 at eclosion to 0.12 ± 0.02 at 12 h maturity. As the insect reached maturity, tan δ plateaued to 0.07 ± 0.01. In the dry state, the decline in tan δ also happened within the first 48 h of maturity.

The frequency exponents of elytra (shown in Fig. 3.10B) dropped rapidly until reaching a plateau around 48 h. For fresh elytra, the frequency exponent reduced almost by half after just 12 h, falling from 0.119 ± 0.034 to 0.073 ± 0.016. It then plateaued to 0.034 ± 0.005 at full maturity. When the elytra were dried, their frequency exponent still declined over the course of maturation, dropping from 0.042 ± 0.008 to 0.016 ± 0.002. This decline was initially rapid, reaching a constant value after 48 h. Figs. 3.10A and 3.10B are both compared to previous data

[20], which demonstrates the reproducibility of these measurements, since the values match within the experimental error.

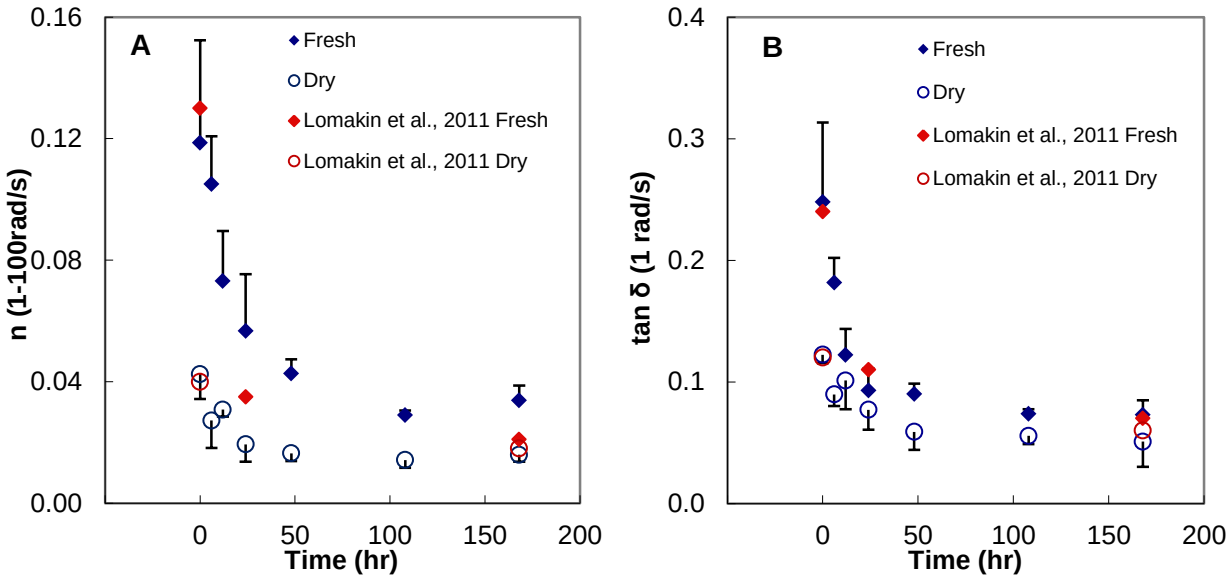

Figure 3.10. The tan δ (A) and frequency exponent, n, (B) decrease rapidly within the first 48 h of maturation time for both fresh and dried elytra of *Tenebrio*. Error bars are standard deviations with sample size ≥ 3 (shown in one direction only for clarity).

3.5 Discussion

The elytron functions as an armor that protects the beetle from damage due to external loads, while being light enough to allow for flight and mobility. A better understanding of the compositional and structural features that enable elytral cuticle to have these functions is important for both understanding the biological development of the elytron as well as capturing the important features to replicate in synthetic biomimetic materials. The aim of this study was to understand the relative importance of microstructure and material composition for cuticle properties. Elytral properties were examined as a function of maturation time in order to provide insight into the overall picture of cuticle development. The results, specifically the linear increase in solid mass, linear decrease in water content, and the rapid changes in color and dynamic mechanical properties (n and tan δ), combine to support a model of cuticle development

as one in which the epidermal cells gradually secrete cuticle components over time, but with each layer maturing within about 48 h.

Microstructure Development

When analysing elytral cuticle, it is important to consider the microstructural features that may influence the properties. Our previous work considered the elytron as a monolithic slab of homogeneous material [20], but clearly there are structural features that play a role in the development of mechanical properties. In particular, there are two cuticular laminations; the microXCT images in Fig. 3.4 showed how the cross-section of the elytron changes from 12 h to 7 days. Only the dorsal lamination underwent significant pigmentation, sclerotization and thickening with development, so it was expected to carry most of the load during the longitudinal tensile tests performed in this study. The cavities between the two cuticular laminations were initially filled with hemolymph. By maturation, however, the hemolymph was resorbed, leaving the cavities filled with air. The liquid or gas components within the cavities were assumed to provide only minor contributions to the mechanical response. The fact that dehydration of the elytron does not occur uniformly throughout the structure is important. A significant amount of water is lost from the cavities between the cuticular laminations rather than from within the lamination materials that support the load; thus the water content measured by the water loss upon drying from the elytron as a whole is an overestimate of the water content within immature cuticle material itself. Additionally, the corrugated shape became more defined as maturation proceeded. The two laminations fused along the striae running lengthwise down the elytron. Although this was not measured in this study, the final shape likely provides resistance to bending forces as corrugated sandwich structures as used in cardboard, for example, are known

to provide resistance to bending in the direction transverse to the corrugation, and such structures have been studied for use in aircraft wings [241]. The striae have been observed to suppress crack propagation during tensile tests to failure [20]. These observations about the microstructural development will be considered later when discussing the change in the material properties measured in this study.

The change in fresh and dry masses over time, shown in Fig. 3.5, demonstrated that the elytron is not a closed system. The dry mass increased linearly with maturation time, nearly doubling by maturation. This is consistent with the model of development in which the epidermal cells continue to secrete precursors to solid material (chitin, pigments and proteins) into the cuticle throughout development. The fresh mass also increased, but at a slower rate than the dry mass, reflecting a gain of material that formed the new cuticle but also some loss of water as hemolymph was gradually resorbed. Fig. 3.6 shows that the total water content declined linearly as the elytron matured, dropping from 75% to 31% of the total mass. Water loss is generally expected to affect the mechanical stability of the elytron [20, 215]. As water is lost from the cuticle, plasticization is reduced and physical interactions such as hydrogen bonding may form, thus stiffening the cuticle. It is important to note, however, that much of the water is lost from within the cavities (Figures 3.2 – 3.4) as hemolymph is resorbed, rather than from within the stress-supporting cuticular material. This contrasts with previous work which has assumed that the change in water content of the elytron with time has been from the cuticle material itself.

DEVELOPMENT OF MOLECULAR INTERACTIONS

Further insight into cuticle development was gained by examining the kinetics of property changes with maturation. The rate of change in the magnitude of the storage modulus

supports the view of a layer-by-layer secretion of cuticle, in which the layers mature within the first two days after secretion of the precursor materials. It should be noted that it was not feasible to measure the exact thickness of every sample. Scanning electron microscopy was used to determine average center-line thicknesses of the dorsal lamination for populations of elytra at 0 h, 24 h, and 7 d maturity [20]. Other thickness values were interpolated. However, there is considerable variation in the biological specimens, so some of the variability in modulus data may have reflected less accurate thickness values used to calculate the stress. Nevertheless, trends were clear. Fig. 3.9 shows that the magnitude of the storage modulus of dried elytra increased and plateaued within the first 48 h. The storage modulus of fresh elytra also increased within the first 48 h, and then increased more before plateauing at 100 h. However, the modulus of the early structures was likely an underestimate of the cuticle modulus because the entire structure was not bearing the load. Only a thin, mature layer was supporting the load, but the thickness value used to calculate the modulus included immature layers of cuticle not supporting the load. Therefore, since the cross-sectional area was overestimated, the stress (which is the force per unit cross-sectional area) was underestimated. In the more mature elytra (beyond 48 h), more of the structure was load bearing and thus the E' was closer to the inherent value of the cuticular material. Therefore, E' for fresh elytra also seemed to plateau within 48 h, indicating that the cuticle materials mature within 48 h of being secreted from the epidermal cells.

Pigmentation of the elytron appears to occur over a similar time-scale (Figs. 3.7). The color change seen in Fig. 3.7 was measured by photographing the elytra from above, so only the color of the top layer of cuticle was reflected in these measurements. Since it darkened almost completely within 48 h, this was direct evidence that each cuticle layer matures within that time

frame. The frequency exponent and tan δ had similar trends. As seen in Fig. 3.10, most of the change happened within 48 h. The similarity may be explained by the fact that the pigmentation and cross-linking reactions are dependent on some of the same precursor molecules [192, 242-244]. In fact, there is a correlation between color intensity and levels of N-β-alanyldopamine (NBAD), a catechol involved in tanning reactions [17, 245]. Schachter *et al.* studied the activity of NBAD synthase in *Tenebrio* and observed narrow spikes in activity levels during the transitions from larva to pupa and pupa to adult [246]. Thus, the rapid changes seen after adult emergence are likely influenced by the availability of NBAD and dopamine leading to cross-linking and pigmentation.

The main finding from the rate of change of the frequency exponent and tan δ was that cross-linking reactions most likely occur over a shorter time frame than the 7 days that it takes for a beetle to fully mature. Based on the dynamic mechanical data in Fig. 3.10, each layer of chitin-protein matrix might mature in about 48 hours, after which the new, immature layers are added as endocuticle but do not significantly contribute to the mechanical stability of the overall structure compared to the previous, fully mature layers that make up the exocuticle. The additional layers increase the thickness, but since n and tan δ are independent of cross-sectional area, they continue to reflect only the properties of the most fully developed, i.e. cross-linked, layers.

Looking at the data for fresh elytra in Fig. 3.10B, the rapid decrease in tan δ (tan δ = E’’/E’) means that the level of elastic components of the cuticle increase more than that of the viscous components. This phenomenon is commonly observed as the cross-link density of a polymeric network increases. In cuticle, covalent cross-links are formed by quinone-tanning reactions. Additionally, non-covalent bonds formed due to dehydration contribute at least on the

time scale of those bonds. This is clear when comparing the data for fresh and dry elytra. Dry elytra had a lower tan δ at all time points. To evaluate whether covalent bonds are, in fact, significant, one can look at just the data for elytra in the dried state (open symbols in Fig. 3.10A). In the dry state, there was no swelling or plasticization to separate the material components, so the importance of dehydration-induced physical stabilization was eliminated. Since there was still a significant decrease in tan δ with maturation, the non-covalent interactions alone were not sufficient to account for the decline in tan δ. Thus, it can be concluded that covalent cross-linking does stabilize the cuticle, and this happens within the first 48 h post-eclosion.

It is clear that both non-covalent and covalent cross-links contribute to the mechanical stabilization of elytral cuticle as the insect matures. Dry elytra were stiffer and more fully elastic than fresh elytra, showing that non-covalent interactions are important. Also, dry elytra were stiffer and more fully elastic when taken from a more mature insect, showing that covalent cross-links are important. The covalent interactions formed by enzymatic cross-linking of the proteins appear to form within the first layers in about 48 h of development. Additional physical interactions due to dehydration are formed simultaneously. The simultaneous formation of the covalent and non-covalent bonds may have a synergistic effect on the final properties of an elytron. In a recent study on enzymatically cross-linked gelatin hydrogels, the simultaneous formation of covalent interactions (enzymatic cross-links) and physical interactions (triple helices) resulted in gels with a higher final modulus than gels formed by sequential chemical and physical interactions [247]. It was concluded that the simultaneous formation of each type of interaction promoted a more ideal spatial distribution of molecules such that intermolecular, elastically active bonds were favored over intramolecular, elastically inactive bonds [247]. The final material was, therefore, more efficiently cross-linked. Insect cuticle also appears to be a

material in which covalent and non-covalent interactions form simultaneously within the first 48 h of secretion from the epidermal cells. The complex, hierarchical design of cuticle provides multi-scale material properties tailored to meet very specific functional needs of the organism. For biomimetic material design, it is important to consider what features of a natural material should be replicated in a synthetic material. From this work, it appears that the chemical composition and molecular interactions influence the physical properties of elytra more than the microstructure, at least in tension. However, the corrugation and layered structure likely play a role in resisting stresses in other directions such as bending [34]. Thus, the development of covalent cross-links and pigmentation within the outer cuticle layers soon after ecdysis may protect the immature insect from injury, but additional changes to the microstructure may ensure that the mature elytron can resist multiple types of loads. Bending tests may provide additional information about the role of microstructural changes in elytral development. Additionally, the hardness of the elytron would be an important physical property to investigate. Nanoindentation could be used to measure the hardness [84] of the dorsal side of the elytron; it would be expected that the hardness would develop on time scale similar to the crosslinking interactions within the initially secreted layers of cuticle.

3.6 Conclusions

This study examined the development of microstructure, mass, water content, pigmentation, and mechanical properties of the beetle elytron as a function of maturation time in order to improve the understanding of structure-function relationships in this biological material. The results were consistent with the model of cuticle development in which material is secreted from the epidermal cells in a layer-by-layer mechanism. The elytron's dorsal cuticle lamination became thicker, drier, darker, and stiffer as the insect matured. The decrease in both tan δ and

frequency dependence of the storage modulus suggested that cross-linking stabilizes the cuticle soon after eclosion. The sclerotization and pigmentation of the first layers occurred within 48 h. Additional layers were added over 7 days, which subsequently matured, but the mechanical properties were dominated by the fully mature layers. Dehydration occurred primarily within the cavities between cuticle laminations, rather than from within the material, so dehydration is likely a less significant determinant of the physical properties of the cuticle than has been previously postulated. The extent and timing of cuticular material interactions are regulated by the epidermal cells, leading to an extracellular structure with robust mechanical properties at a relatively low density. The physical and chemical interactions in the protein and polysaccharide network of elytral cuticle as well as the layered architecture provide important design criteria for developing biomimetic materials with improved tensile properties.

CHAPTER 4: THE ROLE OF COVALENT AND NON-COVALENT CROSSLINKS IN THE STABILIZATION OF ELYTRAL CUTICLE

4.1 ABSTRACT

The relative influence of covalent and non-covalent crosslinks in stabilizing elytral cuticle as an insect matures was examined using mechanical analysis of elytra at different stages of tanning, and after soaking in non-covalent bond-breaking solvents. Results from low frequency dynamic mechanical analysis showed that the storage modulus of fully tanned and dried elytra is much less frequency dependent ($n = 0.013 \pm 0.004$) than the storage modulus of untanned and dried elytra ($n = 0.050 \pm 0.024$) even at frequencies as low as 0.01 rad/s. The more elastic response of fully tanned cuticle at very low frequencies, where polymer relaxation could lead to viscous losses in an uncrosslinked material, is consistent with the idea that covalent crosslinks are formed as an insect matures. The fully tanned elytron did moderately relax at very high temperatures near thermal degradation; from 25°C to 150°C, the storage modulus decreased ~3.5 times and the tan δ increased ~9 times. The extreme temperature required to approach this relaxation mode in fully tanned elytra suggests that crosslinking suppressed the relaxation relative to untanned elytra. Additionally, the material extractability decreased with maturation, suggesting that covalent crosslinks were formed within the network. Non-covalent interactions were also hypothesized to influence the mechanical properties of cuticle. Formic acid, which disrupts non-covalent interactions such as hydrogen bonds, was expected to change properties in a manner consistent with reduced crosslinking. Results showed that elytra soaked in formic acid were less stiff, less strong and more ductile than untreated elytra and the effects were greatest for the fully tanned elytra (formic acid caused a 5 fold decrease in Young's modulus, 2 fold decrease

in fracture stress and 3 fold increase in fracture strain). Toughness, however, was not significantly changed by formic acid. The data suggests that non-covalent interactions, most likely hydrogen bonds, provide strength and stiffness, without sacrificing toughness, most likely because of their ability to dissipate energy. Despite the significant contribution of non-covalent interactions, there was still evidence that tanned elytra were more covalently crosslinked than untanned elytra. The properties of tanned elytra were significantly more stiff, strong and frequency independent than the properties of untanned elytra, even when non-covalent interactions were broken up by formic acid. Thus, the results indicate that both non-covalent and covalent interactions are important for producing a strong and tough material such as the beetle elytron.

4.2 Introduction

The relative role of covalent and non-covalent crosslinks in stabilizing insect cuticle has been debated for many years. The quinone tanning hypothesis, put forward in 1940, asserts that the stabilization of cuticle occurs because proteins become covalently crosslinked by reacting with oxidized catechols [213]. Several studies have supported this view, but the existence of covalent crosslinks has not been explicitly proven [16, 20, 190, 191, 209, 248-250]. A contrasting view holds that the phenolic compounds, whether involved in covalent crosslinking or not, affect cuticle properties solely by contributing to dehydration of the material [188, 215, 251]. The dehydration is hypothesized to induce the formation of non-covalent interactions, such as hydrogen bonds and hydrophobic interactions, which are responsible for the change in cuticle properties as an insect matures. The goal of this study was to clarify the role of covalent and non-covalent interactions; the hypothesis was that non-covalent interactions contribute to the

stiffness of the material but that the dominant role of covalent crosslinks in cuticle stability could be shown by testing the material at low frequencies and high temperatures and by breaking up non-covalent interactions with key solvents. While the elytra are tested whole, the results are interpreted in light of the model of cuticle development discussed in Chapter 3, in which cuticle is continuously secreted throughout maturation and crosslinking appears to be established within 48 hours after ecdysis.

Dynamic mechanical analysis is a common method for evaluating the contribution of crosslinking in synthetic polymer materials [252, 253]. In general, a polymer network that has more crosslinking has an increased elastic response relative to viscous response to an applied load. The movement of polymer chains relative to one another is reduced by crosslinks, thus increasing energy storage and reducing energy dissipation. Since elasticity does not depend on strain rate, the modulus of polymer materials becomes less frequency dependent as crosslinks are introduced. While the elytron is a more complex biological system than synthetic polymers, there is value in modeling the structure in a simplified way to gain new information. Lomakin *et al.* used dynamic frequency sweeps to demonstrate that the storage modulus of fully tanned elytral cuticle was less frequency dependent than untanned elytral cuticle [20]. The decrease in frequency dependence with tanning could not be attributed to drying alone [20]. In fact, fully dried, untanned elytra had more frequency dependence than fresh (hydrated), fully tanned elytra. The results were consistent with the quinone tanning hypothesis, which proposes the development of covalent crosslinks in cuticle as the insect matures. Additionally, RNA interference experiments showed that selective knockdown of an enzyme involved in the metabolic pathway leading to quinone crosslinking (ADC) resulted in a more frequency dependent cuticle material, reinforcing the importance of covalent crosslinking [20]. The

mechanical tests used in that study, however, were only able to show that the crosslinks were permanent on the time-scale of the experiment (0.1-600 rad/s). Extending the data to lower frequencies is hypothesized to provide further evidence that the additional crosslinking interactions present in the fully tanned cuticle is, in fact, covalent in nature. Non-covalent interactions such as hydrogen bonding and hydrophobic interactions would be more likely to break and dissipate energy at very long time-scales and, therefore, would not be expected to contribute as much to the storage modulus at very low frequencies.

Covering a more broad frequency range may also uncover a peak in the tan δ indicating a polymer relaxation mode. In general, polymer systems display characteristic transitions as the frequency of applied stress or the temperature changes [254]. It will be glassy and stiff at high frequencies and low temperatures, rubbery and less stiff at lower frequencies and higher temperatures, and will become even less stiff and may flow at very low frequencies and higher temperatures. Schematic 4.1a shows how the storage modulus (E'), loss modulus (E'') and the ratio E''/E' (tan δ) generally behave with temperature or frequency. E' decreases as polymer chains start to relax with increased temperature or decreased frequency. E'' displays a maximum near the point of the greatest change in E', where viscous losses are greatest. The peaks in tan δ mark thermal transition temperatures, which correspond to the expansion of free volume in the material, allowing for greater chain mobility [255]. The transition from a glassy to rubbery state is a pseudo-second-order transition, which is influenced by the rate of heating or cooling [255]. Part b of Schematic 1 shows how crosslinking affects the viscoelastic behavior. Crosslinks reduce chain mobility and thus increase the storage modulus and decrease the tan δ of the material. Crosslinks also raise and broaden the transition regions due to a decreased conformational entropy of the material [254]. Identifying a peak in the tan δ of cuticle would

deepen the understanding of polymer interactions within this material. Since, at room temperature, a small rise in the tan δ of the untanned elytron was observed at lower frequencies [20], dynamic mechanical tests were performed at even lower frequencies and higher temperatures in an effort to bring the relaxation mode into the time-scale of the experiment.

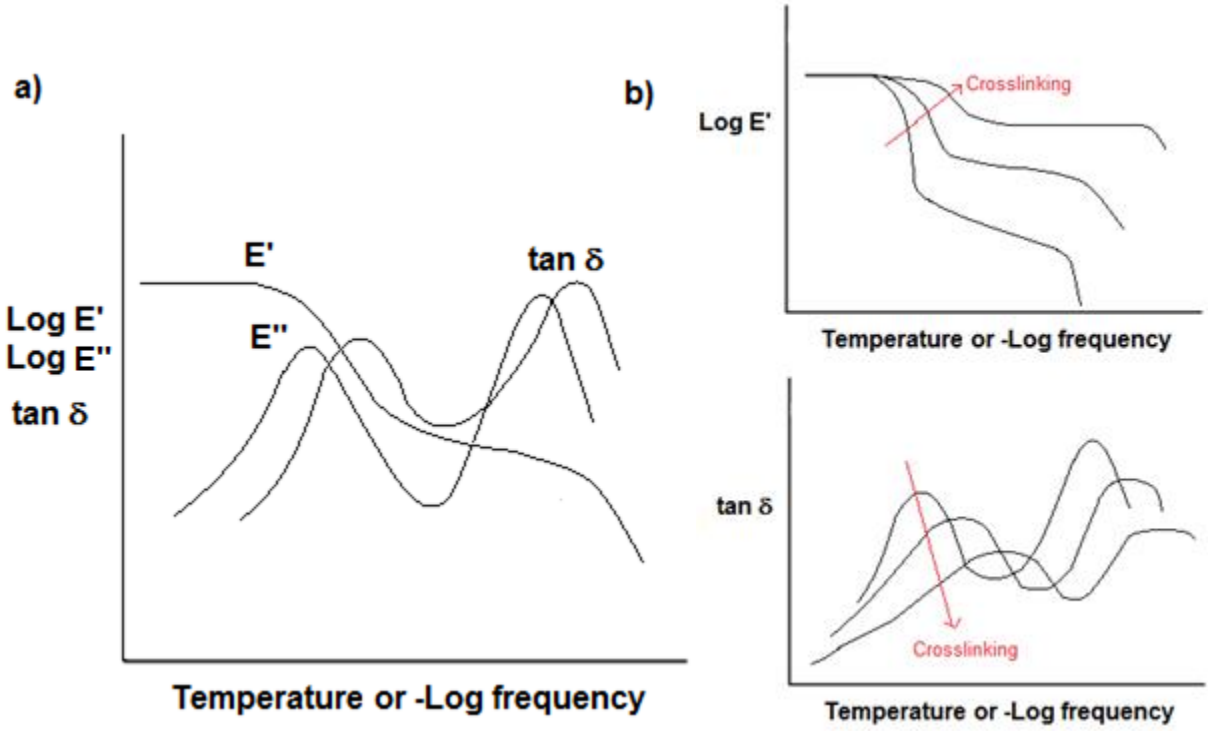

Schematic 4.1. Dynamic mechanical behavior of solid polymer materials. a) E' decreases while E'' peaks as the polymer undergoes a transition with increased temperature or decreased frequency. b) Crosslinking increases E' and decreases tan δ by reducing chain mobility. It also raises and broadens the transition temperatures.

Another way to distinguish between the effects of covalent and non-covalent crosslinking is to study the cuticle after treating with a non-covalent bond breaking solvent. If the level of covalent crosslinking changes as an insect matures, the amount of extractable material should also change. Andersen showed that the proteins in locust cuticle became more inextractible to formic acid as the insect matured, and only artificial crosslinking of immature cuticle with glutardialdehyde caused the proteins to resist extraction to the same degree [250]. In this study, *Tenebrio* elytra were soaked in several non-covalent bond breaking solvents. Trifluoracetic acid

and formic acid are both strong hydrogen bond breaking solvents [256, 257]. Hexafluoroisopropanol is a fluoronated alcohol which can denature proteins by weakening hydrophobic interactions [258]. Lithium bromide is an aqueous solvent that has been shown to dissolve silk [259]. Guanidine hydrochloride is an aqueous solvent used to break up hydrophobic interactions [260]. The extractability of untanned and tanned elytral cuticle when soaked in the solvents was examined to determine whether material becomes covalently bound to the network as the insect matures. The changes in mechanical properties of elytra were also measured after soaking in formic acid to help identify the role of non-covalent crosslinks in cuticular stability. The results were interpreted based on the model of cuticle development presented in Chapter 3, in which cuticle is continuously built up from the underlying epidermal cells during maturation. Thus, the outer layers of cuticle tan first and support the tensile loads while additional material is added and subsequently matures over 7 days.

Additionally, scanning electron microscopy of fractured elytra and Raman spectroscopy of the elytral surface were performed to determine whether microscopic mechanical or chemical heterogeneity existed within the elytral structure. It was hypothesized that there may be differences in crosslinking at the microscopic level, such as within the hexagonal pattern on the surface of elytra produced by the secretion of the material by epidermal cells below. Together with the mechanical analysis and solvent extraction studies, the results help to clarify the role of covalent and non-covalent crosslinks on a molecular and microscopic level in the mechanical stability of insect cuticle.

4.3 Materials and Methods

4.3.1 Materials

Triboilum castaneum and *Tenebrio molitor* insects were reared at the ARS-USDA Center for Grain and Animal Health Research in Manhattan, KS under standard conditions on a diet of equal volumes of wheat flour and rolled oats fortified with 5% brewers' yeast. Pupae were shipped overnight to the University of Kansas. Once ecdysis occurred, the beetles were monitored closely and sacrificed at specific tanning stages by separating the abdomen from the thorax with forceps. Fresh elytra were tested immediately to prevent water loss. Dried elytra were dried in a desiccator for 48 hours prior to testing. Trifluoracetic acid (TFA), hexafluoroisopropanol (HFIP), lithium bromide (LiBr), guanidine hydrochloride (GuHCl) and formic acid (FA) were purchased from Sigma.

4.3.2 Methods

4.3.2.1 Dynamic Mechanical Analysis to uncover a Thermal Transition

Mechanical analyses on *Tenebrio* elytra were performed using a TA Instruments RSAIII dynamic mechanical analyzer using methods analogous to Lomakin *et al* [20]. Elytra from completely untanned insects and fully tanned insects were dried and mounted lengthwise between the tensile grips, such that a rectangular portion of the elytron was left between the grips. The grips were lined with sandpaper to prevent slipping and a torque wrench was used to apply a consistent amount of pressure to each sample at the grips. Frequency sweeps were run from 0.01-100 rad/s at a strain amplitude of 0.1%, which was shown to be within the linear

viscoelastic region by strain sweeps. The elastic modulus (E'), and viscous modulus (E''), and their ratio (tan δ) were measured as a function of frequency. The frequency power law exponent, n, was calculated by fitting the data to a power law model between 0.01 and 100 rad/s. To probe even lower frequencies, fully tanned, dried elytra were tested at elevated temperatures, which correspond to lower frequencies.

4.3.2.2 SOLVENT EXTRACTION

The masses of partially tanned (12-24 hr) and fully tanned (7 d) dried *Tenebrio* elytra were measured on an analytical balance (±0.01 mg). Elytra were then placed in 2 ml of one of the following non-covalent bond breaking solvents: TFA, HFIP, 9.3 M LiBr, 6 M GuHCl and 90% FA and soaked in the solvent overnight (~16 hr) in closed vials. Based on the thickness of a dried *Tenebrio* elytron (9-39 µm) and a typical value for the diffusion coefficient in solids (10^{-9} cm^2/s), 16 hours was estimated (from the equation $L^2/Dt = 1$) to be sufficient for the material to reach equilibrium [261]. Elytra were then redried and weighed. Material extractability was calculated as the loss in dry weight after soaking in solvent overnight [(original dry wt- new dry wt)/original dry wt]*100.

4.3.2.3 STATIC MECHANICAL TESTING AFTER FORMIC ACID TREATMENT

Since formic acid appeared to have the largest qualitative effect on the elytral properties, the mechanical properties of *Tenebrio* elytra after treatment with this solvent were quantified. Elytra at 3 different stages of tanning were tested: untanned (0 hr), partially tanned (24-48 hr) and fully tanned (>7 d). After removing elytra from the formic acid, they were dipped briefly in water to remove excess FA on the surface and immediately mounted in the testing grips. Static

stress-strain measurements were made under tension by extending the elytra to failure at 0.01 mm/s.

4.3.2.4 Dynamic Mechanical Testing after Formic Acid Treatment

Using the same methods as 4.3.2.1, dynamic testing of *Tenebrio* elytra was performed after soaking in formic acid. Dynamic testing of *Tribolium* elytra was also performed after soaking in formic acid and redrying for over 24 hrs in the fume hood.

4.3.2.5 Scanning Electron Microscopy of Fractured *Tenebrio* Elytra

Fully tanned, partially tanned and fully tanned *Tenebrio* elytra treated with formic acid were fractured by pulling them to failure in the same manner as in static tensile testing. The samples were coated with gold using a Technics Hummer II sputter coater. A Leo 1550 field emission Scanning Electron Microscope in the Microscopy and Analytical Imaging Laboratory at the University of Kansas was used to obtain a detailed picture of the fractured edge of the elytra.

4.3.2.6 Raman Spectroscopy

A Horiba Jobin Yvon LabRam ARAMIS Micro-Raman Microscope in the Bioengineering Research Center at the University of Kansas was used to provide a chemical map of elytral surfaces. Spectra of the ventral side of a tanned *Tribolium* elytron were obtained with a HeNe laser, at a wavelength of 785 nm. A 10 point line scan was performed to obtain 10 different spectra at locations along the ventral surface of the cuticle, each 5 μm apart. The spatial resolution of each spectral acquisition is 1-2 μm. Next, the cross-section of a *Tenebrio*

elytron was analyzed. To section the elytron, it was first dehydrated in a series of ethanol solutions including two changes of 70% ethanol for 30 minutes each and two changes of absolute ethanol for 30 minutes each. Next, the sample was infiltrated with LR white resin (Electron Microscopy Sciences) at room temperature overnight inside gelatin pill capsules. The resin was then polymerized by incubating at 60°C for 24 hours [262]. A Leica ultratome in the Microscopy and Analytical Imaging Laboratorty at the University of Kansas was used to cut 1µm-thick sections. The sections were placed on clean microscope slides. The 785 nm laser burned the sample, even when submerged in water, so a 1064 nm laser was used.

4.4 RESULTS

Dynamic mechanical analysis was performed at lower frequencies and higher temperatures in order to clarify the nature of the crosslinks in elytral cuticle and possibly identify a thermal transition. Solvent extraction was used to determine the effect of disrupting non-covalent bonds in terms of protein extractability and mechanical properties. Scanning electron microscopy and Raman spectroscopy were used to examine heterogeneities in the structure.

4.4.1 DYNAMIC MECHANICAL ANALYSIS TO UNCOVER A THERMAL TRANSITION

The frequency dependence of the storage modulus appeared to follow the same trend over a lower frequency range as was observed for the higher frequency range. In Figure 3.1a below, the frequency sweeps performed down to low frequencies (0.01 rad/s) are compared to the previously published data (0.1-600 rad/s) [20]. Lower frequencies could not be measured due to the force resolution of the instrument. Due to the amount of time required for testing at low frequencies, only dried elytra could be tested in this range. Tests were run from low to high

frequency as well as in reverse (high to low frequency) and the data overlapped, suggesting that the microstructure did not change during the long testing times. The tan δ curves are shown in Figure 3.1b. For both untanned and tanned, dry elytra, the storage modulus at 1 Hz and the tan δ at 1 rad/ s were averaged and compared to previous data in Table 4.1. All values were the same, within uncertainty, demonstrating the reproducibility of the tests. Minor differences between the present data set and previously published data could be attributed to differences in mounting techniques or slightly different preloads at the start of the test. There was a higher variability in the E' values measured in this study, possibly due to a different population of insects with more diversity in size. The frequency power law exponents were averaged over the 0.01-100 frequency range, and these were compared to the previously published data from 10-100 rad/s [20]. The results are summarized in Table 4.1. The exponents were the same, within uncertainty, even at frequencies that are a decade lower. The untanned and dried elytra were more frequency dependent ($n = 0.050 \pm 0.024$) than the fully tanned and dried elytra ($n = 0.013 \pm 0.004$), and a two-tailed, paired t-test showed that the difference was statistically significant ($p < 0.05$). Overall, the trends in E' and tan δ remained the same at low frequencies; there was neither a significant drop in modulus nor rise in tan δ that would suggest a transition due to polymer relaxation.

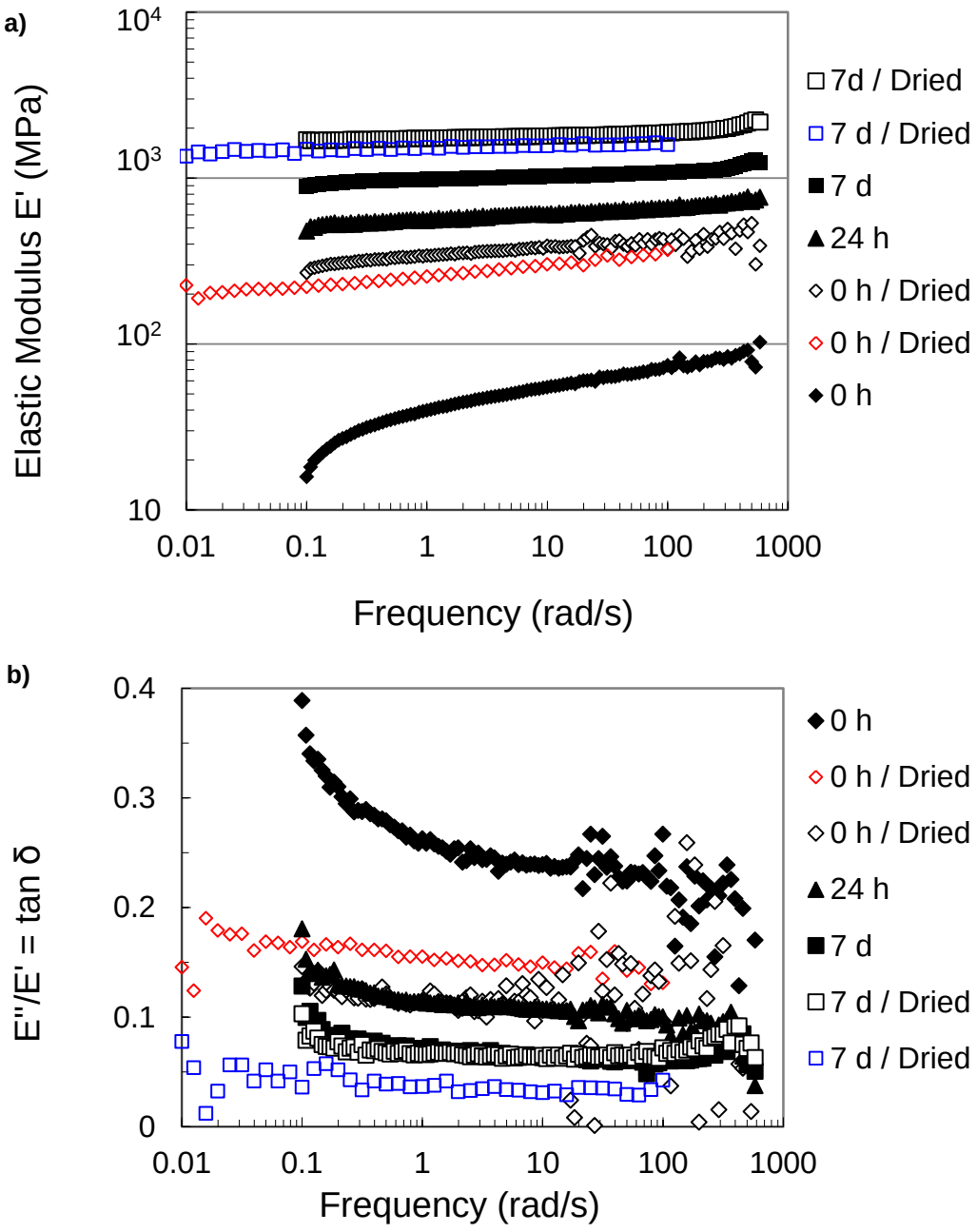

Figure 4.1. Representative frequency sweeps measured down to 0.01 rad/s for dried *Tenebrio* elytra at 0 h and 7 d, compared to the previously published data [20] measured from 0.1-600 rad/s. a) The slopes of the storage moduli remain constant down to 0.01 rad/s. b) There was not a significant rise in tan δ to suggest an approach toward a transition.

Table 4.1. Dynamic mechanical properties of dried *Tenebrio* elytra compared to published data [20].

		E' at 1 Hz (MPa)			tan δ at 1 rad/s			Freuquency Power Law Exponent		
Untanned	Lomakin *et al.* [20]	370	±	80	0.12	±	0.02	0.040	±	0.005*
	This study	290	±	200	0.14	±	0.05	0.050	±	0.024**
Tanned	Lomakin *et al. [20]*	1800	±	300	0.06	±	0.01	0.018	±	0.001*
	This study	3700	±	2000	0.04	±	0.01	0.013	±	0.004**

*power law exponent from 10-100 rad/s
**power law exponent from 0.01-100 rad/s
Sample sizes ≥ 4.

The effect of temperature on a fully tanned and dried elytron is shown in Figure 4.2. The E' and tan δ curves as a function of frequency are shown in Figure 4.2a as temperature was raised from 25 to 175°C. Up to 150°C, increased temperature caused the storage modulus curve to decrease and the tan δ curve to increase. The changes indicate an approach toward the tan δ peak, or a transition temperature. Figure 4.2b shows how the E', tan δ and frequency exponent at given frequencies changed upon temperature increase. The E' at 6.28 rad/s dropped 3.5 times, the tan δ at 1 rad/s increased 9 times and the frequency exponent from 1-100 rad/s increased 5 times from 25 to 150°C. At 175°C, the trends reversed; the modulus increased slightly and the tan δ and frequency exponent dropped. Thermogravimetric analysis of a fully tanned elytron, shown in Figure 4.3, showed a small loss in weight up to 150°C, presumably from the loss of bound water. A second region of weight loss began to occur above 150°C, suggesting that cuticle began to degrade. Deamidation reactions resulting in the degradation of amino acids were shown to occur between 150 and 180°C [263]. Degradation of chitin due to elimination of acetamide was shown to begin just under 100°C [264].

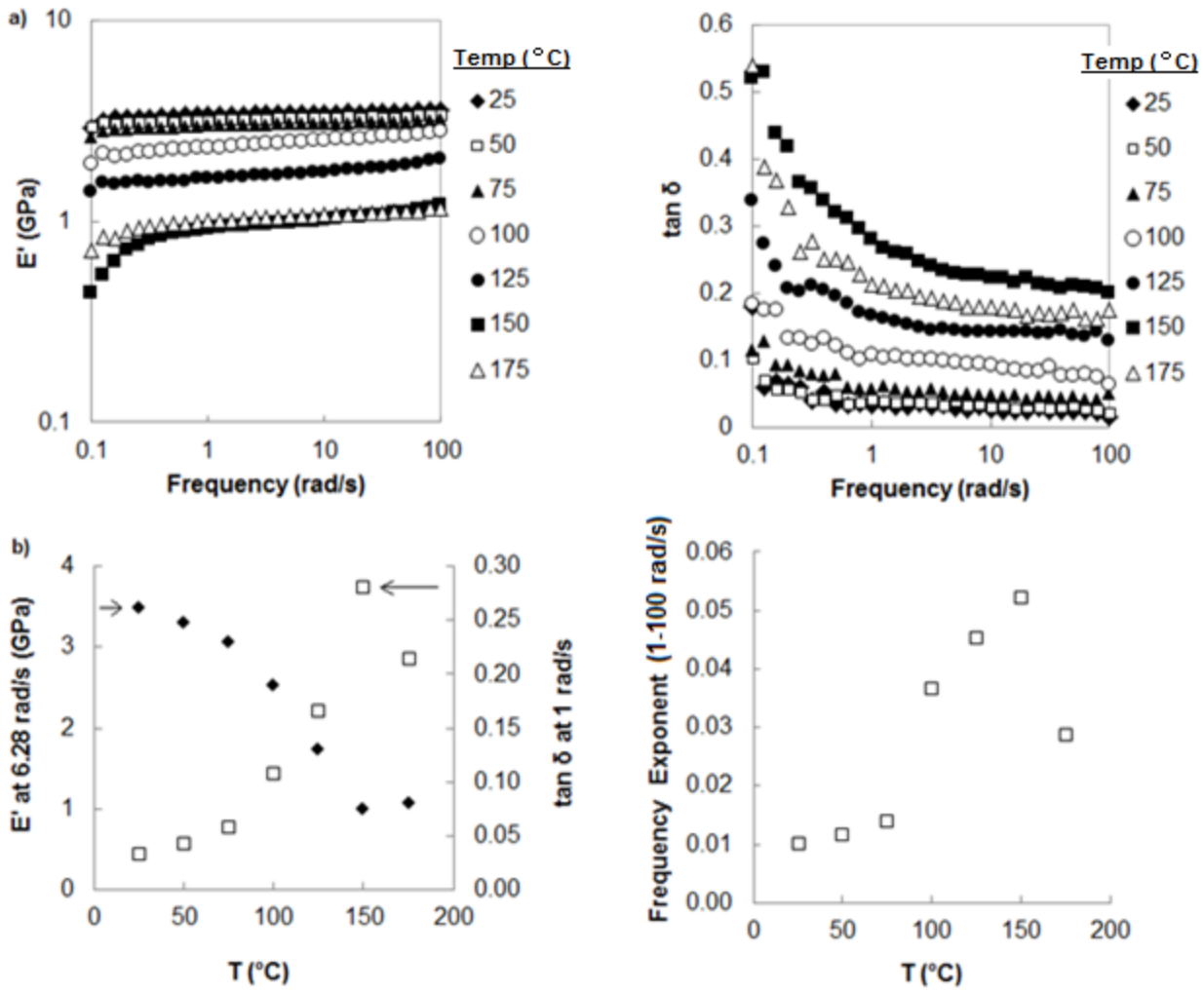

Figure 4.2. a) Frequency sweeps of a fully tanned and dried *Tenebrio* elytron as a function of temperature. b) Increased temperature caused a decrease in the storage modulus and an increase in tan δ and the frequency power law exponent until 150°C, after which the trend reversed.

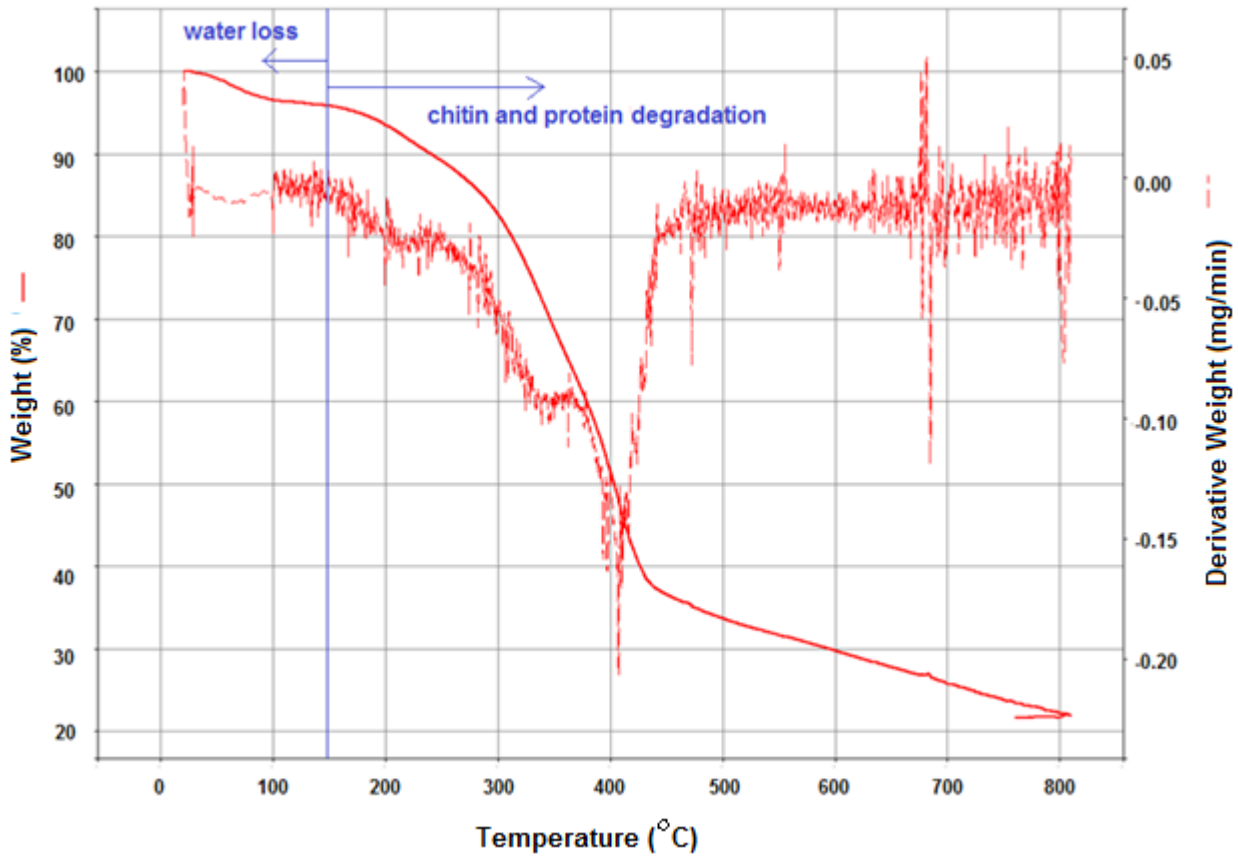

Figure 4.3. Thermogravimetric analysis of the *Tenebrio* elytron. Increasing temperature up to 150°C resulted in loss of bound water while a further increase in temperature resulted in degradation of the chitin and proteins.

4.4.2 Solvent Extraction

The amount of solid material that could be extracted from elytra when soaked overnight in several different non-covalent bond-breaking solvents is shown in Figure 4.3. The filled bars represent the amount extracted from partially tanned (~12-24 hr) elytra and the open bars represent the amount extracted from fully tanned (7d) elytra. For each solvent, more material was extracted from the partially tanned cuticle. That is, more material diffused out once the tissue was swollen in the solvent. Water extracts just over 20% and 10% of the solid material from partially tanned and fully tanned elytra respectively. The strong hydrogen bond breaking solvents, TFA, HFIP and FA, had much larger effects, removing about 60-70% from partially

tanned elytra and 20-30% from fully tanned elytra. TFA had the additional effect of causing the color of elytra to turn black, suggesting degradation. The aqueous salt solutions, LiBr and GuHCl, did not differ much from water even though they were expected to disrupt hydrogen bonds and hydrophobic interactions, respectively. Since FA had the largest effect on the extractability of elytra without indications of chemical degradation, it was chosen as the solvent for subsequent mechanical tests.

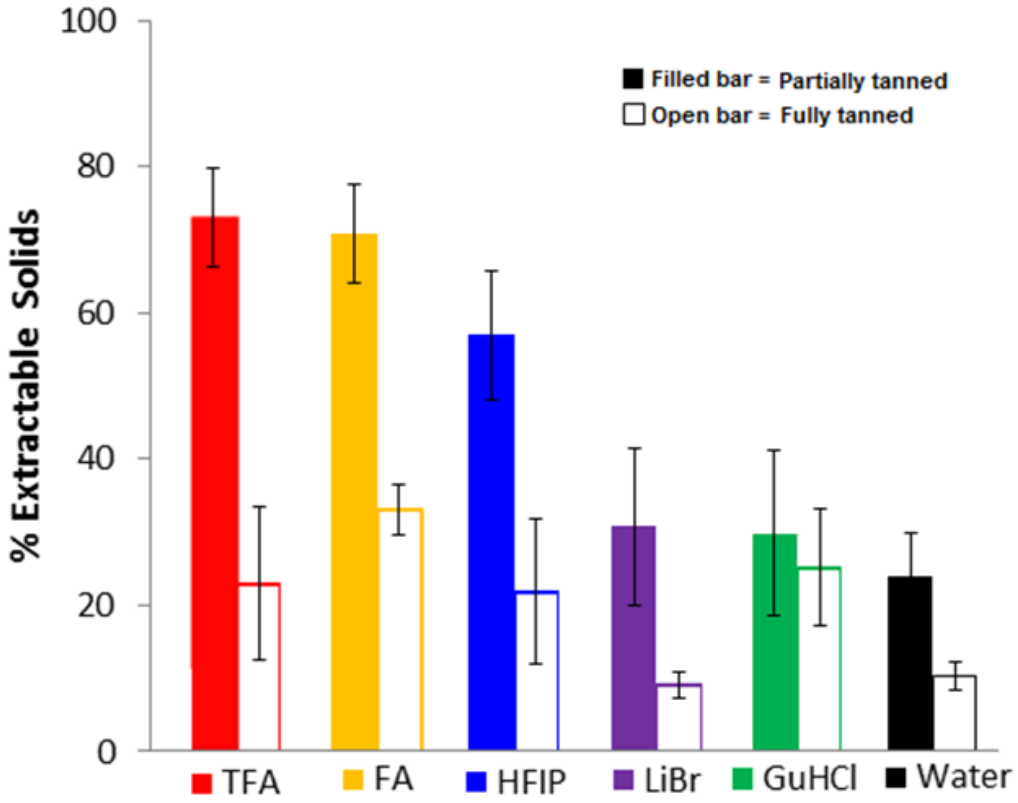

Figure 4.3. The % of solid material that was extracted after soaking elytra in several different solvents. In each case, more material was extracted from the partially tanned elytra than from the fully tanned elytra. Sample size ≥ 5.

4.4.3 Static Mechanical Testing after Formic Acid Treatment

The static mechanical properties of fresh elytra are shown in Figure 4.4 for both untreated and formic acid treated samples. The irregularities, or local maxima before and after the global maximum, in the stress-strain curve occurred due to piece-wise tearing of the elytra which was

interrupted by the rib structures (see Figures in Chapter 3). After soaking in formic acid, the fully tanned elytra, in particular, appeared to tear more steadily, that is, with a gradual decrease in stress rather than abrupt fracture. For elytra at all stages of tanning, formic acid made the material less stiff, less strong and more ductile. Figure 4.5 shows how the Young's modulus, fracture stress, fracture strain and toughness were affected by formic acid for untanned, partially tanned and fully tanned elytra. The Young's modulus was reduced 5 times for fully tanned, 3 times for partially tanned and 2 times for untanned elytra. The fracture stress was reduced 2 times for fully tanned, 2 times for partially tanned and 1.5 times for untanned elytra. The fracture strain was increased 3 times for fully tanned elytra, 1.5 times for partially tanned and 1.5 times for untanned elytra. The toughness, or work to fracture, was calculated based on the energy absorbed up to primary failure. It was not significantly changed by formic acid. After soaking in formic acid, the fully tanned and partially tanned elytra had comparable properties. The stiffness was about 1.6 times higher for fully tanned elytra, but the fracture stress, fracture strain and toughness were not statistically different, based two-tailed, paired t-tests with $p < 0.05$ considered significant. The untanned elytra that were treated with formic acid, however, were significantly less stiff, less strong and more ductile than both fully tanned and partially tanned elytra that were soaked in formic acid.

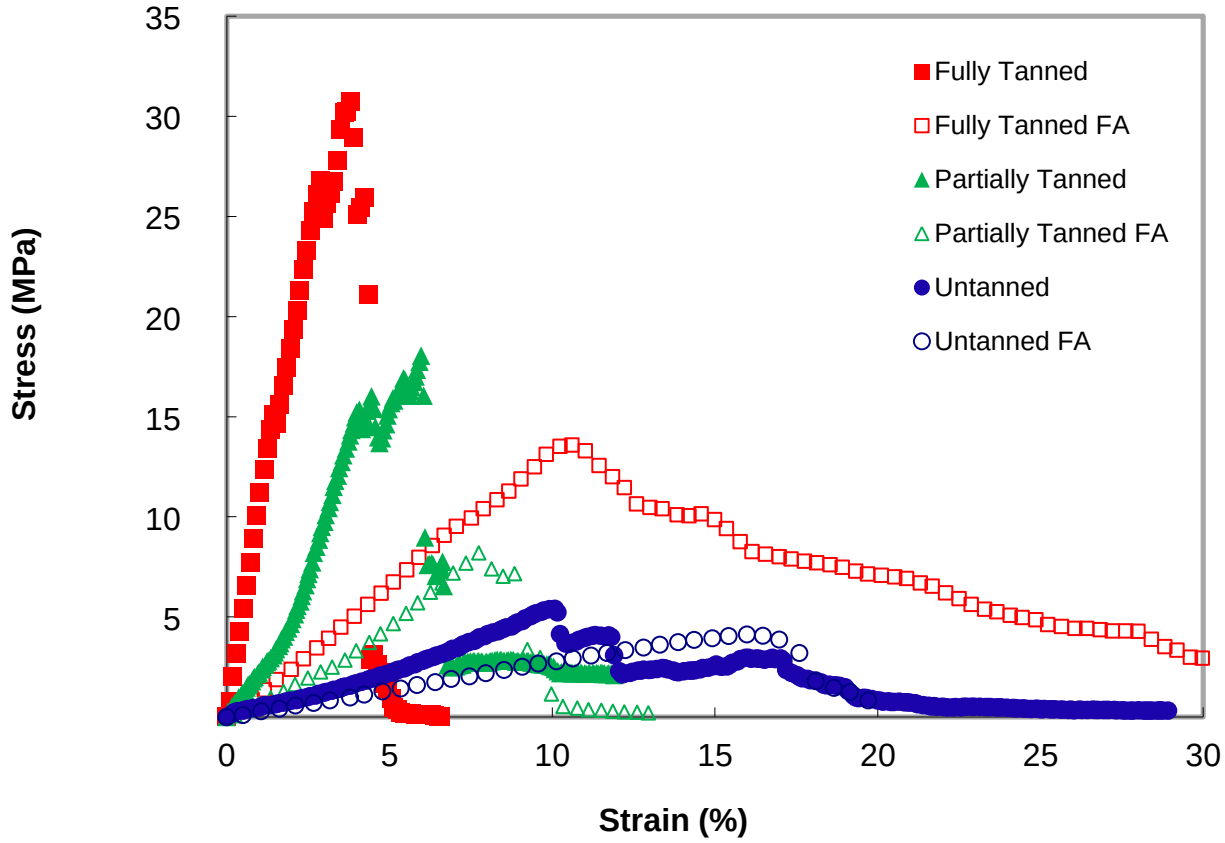

Figure 4.4. Representative stress-strain response of untanned, partially tanned and fully tanned elytra, either freshly harvested from the insect (closed symbols) or after soaking in formic acid (open symbols). Formic acid made the material less stiff, less strong and more ductile. Irregularities after the peak in the stress-strain curve were a result of tearing.

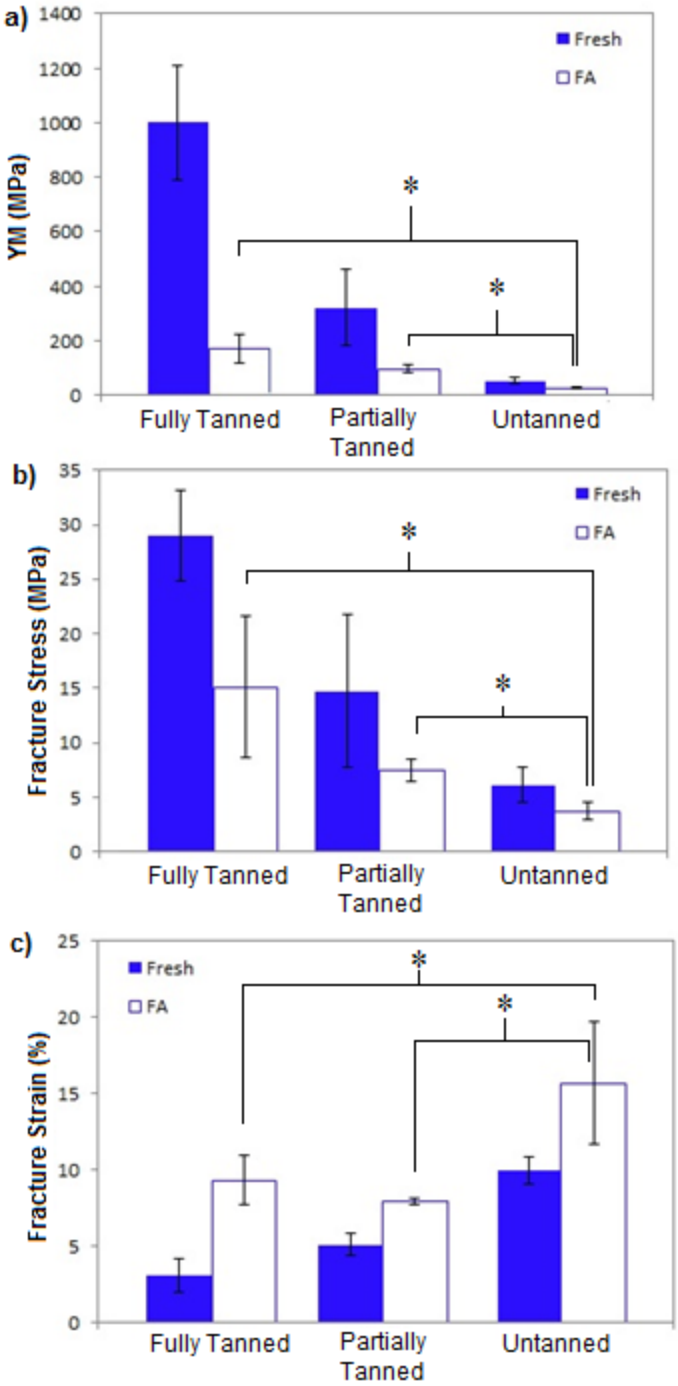
a)
YM (MPa)
1400
1200
1000
800
600
400
200
0
Fresh
FA
*
*
Fully Tanned
Partially Tanned
Untanned
b)
Fracture Stress (MPa)
35
30
25
20
15
10
5
0
Fresh
FA
*
*
Fully Tanned
Partially Tanned
Untanned
c)
Fracture Strain (%)
25
20
15
10
5
0
Fresh
FA
*
*
Fully Tanned
Partially Tanned
Untanned

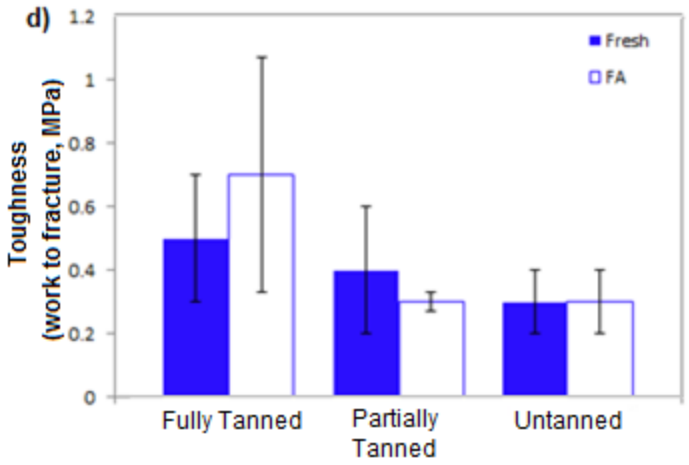

Figure 4.5. For fully tanned, partially tanned, and untanned elytra, the a) Young's modulus, b) fracture stress, c) fracture strain and d) toughness were compared before and after soaking in formic acid. Formic acid decreased the Young's modulus and fracture stress and increased the fracture strain. It did not cause a change in toughness. After soaking in formic acid, the fully tanned elytra had properties comparable to partially tanned elytra. Untanned elytra, however, had a significantly lower Young's modulus and fracture stress and significantly higher fracture strain. Significance was determined by a two-tailed, paired t-test with a p value less than 0.05. Sample sizes ≥ 4.

4.4 4 Dynamic Mechanical Analysis after Formic Acid Treatment

The dynamic mechanical properties of *Tenebrio molitor* are shown in Figure 4.6. Immediately after soaking fully tanned elytra in formic acid, the dynamic mechanical properties were tested and compared to previously published dynamic mechanical data [20]. Results showed that formic acid caused the storage modulus curve to be lowered and the tan δ curve to be increased slightly. At 1 rad/s, the storage modulus dropped about 3.5 times and the tan δ increased about 1.4 times. However, the modulus was still 7 times higher and tan δ was 2.7 times lower than untanned elytra. Soaking fully tanned elytra in formic acid also caused in increase in the frequency exponent; it increased from 0.021± 0.002 for fresh, fully tanned elytra to 0.058 ± 0.004 for formic acid-soaked, fully tanned elytra. However, the frequency exponent was still lower than for the untanned elytra (0.130 ± 0.037).

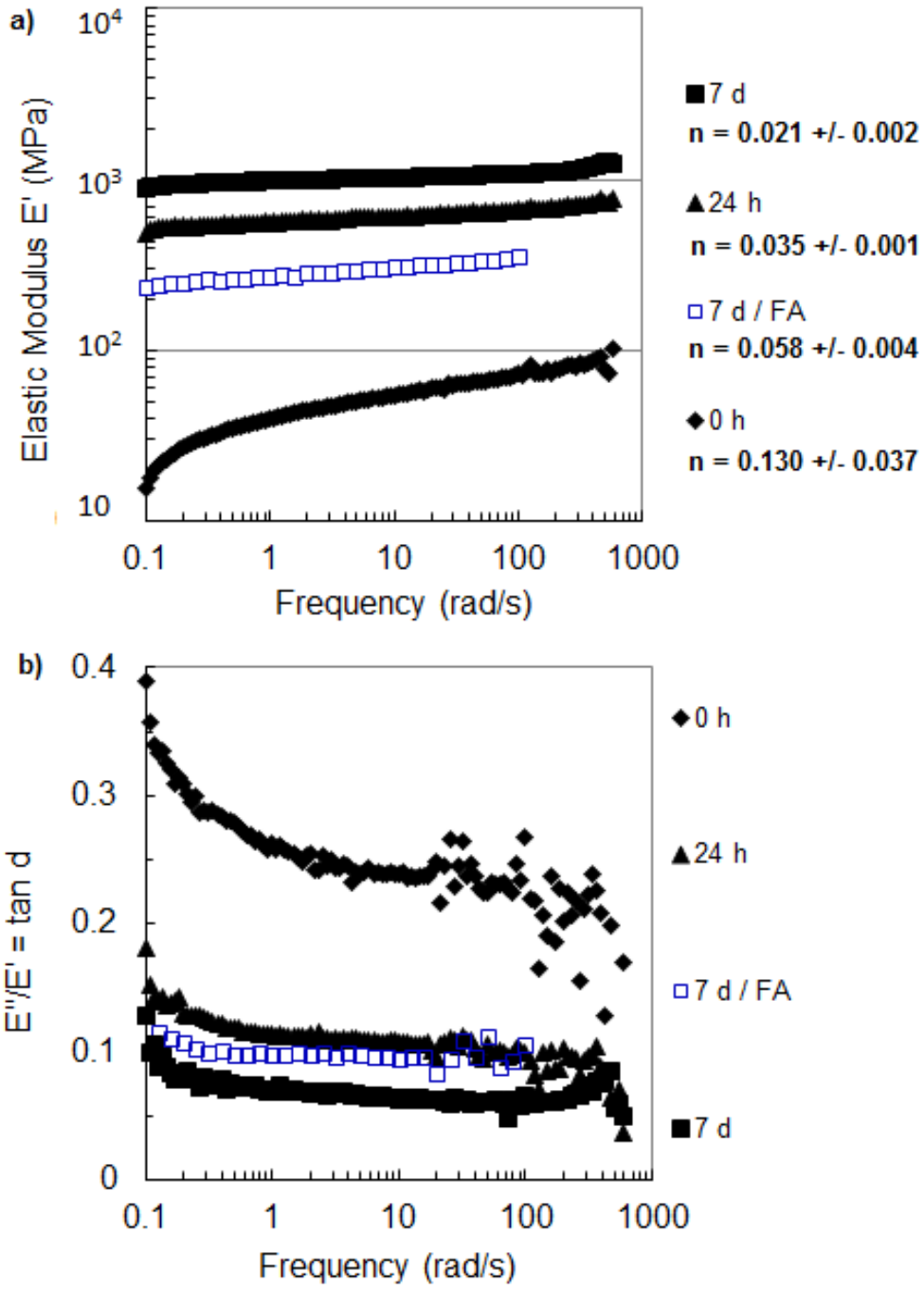

Figure 4.6. Frequency sweeps of fully tanned *Tenebrio* elytra immediately after soaking of formic acid compared to previously published frequency sweeps of *Tenebrio* elytra at 3 different stages of tanning [20]. Formic acid caused a decrease in the modulus and an increase in the frequency exponent and tan δ of fully tanned elytra. However, the modulus was still higher and the tan δ and frequency exponent were still lower than untanned elytra.

The dynamic mechanical properties of *Tribolium castaneum* are shown in Figure 4.7. After soaking a fully tanned elytron in formic acid and redrying, the magnitude of the storage modulus was the same as the original, untreated and dried modulus. The tan δ values were also nearly the same; at 1 rad/s the tan δ of the elytron that was soaked in formic acid and redried was 0.08 (compared to 0.07 originally). The frequency exponent, n, from 1-100 rad/s of the elytron that was soaked in formic acid and redried was 0.042 (compared to 0.025 ± 0.001 originally).

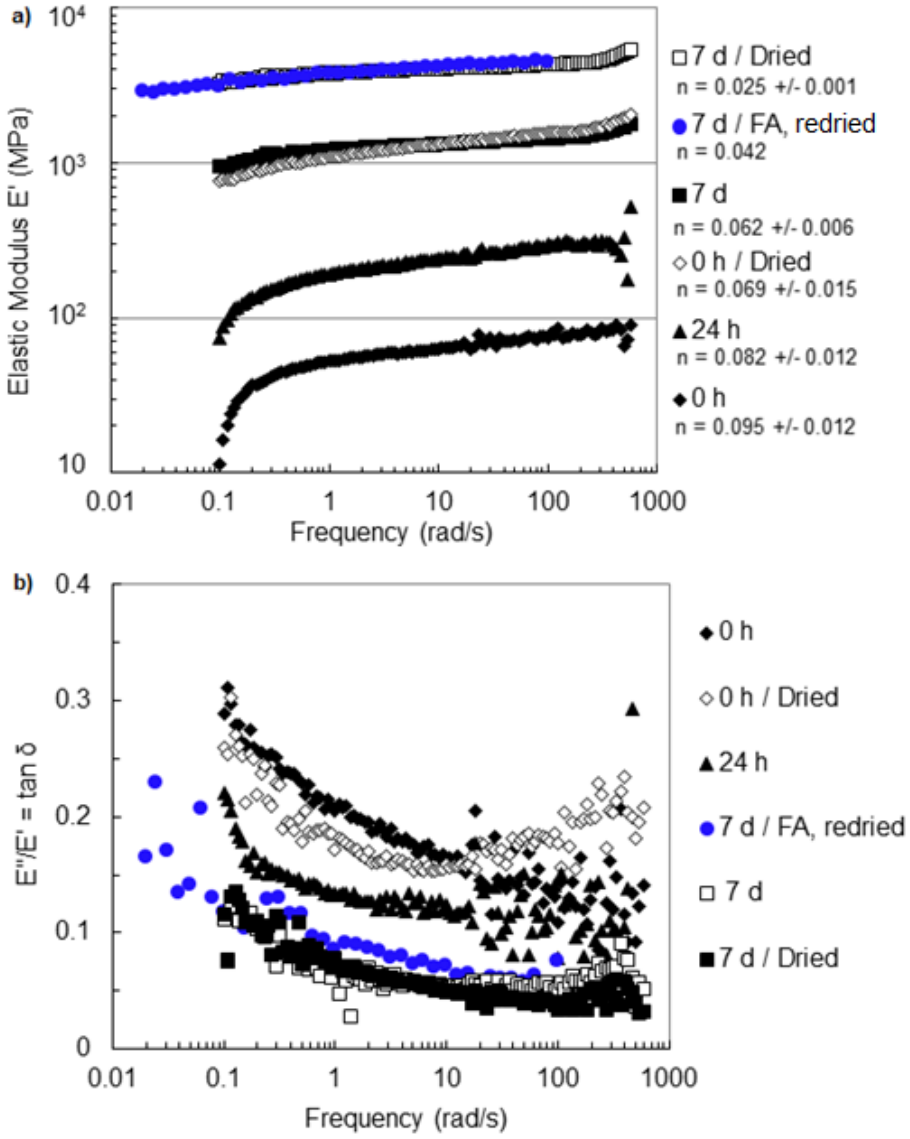

Figure 4.7. a) Storage modulus and b) tan δ for fully tanned elytra after soaking in formic acid and redrying (blue circles) compared to previous data for untreated fully tanned and dried elytra (white squares) [20].

4.4.5 Scanning Electron Microscopy of Fractured Tenebrio Elytra

Fully tanned, partially tanned and fully tanned *Tenebrio* elytra treated with formic acid were fractured by pulling them to failure in the same manner as in static tensile testing. The fractured edges of partially tanned, fully tanned and fully tanned/ formic acid treated elytra are shown in Figure 4.8. It was hypothesized that a preferred break pattern may reveal some mechanical heterogeneity. For example, weak spots may exist where the cuticle within the hexagonal structures were 'glued' together after being secreted. However, the fracture did not preferentially occur along the edges of the hexagonal structures. The fracture was fairly straight, without any distinct pattern or difference based on the stage of tanning or formic acid treatment. Even though the formic acid-treated elytra tore gradually whereas fully and partially tanned native elytra fractured more abruptly (see Figure 4.4), there was no difference observable on the microscopic level.

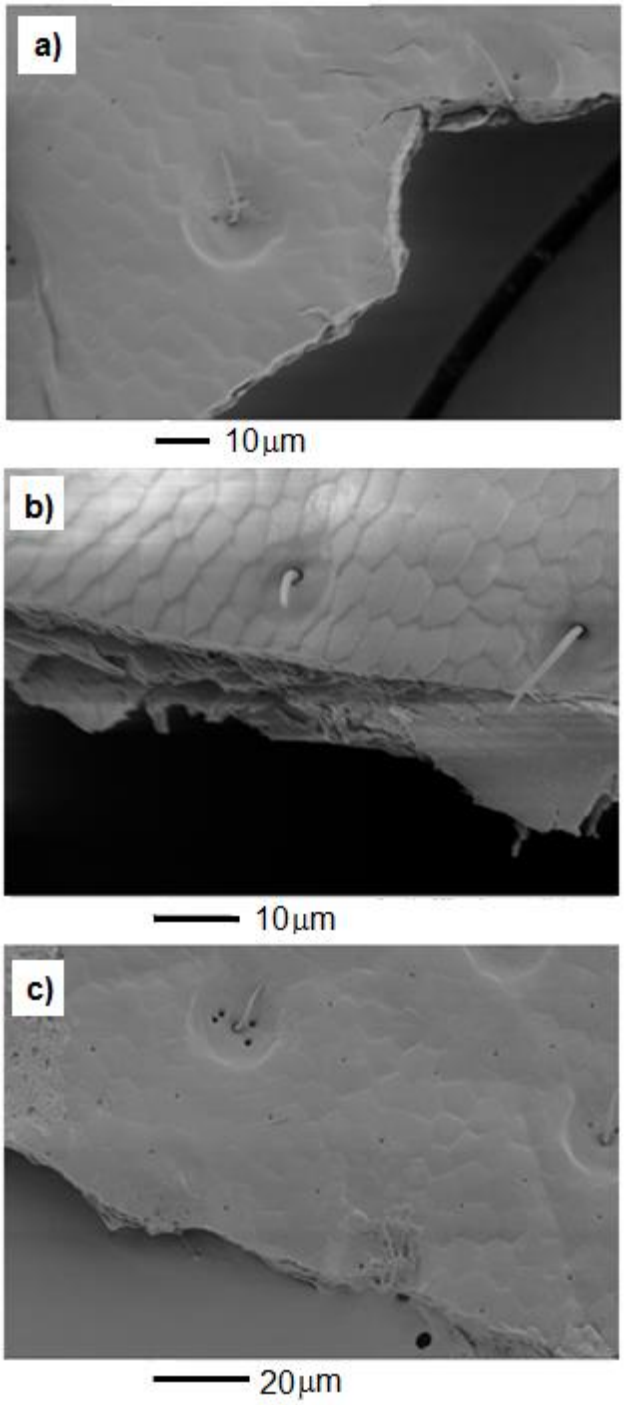

Figure 4.8. SEM images of the fractured edge of a) a partially tanned *Tenebrio* elytron, b) a fully tanned *Tenebrio* elytron, and c) a fully tanned, formic acid treated *Tenebrio* elytron. Fracture appeared to be random through the hexagonal features.

4.4.6 Raman Spectroscopy

Raman spectroscopy was performed on *Tribolium* elytra to determine whether there was significant heterogeneity in the chemical makeup of the cuticle. A 10 point line scan was performed to obtain 10 different spectra at different locations along the ventral surface of the cuticle, each 5 µm apart. The spectra are shown in Figure 4.9. The spatial resolution of each spectral acquisition was 1-2 µm. Of all 10 spectra, only some appeared to have meaningful peaks. The ones without peaks were out of focus because the surface of the cuticle was not completely flat. However, for the scans that were in focus, no significant differences were observed that would suggest a heterogeneous chemical makeup of the cuticle.

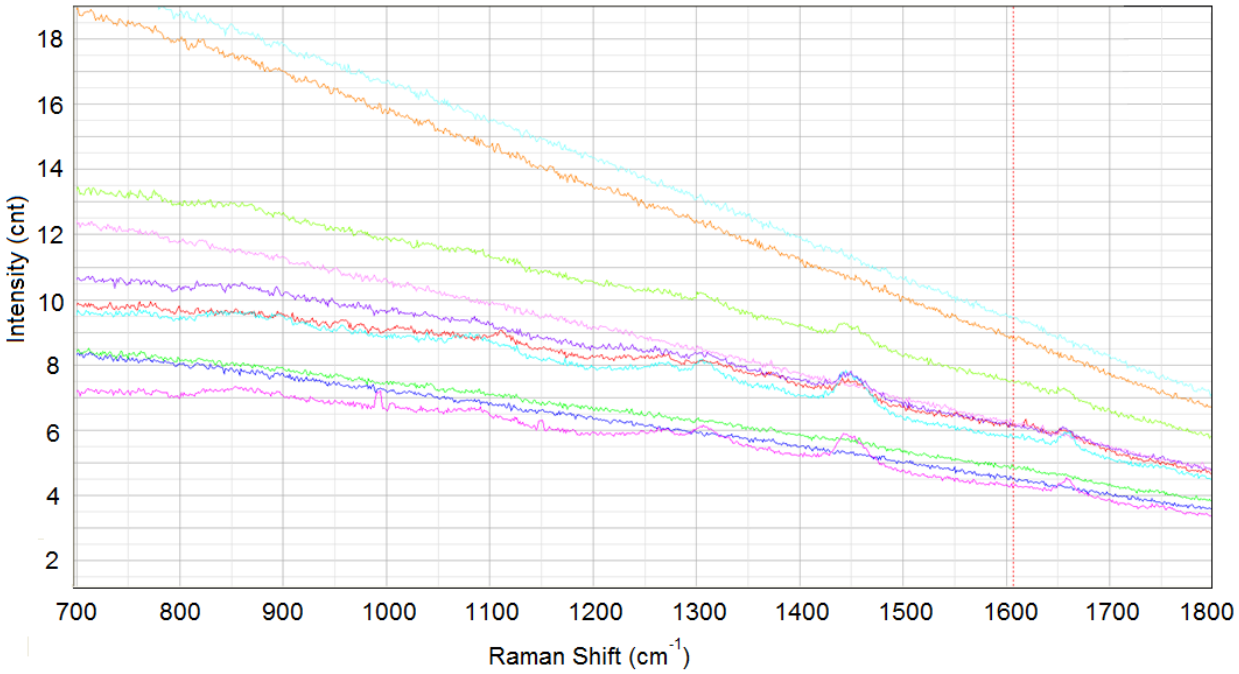

Figure 4.9. Raman spectra at 10 different locations, each 5 µm apart, on the ventral surface of a *Tribolium* elytron. The spectra without significant peaks were taken at locations that were out of focus. Among the spectra with meaningful peaks, no differences were observed that would suggest chemical heterogeneity.

One spectrum from Figure 4.9 was smoothed and baseline corrected using the LabSpec software to remove the effect of fluorescence due to aromatic residues and catechols. Peak assignments, shown in Figure 4.10, were determined based on previous studies involving Raman spectroscopy of chitinous and protein materials [32, 265-271]. The peaks at 895, 1090 and 1443 cm^{-1} were attributed to α-chitin [270, 271]. In the amide I region (1600-1700 cm^{-1}), there was a maximum at 1660 cm^{-1}, which is typical of random coil proteins. In the amide III region, (1230-1320 cm^{-1}) there were two peaks at 1270 and 1308 cm^{-1}, which are typical of α-helical proteins [265-269].

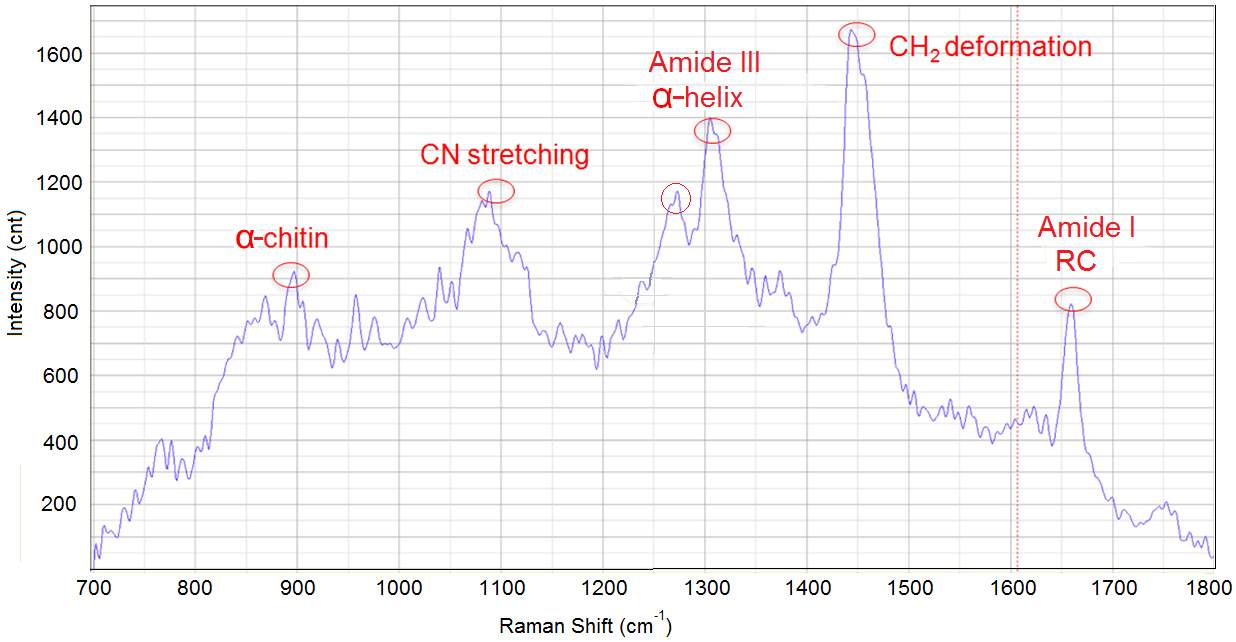

Figure 4.10. Raman spectrum of the ventral surface of a *Tribolium* elytron after baseline correction and smoothing.

Since no significant heterogeneity was seen on the ventral surface of *Tribolium* elytra, *Tenebrio* elytra were embedded in a resin and sectioned to determine if chemical differences existed among the layers of cuticle. Considering the 1-2μm resolution of the Raman instrument, *Tenebrio* samples were used in order to have sufficiently large regions of each layer so that a

Raman spectrum could be acquired for each separate layer. The spectra, however, had significant interference from the embedding resin, making it difficult to interpret the results.

4.5 Discussion

The relative roles of covalent and non-covalent interactions in the stabilization of elytral cuticle were examined using mechanical analysis and solvent extraction. The importance of covalent crosslinking was supported by dynamic mechanical analysis. The dynamic mechanical properties of elytra were tested at lower frequencies and higher temperatures to determine whether a peak in the tan δ would be observed, indicating a transition point where polymer mobility increases. Non-covalent interactions would be expected to undergo viscous dissipation at lower frequencies and higher temperatures, so the importance of covalent crosslinks in stabilizing the structure becomes even more apparent in this range. The low frequency dynamic mechanical testing of *Tenebrio* elytra, shown in Figure 4.1, demonstrated that, even at very long time scales, the elastic modulus did not drop off due to disentanglement of the macromolecules. Instead, the slopes remained constant over the larger frequency range. For fully tanned elytra, the frequency power law exponent previously measured in the range of 10-100 rad/s was 0.018 ± 0.001 [20], and here it was found to be 0.013 ± 0.004 in the range of 0.01-100 rad/s. For untanned elytra, the power law exponent was 0.040 ± 0.005 in the range of 10-100 rad/s [20], and here it was found to be 0.050 ± 0.024 in the range of 0.01-100 rad/s. Since the untanned and dried elytra continued to display a higher frequency dependence ($n = 0.05 \pm 0.024$) than the fully tanned and dried elytra ($n = 0.013 \pm 0.004$) even at low frequencies, the conclusion that additional crosslinking stabilizes the cuticle as it tans [20] was supported. The crosslinks

responsible for the higher elastic response of fully tanned elytra are likely to be covalent, since they are permanent at low time scales.

Since no transition was observed at the lowest frequencies accessible, increased temperature was used to potentially bring the relaxation mode into the time-scale of the experiment. The dynamic mechanical properties of the fully tanned and dried elytron were measured at elevated temperatures, which correspond to lower frequencies. As shown in Figure 4.2, there was a slight decrease in E' and increase in tan δ and n. E' (at 6.28 rad/s) dropped from 3.48 GPa at 25°C to 0.99 GPa at 150°C; tan δ (at 1 rad/s) increased from 0.03 at 25°C to 0.28 at 150°C; n increased from 0.010 at 25°C to 0.052 at 150°C. The changes appeared to begin around 100ºC. The trends reversed slightly at 175°C, where thermogravimetric analysis showed that the material started to degrade. It is likely that protein and chitin degradation above 150°C resulted in the elimination of water and gases and the formation of crosslinks. It has been shown that deamidation of asparagine, glutamine and aspartic acid, resulting in the release of ammonia, occurs around 150ºC [263]. Thermal degradation of chitin, resulting in the release of acetamide, occurs at higher temperatures, around 290º [264]. Below 150°C, the increase in the viscous contribution relative to the elastic contribution to the applied load suggests that the higher temperatures disrupted some non-covalent interactions, leading to viscous energy dissipation. However, there was no observable peak in tan δ nor was there a sharp drop and plateau in E' that would indicate a clear thermal transition. The fact that temperatures near degradation were required to see just the start of a transition suggests that covalent crosslinks greatly suppressed this relaxation mode in tanned elytra relative to untanned elytra. Schematic 4.2 shows how the entire E' and tan δ curves may behave with frequency for untanned and fully tanned elytra. Between the red lines is the behavior shown previously by Lomakin *et al.* [20]. Highlighted in

yellow is the behavior demonstrated in this study (the high temperature data corresponds to low frequencies). It appears that the fully tanned and dry cuticle is a highly crosslinked rubber, with a very high E' (on the order of magnitude of typical glassy materials, 10^9 Pa). High temperatures (very low frequencies) do cause some viscous losses, but the covalent crosslinks prevent any significant long-range motion of the biopolymer chains that would be needed to see a peak in the tan δ curve. There may be a small, broad peak at higher frequencies (colder temperatures), corresponding to the glass transition temperature, but this region has not been measured. It is known that tan δ peaks are lower and more broad in crosslinked materials, so it may be difficult to distinguish a clear T_g in fully tanned elytra. The fact that the tan δ peak only began to emerge near degradation of the fully tanned elytra, while it emerged at room temperature for untanned elytra is consistent with the view that covalent crosslinks suppress this relaxation mode as the insect matures. The trends suggest that tanning moved the tan δ curve down and to the left because covalent crosslinks suppress viscous losses at all times whereas drying moved it to the left only. Thus, it appears that covalent crosslinks imposed constraints on the material that lowered the viscous response at all frequencies, while drying just shift the response to lower frequencies.

Overall, the trends observed at low frequencies and high temperatures are consistent with the previous interpretation of cuticle behavior which said that covalent crosslinks have a larger impact on mechanical properties than non-covalent interactions formed upon dehydration. However, other interpretations are not completely out of the question. It is assumed that the tests performed in this study and previous studies probe the cuticle in the rubbery state and below. However, it is possible that cuticle is, in fact, glassy and the transition being approached at lower frequencies is the glass transition temperature. While this would compromise some of the

meaning drawn from the changes in frequency dependence of the storage modulus, the differences may still reflect important contributions of the crosslinks such as shifting the transition temperatures. Additionally, the differences in the shape of the tan δ curves, as discussed above, would still suggest the importance of covalent crosslinking. Furthermore, if the rubbery state was never reached in fully tanned cuticle before degradation, that alone would suggest it is very highly crosslinked. Another consideration may be that cuticle exhibits multiple glass transition temperatures because it is a multicomponent material. The glass transition of the protein phase may be at lower temperatures (higher frequencies, on the right hand side of Schematic 4.2) while the glass transition of chitin may be at the higher temperatures (lower frequencies, on the left in Shematic 4.2). In this case, the behavior at room temperatures (between the red lines in Schematic 4.2) would be probing the protein in the rubbery state and chitin in the glassy state. The viscous losses at high temperatures/ low frequencies may, therefore, reflect the breaking of hydrogen bonds among the chitin chains.

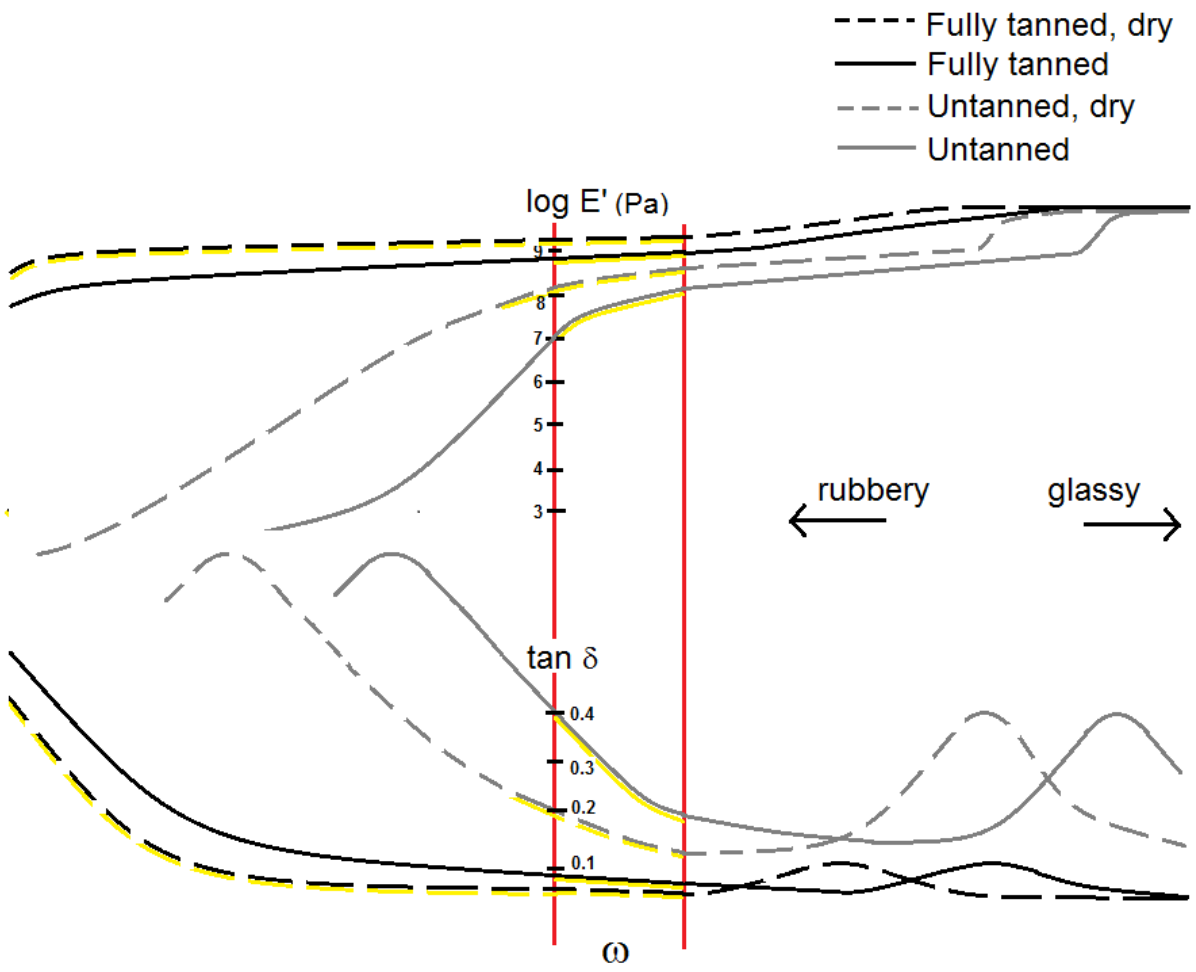

Schematic 4.2. The behavior of fully tanned and untanned elytra over a wide frequency range. The actual behavior that has been measured is highlighted in yellow, while the additional portions of the curves are speculated. It appears that tanning suppresses the relaxation modes in elytra at all frequencies while drying simply shifts them to lower frequencies.

Additionally, soaking elytra in non-covalent bond breaking solvents supported the view that proteins become covalently crosslinked as an insect matures. Figure 4.3 shows that, for each solvent, more solid material was extracted from the less mature elytra. The three hydrogen bond-breaking acids, TFA and FA and HFIP, had the most dramatic effects, removing over ~60-70% of material from partially tanned elytra and 20-30% from fully tanned elytra. The TFA also caused elytra to become black and deformed, suggesting some additional chemical reaction, possibly oxidation of the proteins. The 9M LiBr did not have significantly different effects on

elytra than water. LiBr is a salt that can disrupt protein structures by shielding ions to destabilize salt bridges and by forming ion-dipole interactions that interfere with hydrogen bonding [272, 273]. However, since it is an aqueous solvent, it may not have been able to penetrate the hydrophobic components of the cuticle to affect the proteins. GuHCl, which disrupts hydrophobic interactions, resulted in similar amounts of material to be extracted from the partially and fully tanned elytra. Since hydrophobic pigment molecules are expected to form with maturation, the GuHCl likely had a greater effect on the fully tanned cuticle. Overall, the results suggest that, when non-covalent bonds, most notably hydrogen bonds, were broken, more protein was free to diffuse out of the partially tanned elytra. The lower extractability of fully tanned elytra is hypothesized to result from the covalent crosslinks, which could prevent the loss of protein that would otherwise dissolve when the non-covalent bonds were disrupted. It is important, however, to consider the non-uniform tanning of cuticle layers as they are secreted from the epidermal cells. As discussed in Chapter 3, the covalent crosslinks within the outermost layers of the dorsal cuticle lamination of elytra are formed within 48 hours of secretion from the epidermal cells. Additional layers of cuticle are subsequently added and tanned. Thus, partially tanned elytra likely have a gradient of crosslink density throughout the thickness of the cuticle whereas fully tanned elytra are more uniformly crosslinked throughout the cuticle. Thus, the difference in extractability is likely caused by a very large removal of material from the less-crosslinked layers of partially tanned elytra. The degree of covalent crosslinking in the upper portion of partially tanned elytra may be similar to fully tanned elytra.

It is also possible that some of the difference in extractability was due to the higher solubility of phenolic material in the partially tanned elytra. However, the phenolic portion of the solid material generally ranges from 1% to 15% [274], so this would not account for the large

loss of material (~60-70% in TFA, HFIP and FA) from partially tanned elytra. Additionally, it is possible that protein extractability was reduced in fully tanned elytra due to catecholation (which would reduce solubility) rather than crosslinking. However, Andersen previously showed that proteins within immature locust cuticle were still readily extracted in concentrated formic acid even after treating with reagents that link aromatic material to the free amino groups on proteins, indicating neither decreased charge nor increased aromaticity made the cuticle proteins as resistant to extraction as the natural sclerotization process. Only covalently crosslinking the proteins with glutardialdehyde made immature cuticle resistant to extraction [250]. Thus, the results here are consistent with the view covalent crosslinks play an important role in stabilizing insect cuticle.

Mechanical testing of elytra after soaking in formic acid points to the role of non-covalent interactions, especially hydrogen bonds, in stabilizing the material. It was hypothesized that non-covalent interactions contribute to the stiffness of elytra and that their relative importance increases with maturation. Formic acid, since it is highly polar, can form strong hydrogen bonds which will replace, or 'break up,' the intermolecular hydrogen bonds that existed between proteins and polysaccharides [256]. Figures 4.4 and 4.5 show that the stiffness decreased when elytra were soaked in formic acid, which supports the hypothesis that non-covalent interactions contribute to the stiffness. The largest effect was seen in the fully tanned elytra, where the Young's modulus was lowered about 5 times, which suggests that the importance of non-covalent interactions increases with maturation. This decrease is similar to the drop in E' of fully tanned, dried elytra with increased temperature (3.5 times). Since elytra lose a significant amount of water from the untanned to fully tanned state (71% to 33% water), the fully tanned elytra have less plasticization and are therefore hypothesized to contain more

non-covalent interactions. However, as discussed in Chapter 3, much of the water is lost from between the non-load bearing cavities between the solid cuticle. Even a small loss of water within the solid cuticle, though, may contribute to additional stiffness from non-covalent interactions. The decrease in stiffness of the fully tanned elytra when soaked in formic acid or when heated is consistent with the hypothesized role of non-covalent interactions in contributing to the stiffness of cuticle. Similarly, the fracture stress was lowered and fracture strain increased due to the additional plasticization and loss of non-covalent interactions. The increased fracture strain may reflect the disruption of hydrogen bonds at a higher length scale, thus allowing higher displacements before fracture. The toughness, however, was not considerably changed since the fracture stress was lowered but the fracture strain was increased. Thus, it appears that the major contribution of the non-covalent interactions was the ability to stiffen the material without compromising the toughness. Often, there is a tradeoff between stiffness and toughness [13]. Covalent bonds are very strong, so a high degree of covalent crosslinking results in optimal stiffness; however, the stiffness comes at the expense of reduced toughness because the bonds do not allow for much energy dissipation [13]. The fact that formic acid treatment (i.e. removal of non-covalent interactions) decreased stiffness without changing toughness suggests that the non-covalent interactions were able to impart stiffness without giving up toughness. If the same degree of stiffness had been achieve solely through covalent interactions, the toughness may have been reduced. The partially tanned and untanned elytra, when treated with formic acid, also had lower Young's moduli and fracture stresses and higher fracture strains, but the difference was not as dramatic because they contained fewer non-covalent interactions in the untreated state.

Overall, the static mechanical tests suggest that non-covalent interactions help to stiffen and strengthen the elytral cuticle and that they become more important in the fully mature, less hydrated cuticle. However, the importance of covalent crosslinks remains. It is important to remember here, as well, that the cuticle is not a homogenous structure; the epidermal cells continue to secrete material over the 7 days of maturation to form the final structure. The process of tanning begins as soon as material is secreted and covalent crosslinks are established within the initially secreted cuticle layers within 48 hrs. Therefore, within the load-bearing layers of elytral cuticle, the untanned and partially tanned cuticle should have a significant difference in covalent crosslinking while the partially tanned and fully tanned cuticle differ more in the amount of non-covalent crosslinking. Figures 4.4 and 4.5 show that fully tanned and partially tanned elytra that were soaked in formic acid had similar properties; the stiffnesses were 170 ± 50 MPa and 96 ± 20 MPa respectively, the fracture stresses were 15 ± 7 and 8 ± 1 MPa respectively, and the fracture strains were 9 ± 2 and 8 ± 0 respectively. The similarity in the absence of non-covalent interactions suggests that the main difference between fully and partially tanned elytra, within the load bearing layers, is the amount of non-covalent crosslinking. The untanned elytra that have been treated with formic acid, however, are significantly less stiff and strong and are more ductile (stiffness = 25 ± 3 MPa, fracture stress = 4 ± 1MPa and fracture strain = 16 ± 4%), indicating fewer covalent crosslinks. Thus, the quinone crosslinking theory is supported, and the covalent crosslinks established within elytra stabilize the material within the first 48 hours after eclosion. Additional non-covalent interactions are formed which provide added strength and stiffness while maintaining a high toughness.

The dynamic mechanical testing of fully tanned elytra after treating with formic acid, shown in Figure 4.6, also showed that the stiffness decreased; the E’ was reduced 3.5 times. The

frequency exponent also increased from 0.021 ± 0.002 to 0.058 ± 0.004. These effects were similar to the effects of increasing the temperature of fully tanned elytra, which also caused a 3.5-fold decrease in E' and an increase in the frequency exponent from 0.018 to 0.052. Thus, some of the interactions leading to the lower frequency exponent (and lower viscous dissipation) in fully tanned cuticle were likely non-covalent. However, the formic acid-treated elytra still had a lower frequency exponent than the untanned elytra (0.130 ± 0.037), due to the higher number of covalent crosslinks. The dynamic mechanical testing of a fully tanned *Tribolium* elytron that was soaked in formic acid and redried showed that storage modulus matched the untreated, fully tanned and dried elytron (see Figure 4.7a). Thus, the cuticle remained structurally and mechanically intact despite losing about 33% of its solid material. Non-covalent interactions were likely able to reform once the plasticization of the solvent was removed, thus recovering the stiffness. Also, the material that was lost may have been primarily components from the untanned ventral lamination of cuticle which does not support the load. The frequency exponent of fully tanned elytra that were soaked in formic acid and redried was 0.042, which was higher than untreated, fully tanned and dried elytra (0.025 ± 0.001). This could be due to a less ordered re-formation of non-covalent bonds when the material was re-dried. However, it was still lower than the untanned and dried cuticle (0.069 ± 0.015), showing that the fully tanned material is a more covalently linked network.

Scanning electron microscopy of fractured cuticle showed that there was not a particularly weak microstructural feature that failed first. The fracture occurred through the hexagonal pattern as well as along the edges of the hexagons, within the 'glue,' regardless of the stage of tanning or soaking in formic acid. Elytra that were soaked in formic acid did tend to tear more gradually rather than abruptly fracturing, however. The reason is not clear, but the more

abrupt failure may be due to the cooperative breaking of non-covalent interactions which were not present in formic acid treated elytra. Raman analysis was also unable to detect any chemical heterogeneity on the surface of the elytron. The peaks in the Raman spectra were associated with vibrations of chitin and proteins. The amide I and amide III bands showed that random coil and α-helical conformations were dominant in the cuticle proteins. Further studies may give a more detailed picture of the protein structure. For example, a previous study on soft cuticle structures performed Raman spectroscopy on intact cuticle and cuticle in which the proteins had been extracted [32]. The difference of the two spectra was taken to show the cuticle protein vibrations in the native state [32]. Their results showed that the soft cuticle proteins were predominantly antiparallel β-pleated sheet and the conformation was assumed to control the protein's interaction with chitin [32]. From the results obtained here for elytral cuticle, no observable differences were identified in the spectra whether inside the hexagonal pattern or within the 'glue.' To detect differences among the layers of cuticle, *Tenebrio* must be sectioned within an embedding medium that does not interfere with the Raman spectra.

4.6 Conclusions

Both covalent and non-covalent interactions were hypothesized to play an important role in stabilizing cuticle as an insect matures. The importance of covalent crosslinks within elytral cuticle was verified by measuring the dynamic mechanical properties at lower frequencies and higher temperatures. Even at very low frequencies, the storage modulus of fully tanned and dried cuticle depended less on frequency ($n = 0.013 \pm 0.004$), than untanned and dried cuticle ($n = 0.050 \pm 0.024$). The untanned cuticle most likely contains some covalent crosslinking because the storage modulus did not drop off to low values at very low frequencies, as would occur in an

uncrosslinked material. However, the untanned cuticle still had a higher frequency power law exponent even in the lower frequency range, suggesting it was less crosslinked. Additionally, increasing the temperature of fully tanned elytra to 150°C slightly decreased the stiffness and increased viscous energy dissipation, but no peak in tan δ indicating a thermal transition was observed before it degraded, suggesting it is a highly crosslinked material. The findings reaffirm the conclusion that fully tanned cuticle is more highly crosslinked than untanned cuticle, thus supporting the quinone tanning hypothesis.

The amount of material that could be extracted by swelling in non-covalent bond breaking solvents was higher for partially tanned elytra than fully tanned elytra, most likely reflecting the lower degree of covalent crosslinking within the lower layers of partially tanned elytra. Formic acid did make elytra less stiff and more ductile, showing the importance of non-covalent crosslinks, particularly hydrogen bonds, in cuticle stability. A major contribution of non-covalent interactions appeared to be providing stiffness without sacrificing toughness. However, the importance of covalent crosslinking was not diminished, since fully tanned elytra had significantly higher stiffness and strength than untanned elytra even after breaking up the non-covalent bonds. Fully tanned and partially tanned elytra that were treated with formic acid did not have significantly different mechanical properties, suggesting that, within the load bearing layers of cuticle, there was a similar degree of covalent crosslinking but differing degrees of non-covalent crosslinking. Non-covalent interactions were likely more abundant in the fully tanned, less hydrated elytra. Overall, both covalent and non-covalent crosslinks were found to have an important role in stabilizing the elytral cuticle. Covalent crosslinks increased the stiffness and decrease the time dependence of the material response within 48 hours after the material was secreted from the epidermal cells. The molecular connectivity provided by the

covalent crosslinks is likely critical to protect the insect from injury and possibly to serve as a framework for further assembly of superstructures stabilized via non-covalent interactions. The major contribution of non-covalent interactions, which can dissipate more energy than covalent interactions, appeared to be providing added stiffness and strength without sacrificing toughness.

PART 3: ISOLATION AND EXAMINATION OF KEY HYPOTHESIZED MOLECULAR INTERACTIONS WITHIN INSECT CUTICLE

CHAPTER 5: DIRECT EVIDENCE FROM MICRORHEOLOGY OF COMPLEXATION BETWEEN CHITOSAN AND CPR27, A *TRIBOLIUM CASTANEUM* RR CUTICLE PROTEIN

5.1 ABSTRACT

CPR27 is an abundant protein in the rigid cuticle of the beetle elytron. It contains the Rebers-Riddiford (RR) motif, which is hypothesized to be involved in chitin binding. However, a full length protein binding to chitin has not been explicitly shown and the mechanical influence of the binding is not clear. This study used microrheology to provide evidence of CPR27 complexation with chitosan. The addition of CPR27 to fluorescent chitosan solutions caused a 2-fold drop in viscosity as well as the appearance of fluorescent microparticles, suggesting that complexation led to the formation of insoluble aggregates. The effects were not observed with a non-RR protein, CP30. Thus, the hypothesized binding of RR proteins to chitin was supported. Additionally, microrheology was shown to be a valuable tool for monitoring viscosity changes and simultaneously visualizing the microstructure of solutions using limited quantities of recombinant protein.

5.2 INTRODUCTION

The nature of protein-polysaccharide interactions is an important area of study within the biomedical, pharmaceutical and food science industries [275, 276]. Naturally occurring polymers such as proteins and polysaccharides are excellent building blocks for materials in a wide variety of applications, but understanding the molecular interactions and structure-property relationships is critical to achieving the desired function. A promising strategy for developing

new and improved materials is biomimetics [11, 131, 277-283]. In particular, insect cuticle, which is one of the most widespread biological materials in nature, is an interesting model for biomimetic material design because it has very robust yet versatile properties. Different types of cuticle can have drastically different mechanical properties even though they are made of largely the same limited set of organic materials. Thus understanding the interactions that govern such properties is an important goal in biomaterials research and may lead to the development of novel synthetic materials. The goal of this work was to investigate the interaction between chitosan and a particular type of cuticle protein, which is hypothesized to bind to chitin and contribute to the mechanical stability of the insect exoskeleton.

Cuticle is a composite material made of chitin nanofibers embedded in a matrix of proteins and hydrophobic pigments. Chitin makes up 20-50% of the cuticle dry weight [284]. It is arranged in 18-21 antiparallel chains bundled into nanofibers about 3 nm in diameter [284]. The chitin nanofibers are secreted from the crests of microvilli on the epithelial cell membrane, while the protein matrix is secreted from the grooves between each crest [232]. Therefore, the chitin fibers are surrounded by protein matrix, allowing for many stabilizing interactions between the two components. The hypothesized interaction between the chitin fibers and protein is illustrated in Schematic 5.1, where certain proteins wrap around the chitin chains and are stabilized by hydrogen bonds and aromatic interactions. Chitosan, a derivative of chitin, is also present in cuticle and has been useful in a variety of biomedical applications [285-287]. Chitosan is formed by some degree of deacetylation of chitin, which makes it soluble in acidic conditions. The use of chitin and chitosan in structural materials is limited. In fact, most chitinous structural materials have been developed for biomedical applications due to the biocompatibility, not the mechanical characteristics [1]. A more broad use of chitinous materials

in structural applications would require a more thorough understanding of how nature uses these materials to achieve remarkable material properties, especially through interactions with proteins [1].

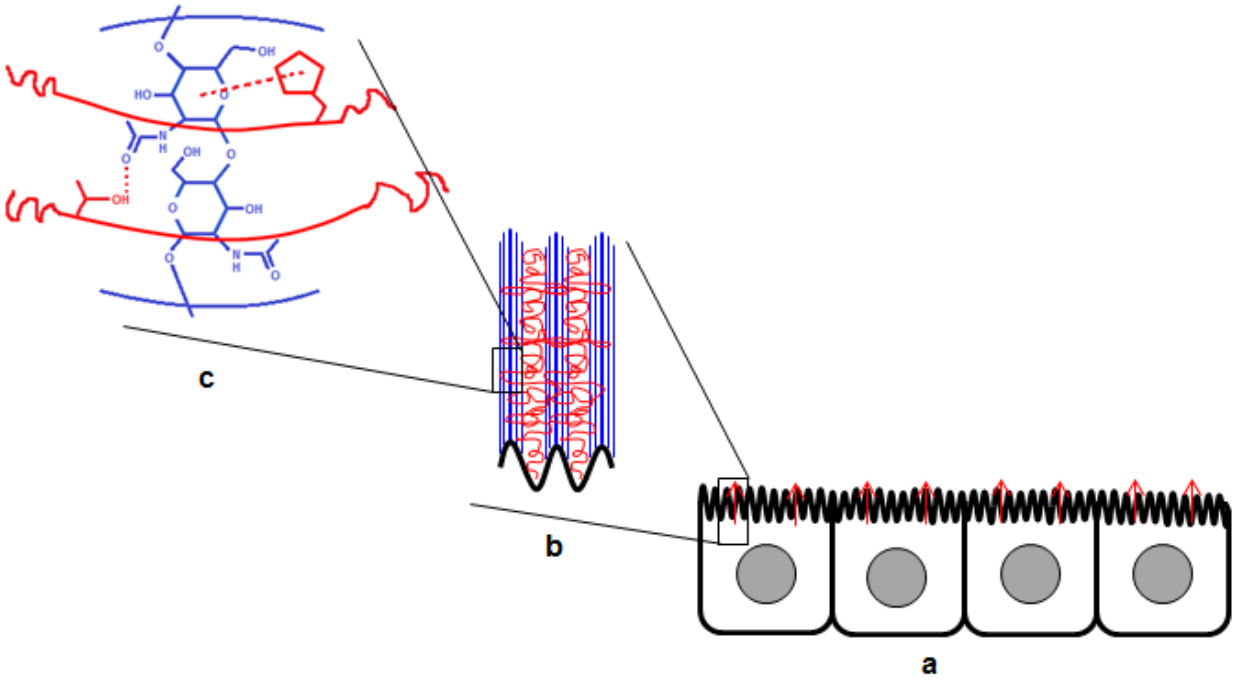

Schematic 5.1. a) Cuticle is secreted from epithelial cells. b) Chitin fibers (blue) are secreted from the crests of microvilli on the apical cell membrane. The protein matrix (red) is secreted from the grooves. c) Certain proteins are hypothesized to form specific interactions with the chitin fibers, contributing to the stability of the cuticle material.

Many different types of proteins have been identified in cuticle. Several conserved regions within those proteins have been found which are responsible for common functions in cuticles from even distantly related species [25]. One such region is called the Rebers-Riddiford (RR) motif, a 28-residue consensus sequence that is involved in chitin binding [26-29, 288]. The nature of the binding is unknown, but a paper using homology modeling suggested that the protein forms an anti-parallel β-sheet with a cleft structure in which the saccharide rings of the chitin chains stack against hydrophobic aromatic residues on the protein [31]. Direct experimental evidence of protein-chitin binding, as well as its mechanical influence, is lacking.

Binding of protein fragments to chitin beads has been shown experimentally, but the binding may not be reflective of *in vivo* chitin binding [28, 288]. The conformation and behavior of the protein most likely depend on the entire sequence. The terminal regions of the protein that flank the RR region are thought to be folded within the spaces between chitin fibers and may link to non-RR proteins to form a unified network [28]. Those domains not directly involved in chitin binding may nevertheless place constraints on the chitin binding region that affects the nature of binding. Also, the protein may interact differently depending on the state of the chitin or chitosan. Subtle difference in the opportunity for hydrogen bonding or stacking of aromatic residues may exist for individual chitin chains, chitin beads, chitin nanofibers or chitosan chains. This study uses rheological measurements of chitosan and a full length RR cuticle protein coupled with microscopy to provide direct evidence of binding. The hypothesis was that the RR protein would induce a change in the viscosity of chitosan solutions and simultaneous visualization of the solutions would verify that complexation occurred.

The two proteins used in this study come from the model insect, *Tribolium castaneum*, or the red flour beetle, which is one of the most widely studied insects from which many cuticle protein sequences have been obtained [289-291]. CPR27 is a 10 kDa RR protein found in the rigid elytra (modified forewings) of *Tribolium castaneum*. It was identified as a major structural protein that is abundant in rigid cuticle but not in flexible cuticle [290]. Furthermore, RNA interference of CPR27 expression led to weak and deformed elytra, suggesting that the protein plays an important role in cuticle structural integrity [290]. CP30 is a 19 kDa protein with low sequence complexity and contains alternating blocks of positive and negative residues in the center of the protein. It is also very abundant in the elytra of *Tribolium castaneum*, but it does not have an RR motif, so it would not be expected to bind chitin. Thus, CP30 acts as a control

for the chitin binding experiments with CPR27. The amino acid sequences of CPR27 and CP30 are shown in Figure 5.1. We have measured the changes in rheological properties of *in vitro* solutions of chitosan with each type of cuticle protein, CPR27 and CP30.

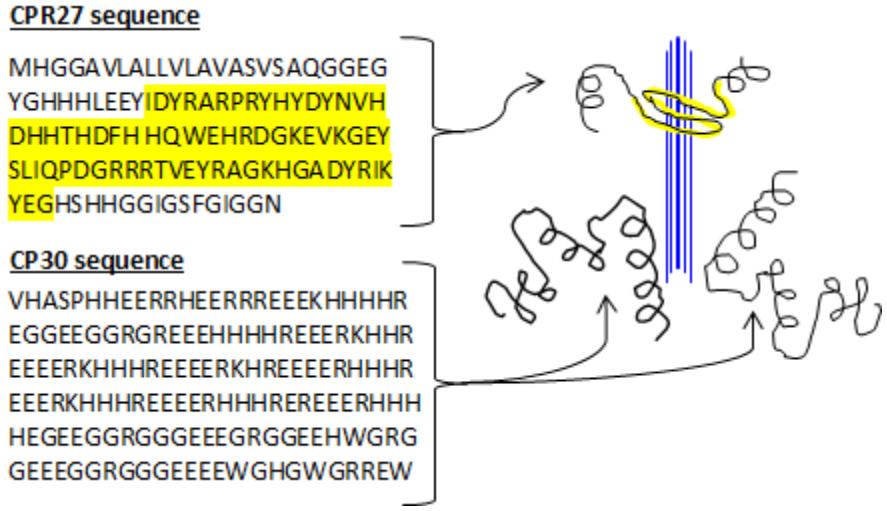

Figure 5.1. Amino acid sequences of CPR27 and CP30. The RR region of CPR27 is highlighted in yellow and is hypothesized to bind to chitin (depicted in blue) via hydrogen bonds and aromatic interactions. CP30 does not have an RR region and is not expected to interact specifically with chitin.

5.3 Materials and Methods

5.3.1 Materials

High purity chitosan was purchased from Sigma-Aldrich. The viscosity average molecular weight was between 140 and 220 kDa and degree of acetylation was less than or equal to 40 mol%. A different, low molecular weight chitosan with a FITC-label (named KITO-3) was purchased from Akina, Inc. (West Lafayette, Indiana).

CPR27 was identified as an important structural protein in the elytra of *Tribolium castaneum* by Arakane *et al*. [290] and CP30 was identified as the third most abundant protein in the elytra of *Tribolium castaneum* by Dittmer *et al.* [291]. In Dr. Michael Kanost's research lab in the Department of Biochemistry and Molecular Biophysics at Kansas State University,

plasmids containing the cDNA for each protein were constructed using RT-PCR. The plasmids were used to transform *Escherichia coli* and the bacteria were grown in LB medium. Expression of the proteins was induced by adding IPTG (isopropyl-beta-D-1-thiogalactopyranoside). The cells were lysed by sonication and the proteins were purified first on a nickel column and then on an anion exchange column.

5.3.2 Solution Preparation

The solvent used for rheological measurements of chitosan was 0.3 M acetic acid/ 0.05 M sodium acetate. The solvent used for KITO-3 was 0.2 M acetic acid/ 0.2 M sodium acetate (pH 5).

Stock solutions of the lyophilized cuticle proteins, CPR27 and CP30, were prepared by dissolving them in sodium acetate buffer (pH 5 and 4 respectively) at 6 mg/ml. The stock solution was added to chitosan solutions in equal volumes to achieve a final concentration of 3 mg/ml protein.

5.3.3 Active Microrheology

Microrheology measures the viscoelastic properties of fluids at micrometer length scales by optically monitoring the motion of probe particles within the fluid [292-295]. The rheological behavior is closely related to the organization and interactions within the fluid [296-298]. Passive microrheology tracks the Brownian motion of probe particles and is, therefore, sensitive to low viscosities and does not risk disrupting the microstructure of the fluid [298, 299]. Active microrheology tracks the forced motion of probe particles by an external electric or magnetic field and can, therefore, measure higher viscosities and can reduce measurement times [296].

Since this study aimed to examine the viscosity of concentrated chitosan solutions with high viscosities, active microrheology was used.

Active microrheology was performed by suspending nickel nanorods in the sample and applying a pair of external magnetic field, 90° apart, to rotate the nanorods. Only a small volume of sample was needed (20 μl) for each experimental condition since the sample was loaded within a small well made from PDMS sandwiched between two glass slides. The nanorods were initially aligned with one magnetic field until time t=0, when the first magnetic field was turned off and a second magnetic field perpendicular to the original field was turned on (see Figure 5.2a). Therefore, the nanorods rotated from 90° to 0° with respect to the second applied field (H), at a speed dependent on the solution viscosity. The rotation of the nanorods was monitored by a CCD Andor Luca video camera attached to a Leica DM 2500M microscope. The videos were converted to images from which the angle of the nanorods could be measured with respect to time using Image J software.

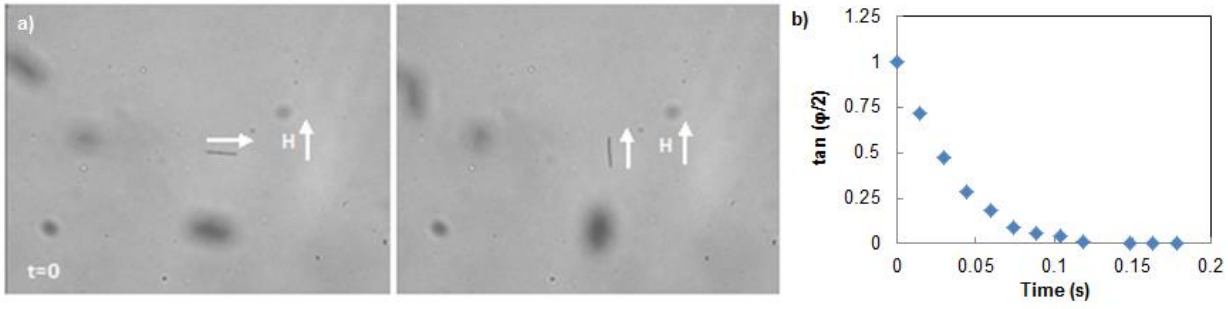

Figure 5.2. a) The magnetic nanorod rotates to align with the applied magnetic field H. b) A plot of the angle of the rod with time allows for the calculation of the relaxation time.

The solution viscosities were calculated by first looking at a balance of the viscous and magnetic torques: $\mu_o mHsin\varphi = -f_r \eta l^3 d\varphi/dt$, where $\mu_o m$ is the magnetic moment, H is the

magnitude of the magnetic field, φ is the angle of the rod with respect to the applied magnetic field, f_r is drag coefficient, η is the viscosity of the solution, and l is the length of the nanorod [296]. The solution to the equation is: $\tan(\varphi/2) = \exp(-t/\tau)$, where $\tau = f_r \eta l^3/\mu_o mH$ is the relaxation time [300]. Thus, by plotting the angle of the rod versus time, as shown in Figure 5.2b, and fitting the data to an exponential decay function, we calculated the relaxation time. The viscosity was then calculated from: $\eta = \tau \mu_o mH/f_r l^3$. This equation can be rewritten in terms of the magnetic field, B (=$\mu_o H$), and the magnetization, M (= m/V, where $V$is the volume of the nanorod). In this case, $\eta = \tau BMV/f_r l^3$. The magnetic field, B, was measured for each experiment using a Gauss meter. The magnetization, M, was averaged from a set of calibration experiments performed on water. The volume and length of the nanorods are also measured for each experiment. The drag coefficient, f_r, is found from the equation: $f_r = \pi/(3(\ln\left(\frac{2l}{d}\right) - 0.8)$, where d is the diameter of the nanorod.

5.3.4 Fluorescence Microscopy

Fluorescence microscopy was used to monitor KITO distribution directly after rheological measurements. An upright fluorescence microscope (Leica DM 2500M) with an extra working distance lens was used at 40x magnification. An 89 North PhotoFluor II 200 W Metal Halide lamp with an excitation wavelength of 500 nm was used as the fluorescent light source and 358-461 nm filters were used to capture the emission. Images were taken with an Andor Luca camera.

5.3.5 Statistical Analysis

Statistical analyses were performed using two tailed, paired t-test in Excel. Statistical significance was detected as $p < 0.05$. Quantitative results were expressed as average ± standard deviation with sample sizes ≥ 4.

5.4 Results

5.4.1 Active microrheological measurements of viscosity

The viscosity of chitosan as a function of concentration is shown in Figure 5.3a. The viscosity increased with increasing concentration. The power-law dependence of viscosity on concentration was typical of polyelectrolyte solutions in excess salt, in which viscosity scales with concentration according to: $\eta \propto C^m$, where m is around 1.25 in the semidilute unentangled region and 3.75 in the semidilute entangled region [301]. The power law exponents for chitosan were 1.21 ± 0.10 and 3.87 ± 0.08 in the semidilute unentangled and semidilute entangled regions, respectively. As shown in Figure 5.3a, the overlap concentration (c*), found from the inflection point marking the transition between the unentangled and entangled regions, was about 5.5 mg/ml.

Next, the viscosity of the fluorescent chitosan, KITO-3, was measured with and without the addition of 3 mg/ml CPR27. As shown in Figure 5.3b, without the protein, KITO-3 viscosities increased with increasing concentration. Here, the power law exponents were 0.26 ± 0.09 and 2.24 ± 0.20 in the semidilute unentangled and semidilute entangled regions respectively. The c* was about 82 mg/ml. With the addition of CPR27, the viscosities of KITO-3 solutions were reduced in the semidilute entangled region (the average viscosities of KITO-3 at 200, 250 and 300 mg/ml were significantly reduced with protein). The power law exponent in

the semidilute entangled region was also lowered to 1.37 ± 0.08. The data in Figure 5.3b is also presented on a linear scale in the appendix.

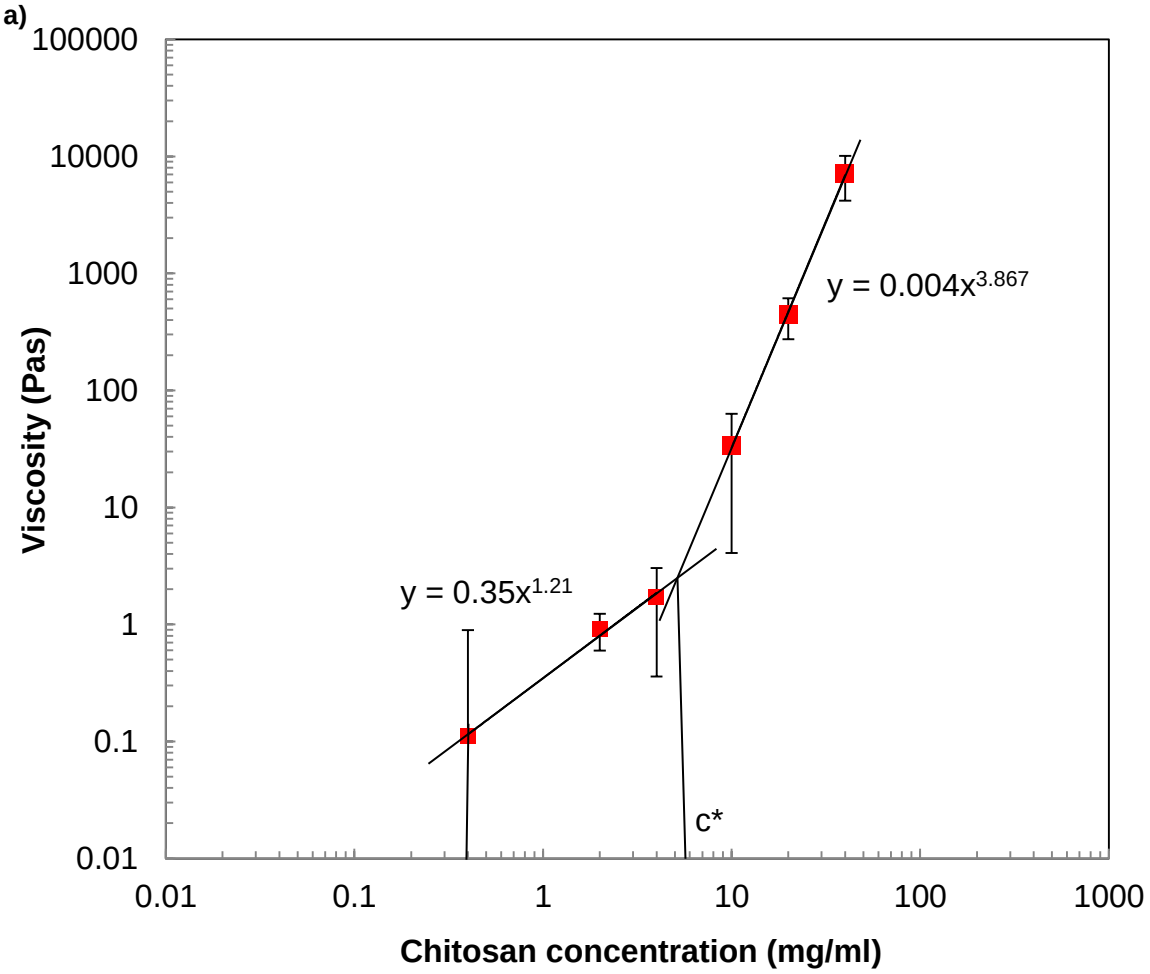

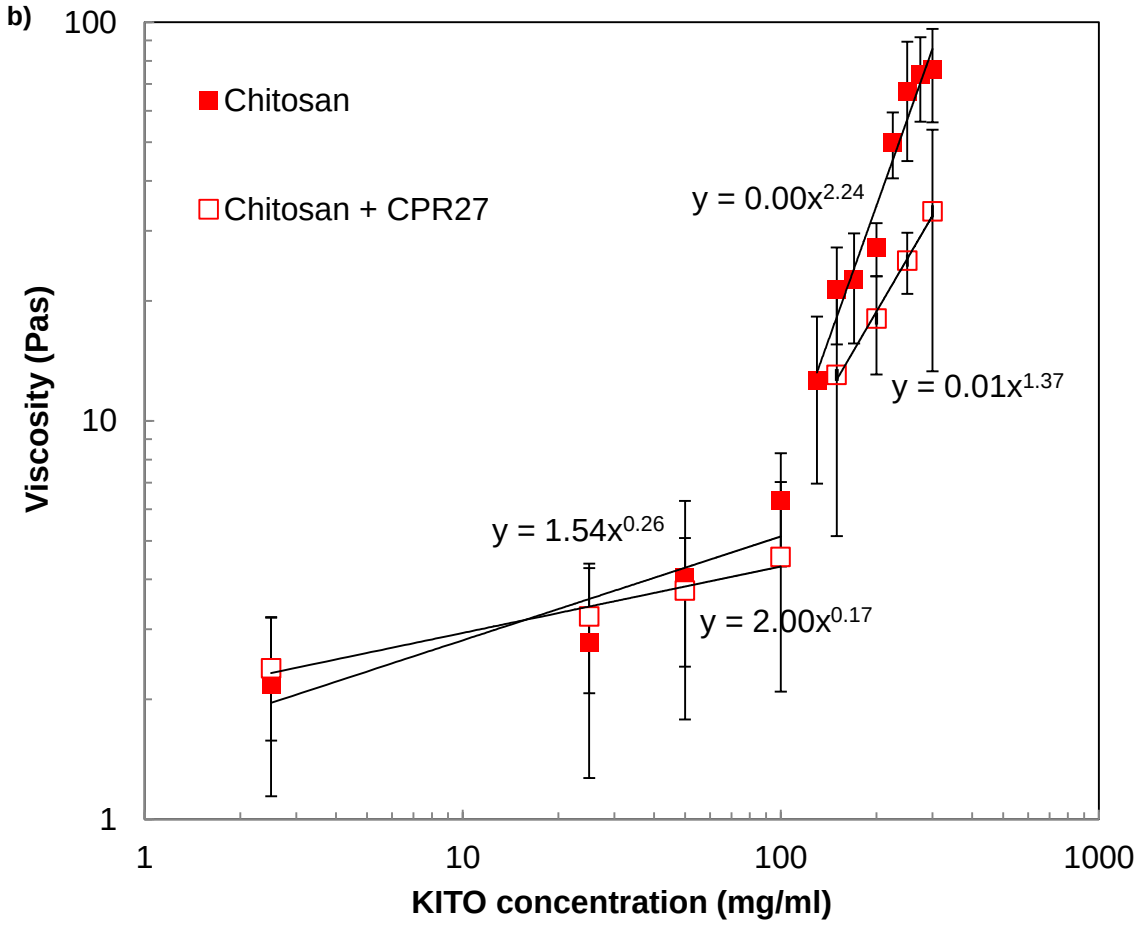

Figure 5.3. a) Dependence of viscosity on concentration for chitosan solutions. b) Dependence of viscosity on concentration for KITO solutions with and without 3 mg/ml CPR27. The protein caused a drop in viscosity at the higher chitosan concentrations. The solvent was 0.2 M acetic acid/ 0.2 M sodium acetate (pH 5). The isoelectric point of chitosan and CPR27 are about 6.5 and 6.72, respectively. Error bars are standard deviations with sample sizes ≥ 4.

Since protein quantities were limited and since CPR27 had the greatest effect on KITO-3 viscosities at the higher KITO-3 concentrations, the effect of CP30 on KITO-3 was tested as a control at the highest KITO-3 concentration. The KITO-3 and CP30 viscosity measurements were made in the same buffer, but at pH 4 because the solubility of CP30 goes down at pH 5-6. When 3 mg/ml CP30 was added to 300 mg/ml KITO-3, there was not a reduction in viscosity, as there was with CPR27. Figure 5.4 shows that the viscosity of a 300 mg/ml KITO-3 solution was

reduced over two times when CPR27 was added (same data as shown in Figure 5.3), but was not significantly reduced when CP30 was added.

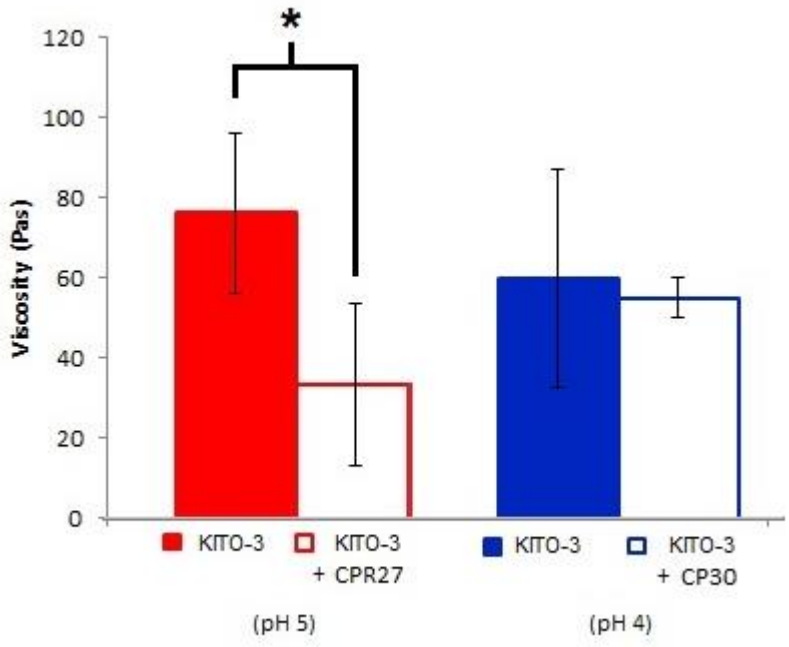

Figure 5.4. The effect of adding 3 mg/ml protein to 300 mg/ml KITO-3 solutions. CPR27 causes a significant reduction in viscosity whereas CP30 does not alter the viscosity. The isoelectric points of chitosan, CPR27 and CP30 are about 6.5, 6.72 and 5.82, respectively. Error bars are standard deviations with sample sizes ≥ 4. The star denotes statistical significance detected as $p \leq 0.05$.

5.4.2 Fluorescence Imaging of Complexation

Fluorescence images of KITO-3 solutions are shown in Figure 5.5. Plain KITO-3 solutions showed a constant, overall fluorescence throughout the solution. With the addition of CPR27, however, bright regions of fluorescence appeared within the solutions. The addition of CP30 did not cause the formation of bright fluorescent regions.

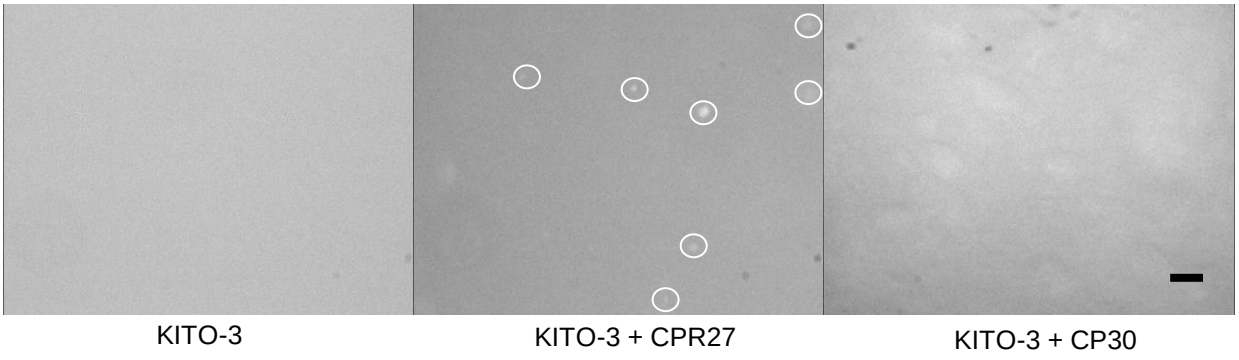

Figure 5.5. KITO solutions have an overall fluorescence. In the presence of CPR27, KITO solutions have bright spots of concentrated fluorescence, suggesting complexation. In the presence of CP30, there are no bright spots to indicate complexation. Scale bar = 20 μm.

5.5 Discussion

This study used microrheology and fluorescence microscopy to provide direct evidence of complexation between chitosan and CPR27, an RR cuticle protein. Validation of the microrheological testing method was accomplished using the higher molecular weight, unlabeled chitosan. The increase in viscosity with concentration fit with a power law model where the viscosity of polyelectrolytes in excess salt is expected to scale with concentration to the power m, where m is around 1.25 in the semidilute unentangled region and 3.75 in the semidilute entangled region [301]. At low concentrations, the viscosity is less sensitive to the concentration because the polymer chains are far apart. At the overlap concentration, or the point at which individual chains begin to contact one another, the viscosity increases more rapidly because of entanglements between the crowded polymer chains [302]. Entanglements slow the motion of polymer chains by restricting it to reptation, or a snake-like motion along the polymer's own contour [303]. The power law exponent for the chitosan data shown in Figure 5.3a was 1.21 ± 0.10 in the semidilute unentangled region and 3.87 ± 0.08 in the semidilute entangled region, which was an excellent fit to the scaling theory, thus validating the methods.

The lower molecular weight, FITC-labeled chitosan (KITO-3) was used for experiments testing the complexation with cuticle protein for two reasons. First, it is water soluble and therefore required a less acidic solvent for dissolution than higher molecular weight chitosans, which is important for the stability of the cuticle proteins in solution. Second, the fluorescent tag on the chitosan allowed for simultaneous visualization of the complexation together with the rheological measurements, thus reinforcing the interpretation of each type of data.

The viscosity of KITO-3 was measured over a range of concentrations from 2.5-300 mg/ml using active microrheology. The concentrations were chosen to span the range of KITO-3 solubility in the sodium acetate buffer at pH 5, which was the highest pH possible for the solubility of CPR27. Without the protein, the viscosity of KITO-3 increased up to a critical concentration, after which it increased even more rapidly with concentration. That critical concentration was about 82 mg/ml, which is a reasonable match with the prediction of c* based on the intrinsic viscosity. The c* can be estimated from the intrinsic viscosity, by assuming that, in the dilute region, each polymer coil affects viscosity as would a hard sphere with a radius equal to the coils' radius of gyration, which is reasonable because hydrodynamic interactions limit solvent flow within the coils [304]. Therefore, using the Einstein equation, which describes the viscosity of hard sphere suspensions ($\eta_0 - \eta_s = 2.5\eta_s\phi$) and the definition of intrinsic viscosity, the intrinsic viscosity can be related to concentration by: $[\eta]_0 = \frac{2.5\phi}{c}$. Since the spheres are expected to overlap at about ϕ=0.40, the c* can be estimated as: $c^* \cong \frac{1}{[\eta]_0}$. Based on the intrinsic viscosity of KITO-3 (0.058 dL/g), the c* should be roughly equal to 172 mg/ml. Other sources state that c* should fall between $\frac{0.5}{[\eta]}$ and $\frac{2}{[\eta]}$ [305], which means the c* of KITO-3 should be around 86-345 mg/ml. The c* measured here for the KITO-3 without protein (82

mg/ml) is at the low end of this range, so the reasonable agreement with theory provides validation of the experimental method.

The power law exponents above and below the c* were 0.26 ± 0.09 and 2.24 ± 0.20 respectively. These are lower than theory suggests for polyelectrolytes in the semidilute unentangled and semidilute entangled regions, in which the power law exponents are expected to be 1.25 and 3.75. The low exponents can most likely be attributed to low molecular weight of the KITO-3. While the exact molecular weight of was not provided by the manufacturer, it can be estimated from the Mark-Houwink equation. Based on the intrinsic viscosity (0.058 dL/g), the degree of acetylation (15-25%), and the Mark-Houwink parameters found by Kasaai *et al*. [306], the viscosity average molecular weight is estimated to be about 2125 Da, which translates to about 9 repeat units plus the FITC label. This is well below the molecular weight of most of the polymers used to develop the scaling theories [301]. It is reasonable to think that such a low molecular weight polymer would have a more limited ability to form entanglements, and the viscosity would therefore depend less on the concentration.

Next, the viscosities of KITO-3 solutions with the addition of 3 mg/ml CPR27 were measured and compared to the viscosities of pure KITO-3 solutions. In the presence of CPR27, the viscosities of KITO-3 solutions were significantly reduced at the highest KITO-3 concentrations (200, 250 and 300 mg/ml KITO-3). The reduced viscosity was accompanied by the appearance of bright fluorescent spots around 2-3 μm in size when CPR27 was added to the fluorescently labeled KITO-3 solutions. The reduction in viscosity, therefore, can be attributed to the formation of insoluble complexes which effectively removed some KITO-3 from solution and lowered the viscosity in the vicinity of the microrheology probes. The power law exponent in the semidilute entangled region was also lowered with the addition of CPR27, suggesting that

there were fewer entanglements once the complexation and aggregation of some KITO-3 occurred. The drop in viscosity along with the formation of insoluble aggregates was evidence that the interaction between KITO-3 and CPR27 leads to complexation.

Several other types of protein-polysaccharide complexes have been studied, with differences in the microstructures of coacervates, but the natures of the complexations were mainly electrostatic [307-310]. A study on the coacervation of chitosan and gelatin showed that the complexation between the polysaccharide and protein resulted in phase-separated, heterogeneous solutions with polymer-rich and polymer-poor regions [310]. At higher pH, insoluble complexes began to form, which corresponded to a lowering of viscosity [310], similar to the phenomenon observed here between chitosan and CPR27. The mechanism of binding was charge selective patch binding, in which the ampholyte gelatin had a net positive charged but contained enough negative charge to bind electrostatically to the positively charged chitosan [310].

The influence of electrostatic interactions on the KITO-3 and CPR27 complexation cannot be ruled out. The pKa of the amino group on chitosan is about 6.5, so the KITO-3 would have been positively charged at the pH used (pH 5). The isoelectric point of CPR27 is 6.72, so it would have had a net positive charge as well. However, 6% of the sequence is aspartic acid (pKa = 3.71) and 7% is glutamic acid (pKa = 4.15). Those residues would certainly have some negative charge at pH 5. However, electrostatics was not likely the main factor leading to complexation because CP30, the control, non-RR cuticle protein, did not appear to complex with the KITO-3. The CP30 has a high glutamic acid content, so it should contain some negative charge at pH 4. Therefore, some degree of electrostatic interaction between the positively charged chitosan and negative residues on CP30 would be expected, yet it does not display

evidence of complexation. Figure 5.4 shows that there was no significant drop in the viscosity of KITO-3 with the addition of CP30 as there was with the addition of CPR27. Additionally, Figure 5.5 shows that there were no distinct bright, fluorescent spots seen as evidence of insoluble aggregates forming with the addition of CP30. Quenching of the KITO fluorescence by the CP30 was not likely because FITC emits light at 520 nm whereas the Trp residues on CP30 absorb at 280 nm. The difference in chitosan-binding abilities of the two proteins points to the different roles within cuticle. CPR27, an RR protein that is abundant in rigid cuticle, is thought to stabilize the material by binding the protein network to the chitin fibers. The nature of the chitosan-RR protein interaction is not well understood, but is thought to occur because the RR region forms a β-sheet cleft structure that can wrap partially around a chitin or chitosan molecule, forming hydrogen bonds as well as aromatic interactions between the saccharide rings of the chitosan and aromatic residues on the protein [31]. The CP30, on the other hand, does not have an RR region and likely has a unique structure and function within cuticle that is still unknown.

This study supports the view that RR proteins complex in a specific manner with chitosan, and not just through general electrostatic interactions because the complexation was not observed with a protein capable of electrostatic interaction yet lacking the RR region. The results emphasize the unique biological function of the proteins within insect cuticle. Incorporating the RR motif into biomedical materials is a potentially useful design strategy, especially considering the biocompatibility of chitinous materials [1]. The organization of insect cuticle offers insight into how chitin and chitosan can be combined with protein or polypeptide materials to produce novel biomaterials with improved mechanical properties. In fact, recent studies have shown improved strength and toughness in composites by combining chitin

nanofibers and silk in a biomimetic design [131, 132]. The combination of chitin with RR cuticle proteins or with polypeptides containing the RR motif would be an interesting avenue to explore in the future.

5.6 Conclusions

The first direct evidence of chitosan complexation with a full length RR cuticle protein, CPR27, was shown by microrheology and fluorescence imaging. The addition of CPR27 to a fluorescently labeled chitosan caused about a 2-fold drop in viscosity at higher chitosan concentrations as well as the appearance of bright fluorescent spots within the solution. Together, the results suggest that the protein bound to chitosan, forming insoluble aggregates and lowering the viscosity of the solution. The evidence of complexation was not seen with CP30, indicating that the chitosan binding is specific to RR proteins. The influence of this important binding motif on the rheology of chitosan solutions suggests that it likely has an important role in determining the mechanical properties of insect cuticle as well. It was also found that microrheology is a valuable tool for studying such protein-polysaccharide interactions because it allows for simultaneous visualization of microscopic structure and it uses small quantities of materials that are often available in limited amounts, such as the recombinant cuticle proteins used here. The protein-chitosan binding motif could be an effective approach for the biomimetic design of high performance structural biomaterials.

CHAPTER 6: VISCOELASTICITY OF CUTICLE PROTEINS UNDERGOING SCLEROTIZATION REACTIONS

6.1 ABSTRACT

One of the most important contributors to mechanical stability in sclerotized insect cuticles is thought to be quinone crosslinking of proteins, yet the specific mechanical contribution of these interactions has never been characterized in isolation. Therefore, the rheological testing of cuticle protein solutions undergoing quinone crosslinking reactions was performed in order to establish a link between molecular composition and viscoelastic properties. The hypothesized mechanism of quinone crosslinking consists of catechols that are oxidized by a phenoloxidase to quinones, making them reactive toward multiple protein molecules to form crosslinks. Model reactions involving the catechol, NBAD, the phenoloxidase, laccase, and the cuticle proteins from *Tribolium castaneum*, CPR27 and CP30 were studied using microrheology. The results showed that microparticles were formed within solutions containing protein and laccase, NBAD and laccase, and protein, NBAD and laccase. Passive microrheology suggested that elasticity developed within solutions of CP30 and laccase as well as CP30, NBAD and laccase. Elasticity in solutions containing protein, NBAD and laccase may have been caused by quinone crosslinking of proteins, but further work is needed to connect the viscoelastic changes with specific interactions within these model reactions.

6.2 INTRODUCTION

Insect cuticle can have remarkably diverse mechanical properties despite being made of a limited set of components, primarily chitin, proteins, catechols and water [8, 34]. Cuticle is often

classified into either soft or hard cuticle [17]. Soft cuticle, such as the cuticle found in joint regions, is flexible and resilient, allowing for locomotion [18]. Hard cuticle provides structure and protection from injury and is, therefore, hard and stiff [19]. Recent studies have suggested cuticle may be an excellent model for the design of biomaterials [20, 78, 217-220]. The elytron (or the outer wing cover) of beetles is particularly interesting because it is strong, yet lightweight [219, 220, 311]. However, the molecular interactions that govern the mechanical properties in elytral cuticle are not well understood.

Elytra and other hard cuticle structures go through a process known as sclerotization in which the material becomes stiffer and the proteins become less extractable [27, 214, 238]. The widely accepted view of sclerotization is that catechols become oxidized to quinones, a process which is catalyzed by the phenyloxidase laccase and requires oxygen [195, 312, 313]. The catechols identified in insect cuticle are dopamine, N-acetyldopamine (NADA) and N-β-alanyldopamine (NBAD) [16, 191]. The quinones then react with multiple nucleophilic groups such as histidine and lysine on proteins to form covalent crosslinks [191, 249]. An overview of the mechanism is shown in Figure 6.1. While many studies have shown protein-catechol conjugates in cuticle [191, 206, 207, 209, 248, 314-317], no one has proven the existence of a crosslink (two proteins connected by a catechol) due to the inextractable nature of the cuticle. However, cuticle protein crosslinking by catechols has been shown in model reactions *in vitro* [249]. Using SDS-PAGE analysis of *in vitro* crosslinking reactions, Suderman *et al.* showed that enzymatic oxidation of catechols induced the polymerization of cuticle proteins. It was also concluded that the binding was covalent because urea had no effect. The authors stated that the next step was to evaluate the mechanical properties of these model reactions and compare them to cuticle and cuticle-mimetic materials [249, 280]. Covalent crosslinking of proteins via

quinone compounds is thought to confer stiffness and hardness to cuticle, but the link has not been explicitly proven. Additionally, the polymerization of catechols into pigment molecules may also contribute to mechanical properties, but the relative importance of this is not clear. Therefore, the goal of this study was to establish a link between specific cuticle reactions (protein crosslinking and catechol polymerization) and their effects on rheological properties of model solutions *in vitro*.

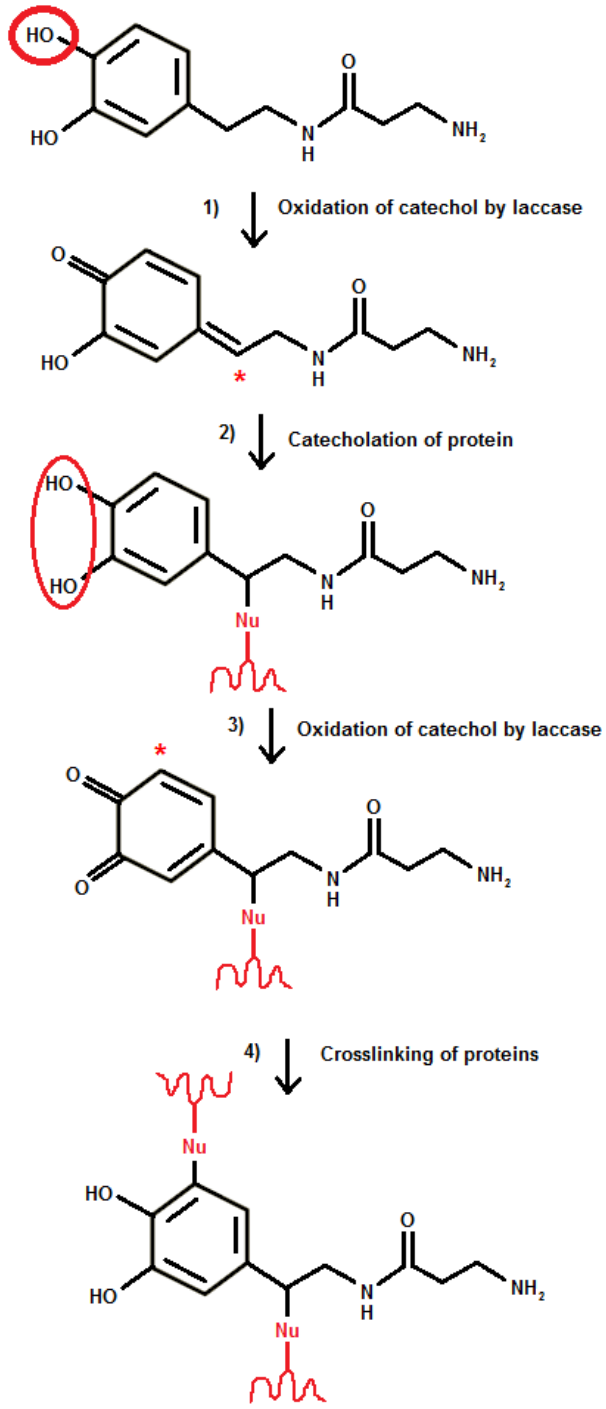

Figure 6.1. Hypothesized crosslinking mechanism of cuticular proteins. In step 1, laccase catalyzes the oxidation of the catechol, NBAD, to a p-quinone methide. In step 2, the quinone reacts with a nucleophilic side chain on a cuticle protein to form a catecholated protein. In step 3, oxidation again occurs to form an o-quinone. And in step 4, the quinone reacts with another protein molecule to form a crosslink.

The model reactions consisted of recombinant proteins from elytral cuticle of *Tribolium castaneum* (CPR27 and CP30), the catechol (NBAD) and the phenoloxidase (laccase). The two proteins chosen were CPR27 and CP30 because they are highly abundant in the elytra of *Tribolium castaneum* and are hypothesized to undergo quinone crosslinking reactions and therefore provide structural stability to the cuticle [290, 291]. CPR27 was identified as an important structural protein in the elytra of *Tribolium castaneum* by Arakane *et al*. [290] and CP30 was identified as the third most abundant protein in the elytra of *Tribolium castaneum* by Dittmer *et al.* [291]. The sequences of CPR27 and CP30 are shown in Figure 6.2. The histidine and lysine residues, which are the strongest nucleophiles and hypothesized to react with quinones, are shown in bold and underline, respectively. Tyrosine residues, which may also react with quinones and may form direct dityrosine crosslinks, are highlighted in grey. Since the recombinant proteins were available in limited quantities, microrheology was used to study the viscoelastic properties of *in vitro* protein solutions undergoing model crosslinking reactions. The main hypothesis was that covalent crosslinking of proteins via enzymatically oxidized catechols would induce elasticity in the solutions. However, the possibility of forming branched polymers or aggregated particles in the dilute solutions studied here were also considered. For example, the frequency at which G’ exceeds G’’ should depend on the molecular weight of the branch arms for branched polymers [318]. Particles in suspension can induce elasticity in a fluid and a higher volume fraction of particles causes the G’ and G’’ curves to shift toward lower frequencies and higher moduli [319].

CPR27 sequence (MW = 10 kDa)

MHGGAVLALL VLAVASVSAQ
GGEGYGHHHL EEYIDYRARP
RYHYDYNVHD HHTHDFHHQW
EHRDGKEVKG EYSLIQPDGR
RRTVEYRAGK HGADYRIKYE
GHSHHGGIGS FGIGGN

CP30 sequence (MW = 19 kDa)

VHASPHHEER RHEERRREEE
KHHHHREGGE EGGRGREEEH
HHHREEERKH HREEEERKHH
HREEEERKHR EEEERHHHRE
EERKHHHHEE EERHHHRERE
EERHHHHEGE EGGRGGGEEE
GRGGEEHWGR GGEEEGGRGG
GEEEEWGHGW GRREW

Figure 6.2. Sequences of CPR27 and CP30. Histidine and lysine, the strongest nucleophiles to possibly react with quinones, are shown in bold and underline, respectively. Tyrosine residues, which may also react with quinones and may form direct dityrosine crosslinks, are highlighted in grey.

6.3 Materials and Methods

6.3.1 Materials

CPR27 and CP30 were expressed in Dr. Michael Kanost's research lab in the Department of Biochemistry and Molecular Biophysics at Kansas State University. Plasmids containing the cDNA for each protein were constructed using RT-PCR. The plasmids were used to transform *Escherichia coli* and the bacteria were grown in LB medium. Expression of the proteins was induced by adding IPTG (isopropyl-beta-D-1-thiogalactopyranoside). The cells were lysed by sonication and the proteins were purified first on a nickel column and then on an anion exchange column.

NBAD was synthesized in the Kanost laboratory according to Yamasaki *et al*. [320]. A 100 mM NBAD stock solution was prepared in 1 mM HCl to prevent auto-oxidation. Fungal laccase (*Pyricularia oryzae*) was purchased from Sigma. The laccase powder was found to contain ~1000 units of activity per 1 mg powder by the Kanost group. A laccase stock solution

of 10 U/µl was prepared by dissolving 10 mgs laccase in 1 ml buffer (50 mM sodium phosphate buffer at pH 5 or 7 depending on the protein). The laccase was also found to contain a protease, so for the passive microrheology experiments, the stock solution was heated at 60°C for 15 minutes to degrade the protease. It was then centrifuged at 16,000 x g for 10 min to remove the insoluble material.

6.3.2 Methods

Passive and active microrheology track the Brownian motion and forced motion, respectively, of probe particles to measure viscoelastic properties of solutions [292-295]. Microrheology provides information on the microstructure as well as the storage and dissipation of mechanical energy in microliter volumes of complex fluids [321]. It has been used to study biological interactions such as the polymerization and crosslinking of proteins, actin filaments, microtubules, and extracellular matrix components [292, 321-330], but has not been used to study cuticle protein interactions.

Active microrheology was used to measure the viscosity of CPR27 solutions as it reacted with laccase or with both NBAD and laccase. Each reactant was used at concentrations that were determined to yield the most efficient crosslinking by Suderman *et al*. (0.16 mM CPR27, 4.4 mM NBAD, and 0.1 U/µL laccase in 50mM sodium phosphate buffer at pH 5) [249]. In the conditions in which a reactant was left out, buffer was used in its place. The active microrheology methods were described in detail in Chapter 5. Briefly, nickel nanorods were suspended in 20 µl samples loaded in a well made from PDMS sandwiched between two glass slides. Perpendicular magnetic fields were used to rotate the rods 90° and the rotation was monitored by a CCD Andor Luca video camera attached to a Leica DM 2500M microscope. The

angle of the nanorods as a function of time as well as the magnetic field were used to calculate the viscosity of the solution.

Since the nanorods were interacting with the solution material, causing heterogeneity and poor reproducibility, passive microrheology was instead used to measure G', G'' tan δ, and viscosity for each reaction condition shown in Table 6.1. CP30 was used since the CPR27 appeared to experience some aggregation during storage. The concentrations were again determined based on the findings of Suderman *et al*. (0.16 mM CP30, 4.4 mM NBAD, and 1 U/μL laccase in 50mM sodium phosphate buffer at pH 7) [249]. CP30 is most soluble at pH 7, and the laccase is less reactive at this pH, so a higher concentration of laccase was used. In the conditions in which a reactant was left out, buffer was used in its place. For each condition, the viscoelastic properties were measured at 0, 0.5, 1, 2, 4 and 24 hr reaction time.

Since microparticles were observed as some reactions took place, image analysis was used to quantify the accumulation of particles. Image J software was used to count the particles as a function of reaction time and measure the average size of the particles. Brightfield images were converted to black and white images by applying a threshold. Particles within a certain range of pixel size and circularity were then counted. Figure 6.2 shows an example. Details of the method are described in the appendix.

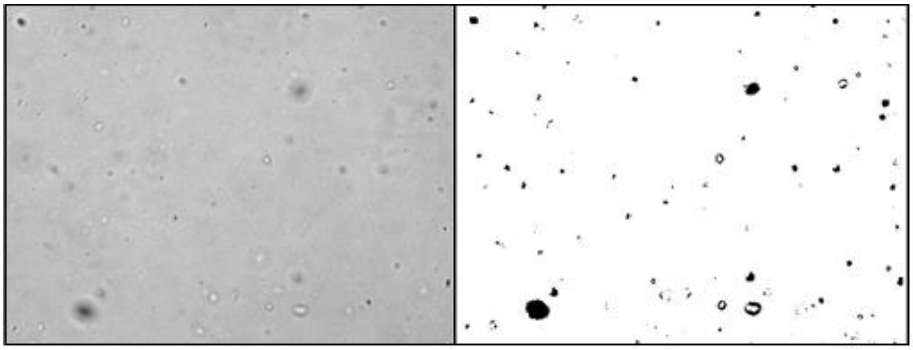

Figure 6.2. Image J was used to count the number of particles in the solution at a given time. A threshold was applied to get a black and white image and then particles within a certain range of pixel size and circularity were counted. In this image, 36 particles were counted with an average size of 41.6 pixels.

Table 6.1. Experimental groups and expected interactions.

Condition	CP30	NBAD	Laccase	Expected Interactions
1 Protein	+	-	-	None
2 Catechol	-	+	-	None
3 Enzyme	-	-	+	None
4 Protein + Catechol	+	+	-	None
5 Protein + Enzyme	+	-	+	None
6 Catechol + Enzyme	-	+	+	Pigment formation due to catechol polymerization
7 Protein + Catechol + Enzyme	+	+	+	Quinone crosslinking, pigment formation

Passive microrheology was performed by monitoring the thermal motion of fluorescent particles in the solution. Specifically, 0.5 µl of a fluorescent latex bead (Polysciences, Inc.) solution (10 µl of 0.1 µm beads in 2 ml buffer) was added to 20 µl solutions of each sample. The thermal motion of the fluorescent particles was monitored in each solution using a CCD AndorLuca video camera attached to an upright fluorescent microscope (Leica DM 2500M). Brightfield images of the particles were taken as well. The videos were converted to frames of images and sent to collaborators in Dr. Eric Weeks' research group in the Department of Physics at Emory University. They have a well-established method for tracking particles, calculating the mean squared displacement of the particles and converting that to viscoelastic moduli using IDL (Interactive Data Language) software (see http://www.physics.emory.edu/faculty/weeks// idl/tracking.html and http://www.physics.emory.edu/faculty/weeks/idl/rheo.html). The mean squared displacement is calculated by tracking the random diffusive motion of the particles. Specifically, the x and y positions of each particle are recorded as a function of time. The displacements are then calculated by taking the difference between the positions at a certain time in reference to the position at an earlier time, $\Delta x = x(t+\tau) - x(t)$ and $\Delta y = y(t+\tau) - y(t)$. The mean squared displacement is then calculated at each time interval by taking the ensemble average of these displacements over all initial times and all particles. That is, $\langle \Delta x^2 \rangle = \sum_{i=1}^{n} \Delta x_i^2 / N$ and $\langle \Delta y^2 \rangle = \sum_{i=1}^{n} \Delta y_i^2 / N$ [331]. The mean squared displacement data can then be used to find viscoelastic moduli as a function of frequency, G'(ω) and G''(ω), through the Generalized Stokes-Einstein equation: $\widetilde{G}(s) = \frac{k_B T}{\pi a s \langle \Delta \tilde{r}^2(s) \rangle}$, where $\widetilde{G}(s)$ is the Laplace transform of G*, s is the Laplace frequency, a is the radius of the tracer particle, and $\langle \Delta \tilde{r}^2(s) \rangle$ is the Laplace transform of the mean squared displacement [321, 332]. The process is illustrated in Figure 6.3.

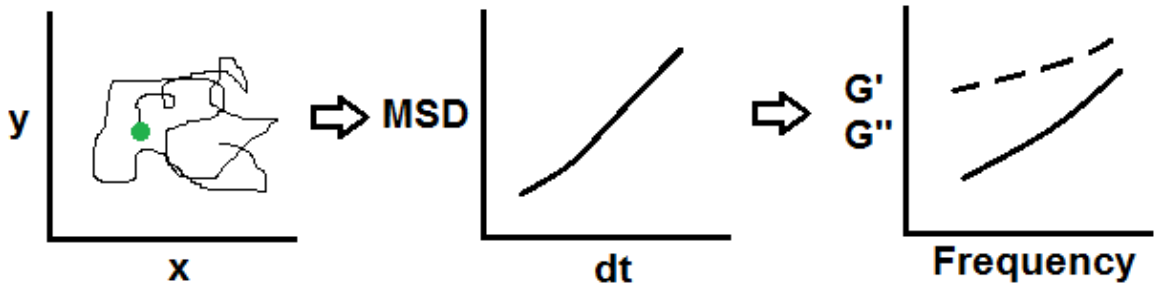

Figure 6.3. Calculating the dynamic moduli as a function of frequency from particle tracking microrheology experiments.

6.4 Results and Discussion

Microrheology was used to determine the rheological behavior of solutions undergoing model cuticle protein reactions. It was hypothesized that cuticle proteins would be crosslinked via enzymatically oxidized catechols, thus affecting the viscoelastic properties of the fluids. Active microrheology was used to measure the viscosity as a function of time for mixtures of CPR27, NBAD and laccase. Results showed that viscosity increased when CPR27 was mixed with laccase and NBAD, as would be expected from protein crosslinking (see Figure 6.4). There was also an even more rapid increase in the viscosity of the CPR27 solutions with just laccase, which was consistent with SDS-page results that suggested that laccase directly induced cross-linking of tyrosine residues on the protein (unpublished data from the Kanost group at Kansas State University). In the presence of NBAD, however, the oxidized NBAD could also react with Tyr side chains on the protein (forming branches rather than crosslinks), and would therefore compete for the tyrosine residues that could otherwise be involved in direct dityrosine crosslinking. Further reaction could allow for the NBAD to link with another protein thus forming a crosslink, but at slower rate than direct dityrosine crosslinking alone. The graphics next to the curves in Figure 6.4 illustrate the different routes to crosslinking.

While these initial results supported the crosslinking hypothesis, attempts to reproduce the data using active microrheology were poor. Visual observation of the solutions under 40x magnification revealed that particles were forming in the solutions and actually aggregating around the microrheology probes, causing considerable heterogeneity (see inset of Figure 6.4). Thus, depending on the amount of material aggregating on a nanorod, viscosity measurements were highly variable. Therefore, subsequent experiments were aimed at quantifying the accumulation of microparticles and measuring the viscoelastic properties using passive microrheology probes which would not interact with the solution material.

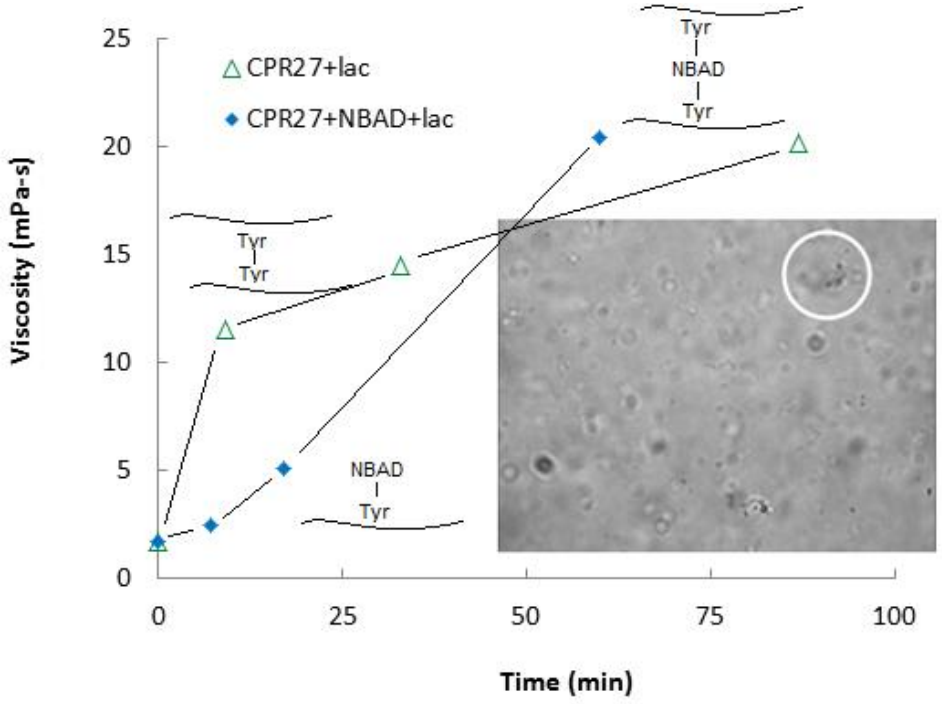

Figure 6.4. Viscosity increased with time for reactions involving CPR27 and laccase as well as CPR27, NBAD and laccase. The slightly faster increase in viscosity for CPR27 and laccase solutions was most likely due to the formation of direct dityrosine crosslinks whereas crosslinking in CPR27, NBAD and laccase solutions had to go through the step of catecholation of the protein before crosslinking. Inset: Material aggregated onto the nanorods (shown in the circle), creating heterogeneity in the solution.

The results of active microrheology experiments on CPR27 reactions were proof of concept that the reactions were causing a significant effect, that is, the formation of particles and

a noticeable change in viscosity, at least locally. Subsequent experiments were performed with the protein CP30 because of the availability of quality material (CPR27 had aggregated somewhat after a few months in storage). The experimental conditions and hypothesized interactions are shown in Table 6.1. Since the formation of microparticles (shown in Figure 6.5) was observed, the number and size of particles were quantified over the first hour of the reaction. The results, shown in Figure 6.6a, show that the number of particles increased with time for both NBAD+lac and CP30+NBAD+lac. The average size of the particles, shown in Figure 6.6b, remained relatively constant (~2.2 μm), suggesting that the particles were not flocculating. In each case, the microparticles most likely included polymerized NBAD pigment molecules, similar to the melanin-like nanoparticles formed from the auto-oxidization of dopamine [333]. The melanin-like nanoparticles in that study were 100-300 nm in diameter, and the size depended on the rate of auto-oxidation of the catechol (higher pH increased the rate of auto-oxidation of dopa) [333]. The particles seen here, presumably polymerized NBAD, were much larger (~2 μm), perhaps because the kinetics of NBAD oxidation by laccase is faster. A more precise way to determine the particle size would be dynamic light scattering, but this method gave us an idea of the particle size with the images that were already available from the microrheology experiments.

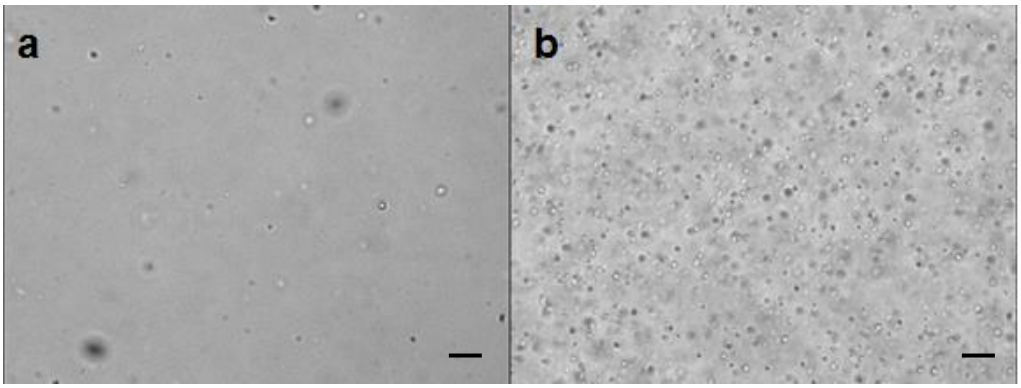

Figure 6.5. Brightfield images (40x) of a solution of 0.16 mM CP30, 4.4 mM NBAD, and 1 U/µL laccase in 50mM sodium phosphate buffer at pH 7 at a) 20 minutes after the start of the reaction and b) 45 minutes after the start of the reaction, showing the accumulation of microparticles with time. Scale bars = 20 µm.

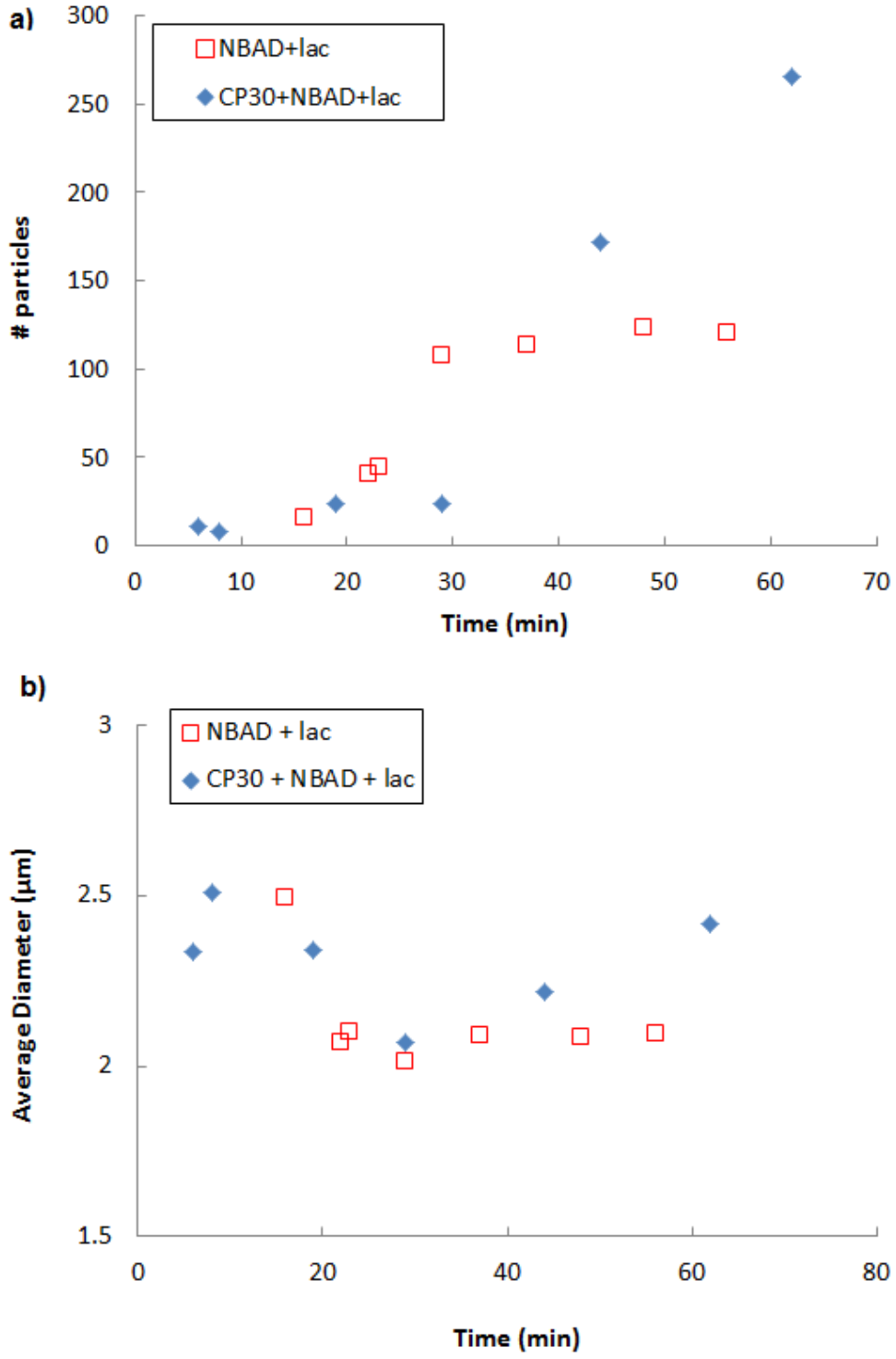

Figure 6.6. Microparticle formation as a function of reaction time. a) The number of particles increased with time for both NBAD+lac and CP30+NBAD+lac. b) The average diameter of the particles remained constant with time.

Passive microrheology was used to monitor changes in the viscoelastic properties of the solutions over 24 hours. For conditions 1, 2 and 3, which contained each reactant by itself, no significant qualitative changes were noted by visually observing the solutions under 40x magnification. For condition 4, with only protein and catechol, no visual changes in solution properties were observed either. No interactions were expected for this condition because there was no enzyme to oxidize the catechol and make it reactive toward itself or the proteins. Figure 6.7 shows qualitative observations for conditions 5 (CP30+lac), 6 (NBAD+lac) and 7 (CP30+NBAD+lac). For condition 5, very small particles formed slowly. After 24 hours, there were many small particles (~1 μm diameter) suspended within the solution. The formation of particles was not expected with just CP30 and laccase because CP30 does not contain any Tyr residues, so laccase-induced dityrosine crosslinking would not be possible for this protein. Thus, the makeup of these particles was unknown. For condition 6, with just NBAD and laccase, larger particles (~1.4-2 μm) were formed and began to settle after a few hours. Most likely, the particles were made of polymerized NBAD molecules which became insoluble after reaching a certain molecular weight. As shown in Figure 6.8, the solution also turned orange in the cases where NBAD and laccase were present. For condition 7 which contained CP30, NBAD and laccase, even larger particles (~ 2.4-2.8 μm) were formed and began to settle within a few hours. The particles were almost completely settled to the bottom of the slide by 4 hours. Since the particles were larger and settled more quickly with the presence of protein, the protein was most likely involved in the reaction. This is consistent with the observations of Suderman *et al*., in which NBAD and laccase caused the polymerization of *Manduca sexta* cuticle proteins in addition to the formation of pigment molecules.

a) CP30+Lac

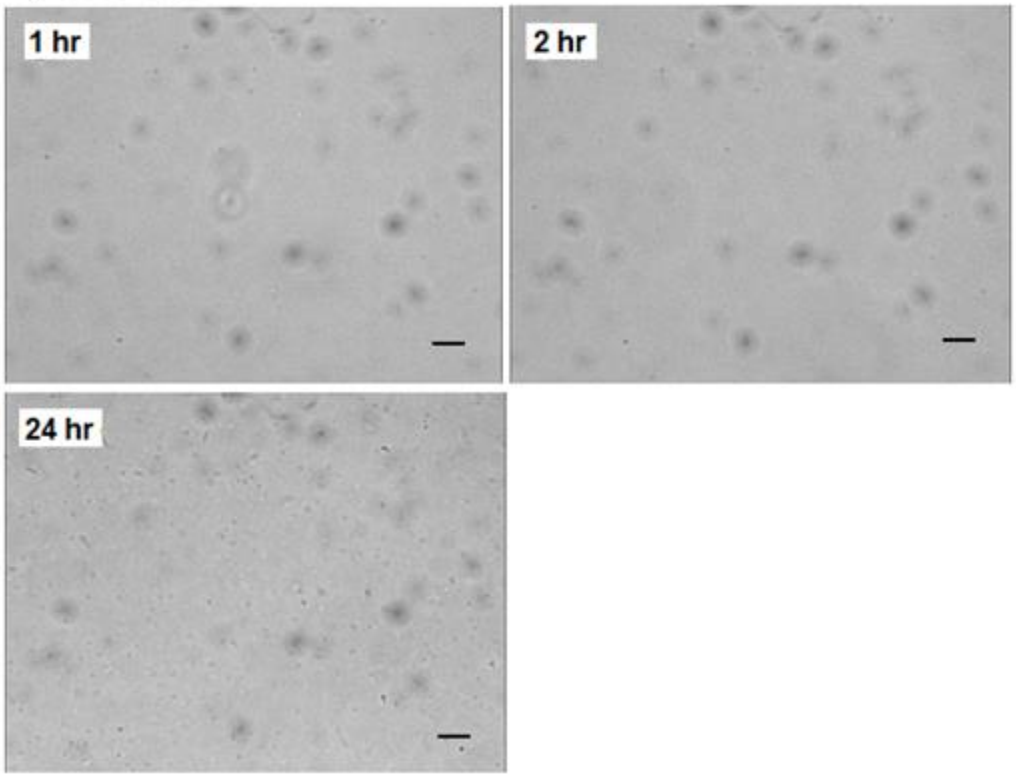

b) NBAD+Lac

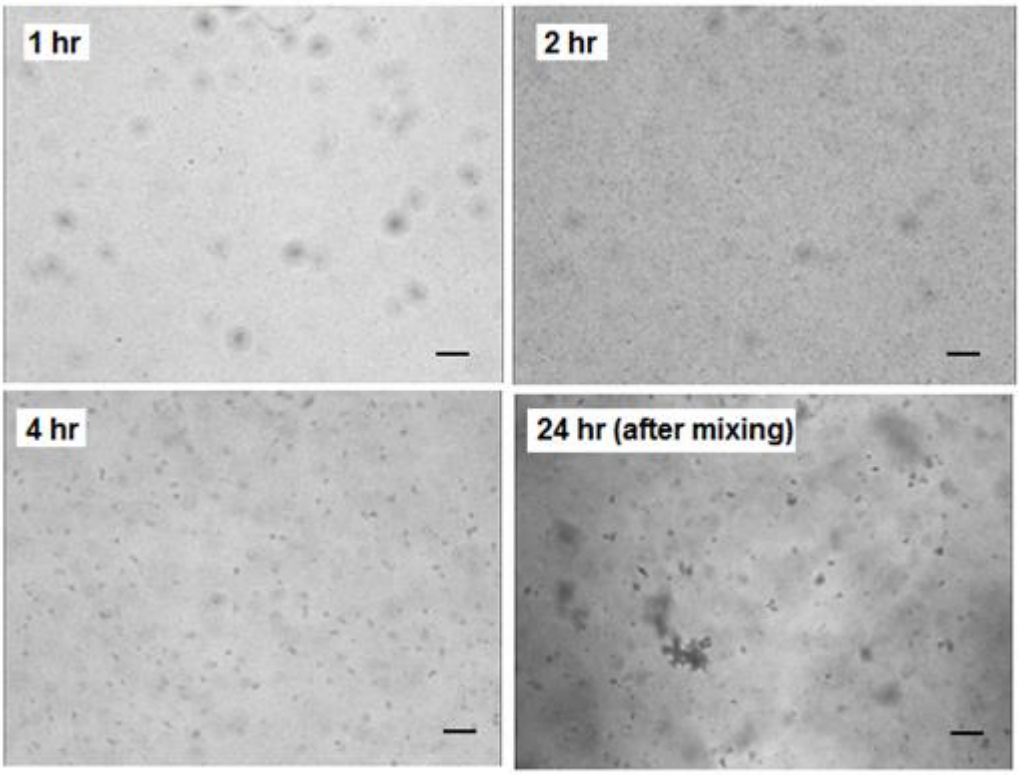

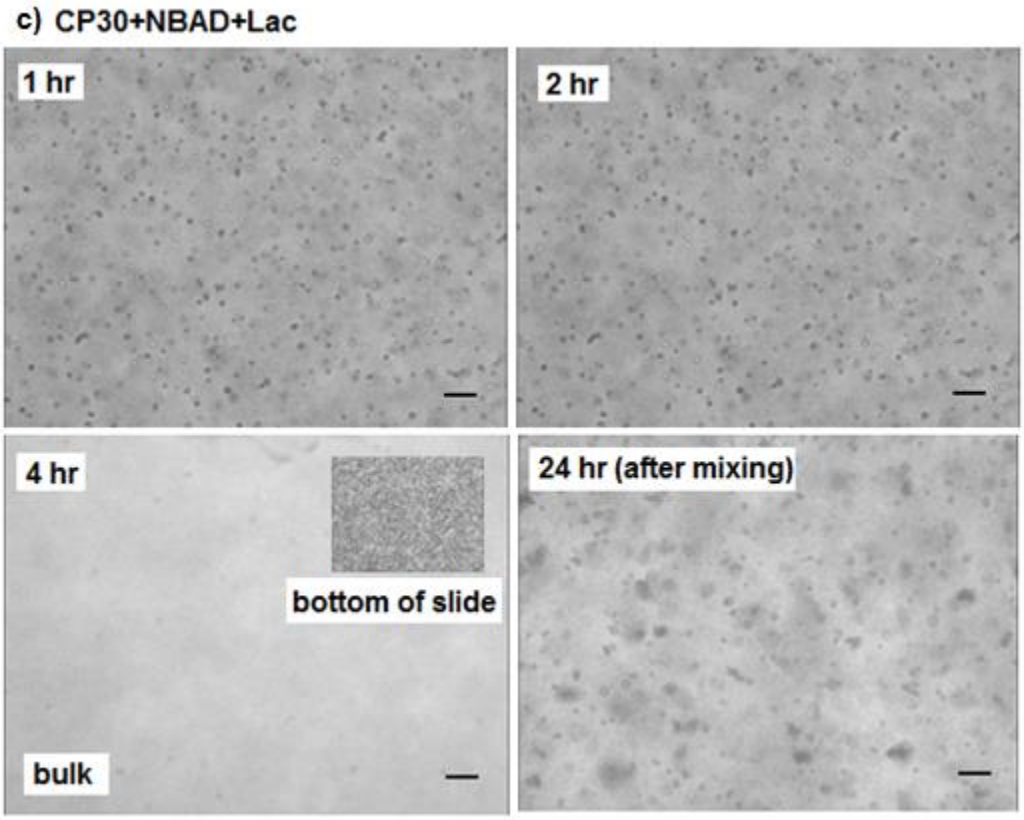

Figure 6.7. Observations of microparticle formation within solutions at 40x magnification. a) For CP30+lac, small particles, ~1µm in diameter, were formed very gradually over 24 hours and remained suspended in solution. b) For NBAD+lac, larger particles, ~1.4-2 µm in diameter, were formed and settled after several hours. c) For CP30+NBAD+lac, even larger particles, ~2.4-2.8 µm in diameter, were formed and settled almost completely within 4 hours. Scale bars = 20 µm.

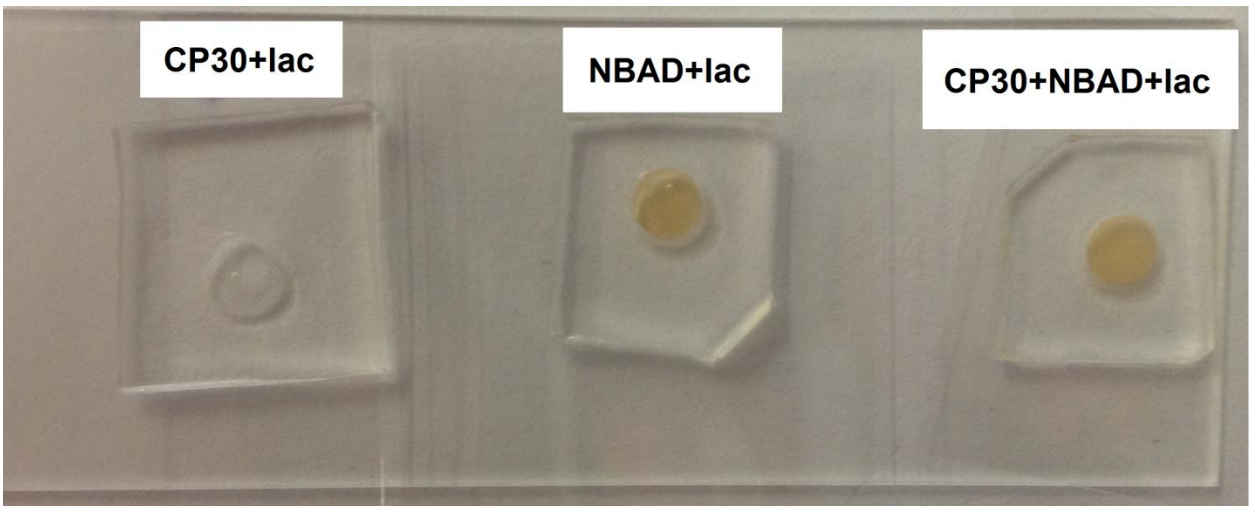

Figure 6.8. Reaction solutions in PDMS molds between glass slide and coverslips (wells are ~2 mm diameter x 1.5 mm depth). After 1 hour, CP30+lac solutions were clear whereas the NBAD+lac solutions and the CP30+NBAD+lac solutions changed to an orange color.

The results from passive microrheology are shown in Figures 6.9 and 6.10. Figure 6.9 shows the MSD of fluorescent latex beads that were added to solutions for each experimental condition. In general, for all the data, there was considerable drifting that could not be completely removed with the particle tracking software. The drifting was found to occur in non-uniform directions for the various particles within a solution. The reason for the drifting was not known, but possibilities include sample heating from the light source, interactions among the fluorescent beads or convection of the sample fluid, possibly from small quantities of solution leaking from the PDMS mold. The drifting primarily affected the slope of the MSD data, making it appear as if the slope was greater than 1 in many cases, suggesting super-diffusive, or forced, motion. Thus the slopes were not considered when interpreting the data. However, the shape of the MSD data could be used to indicate whether elasticity was present in the solution. In general, the MSD of particles diffusing in purely viscous solutions is proportional to time, so the data is linear [321]. However, when an elastic element is added to the system, the time dependence of the MSD is reduced at short times, causing curvature in the data. Therefore, MSD data characterized by a reduced slope at short times indicates viscoelasticity.

As shown in Figure 6.9, no curvature was seen in the control samples, suggesting that they were purely viscous solutions. For CP30+lac solutions, however, some curvature was seen at the end of the reaction. The elasticity corresponds to the formation of many small microparticles within the solutions. The composition of the particles is unknown because the CP30 was not expected to interact with laccase alone because there are no tyrosine residues to enable dityrosine crosslinking reactions. It is known that hard sphere suspensions can make a fluid slightly elastic because the packing of particles prevents purely diffusive motion [319]. Thus, the elasticity in CP30+lac solutions was likely produced by the particles. The NBAD+lac

solutions did not display evidence of elasticity even though microparticles were formed over time. Since the particles in this case were settling, they may not have reached a sufficient volume fraction in the bulk solution to induce elasticity. For the CP30+NBAD+lac solutions, elasticity was seen at 1 hour and 4 hours. Since microparticle formation was similar to the NBAD+lac solutions (larger particles that settled quickly), the origin of the elasticity may not have been from the particle packing. In particular, elasticity was seen at 4 hours, at which time most of the particles had settled to the bottom of the slide. Thus, the elasticity may have been due to crosslinked protein that remained in solution even after some material had precipitated as particles.

The viscosities of solutions from conditions 5, 6 and 7 (in which microparticle formation was observed), were calculated by dividing the loss modulus (G'') by frequency at 1 rad/s. The results are shown in Figure 6.10 as a function of reaction time. There was no trend and considerable variability in the viscosity of CP30+lac solutions. Since the particles, in this case, remained suspended in solution, they likely contributed to the viscosity, but perhaps in a non-homogenous manner. The viscosities of the NBAD+lac solutions and the CP30+NBAD+lac solutions appeared to decrease with reaction time. The decreased viscosities were likely due to the precipitation and settling of large amounts of material.

a) Controls (10 min)

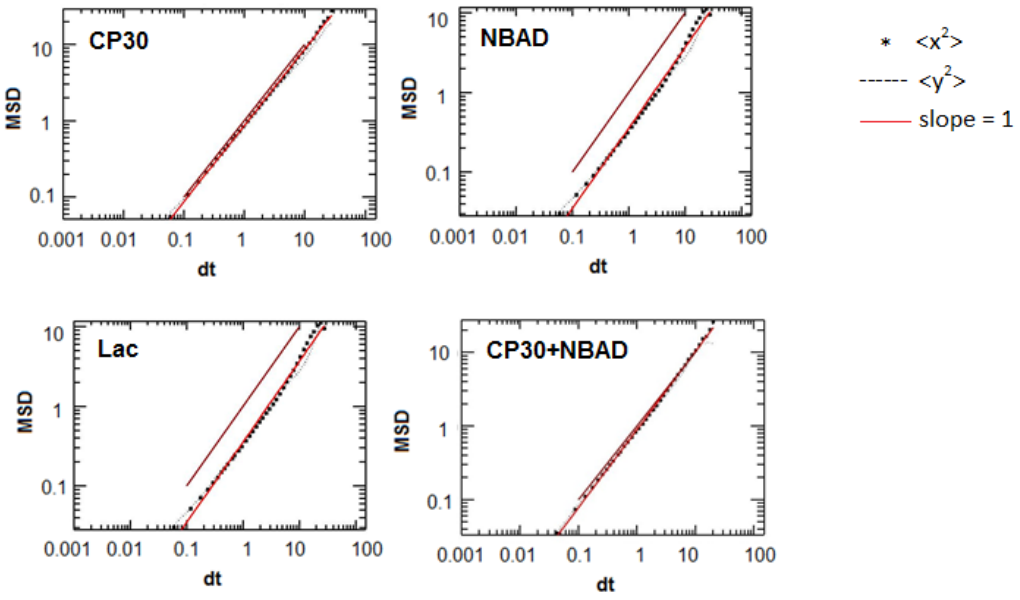

b) CP30+Lac

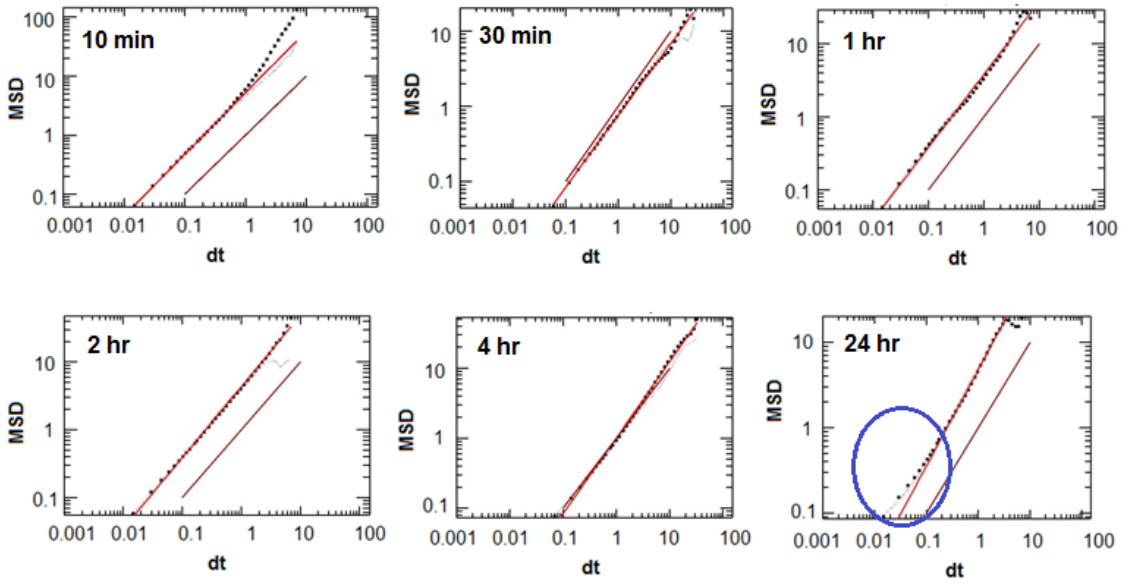

c) NBAD+Lac

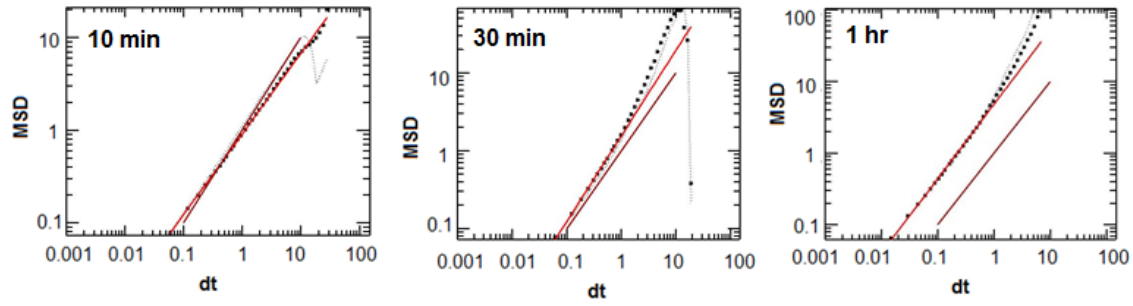

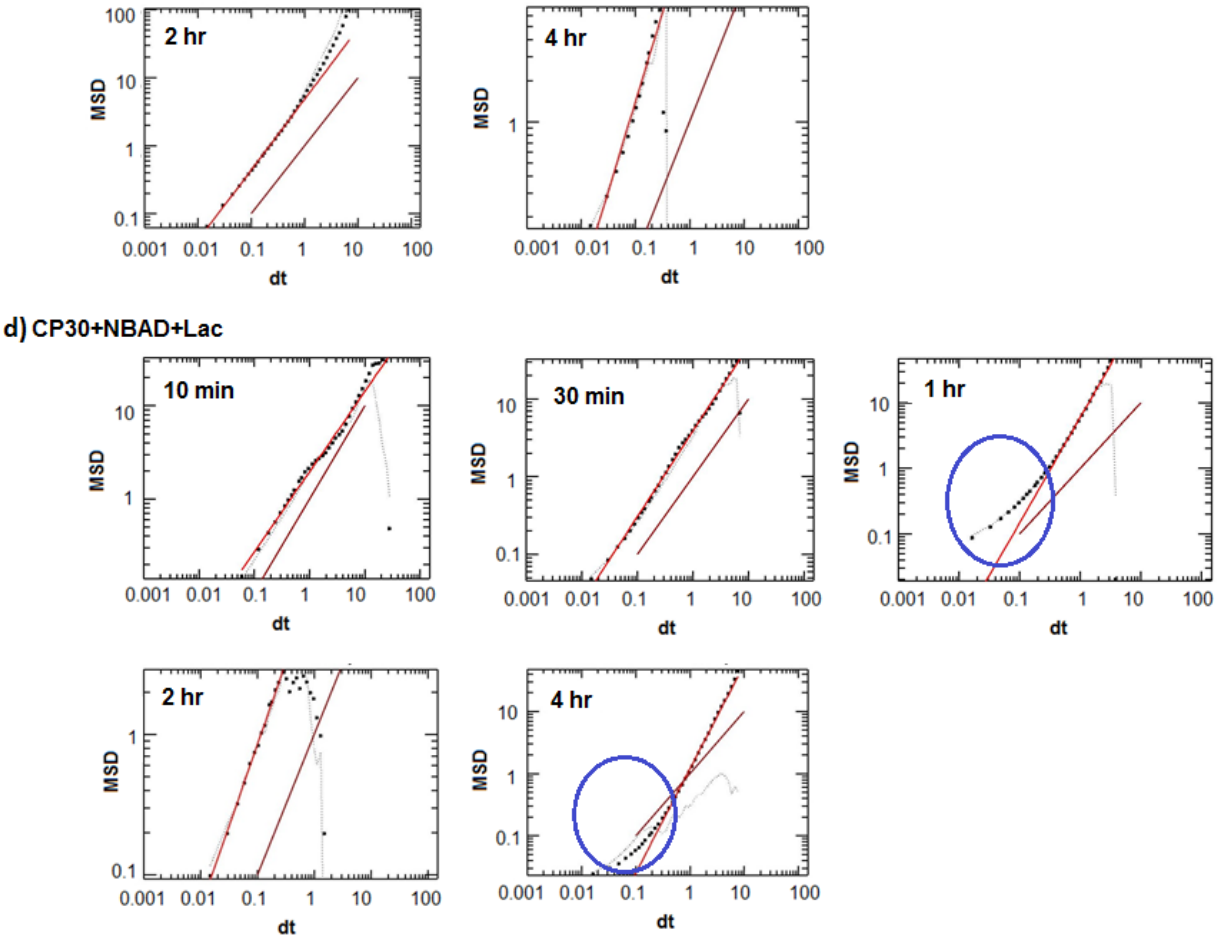

Figure 6.9. MSD of fluorescent beads in each experimental condition. Stars (*) represent $\langle x^2 \rangle$, dashed lines represent $\langle y^2 \rangle$ and red lines are reference lines with a slope = 1. Curvature at short times, suggesting elasticity, is circled. a) The control conditions, measured at 10 minutes, had linear MSD data indicating purely viscous solutions. b) CP30+lac solutions had some curvature, suggesting elasticity, at the end of the reaction. c) NBAD+lac solutions did not have curvature at short times, suggesting there was no elasticity. d) CP30+NBAD+lac solutions had curvature at 1 hour and 4 hours but not at 2 hours, possibly because of different reaction rates involved with NBAD polymerization vs. catecholation and crosslinking of proteins.

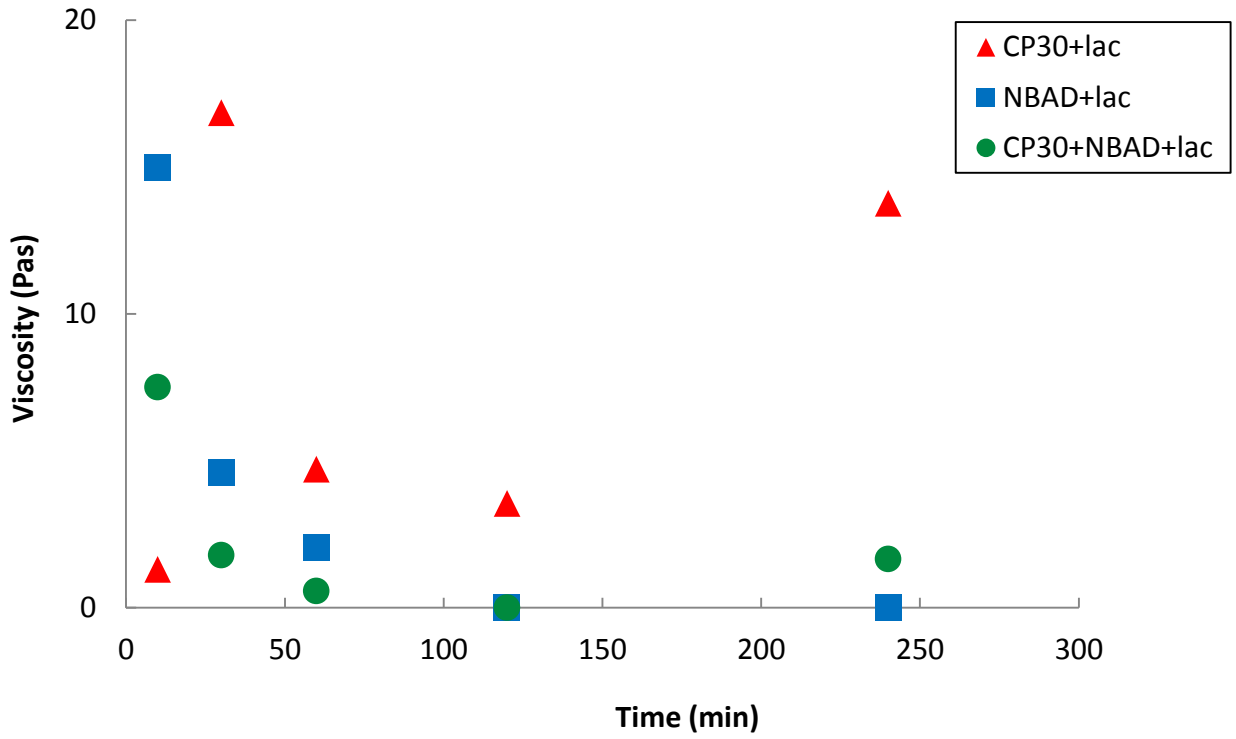

Figure 6.10. The change in viscosity with reaction time for the experimental conditions in which microparticles were observed. No trend was seen for CP30+lac solution viscosity, perhaps because the suspended particles were non-homogeneous. However, the NBAD+lac and CP30+NBAD+lac solution viscosities appeared to decrease with time, perhaps due to the large amount of precipitated material.

Overall, the experiments showed several important results from model cuticle protein crosslinking reactions. First, microparticles were formed with CP30 and laccase, NBAD and laccase, and CP30, NBAD and laccase. The composition of the particles in CP30 and laccase solutions is unknown, because CP30 has no tyrosine residues, so direct dityrosine crosslinking was not expected. The particles formed in NBAD and laccase solutions and CP30, NBAD and laccase solutions were larger and settled quickly. They were most likely composed of polymerized pigments, which are known for becoming very insoluble [333]. Whether the protein was included in the particles is not completely clear. However, particle tracking microrheology did suggest a difference between the viscoelastic properties of each solution. Elasticity was seen in the CP30, NBAD and laccase solutions while it was not seen for just

NBAD and laccase. Thus, the origin of the elasticity may have been from crosslinked protein that remained in solution. However, additional experiments are needed to 1) get reproducible data after solving the drifting problem and 2) analyze the composition of material in the solution and precipitate. Furthermore, the conditions of the experiments could be altered to favor more soluble reaction products or, at the least, smaller particles that remain suspended in solution.

To verify the interpretations based on the data in this chapter, the experiments should be repeated after solving the drifting problem and further analysis should aim to identify the composition of the reaction products. To solve the drifting problem, particle tracking should be performed with the fluorescent latex beads by themselves to rule out any interactions among the fluorescent probes. Other probe particles, such as polystyrene particles could be used instead [334]. Particle tracking should also be done with careful monitoring of temperature to rule out any heating of the samples from the light source. Lastly, the particle tracking in the PDMS wells sandwiched between glass slides should be compared to particle tracking in petri dishes to rule out any convective flow disturbances arising from small leaks between the PDMS and glass. A different mold could be made that would ensure no leaking would be causing convection. Dasgupta and Weitz used a glass spacer between a glass slide and coverslip and sealed them using a UV-curing, optical grade glue [334]. Once reliable data is attained, the experiments should be repeated to verify the reproducibility of the data shown here.

The viscoelastic data must also be supplemented with biochemical techniques aimed at analyzing the composition of the reaction products. First of all, the solutions should be centrifuged and both the soluble and pellet fraction should be separated using SDS-PAGE. Immunoblot analysis should then be performed to detect the protein and determine its size. Thus, the times at which protein dimers, trimers, oligomers and polymers form can be

determined, as well as the point at which protein appears in the insoluble pellet fraction. These procedures are analogous to the procedures in Suderman *et al.* [249]. It is important to know when material is precipitating and what is in the precipitate vs. what is left in solution in order to interpret the rheological behavior of the fluids. Knowing whether the CP30 precipitates with the NBAD polymers would be key to understanding the difference in their rheological behavior. The particle tracking analysis should also be done at more frequent time intervals within the first 2 hours of the reaction, since this is most likely when the interesting changes in the properties of the soluble material occur. The combination of these techniques with microrheology will clarify how specific reaction products affect the viscoelastic properties of the solutions.

In addition to the reaction conditions tested here, changes could be made that would encourage solubility of the products or smaller particle sizes. Suderman *et al.* showed that the type of protein and catechol used for crosslinking affects the solubility of the products. In their model reactions, proteins crosslinked by NADA remained soluble for a longer time than protein crosslinked by NBAD [249]. Additionally, the products formed from crosslinking of the protein MsCP27 were soluble whereas the products formed from MsCP20 and MsCP36 became insoluble shortly after catecholation [249]. The reasons for the differences in solubility were not mentioned, but could be attributed to the distribution of reactive groups on the proteins or differences in reactivity of the catechols. Nevertheless, the microrheology experiments would be more effective if they were performed using conditions that achieved optimal solubility of cross-linked proteins. Thus, the experiments could be performed using the *Manduca sexta* protein, MsCP27, and NADA since that has already been shown to result in more soluble products.

If solubility could be improved, there is still a good possibility that an elastic gel network would not form at the low concentrations of protein used here. Instead, branched polymers may

form that affect viscoelastic properties in unique ways. In general, branching prevents reptation of polymers, so the chains have to relax via primitive path motions [319]. Such motions involve the extension and retraction of one end of a chain which is tethered at the other end by a branch point. Branched chains have a wide distribution of relaxation times because the chain ends can fluctuate much faster than the segments near the tether point. The frequency dependent behavior of the viscoelastic moduli differ from linear polymers in several ways. For example, the crossover between G' and G'' occurs at higher frequencies in branched polymers. Also, the magnitude of G' at the crossover point depends on the molecular weight of the branch arms in branched polymers whereas it is independent of molecular weight in linear polymers [318]. For branched polymers such as star molecules, there are very good theoretical predictions for the behavior of G' and G'' with frequency [335-337]. However, they require information about the plateau modulus, the entanglement molecular weight and the Rouse time of an entanglement segment that can be found from linear polymer solutions [337]. Thus, high concentrations of protein may still be needed to obtain all the necessary information for interpreting the viscoelastic data.

If particles formation cannot be avoided, some parameters could be changed to encourage smaller particles that would remain suspended in solution (they would need to be < 1 μm [319]). Ju *et al.* found that melanin-like nanoparticles could be formed from the auto-oxidation of dopamine and the particle size could be controlled down to <100 nm [333]. The smaller sizes were achieved by increasing the rate of oxidation, increasing the temperature and decreasing the concentration of the catechol [333]. Thus, in the model reactions studied here, the concentration of catechol could be decreased and the concentration of enzyme could be increased (to encourage faster oxidation), and the temperature could be increased to result in smaller particle formation.

If the particle size could be reduced to prevent sedimentation, the rheological properties would likely be dominated by the particle phase of the solutions. In that case there are theories that relate the viscosity as well as the G' and G'' to the volume fraction of spherical particles [319]. In general, hard sphere suspensions can induce elasticity in a system because the packing of particles prevents them from moving rapidly without generating forces, so the particle configurations are slow to relax [319]. Thus, the G' and G'' shift toward lower frequencies and higher moduli with increased particle volume fraction [319].

Another good option would be to increase the protein concentration to encourage gelation. To get a gel, synthetic monomers generally require 2-3 wt% of monomer and about 0.03 wt% crosslinker in the initial solution [338, 339]. This would translate to a protein concentration of 20-30 mg/ml (7-10x higher than the 3 mg/ml used here) and a catechol concentration of 0.3 mg/ml (3.3x lower than the 1 mg/ml used here). The lower catechol concentration compared to protein concentration may result in a lower crosslink density, but perhaps with more soluble products. These concentrations would likely result in more soluble products that form a network rather than insoluble particles. The elastic component of the viscoelastic response would likely be more clear under these conditions, making it easier to determine the contribution of protein crosslinking. The results may shed light on the roles of cuticle proteins *in vivo* as well as the potential for developing cuticle-mimetic structural biomaterials.

6.5 Conclusions

The viscoelastic effects of model cuticle protein crosslinking reactions were investigated using microrheology. A strength of microrheology is that it combines microscopy with

quantitative rheological measurements so that microscopic structures can be detected along with the property changes. In the model reactions tested here, small particles that remained suspended in solution were observed in solutions of CP30 and laccase. The composition of the particles was unclear, but the suspension resulted in elasticity after 24 hours. Larger particles that settled out of solution were observed in NBAD+laccase solutions and CP30+NBAD+laccase solutions. However, elasticity was only observed in solutions that contained the protein, suggesting that perhaps crosslinked protein remained soluble and contributed to the elasticity. Thus, the potential for microrheology to provide valuable information about model systems has been demonstrated. However, further experiments are needed to achieve reproducible results and to verify whether the protein was in the soluble or insoluble portion of the products. Additionally, further optimization of reaction conditions that lead to more soluble products or even gelation could provide valuable information contribution of the protein to rheological properties.

CHAPTER 7: EVALUATING THE STRUCTURE AND POTENTIAL SELF-ASSEMBLY OF CP30, AN ABUNDANT PROTEIN IN BEETLE ELYTRAL CUTICLE

7.1 ABSTRACT

CP30 is an abundant protein in the rigid cuticle of the beetle elytron. It has an unusual amino acid sequence that is hypothesized to self-assemble via electrostatics or metal ion coordination. The structure of CP30 was evaluated at a variety of pH, ionic strength and temperature conditions to determine whether association occurs. Circular dichroism, fluorescence spectroscopy and static and dynamic light scattering showed that the protein had an extended α-helical structure at pH 3, 5 and 7 which unfolded around 60°C and reformed upon cooling back to 10°C. Thus the electrostatic self-assembly of the protein was not directly supported. However, the protein aggregated at pH 5, low salt, which is close to the protein's isoelectric point (5.82), preventing analysis at that condition. Further studies aimed at solubilizing the protein near that condition may uncover evidence of assembly. Microrheology experiments indicated that CP30 does interact with nickel ions by forming microparticles and elasticity in the fluid, which supports the view that metal coordination crosslinking of proteins has a mechanical role in cuticle. The unique structure of CP30 may offer new design motifs for the development of tunable biomaterials.

7.2 INTRODUCTION

Protein self-assembly is the spontaneous association of proteins, through non-covalent interactions, into an organized structure [340]. For example, the coiled-coil motif is a well-known self-assembly pattern within many different types of proteins such as muscle proteins,

transcription factors, cytoskeletal proteins, cell surface proteins, molecular motors and antigens [341, 342]. It is formed when helical proteins associate at specific locations to form a superhelix. Coiled-coil proteins have characteristic sequences, illustrated in Figure 7.1, in which one hydrophobic residue is followed by two polar residues, another hydrophobic residue, and 3 more polar residues. Several helices assemble by association of the hydrophobic groups while the polar groups face out and electrostatic interactions further stabilize the structure [342]. Another self-assembly motif in proteins such as silk is a β-sheet, in which hydrogen bonding among several protein strands causes them to line up in a parallel or antiparallel manner [342]. Many of nature's structural materials such as silk, collagen, elastin, muscle, bone and teeth have self-assembled proteins as their building blocks [340]. The self-assembled organization is essential to the function of these proteins within biological organisms. Even though *in vivo* self-assembly of proteins differs from *in vitro* self-assembly, the motifs discovered in native proteins can be used to control the structure and properties of engineering materials [343].

In fact, self-assembled motifs have been exploited to make "smart" self-assembling structures that respond to changes in pH, temperature, ionic strength or concentration, making them useful materials for tissue engineering scaffolds [340]. For example, the self-assembly of genetically engineered triblock peptides including the coiled-coil motif was pioneered by Tirrell's research group, allowing them to produce pH and temperature dependent hydrogels [114]. Many other protein-inspired materials based on the repeat sequences in silk [344, 345], elastin [118, 346, 347], titin [348] and resilin [123, 349-351], as well as combinations of sequences from different proteins [343, 352-354] have been produced with highly tunable material properties. Identifying novel motifs in native proteins can lead to new strategies for controlling and improving biomaterial properties.

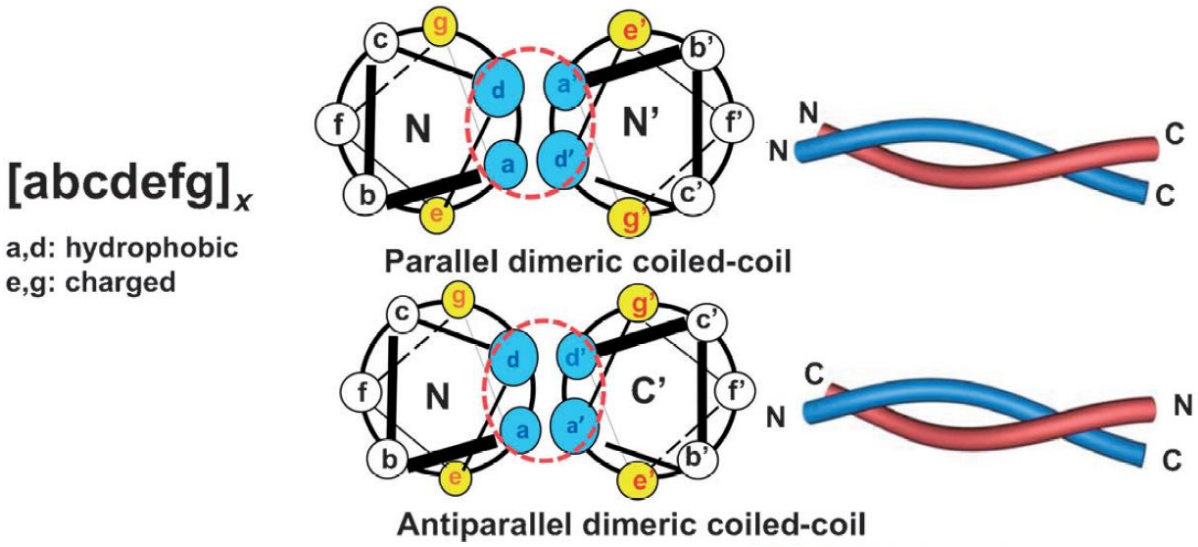

Figure 7.1. Characteristic sequence and structure of the coiled-coil motif. Adapted from [342] with permission from Wiley and Sons.

The overall goal of this study was to evaluate the structure and self-assembly potential of protein that is highly abundant in a rigid cuticle structure, the elytron. Insect cuticle is an abundant biomaterial with extremely versatile mechanical properties; within a narrow density range, it can span 8 orders of magnitude in stiffness [34]. The main structural components are proteins and chitin, but the molecular-level structures of these components that account for the mechanical properties are not well understood. *Tribolium castaneum*, or the red flour beetle, is an insect whose genome has been sequenced, making it a good source for studying biochemical processes and biomolecules in cuticle [355-358]. Several abundant proteins within the elytral cuticle of *Tribolium castaneum* were identified and sequenced[291]. The third most abundant protein in the elytron is CP30 (or GLEAN no. 14462) [291]. CP stands for cuticle protein and 30 reflects the fact that it tracks with the 30 kDa standard protein in SDS-PAGE. It is 19 kDa with an isoelectric point of pH 5.82 and the sequence is shown in Figure 7.2a. It has a very unusual sequence; three charged residues, glutamic acid, arginine and histidine, make up 76% of the

sequence [291]. It has a sort of triblock structure in which the C-terminus has a net positive charge, the central portion (highlighted in yellow in Figure 7.1a) contains alternating blocks of consecutive positive and negative amino acid residues, and the N-terminus has a net negative charge. The sequence suggests that it may self-assemble via electrostatic interactions and therefore, have a unique role within cuticle. Figure 7.2b shows one hypothesis regarding how it may align to promote electrostatic self-assembly. If each chain is offset by 4 residues, the positive and negative blocks of amino acids could electrostatically interact to produce self-assembled fibrils, nanoparticles or other structures. Therefore, the first aim of this study was to characterize the structure of CP30 in a variety of pH and ionic strength conditions to find evidence of self-assembly.

A second hypothesized interaction, illustrated in Figure 7.2c, is the formation of coordination crosslinks between the histidine residues and multivalent metal ions, which could be the driving force for association into unique structures. Coordination bonds between proteins and multivalent metal ions have been linked to increased hardness and stiffness of arthropod cuticle [85-88, 359]. Many of the hard 'tools' such as jaws, leg claws and mandibles are enriched in transition metals and halogens. However, a study on jewel beetles showed that larval mandibles lacking metal are harder than adult mandibles with metal, thus putting the actual role of the protein-metal interactions into question [89]. Protein-metal coordination bonds are also thought to be responsible for the self-healing characteristics of mussel byssal threads [82, 360]. The stiffness of the threads can be partially recovered after stressing past the yield point [360]. The self-healing properties are thought to arise, in part, from reversible binding between multivalent metal ions and the specialized collagen proteins that are rich in histidine [360, 361]. The modulus of byssal threads was reduced when treated with a metal chelating agent, thus

supporting this view [360]. Since CP30 is also rich in histidine, it may also participate in metal coordination bonds. In fact, Dr. Karanicolas in bioinformatics at the University of Kansas thought that CP30 would likely have just loose associations by itself, but may take on an interesting structure in the presence of another associating molecule. Furthermore, the histidine and lysine residues in CP30 may also be involved in covalent crosslinking reactions with chitin-binding proteins [195, 248], thus linking the cuticle network as a whole. The support for protein-metal crosslinks having an important mechanical role in insect and marine structures is strong, but direct evidence of protein-metal bonds is lacking. Therefore, the second aim of this study was to find evidence of interaction between CP30 and Zn^{2+} ions.

It is important to note that the *in vitro* interactions examined in this study will likely differ from *in vivo* interactions because there will be a reduced ability to form higher order structures in solution. However, isolating the components in solution is important for establishing the unique role of this interaction apart from other components in the native tissue. The results may also point to new motifs for designing biomaterials.

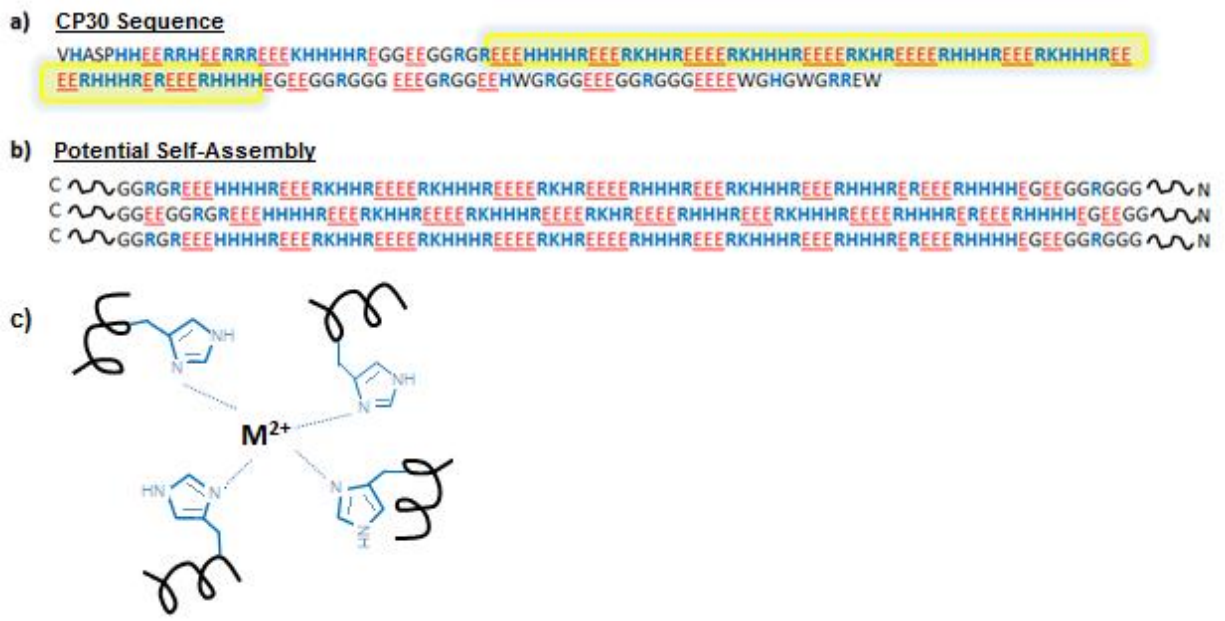

Figure 7.2. a) The primary sequence of CP30 has many alternating blocks of consecutive positive (blue) and negative (red) residues and very few hydrophobic residues in the central region of the protein (highlighted in yellow). b) One hypothesis is that electrostatic self-assembly may occur since the positive and negative blocks of residues within the central region of the protein align when each chain is offset by 4 residues. c) Another hypothesis is that multivalent metal ions may promote the assembly of the protein by forming coordination bonds with histidine residues.

7.3 Materials and Methods

7.3.1 Materials

CP30 was first identified and sequenced by Dittmer *et al.* using a combined proteomics and transcriptomics approach with *Tribolium castaneum* [291]. In Dr. Michael Kanost's research lab in the Department of Biochemistry and Molecular Biophysics at Kansas State University, plasmids containing the cDNA for CP30 were constructed using RT-PCR. The plasmids were used to transform *Escherichia coli* and the bacteria were grown in LB medium. Expression of the protein was induced by adding IPTG (isopropyl-beta-D-1-thiogalactopyranoside). The cells were lysed by sonication and the proteins were purified first on a nickel column and then on an anion exchange column. The protein was then eluted in a 25

mM Tris buffer (pH 7.5) with 330 mM sodium chloride. The protein was assayed at 0.7 mg/ml using a Coomassie Plus Protein Reagent (Thermo Scientific) and shipped frozen from Kansas State University.

7.3.2 METHODS

7.3.2.1 SAMPLE PREPARATION. The stock protein was dialyzed in 3 ml aliquots against a series of pH conditions (pH 3, 5, and 7) and either low salt (~0.04 M sodium chloride) or high salt (~0.33 M sodium chloride) in a 20 mM citrate phosphate buffer for ~ 18 h at 2^{o}C using 3500 MWCO dialysis cassettes (Thermo Scientific).

After dialysis, a bicinchoninic acid assay (BCA) was used to determine the concentration of samples after dialysis as well as the stock [362, 363]. Bovine serum albumin was used as a standard with known concentration, and a calibration plot was created. Working concentrations were 0.050 mg/mL for fluorescence, light scattering and UV-visible absorption experiments and 0.060 mg/mL for circular dichroism.

7.3.2.2 UV-VISIBLE ABSORPTION SPECTROSCOPY. The absorption spectrum was measured for the stock solution to estimate the concentration. Since the Beer-Lambert law relates the absorbance to the concentration, this technique gave another measure of concentration to which the results from the BCA assay were compared.

7.3.2.3 CIRCULAR DICHROISM. Circular dichroism detects the differential absorption of right and left handed circularly polarized light. Since proteins are optically active molecules, they absorb the two components (electric and magnetic) of circularly polarized light in unequal

amounts, thus transforming it into elliptically polarized light. Different types of secondary structures in proteins result in different absorption behavior, and several structures such as α-helices, β-sheets and random coils have been shown to produce characteristic circular dichroism spectra. Therefore, circular dichroism spectra were obtained for CP30 solutions to identify the dominant secondary structure as well as any structural alterations that were caused by pH, ionic strength and temperature. CD spectra were collected from 200-260 nm as a function of pH, ionic strength, and temperature (10-90°C).

7.3.2.4 FLUORESCENCE SPECTROSCOPY. Fluorescence spectroscopy can detect conformational changes in a protein by tracking the emission of light by aromatic side chains as a perturbation that alters the structure, such as temperature, is applied. Shifts in the emission wavelength occur when the local environment (such as exposure to solvent) of the fluorescent side chains occurs, thus enabling the detection of protein unfolding. Fluorescence spectra were obtained by exciting the solutions with 295 nm light and monitoring the emission wavelength peak position and peak intensity as the temperature was increased from 10 – 90°C.

7.3.2.5 LIGHT SCATTERING. Dynamic light scattering can provide a measure of protein size by measuring the fluctuation in intensity of scattered light. Since the molecules causing the light scattering experience Brownian motion, the intensity of scattered light will fluctuate slightly over time. The Brownian motion of a larger molecule will be much slower than the motion of a small molecule. Therefore, the diffusion coefficient can be found and related to the hydrodynamic radius of the molecule. Here, dynamic light scattering of the stock solution was measured to obtain the size of CP30.

Static light scattering measures the intensity of scattered light to provide a measure of the size or molecular weight of a macromolecule in solution. An increase in size would manifest itself as an increase in the intensity of scattered light because a larger molecule can scatter more light. Therefore, static light scattering measurements of CP30 solutions were performed by measuring the intensity of scattered light (295 nm) as temperature was increased from 10 – 90°C to detect any association or aggregation of the protein.

7.3.2.6 MICRORHEOLOGY. Passive microrheology was used to measure the dynamic viscoelastic properties of solutions of CP30 and nickel ions. Passive microrheology monitors the thermal motion of probe particles in a fluid. The motion of the particles depends on the viscoelastic properties of the fluid; particles in purely viscous fluids experience simple Brownian diffusion whereas particles in viscoelastic fluids exhibit sub-diffusive motion [332]. Relationships have been established between the microscopic motion of particles and the viscoelastic properties of complex fluids [332], making microrheology a valuable tool for studying materials in which quantities are limited.

To prepare samples for microrheology a 100 mM Bis-Tris buffer was prepared at pH 7. Fullenkamp *et al.* showed that pH 7 resulted in optimal histidine-metal coordination bond stability; at low pH, protonation of the imidazole group on histidine reduced bond stability and, at high pH, hydroxyl ions interfered with the metal binding [82]. Next, a 0.3 mM (6 mg/ml) CP30 solution, a 2.5 mM (0.147 mg/ml) $NiCl_2$ solution, and a combined 0.3 mM CP30 + 2.5 mM $NiCl_2$ solution were prepared in the Bis-Tris buffer. Since each metal ion can coordinate with 4 histidine residues, and there are 33 histidine residues per protein molecule, the concentrations were calculated such that the ratio of metal: histidine was 1:4. Next, 0.5 µl of a

fluorescent latex bead (Polysciences, Inc.) solution (10 µl of 0.1 µm beads in 2 ml buffer) was added to 20 µl solutions of each sample (Ni, CP30 and Ni+CP30). The thermal motion of the fluorescent particles was monitored in each solution using a CCD AndorLuca video camera attached to an upright fluorescent microscope (Leica DM 2500M). Brightfield images of the particles were taken as well. The videos were converted to frames of images and sent to collaborators in Dr. Eric Weeks' research group in the Department of Physics at Emory University. They have a well-established method for tracking particles, calculating the mean squared displacement of the particles and converting that to viscoelastic moduli using IDL (Interactive Data Language) software (see http://www.physics.emory.edu/faculty/weeks// idl/tracking.html and http://www.physics.emory.edu/faculty/weeks/idl/rheo.html). The process involves taking the Laplace transform of the mean squared displacement and relating it to G'(ω) and G''(ω) through the Generalized Stokes-Einstein equation: $\widetilde{G}(s) = \frac{k_B T}{\pi a s \langle \Delta \tilde{r}^2(s) \rangle}$, where $\widetilde{G}(s)$ is the Laplace transform of G*, s is the Laplace frequency, a is the radius of the tracer particle, and $\langle \Delta \tilde{r}^2(s) \rangle$ is the Laplace transform of the mean squared displacement [321, 332].

7.4 RESULTS

Several characterization methods were used to determine the secondary structure of CP30 at various pHs, ionic strengths and temperatures. Each technique helped to identify aspects of the structure. While dramatic evidence of association was not observed, subtle differences based on pH, ionic strength and temperature were noted and may shed light on the possible *in vivo* assembly of the protein where it is much less hydrated. The results suggest future experiments needed to gain a better understanding of the structure and function of CP30 within insect cuticle.

7.4.1 SAMPLE PREPARATION. The protein was prepared in a variety of pH and ionic strength conditions because the electrostatic self-assembly of the protein was hypothesized to be influenced by pH and ionic strength. After dialyzing the protein into the various conditions from the stock solutions provided by Kansas State University, the concentration in each experimental condition was determined from BCA analysis. The results are shown in Table 7.1. The concentration of protein dropped to levels below useful analysis at pH 5, low salt. No aggregation of the protein was observed; so it may have been lost because it stuck to the dialysis membrane during the sample preparation. Therefore, the protein could not be analyzed in this condition (pH 5, low salt).

Table 7.1. CP30 concentrations determined from BCA analysis for each condition. Note that the protein concentration dropped significantly at pH 5, low salt.

Ionic Strength	pH	Concentration (mg/ml)
Low Salt (0.04 M NaCl)	3	0.176
	5	0.021
	7	0.058
High Salt (0.33 M NaCl)	3	0.173
	5	0.057
	7	0.183
Stock	7.5	0.178

7.4.2 UV-VISIBLE ABSORPTION SPECTROSCOPY

The UV-Visible absorption spectrum was obtained to provide another measure of protein concentration. The spectrum of the stock CP30 solution is shown in Figure 7.3. The absorption peak around 220 nm is about 2.7 and corresponds to the absorption of UV-light by the peptide bonds. The peak around 280 nm is about 0.5 and corresponds to the absorbance of UV-light

from the Trp side chains. The Beer-Lambert Law relates the absorbance to the concentration by the equation, $A = \varepsilon C L$, where A is the absorbance at a particular wavelength, ε is the extinction coefficient at a particular wavelength, C is the concentration and L is the path length through the sample [364]. The absorbance at 280 nm was 0.5, the path length was 1 cm and the extinction coefficient at 280 nm was calculated from an online peptide property calculator to be 22000 $cm^{-1}M^{-1}$. The calculation is based on the protein sequence and the spectral contributions of Tyr, Trp and Cys residues [365], however, CP30 has no Tyr or Cys residues. It has been shown to be accurate to ±5% in most cases [365]. The concentration of the stock solution was, therefore, calculated to be 0.440 mg/ml. Since the BCA assay calculated the concentration at 0.178 mg/ml, this method likely provided underestimates of the true CP30 concentrations. The BCA assay is highly influenced by cysteine, tyrosine and tryptophan side chains because they contribute to the reduction of Cu^{2+} to Cu^{+}, which then reacts with the bicinchoninic acid to form the purple product [362]. Since only 2.6% of CP30 is made of Trp (there are no Tyr or Cys) residues while 9.7% of BSA is made of Trp, Tyr and Cys [366], the CP30 may not produce as much purple color per gram as the standard BSA.

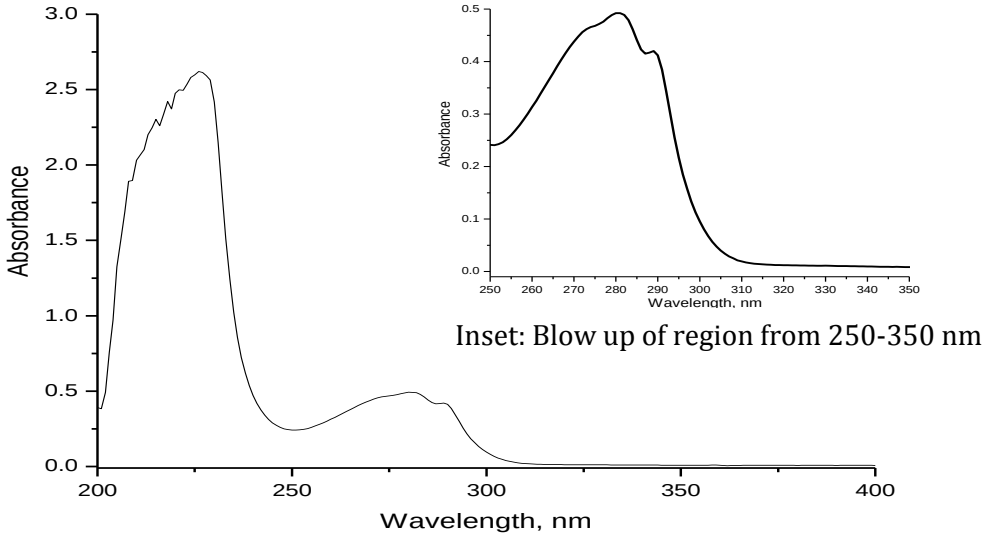

Figure 7.3. UV-visible absorption spectrum of the CP30 stock solution. The peak at 220 nm is from the absorption of light by the peptide bond while the peak at 280 nm is from the absorption by the Trp residues. The inset shows an expanded view of the Trp absorption peak.

7.4.3 Circular Dichroism Spectroscopy

Circular dichroism spectra were obtained as a function of temperature for each pH and ionic strength condition to identify secondary structural features in the protein. Results are shown in Figure 7.4 (high salt) and Figure 7.5 (low salt). In each case, double minima at about 208 and 222 nm were observed, which is indicative of α-helical secondary structure. As the temperature increased, the double minima diminished into a single minimum ~200 nm, which is typical of a random coil secondary structure. When the solutions were cooled to 10°C, after heating the α-helical characteristics were almost completely recovered (the dashed lines in Figures 7.4 and 7.5 are after cooling back to 10°C). Since an increase in temperature caused the secondary structure to change from α-helical to random coil, an attempt to determine the temperature of unfolding (Tm) was made. The temperature of unfolding is the point at which half the protein has undergone a structural change and the ellipticity changes most rapidly. Thus,

the molar ellipicity values at key wavelengths were plotted as a function of temperature for selected wavelengths in Figure 7.6. The change in ellipticity was gradual, so a distinct unfolding temperature was not observed. However, the ellipticity values plateaued around 60ºC, suggesting that the protein was completely unfolded at that point. This result is for pH 7, high salt but the result is representative of all samples. Figure 7.7 shows the CD spectrum for each pH and ionic strength condition at 10°C for direct comparison. No differences can be distinguished in the secondary structure.

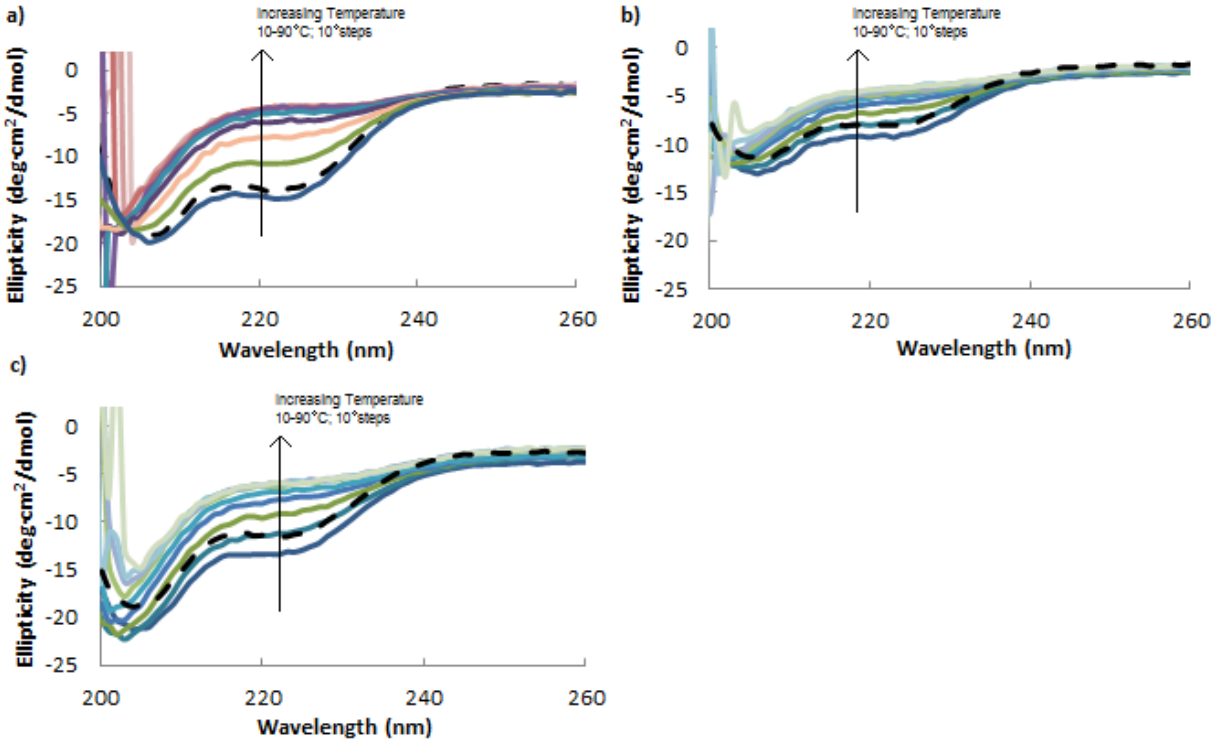

Figure 7.4. Circular dichroism spectra of CP30 at a) pH 3, b) pH 5 and c) pH 7 in high salt conditions. The high salt conditions obscured the data below about 205 nm. In each case there was a double minima at about 208 and 222 nm, which diminished upon heating from 10-90ºC. The dashed line is the spectrum after cooling back to 10ºC. The conformation was almost completely recovered in each case.

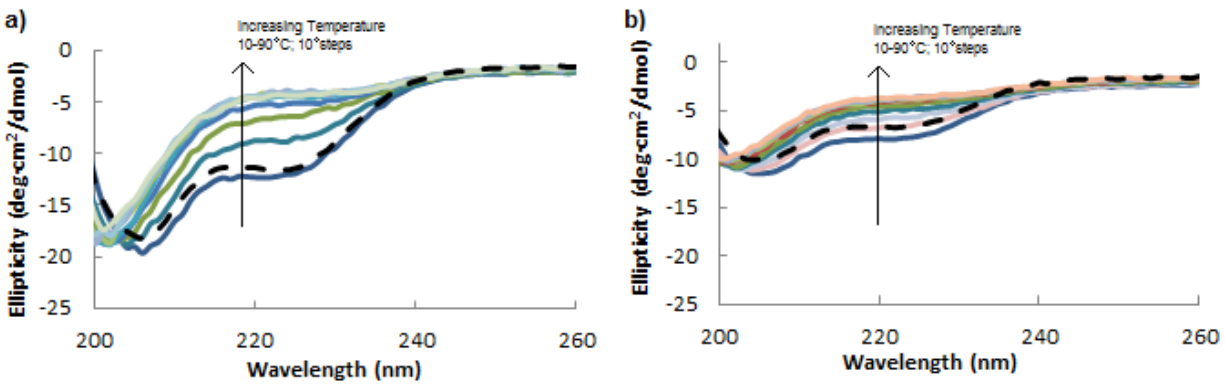

Figure 7.5. Circular dichroism spectra of CP30 at a) pH 3 and b) pH 7 in low salt conditions. In each case there was a double minima at about 208 and 222 nm, which diminished upon heating from 10-90ºC. The dashed line is the spectrum after cooling back to 10ºC. The conformation was almost completely recovered in both cases.

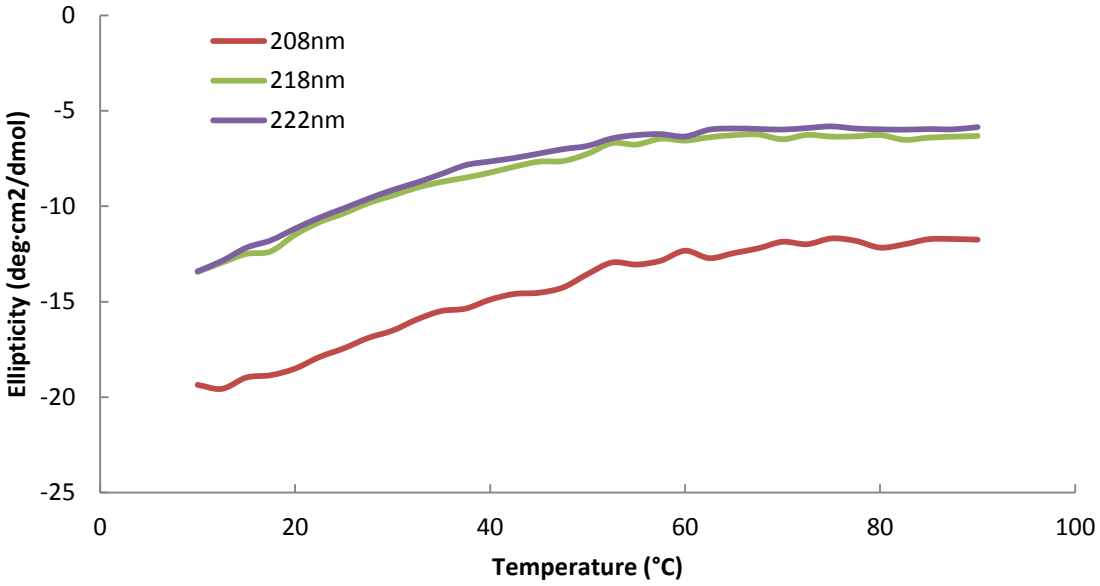

Figure 7.6. Ellipticity of CP30 solutions (pH 7, HS) for select wavelengths as a function of temperature. The values plateaued around 50-60°C, suggesting the protein was unfolded.

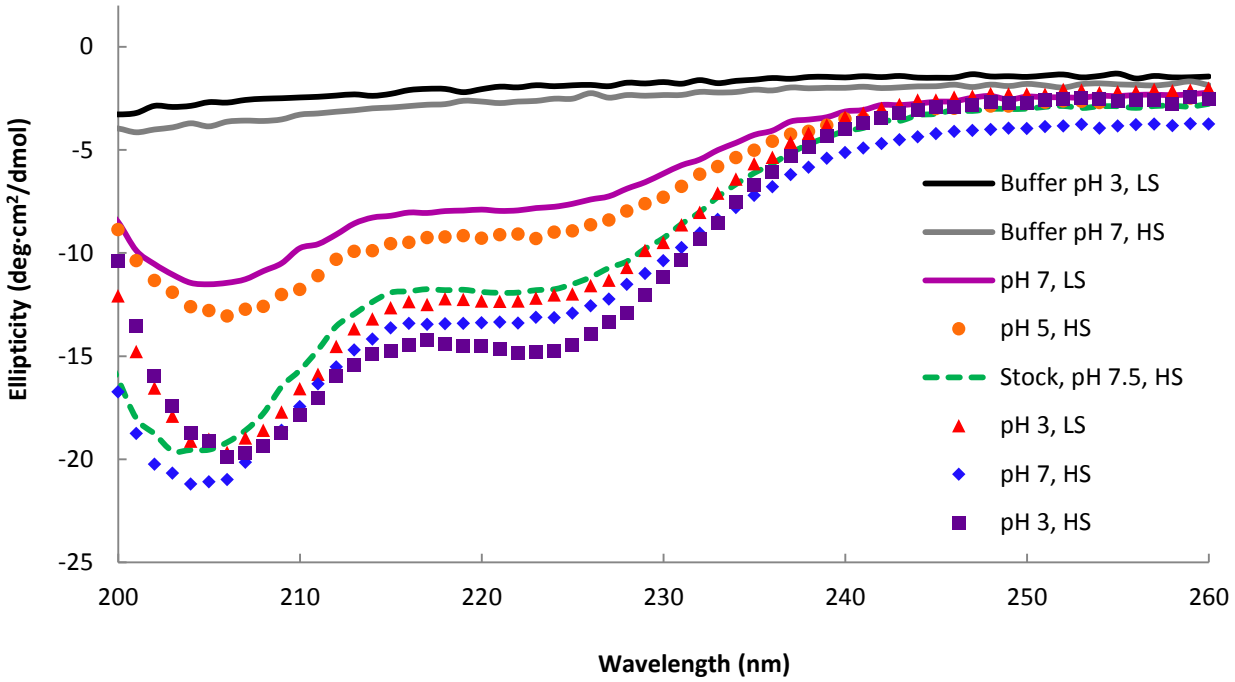

Figure 7.7. Comparison of CD spectra for each experimental condition at 10°C. No differences in secondary structure were observed among the various pH and ionic strength conditions tested.

7.4.4 Fluorescence Spectroscopy

CP30 has 4 tryptophan (Trp) residues at the N-terminus of the protein (see Figure 7.2a). The fluorescence emission spectrum of Trp was obtained as a function of temperature to detect changes in the folded state of the protein. The fluorescence spectra for each pH and ionic strength were similar. Representative spectra as a function of temperature are shown for CP30 at pH 7, high salt in Figure 7.8. At 10 °C, The tryptophan emission peak position maximum was observed to be at 349 nm, indicating that the aromatic residue is already exposed to the solvent. Typical emission wavelengths for a buried tryptophan residue are approximately 330 nm. Upon temperature increase to 87.5 °C, the peak red shifted to slightly higher wavelengths and the intensity decreased, indicating a slight unfolding of the protein. The peak red shifts due to additional exposure of the indole rings to solvent, which lowers the energy of transition, thus increasing the emission wavelength.

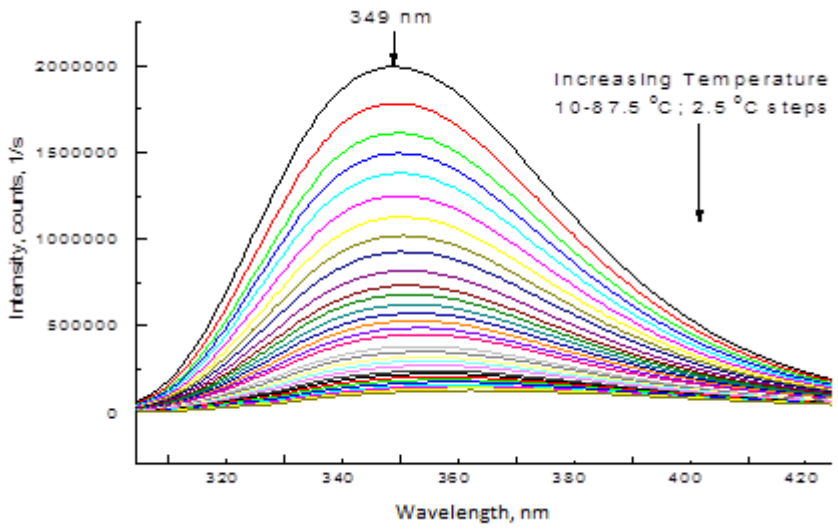

Figure 7.8. Fluorescence spectra of CP30, high salt, pH 7 (excitation 295 nm). The emission peak maximum occurs at 349 nm and red shifts to slightly higher wavelengths as temperature increases.

The shift in the fluorescence peak position as a function of temperature is shown for each condition in Figure 7.9. For a protein that undergoes a transition from a folded to completely unfolded state with temperature, a more distinct rise would be expected in the peak position vs. temperature curve, corresponding to cooperative changes in the protein structure. The temperature at which the greatest change in peak position occurred would be the melting temperature. In this case, however, the shift is very gradual, so a Tm could not be calculated. Instead, an initiation temperature, the temperature at which the protein underwent the greatest change in conformation, was estimated from where the curve started to deviate from linearity (between 55 and 70°C).

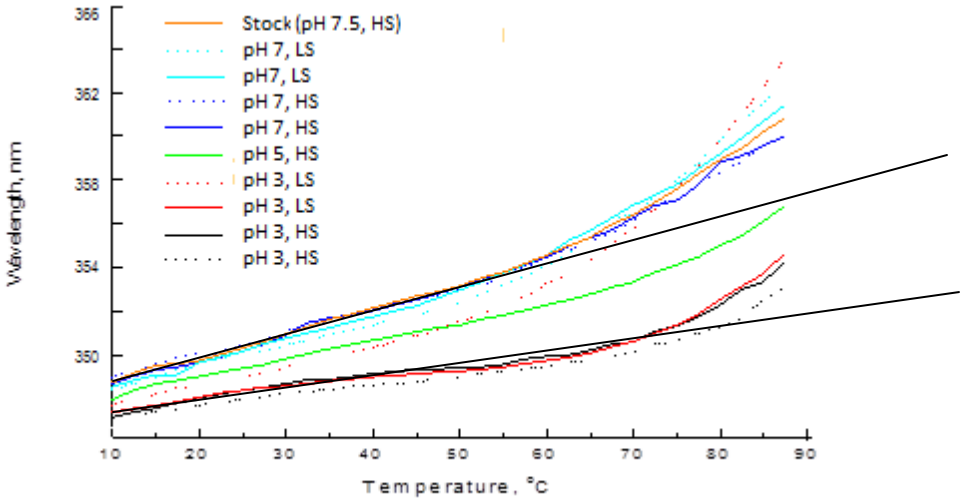

Figure 7.9. Shift in fluorescence peak position plotted using the mean spectral center of mass method (msm). Two samples were run each for pH 3, LS and HS and pH 7, LS and HS. The black lines follow the upper and lower curves until they deviate from linearity at 55and 70°C, respectively, indicating the temperature at which the protein begins to change conformation.

The decrease in the fluorescence emission peak intensity values as a function of temperature is shown in Figure 7.10. The fluorescence intensity decreased because Trp, the fluorophore, became more exposed to the solvent which quenches the emission.

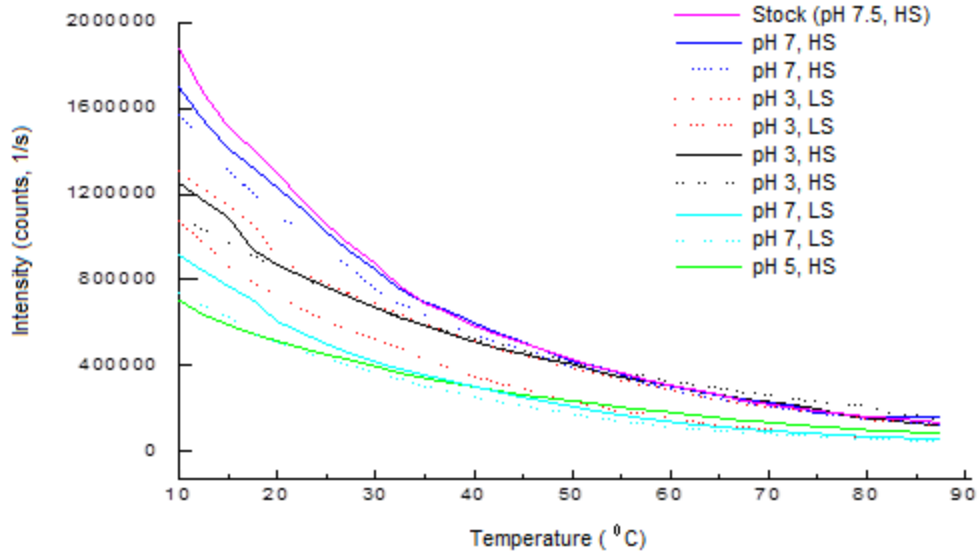

Figure 7.10. Decrease in fluorescence peak intensity values as a function of temperature.

7.4.5 LIGHT SCATTERING

Dynamic light scattering was measured to find the hydrodynamic radius of CP30 in the stock solution (pH 7.5, high salt). Results showed that the radius at 20° C was around 1.8 nm. The polydispersity, which describes the width of the Gaussian distribution of the autocorrelation function used to analyze the fluctuations in scattering intensity [367], was 23.6%, indicating a moderately homodisperse population (V 15-20% is considered monodisperse according to the Wyatt manual).

Static light scattering as a function of temperature was measured to determine if the scattering intensity of the molecule increased, possibly indicating conditions of aggregation. Results are shown in Figure 7.11. There was very little increase in scattering intensity until a slight increase is seen at elevated temperatures (>55^{o} C). No visible aggregation was observed in any solutions after heating. The increased scattering may be due to an increase in molecular size as the protein unfolds rather than aggregation or association of proteins.

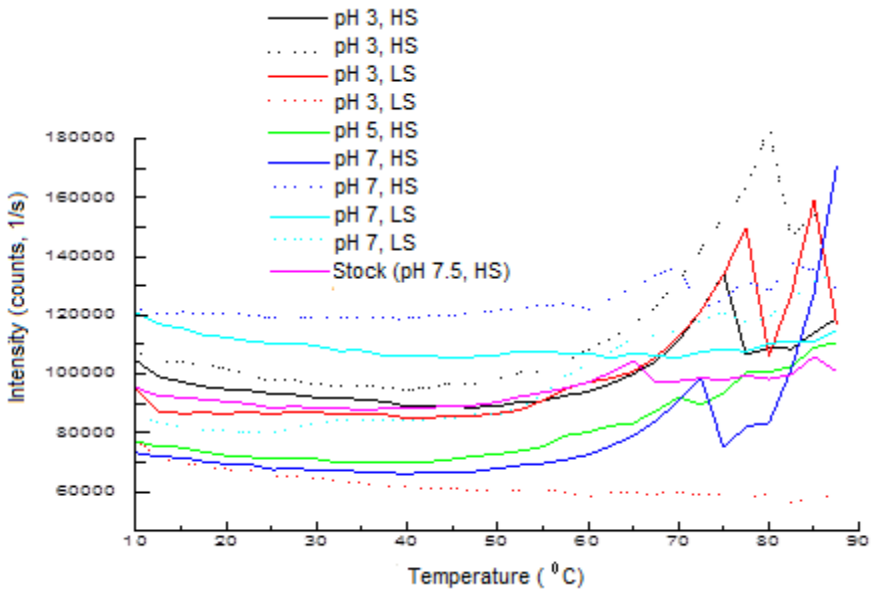

Figure 7.11. Static Light Scattering at 295 nm as a function of temperature. The scattering intensity increases slightly above 55°C, possibly reflecting an increase in molecular size as the protein unfolds.

7.4.6 Microrheology of CP30 and Nickel Ion Solutions

To address the second aim, regarding whether CP30 interacts with Ni^{2+} ions, microrheology was used to visually and mechanically characterize CP30 and $NiCl_2$ solutions. Since microrheology can simultaneously measure rheological properties of very small volumes of fluid and visualize microscopic structures, it is a valuable tool for studying self-assembly in solutions in which materials are limited. Therefore, microrheology was used to compare mixtures of 0.3 mM CP30 and 2.5 mM $NiCl_2$ in 100 mM Bis-Tris buffer (pH 7) to each reactant alone. Since each metal ion could theoretically coordinate with 4 His residues, the concentrations were chosen such that the Ni^{2+} to His ratio was 1:4. The brightfield images of CP30 and $NiCl_2$ solutions are shown in Figure 7.12. By themselves, CP30 solutions and $NiCl_2$ solutions had no particles. When combined, however, many particles formed within the 10 minutes required to prepare the sample and look at in under the microscope. Using Image J software, the particles were measured to be about 1 µm in diameter.

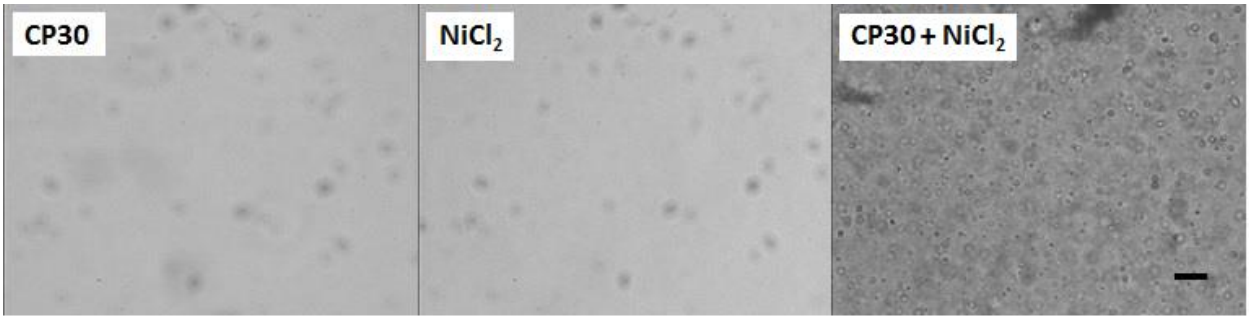

Figure 7.12. Brightfield images of CP30 and $NiCl_2$ solutions. By themselves CP30 and $NiCl_2$ solutions had no particles (dark spots in these images are from the objective lens). However, a mixture of CP30 and $NiCl_2$ resulted in the formation of particles, about 1 µm in diameter. Magnification = 40x and scale bar = 20 µm, which applies to each image.

The viscoelastic character of each solution was also studied using passive microrheology. Particle tracking analysis was performed on fluorescent latex beads suspended in each solution and the mean squared displacement vs. time is shown in Figure 7.13. CP30 and $NiCl_2$ solutions were purely viscous, with linear MSD data and slopes close to 1, indicating that the fluorescent beads were freely diffusing in the solution medium. The mixture of CP30 and $NiCl_2$, however, resulted in some viscoelasticity in the solution. The MSD data was curved, indicating that the solution properties are partially elastic.

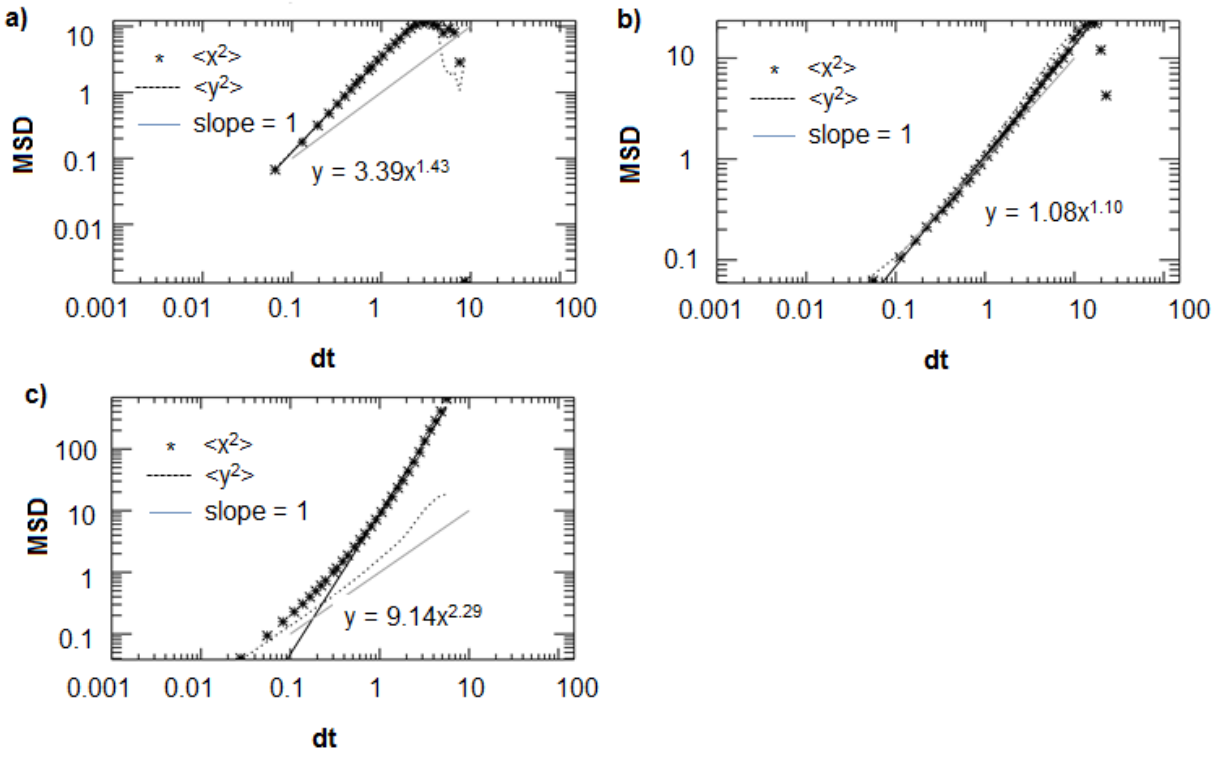

Figure 7.13. MSD data for fluorescent latex beads in a solution of a) CP30 b) $NiCl_2$ and c) CP30 + $NiCl_2$. The CP30 and $NiCl_2$ solutions are purely viscous, while the combination of CP30 and $NiCl_2$ has some elasticity as evidenced by the curvature in MSD data.

7.5 Discussion

The goal of this study was to examine the structure and self-assembly potential of CP30, a highly abundant protein in rigid insect cuticle with a very unique amino acid sequence. The first hypothesized interaction was electrostatic self-assembly due to charge complexation between the many consecutive blocks of positive and negative amino acids in the central region of the protein. A range of techniques were used to examine the structure of the protein in a variety of pH, ionic strength and temperature conditions to identify evidence of assembly into ordered structures. Together the circular dichroism, fluorescence, and light scattering data suggest that CP30 has an extended α-helical structure that unfolds with increased temperature, which reforms when cooled.

Circular dichroism spectra, shown in Figures 7.5 and 7.6, revealed that CP30 solutions had minima in ellipticity values around 208 and 222 nm, suggesting that the protein has an α-helical structure at 10ºC. Upon heating to 90ºC, the double minima disappeared and a single minimum at about 200 nm appeared, suggesting the structure unfolded to become random coil. The α-helical structure, however, was almost completely recovered upon cooling back to 10ºC. Plotting the ellipticity versus concentration for select wavelengths in Figure 7.6 showed that there was not a distinct unfolding temperature at which half the protein had changed conformation. This is likely because the helices were not bound into a very compact form initially, so the shift to the unfolded state was more subtle. Nevertheless, the values plateaued around 60°C, suggesting that the protein had changed completely from α-helix to random coil conformation. There did not seem to be a significant pH or ionic strength dependence, as shown in the direct comparisons in Figure 7.7. The expectation was that lower ionic strength would have resulted in less screening of electrostatic interactions and a pH closer to the protein's pI (5.82) would have resulted in more electrostatic interactions because the residues Arg, His and Lys would be positively charged and the residues Asp and Glu would be negatively charged. These conditions were expected to promote stronger associations and provide stronger evidence of structure, such as a clear melting temperature. However, the protein was lost during dialysis against buffer at pH 5 and low salt. This may indicate that the hypothesized electrostatic assembly caused the protein to precipitate out of solution or stick to the dialysis membrane and minimize recovery. The remaining conditions tested must have either had sufficient screening from salt ions or insufficient electrostatic attractions to promote the expected assembly. Instead, a loose helical structure was seen, most likely stabilized by sparsely packed hydrogen bonds and electrostatic interactions.

The fluorescence data further indicated that the structure was relatively loose, even at low temperatures. Trp normally emits light at 350-355 nm when exposed to a polar environment. When buried in a folded protein, the emission occurs at lower wavelengths (~down to 330 nm) because the energy of the excitation transition is higher when the Trp indole ring is not quenched by the solvent. Therefore, the fact that the fluorescence peak for CP30 was initially at 348 nm at 10°C suggests that the α-helical structure is loose, allowing for most of the protein to be in contact with the solvent. When the temperature was increased, the peak shifted to higher wavelengths (Figure 7.9) and the peak intensity values decreased (Figure 7.10), indicating that the Trp residues became even more exposed. This change was subtle, most likely because the helices were in a loose conformation initially, so a distinct melting temperature was not observed. However, an initiation temperature around 55-70°C was observed (Figure 7.9), indicating that the largest change in structure occurred in that temperature range. It is important to note that the Trp residues are all located near the N-terminus of the protein. Therefore, the fluorescence data may only reflect the structural properties of that part of the protein.

Dynamic light scattering showed that the hydrodynamic radius of the stock solution at 20°C was about 1.8 nm, which is typical of a single α-helical protein [368]. Static light scattering showed there was a slight increase in scattering intensity above 55°C. However, there was no visible aggregation so the effect might have been due to an increase in molecular size of the protein as it unfolded from an α-helical to a random coil conformation.

To summarize the results of the spectroscopic and light scattering experiments, CP30 was found to have an extended α-helical structure at low temperatures. The structure unfolds into a random coil configuration around 60°C but reforms when cooled. Additional work is needed to clarify the structure at pH 5, low salt to determine if the protein is aggregating, associating or

sticking to membranes in that condition. Attempts could be made to solubilize the protein in buffer directly from the dry state to avoid the dialysis step, thus helping to understand whether sticking to the dialysis membrane was the problem. If the protein is still not soluble, then attempts should be made to prepare the protein in conditions that more closely bracket the pH 5, low salt condition. Specifically, pH 4, 4.5, 5 and 5.5 and intermediate salt concentrations (0.11, 0.18 and 0.25 M sodium chloride) could be tested to see if the structure changes as that condition of aggregation or association is approached. Also, higher concentrations should be tested, which would more closely reflect the *in vivo* state of the protein because rigid cuticle such as the elytron becomes less hydrated as it matures, possibly promoting self-assembling interactions. Additional circular dichroism scans could also be performed in the near UV to probe for changes in tertiary structure. In the near UV range, the absorption by aromatic groups is sensitive to the location within the protein, so the spectrum changes based on tertiary structural changes. It requires higher concentrations and longer path lengths, however, to achieve an acceptable signal-to-noise ratio so this should be attempted after evidence of stronger secondary structural features are observed in the additional pH, ionic strength and concentration conditions mentioned above. FTIR could also be used to provide a more sensitive measure of secondary structure, but it does require higher concentrations.

The second hypothesized interaction was the formation of coordination crosslinks between the His residues in CP30 and nickel ions. Since CP30 has a high histidine content, it may form coordination bonds with multivalent metal ions in a manner similar to the mussel adhesive proteins [82]. Microscopic imaging results, shown in Figure 7.12, provided evidence that that CP30 and $NiCl_2$ immediately formed microparticles when combined, thus supporting this hypothesized interaction. The viscoelastic character of the solution also changed; as shown

in Figure 7.13, the associations within the protein-metal ion solution restricted the free diffusion of probe particles, suggesting that it changed from a purely viscous liquid to a viscoelastic liquid. This supports the view that protein-metal ion interactions have a mechanical function in hard and stiff marine and arthropod structures.

7.6 Conclusions

CP30, a unique cuticle protein, has an extended helical structure at pH 3, 5 and 7 and high ionic strengths as well as pH 3 and 7 and low ionic strengths. Further work should be conducted to investigate whether association and/or aggregation occurs in conditions closer to pH 5, low salt, where the protein was lost during the sample preparation in this study and is expected to form the strongest electrostatic interactions. Thus the first hypothesized self-assembling motif was not directly supported but cannot be ruled out. The second hypothesized interaction, between CP30 and nickel ions, was supported by the formation of microparticles and the development of elasticity in the fluid when the protein was mixed with $NiCl_2$. The findings support the view that metal coordination crosslinking with His residues in cuticle proteins has an important role of stabilizing the mechanical properties of marine and arthropod structures. The cuticle protein CP30 has a unique sequence that may inspire novel motifs for developing biomaterials with controlled structures and mechanical properties.

Chapter 8: Conclusions

Biomimetic material design is an effective approach to developing materials with excellent, often multifunctional, properties. The insect cuticle is a particularly interesting material for biomimetic research. It has a wide range of mechanical properties with a relatively low density [34]. It serves important mechanical functions for the insect; hard cuticles such as elytra must be strong and tough to protect the organism from injury whereas soft cuticle within joints must be ductile and resilient to allow for locomotion. Some of the organization of components has been established, but many of the molecular interactions among the proteins, chitin and catechols are not yet understood. The objective of this thesis, therefore, was to identify key molecular interactions and their mechanical roles to provide new design criteria for structural biomaterials. Two major aims addressed this objective; first, the importance of covalent and non-covalent interactions within an intact cuticle structure was examined using static and dynamic mechanical tests as well as extraction in solvents and second, hypothesized interactions were isolated and their specific properties were studied *in vitro* using microrheology and structural analyses.

The cuticular structure of interest was the beetle elytron (outer wing cover). It is a strong and tough structure and several of the abundant proteins have been identified and expressed in bacteria by collaborators on this project. Previous graduate students at KU developed dynamic mechanical analysis methods that were used to demonstrate the importance of crosslinking for stabilizing the structure as the insect matures [20]. Important questions remained, however, concerning the relative importance of covalent and non-covalent crosslinks. Thus, the first major aim of this work was to clarify the influence of covalent and non-covalent interactions in governing the mechanical properties of the intact elytron. Together, Chapters 3 and 4

demonstrated that the elytron is a non-homogenous cuticle structure in which covalent interactions stabilize the material within 48 hours of secretion from the epidermal cells and non-covalent interactions add further stiffness without sacrificing toughness.

Specifically, the relative importance of each type of interaction was examined using static and dynamic mechanical analysis. While the tensile testing of the whole structure requires that it be modeled as a monolithic structure, details regarding the microstructural changes were considered when interpreting the results. Frequency, temperature, hydration, maturation time and bond-disrupting solvents were used to manipulate the conditions and elicit new information. The hypothesis of the dominant contribution of covalent crosslinking was supported. Even in the dried state, the storage modulus, E', was close to 10 times higher for tanned elytra than untanned elytra. Additionally, the frequency dependence of E' was lower for fully tanned, dry elytra ($n = 0.013 \pm 0.004$) than for untanned, dry elytra ($n = 0.050 \pm 0.024$) even at low frequencies, supporting the idea that covalent crosslinks stabilize the structure as the insect matures. Temperatures near degradation were required to lower the stiffness of tanned, dry elytra by 3.5 times and to increase the tan δ and frequency dependence, suggesting that covalent crosslinks greatly suppress the relaxation of biopolymer chains in cuticle. Overall, the view that tanning shifted the tan δ curve down and left because covalent crosslinks suppress viscous losses at all time scales whereas drying shifted it to the left only, was supported.

The increase in E' and decrease in frequency dependence with maturation was also found to plateau after 48 hours post-eclosion, suggesting that the initially secreted cuticle layers mature within a shorter time frame than the 7 days of cuticle development. The dorsal surface of the elytron also reached its mature color around 48 hours, suggesting that quinone crosslinking and pigmentation, which rely on some of the same precursor molecules, occur within that time frame.

The water content declined linearly over 7 days, but the majority of water was lost within the cavities between cuticular laminations, suggesting a relatively minor role of dehydration in governing the mechanical properties as this indicates that the water content of the fully mature load-bearing portion of the elytron's water content is not changing by this amount. The fact that more material could be extracted from partially tanned elytra than from fully tanned elytra most likely reflects the lower degree of covalent bonding within the material secreted at later times. Soaking elytra in formic acid, a strong hydrogen-bond breaking solvent, caused the static mechanical properties of fully tanned elytra to resemble those of partially tanned elytra, suggesting that the mature outer layers contained comparable degrees of covalent crosslinks. The untanned elytra, however, were significantly less stiff, less strong and more ductile than either the partially or fully tanned elytra, showing that they were less covalently crosslinked throughout the entire structure.

While the hypothesis of the dominant role of covalent crosslinking was supported, the importance of non-covalent interaction was also brought to light. Soaking elytra in non-covalent bond breaking solvents revealed the importance of non-covalent interactions, specifically H-bonds, for contributing to the stiffness. The toughness was not affected, possibly because non-covalent interactions can dissipate energy under loads. If the same level of stiffness had been achieved solely through covalent crosslinks, the material may have been significantly more brittle and less tough. Overall, covalent crosslinks stabilized the structure shortly after secretion from the epidermal cells, possibly providing a framework for the assembly and non-covalent bonding of other molecules. Non-covalent crosslinks stiffened the network, possibly at a higher length scale than the molecular level covalent crosslinks, thus allowing higher fracture strains than pure covalent crosslinks could provide. For example, non-covalent bonds among the

protein-wrapped chitin bundles at the micron scale may allow for higher displacements before the nano-scale interactions between individual proteins and chitin chains are stressed.

The first major aim answered important questions regarding the role of covalent and non-covalent interactions in the properties of the intact elytron; that is, covalent interactions stiffen the cuticle and reduce viscous dissipation shortly after eclosion and non-covalent interactions provide additional stiffness, possibly at higher length scales. However, some features of the complex biological structure, such as specific interactions between proteins and chitin or individual protein conformations and self-assembly, remained inaccessible. Thus, the second aim applied a different approach, in which key hypothesized interactions were studied apart from the complex biological system to shed light on the function of that feature *in vivo* and to assess the potential of that feature as a biomaterial design component. Specifically, protein-chitin binding, quinone crosslinking of proteins and protein self-assembly or metal-ion mediated coordination were examined. Chapters 5, 6 and 7 examined the hypothesized interactions within solutions of two of the most abundant proteins in the beetle elytron, CPR27 and CP30.

CPR27 contains a Rebers-Riddiford consensus sequence which is hypothesized to bind chitin. Active microrheology was used to detect a 2-fold decrease in the viscosity of aqueous, fluorescently labeled chitosan solutions with the addition of CPR27 (100:1 weight ratio chitosan:protein). The decrease was accompanied by the formation of fluorescent spots in the solutions, suggesting that complexation between the protein and the fluorescent chitosan produced aggregates that reduced the viscosity in the vicinity of the microrheology probes. CP30, a non-RR protein, did not affect the chitosan solutions, suggesting a specific interaction between the hypothesized chitin-binding sequence and chitosan. Thus, the RR motif likely plays

an important mechanical role in cuticle and may suggest a new motif for protein-polysaccharide composite biomaterial design.

Both CPR27 and CP30 were hypothesized to undergo quinone-mediated crosslinking reactions via histidine residues. Passive microrheology was used to monitor the viscoelastic properties of solutions of proteins, catechols and enzymes as reactions proceeded over time. The reaction between protein, catechol and enzyme as well as catechol and enzyme caused the formation of microparticles. Evidence of elasticity was observed in solutions containing the protein, but not in solutions containing just the catechol and enzyme. Thus, crosslinked proteins may have limited the diffusive motion of the microrheology probes. The strength of microrheology as a method for providing rheological data as well as microscopic structural information was demonstrated by these studies. However, further tests are needed to ensure the reproducibility of the results and to establish the origin of the elasticity.

The last hypothesized interaction studied *in vitro* was CP30 self-assembly and coordination crosslinking with metal ions. CP30 has a unique sequence with many short blocks of consecutive positive and negative amino acids, which was hypothesized to promote assembly into aggregates or fibers. It also has a high histidine content that may promote coordination crosslinking with multivalent metal ions. The CD, fluorescence, and light scattering studies on CP30 solutions revealed that the protein had an extended α-helical conformation at pH 3, 5 and 7 which unfolded around 60°C and reformed upon cooling back to 10°C. The results did not directly support the electrostatic self-assembly hypothesis. However, considering that the protein aggregated or adsorbed to membranes, preventing analysis at pH 5, low salt (0.04 M sodium chloride), further experiments at conditions that bracket this pH may indicate assembly. Evidence of interaction between CP30 and nickel ions was observed by the formation of

microparticles and the development of elasticity (shown by curvature in the MSD data) in the fluid. The ion coordination bonds could provide a useful motif for biomaterial design.

As a whole, this thesis demonstrates a truly biomimetic approach to material design. The structure-property relationships of an intact cuticle structure was studied, followed by the study of isolated, *in vitro* model systems which feeds back into the understanding of the structure as a whole and indicates the potential for cuticle-mimetic motifs in biomaterial synthesis. Covalent bonds were found to stabilize the cuticle within 48 hrs of maturation while non-covalent interactions were found to further increase stiffness without sacrificing toughness. RR protein-chitin binding, histidine-metal ion coordination crosslinking, and protein-catechol crosslinking were shown to affect rheological properties of model cuticle solutions, suggesting their importance in the *in vivo* material as well as their potential as design motifs. A major strength, yet challenge, of this work is that expertise in a diverse set of experimental techniques is needed to answer important questions about biological design features. This project is highly interdisciplinary and collaborative, making it exciting and worth studying from multiple perspectives.

Recommendations

While the results of this thesis advance the understanding of molecular interactions within insect cuticle that could be useful in the future for developing new biomaterial design strategies, the potential for further advances is great. Regarding the studies on the intact beetle elytron, one valuable experiment may be to perform dynamic mechanical analysis at lower temperatures to possibly identify the glass transition. The work here focused on the higher temperature transition since it was already emerging for untanned elytra. However, additional

low-temperature data would help confirm that the current and previous testing was, in fact, performed in the rubbery region of the elytron material. As discussed in Chapter 4, it was not unambiguous whether the testing was actually within the rubbery region. An additional transition observed at lower temperatures, if possible, would confirm that the previous results were in the rubbery state.

Additionally, micromechanical tests and mathematical modeling may reveal some important differences in the physical properties at different length scales. The tensile tests on the bulk material performed in this thesis revealed information about the overall connectivity of the structural components, but the length scale of these interactions cannot be precisely identified. The beetle elytron is a hierarchical structure in which the viscoelastic properties may vary depending on the direction or length scale of the applied load. Compact cortical bone, for example is a complex, hierarchical tissues that has been shown to have anisotropic material properties in which several different elastic constants are needed to properly model the mechanics of the multi-scale structure [369-371]. Thus, it may be interesting to use nanoindentation along with analytical modeling such as finite-element analysis of the elytral structure to reveal how the hierarchical structure influences the mechanical properties [372]. Overall, however, the transition from studies on the intact structure to *in vitro* studies of isolated cuticular interactions was motivated by the complexity of biological structure which ultimately limited to precision to which properties could be connected to exact molecular interactions.

Microrheology was shown to be a valuable tool for studying the interactions within *in vitro* cuticle systems. The small volumes required to obtain quantitative rheological data is extremely valuable because the recombinant cuticle proteins and highly purified and well-characterized chitosan are available in limited amounts. Additionally, the fact that

microrheology allows for the simultaneous visualization of microscopic structures has been an important part of interpreting the quantitative results. The sealed system also prevents evaporation which can cause problems in conventional rheology. Several recommendations can be made, however, to address some limitations of the studies described in the second part of this thesis, as well as to extend the method to other hypothesized interactions.

First of all, the passive microrheology studies of hypothesized covalent crosslinking of cuticle proteins could be improved. The drifting of the passive microrheology probes should be solved to obtain reliable viscoelastic moduli, as discussed in Chapter 6. It is most likely that the drifting was an artifact of my experimental setup and could be solved to obtain more reliable results for these experiments. Furthermore, a few modifications to the reaction conditions, explained in Chapter 6, could make the products soluble for longer times. The lack of solubility of the products limits the usefulness of microrheology for this particular interaction. While particle suspensions can affect rheological properties in unique ways, the phenomena causing the changes are different from what is expected by crosslinking of soluble polymers. Microrheology is a very useful tool for monitoring the crosslinking reactions of polymer solutions as well as biological systems [325, 327, 338, 373]. Pioneers of the method have shown that the viscoelastic properties of crosslinked polymer solutions as gelation occurred could be accurately measured using particle tracking microrheology. The measurements of G' and G'' were in agreement with conventional "macro"-rheological measurements for the material in both the sol and gel states as well as near the sol/gel transition [338]. As the reaction proceeded, G' increased relative to G'' and became more frequency-independent, as expected for crosslinking in the rubbery state [338]. Microrheology has also been used to characterize the physical properties of comb polyelectrolytes such as aggrecan [327] and cytoskeletal structures such as actin filaments and

microtubules [325, 374]. However, the measurements rely on solubility of the products. Thus, conditions for optimal solubility, or possibly gel formation, of the cuticle protein crosslinking products, as discussed in Chapter 6, should be investigated.

Additionally, the viscoelastic data must be supplemented with spectroscopic techniques to connect the viscoelastic changes with specific structural and chemical interactions. Microrheology, by itself, is useful for quantifying the viscoelastic properties of the fluids, but it is most useful when supplemented by additional techniques to identifying the precise structures and interactions. Optical microscopy, which can be done simultaneously with particle tracking microrheology, can detect only very large structures (greater than 0.5 μm) such as actin DNA and microtubules [319]. However, for smaller structures such as protein networks, light scattering would be useful [319, 375]. Static light scattering from multiple angles can provide information regarding the length scale and shape of structures within complex fluids [319, 375]. Fourier transform infrared (FTIR) spectroscopy and nuclear magnetic resonance (NMR) spectroscopy would also be particularly useful for resolving the structure of the cuticle proteins and for detecting binding to other molecules. FTIR can detect vibrational motions of certain functional groups that absorb infrared light, which are sensitive to structure, thus allowing detection of structural changes. It may, therefore, detect changes in CPR27 as it binds to chitosan or changes to CP30 as it binds to metal ions. Heteronuclear and multidimensional NMR spectroscopy can distinguish between the signals of neighboring nuclei and can determine dihedral angles as well as distance measurements between non-covalently bonded atoms, thus providing information on the 3D structure of proteins [376, 377]. Also, interactions between other molecules and proteins can be detected, even when binding affinities are very weak. Since binding changes the electron shielding around the protein nuclei, NMR spectra can detect the

interaction by a change in the chemical shift for the particular region of the protein in which binding occurred [376]. A combination of these structural probes should be used in addition to microrheology to relate the specific structures to the viscoelastic properties.

Beyond the hypotheses addressed in this thesis, there is more potential for future work in the area of cuticle biomimetics. In considering the hierarchical design of insect cuticle, I think that the focus should be on the nanometer-scale interactions among the structural biopolymers (level III in Figure 2.1 of Chapter 2). The work in this thesis has consistently supported the dominant role of molecular interactions in governing the physical properties of the elytron, while higher-level features appear to be specific to the biological conditions or needs of the insect during development. Thus, future work should focus on cuticle-mimetic protein and/or polysaccharide systems in which the properties are highly tuned to a particular application. For example, the concept of chitin nanofibers embedded in a highly crosslinked protein network may lead to the design of tissue engineering scaffolds that have stiffnesses comparable to bone, but without the need for mineral reinforcement. Artificial proteins with the RR motif could be used with chitin nanofibers to achieve even better properties than chitin-silk composite materials recently made with a modulus of 2.7 GPa [132]. Additionally, the ratio of chitin to protein could be varied to tune the modulus or perhaps develop a modulus gradient for tissue engineering at the bone-cartilage interface.

Another cuticle protein, resilin, has been identified by the KSU group in *Tribolium castaneum*. It is very highly resilient and also contains the RR chitin-binding motif. It also has very few ionizable groups compared to other resilin proteins. *In vitro* interactions between resilin and chitosan or chitin nanofibers would be interesting to study if it could be expressed in higher quantities. If not, resilin-like polypeptides could be synthesized and their interactions

with polysaccharide polymers could be studied using microrheology and spectroscopy to connect viscoelastic properties with structural and chemical interactions. Additionally, the motifs within CPR27 and CP30 could be combined with motifs from elastic cuticle proteins such as resilin to achieve stiff yet resilient materials. Other polypeptides could be incorporated as well, such as cell binding or biodegradable sequences, for tissue engineering applications. Multicomponent networks could be synthesized that mimic the mechanisms within cuticle that both store and dissipate energy to form tough hydrogels. Such materials would be valuable for the development of biomedical materials such as tissue-engineering scaffolds that require specific mechanical responses to a variety of loads.

REFERENCES

[1] Fernandez JG, Ingber DE. Bioinspired Chitinous Material Solutions for Environmental Sustainability and Medicine. Advanced Functional Materials 2013;23:4454-66.

[2] Gruber P. The signs of life in architecture. Bioinspiration & biomimetics 2008;3:023001.

[3] Knippers J, Speck T. Design and construction principles in nature and architecture. Bioinspiration & biomimetics 2012;7:015002.

[4] Studart AR. Towards High-Performance Bioinspired Composites. Advanced Materials 2012;24:5024-44.

[5] Sarikaya M, Tamerler C, Jen AK-Y, Schulten K, Baneyx F. Molecular biomimetics: nanotechnology through biology. Nat Mater 2003;2:577-85.

[6] Que L, Tolman WB. Biologically inspired oxidation catalysis. Nature 2008;455:333-40.

[7] Parker AR, Townley HE. Biomimetics of photonic nanostructures. Nature Nanotechnology 2007;2:347-53.

[8] Wegst UGK, Ashby MF. The mechanical efficiency of natural materials. Philos Mag 2004;84:2167-81.

[9] Altman GH, Diaz F, Jakuba C, Calabro T, Horan RL, Chen J, et al. Silk-based biomaterials. Biomaterials 2003;24:401-16.

[10] O'Brien JP, Fahnestock SR, Termonia Y, Gardner KH. Nylons from nature: synthetic analogs to spider silk. Advanced Materials 1998;10:1185-95.

[11] Langer R, Tirrell DA. Designing materials for biology and medicine. Nature 2004;428:487-92.

[12] Buehler MJ. Tu (r) ning weakness to strength. Nano Today 2010;5:379-83.

[13] Dunlop JW, Fratzl P. Biological composites. Annual Review of Materials Research 2010;40:1-24.

[14] Fratzl P. Biomimetic materials research: what can we really learn from nature's structural materials? Journal of the Royal Society Interface 2007;4:637-42.

[15] Neville AC. Biology of the arthropod cuticle: Springer-verlag Berlin; 1975.

[16] Andersen SO. Cuticular sclerotization and tanning. In: Gilbert LI, Iatrou K, Gill S, editors. Comprehensive Molecular Insect Science: Elsevier, Oxford, U.K.; 2005. p. 145–70.

[17] Andersen SO. Cuticular sclerotization and tanning. In: Kerkut GA, Gilbert LI, editors. Comprehensive Insect Physiology, Biochemistry and Molecular Biology. New York: Pergamon Press; 2005. p. 145-70.

[18] Bayley T, Sutton G, Burrows M. A buckling region in locust hindlegs contains resilin and absorbs energy when jumping or kicking goes wrong. The Journal of Experimental Biology 2012;215:1151-61.

[19] Barbakadze N, Enders S, Gorb S, Arzt E. Local mechanical properties of the head articulation cuticle in the beetle *Pachnoda marginata* (Coleoptera, Scarabaeidae). J Exp Biol 2006;209:722-30.

[20] Lomakin J, Huber PA, Eichler C, Arakane Y, Kramer KJ, Beeman RW, et al. Mechanical properties of the beetle elytron, a biological composite material. Biomacromolecules 2011;12:321–35.

[21] Vincent JF. Arthropod cuticle: a natural composite shell system. Composites Part A: Applied Science and Manufacturing 2002;33:1311-5.

[22] Romano P, Fabritius H, Raabe D. The exoskeleton of the lobster *Homarus americanus* as an example of a smart anisotropic biological material. Acta Biomater 2007;3:301-9.

[23] Gardiner B, Khan M. A new form of insect cuticle. Zoological Journal of the Linnean Society 1979;66:91-4.

[24] Andersen S. Characteristic properties of proteins from pre-ecdysial cuticle of larvae and pupae of the mealworm Tenebrio molitor. Insect biochemistry and molecular biology 2002;32:1077-87.

[25] Andersen SO, Hojrup P, Roepstorff P. Insect cuticular proteins. Insect biochemistry and molecular biology 1995;25:153-76.

[26] Rebers JE, Riddiford LM. Structure and expression of a Manduca sexta larval cuticle gene homologous to Drosophila cuticle genes* 1. Journal of molecular biology 1988;203:411-23.

[27] Willis JH, Iconomidou VA, Smith RF, Hamodrakas SJ. Cuticular proteins. Comprehensive molecular insect science Oxford, UK: Elsevier 2005.

[28] Rebers JE, Willis JH. A conserved domain in arthropod cuticular proteins binds chitin. Insect biochemistry and molecular biology 2001;31:1083-93.

[29] Togawa T, Nakato H, Izumi S. Analysis of the chitin recognition mechanism of cuticle proteins from the soft cuticle of the silkworm, Bombyx mori. Insect Biochemistry and Molecular Biology 2004;34:1059-67.

[30] Andersen S. Amino acid sequence studies on endocuticular proteins from the desert locust, Schistocerca gregaria. Insect biochemistry and molecular biology 1998;28:421.

[31] Iconomidou VA, Willis JH, Hamodrakas SJ. Unique features of the structural model of 'hard' cuticle proteins: implications for chitin-protein interactions and cross-linking in cuticle. Insect Biochemistry and Molecular Biology 2005;35:553-60.

[32] Iconomidou VA, Chryssikos GD, Gionis V, Willis JH, Hamodrakas SJ. “Soft”-cuticle protein secondary structure as revealed by FT-Raman, ATR FT-IR and CD spectroscopy. Insect biochemistry and molecular biology 2001;31:877-85.

[33] Locke M. The structure and formation of the integument in insects. The physiology of Insecta 1964;3:379-470.

[34] Vincent JFV, Wegst UGK. Design and mechanical properties of insect cuticle. Arthropod Struct Dev 2004;33:187-99.

[35] Guild F, Harris B, Atkins A. Cracking in layered composites. Journal of Materials Science 1978;13:2295-9.

[36] Andersen SO. Cuticular sclerotization and tanning. 2011.

[37] Cunniff PM, Fossey SA, Auerbach MA, Song JW, Kaplan DL, Adams WW, et al. Mechanical and thermal properties of dragline silk from the spider Nephila clavipes. Polymers for advanced technologies 1994;5:401-10.

[38] Keten S, Buehler MJ. Nanostructure and molecular mechanics of spider dragline silk protein assemblies. Journal of the Royal Society Interface 2010;7:1709-21.

[39] Giesa T, Arslan M, Pugno NM, Buehler MJ. Nanoconfinement of spider silk fibrils begets superior strength, extensibility, and toughness. Nano letters 2011;11:5038-46.

[40] Papadopoulos P, Sölter J, Kremer F. Hierarchies in the structural organization of spider silk—a quantitative model. Colloid and Polymer Science 2009;287:231-6.

[41] Vollrath F, Knight DP. Liquid crystalline spinning of spider silk. Nature 2001;410:541-8.

[42] Shao Z, Vollrath F. Materials: Surprising strength of silkworm silk. Nature 2002;418:741-.

[43] Qin Z, Buehler MJ. Cooperative deformation of hydrogen bonds in beta-strands and beta-sheet nanocrystals. Phys Rev E 2010;82:061906.

[44] Barthelat F. Biomimetics for next generation materials. Philosophical Transactions of the Royal Society A: Mathematical, Physical and Engineering Sciences 2007;365:2907-19.

[45] Dubey D, Tomar V. Role of Molecular Level Interfacial Forces in Hard Biomaterial Mechanics: A Review. Annals of biomedical engineering 2010;38:2040-55.

[46] Dunlop J, Fratzl P. Biological Composites. Annual Review of Materials Research 2010;40:1-24.

[47] Pokroy B, Demensky V, Zolotoyabko E. Nacre in Mollusk Shells as a Multilayered Structure with Strain Gradient. Advanced Functional Materials 2009;19:1054-9.

[48] Bonderer LJ, Studart AR, Gauckler LJ. Bioinspired design and assembly of platelet reinforced polymer films. Science 2008;319:1069-73.

[49] Deville S, Saiz E, Nalla RK, Tomsia AP. Freezing as a path to build complex composites. Science 2006;311:515-8.

[50] Munch E, Launey ME, Alsem DH, Saiz E, Tomsia AP, Ritchie RO. Tough, bio-inspired hybrid materials. Science 2008;322:1516-20.

[51] Tang Z, Kotov NA, Magonov S, Ozturk B. Nanostructured artificial nacre. Nat Mater 2003;2:413-8.

[52] Yao HB, Tan ZH, Fang HY, Yu SH. Artificial Nacre-like Bionanocomposite Films from the Self-Assembly of Chitosan–Montmorillonite Hybrid Building Blocks. Angewandte Chemie International Edition 2010;49:10127-31.

[53] Walther A, Bjurhager I, Malho J-M, Pere J, Ruokolainen J, Berglund LA, et al. Large-area, lightweight and thick biomimetic composites with superior material properties via fast, economic, and green pathways. Nano letters 2010;10:2742-8.

[54] Cheng Q, Li M, Jiang L, Tang Z. Bioinspired Layered Composites Based on Flattened Double-Walled Carbon Nanotubes. Advanced Materials 2012;24:1838-43.

[55] Launey ME, Ritchie RO. On the fracture toughness of advanced materials. Adv Mater 2009;21:2103ñ10.

[56] Fantner GE, Hassenkam T, Kindt JH, Weaver JC, Birkedal H, Pechenik L, et al. Sacrificial bonds and hidden length dissipate energy as mineralized fibrils separate during bone fracture. Nat Mater 2005;4:612-6.

[57] Gupta HS, Fratzl P, Kerschnitzki M, Benecke G, Wagermaier W, Kirchner HO. Evidence for an elementary process in bone plasticity with an activation enthalpy of 1 eV. Journal of the Royal Society Interface 2007;4:277-82.

[58] Lawn B, Lee J, Chai H. Teeth: Among Nature's Most Durable Biocomposites. Annual Review of Materials Research 2010;40:55-75.

[59] Hannig M, Hannig C. Nanomaterials in preventive dentistry. Nature nanotechnology 2010;5:565-9.

[60] Bentov S, Zaslansky P, Al-Sawalmih A, Masic A, Fratzl P, Sagi A, et al. Enamel-like apatite crown covering amorphous mineral in a crayfish mandible. Nature Communications 2012;3:839.

[61] Chai H, Lee JJW, Constantino PJ, Lucas PW, Lawn BR. Remarkable resilience of teeth. Proceedings of the National Academy of Sciences 2009;106:7289.

[62] Miserez A, Li Y, Waite JH, Zok F. Jumbo squid beaks: Inspiration for design of robust organic composites. Acta Biomaterialia 2007;3:139-49.

[63] Miserez A, Schneberk T, Sun C, Zok FW, Waite JH. The transition from stiff to compliant materials in squid beaks. Science 2008;319:1816-9.

[64] Pisano J, Finlayson J, Peyton MP. Cross-link in fibrin polymerized by factor XIII: ε-(γ-glutamyl) lysine. Science 1968;160:892-3.

[65] Doolittle RF, Chen R, Lau F. Hybrid fibrin: Proof of the intermolecular nature of γ-γ crosslinking units. Biochemical and biophysical research communications 1971;44:94-100.

[66] Sobel JH, Gawinowicz MA. Identification of the α chain lysine donor sites involved in factor XIIIa fibrin cross-linking. Journal of Biological Chemistry 1996;271:19288-97.

[67] Sanborn TJ, Messersmith PB, Barron AE. In situ crosslinking of a biomimetic peptide-PEG hydrogel via thermally triggered activation of factor XIII. Biomaterials 2002;23:2703-10.

[68] Lorand L. Fibrin clots. 1950.

[69] Schense JC, Bloch J, Aebischer P, Hubbell JA. Enzymatic incorporation of bioactive peptides into fibrin matrices enhances neurite extension. Nature biotechnology 2000;18:415-9.

[70] Cooper A, Eyles SJ, Radford SE, Dobson CM. Thermodynamic consequences of the removal of a disulphide bridge from hen lysozyme. Journal of molecular biology 1992;225:939-43.

[71] Morozova LA, Haynie DT, Arico-Muendel C, Van Dael H, Dobson CM. Structural basis of the stability of a lysozyme molten globule. Nature Structural & Molecular Biology 1995;2:871-5.

[72] Li B, Haynie DT. Multilayer biomimetics: reversible covalent stabilization of a nanostructured biofilm. Biomacromolecules 2004;5:1667-70.

[73] Smith BL, Schäffer TE, Viani M, Thompson JB, Frederick NA, Kindt J, et al. Molecular mechanistic origin of the toughness of natural adhesives, fibres and composites. Nature 1999;399:761-3.

[74] Keten S, Buehler MJ. Geometric confinement governs the rupture strength of H-bond assemblies at a critical length scale. Nano Letters 2008;8:743-8.

[75] Nissan AH. H-bond dissociation in hydrogen bond dominated solids. Macromolecules 1976;9:840-50.

[76] Reynolds SE. The mechanical properties of the abdominal cuticle of Rhodnius larvae. The Journal of experimental biology 1975;62:69-80.

[77] Tychsen PH, Vincent J. Correlated changes in mechanical properties of the intersegmental membrane and bonding between proteins in the female adult locust. Journal of Insect Physiology 1976;22:115-25.

[78] Klocke D, Schmitz H. Water as a major modulator of the mechanical properties of insect cuticle. Acta Biomater 2011;7:2935-42.

[79] Gutsmann T, Hassenkam T, Cutroni JA, Hansma PK. Sacrificial bonds in polymer brushes from rat tail tendon functioning as nanoscale velcro. Biophys J 2005;89:536-42.

[80] Currey J. Biomaterials: sacrificial bonds heal bone. Nature 2001;414:699-.

[81] Thompson JB, Kindt JH, Drake B, Hansma HG, Morse DE, Hansma PK. Bone indentation recovery time correlates with bond reforming time. Nature 2001;414:773-6.

[82] Fullenkamp DE, He L, Barrett DG, Burghardt WR, Messersmith PB. Mussel-Inspired Histidine-Based Transient Network Metal Coordination Hydrogels. Macromolecules 2013.

[83] Lichtenegger HC, Schöberl T, Ruokolainen JT, Cross JO, Heald SM, Birkedal H, et al. Zinc and mechanical prowess in the jaws of Nereis, a marine worm. Proceedings of the National Academy of Sciences 2003;100:9144-9.

[84] Oliver WC, Pharr GM. An improved technique for determining hardness and elastic modulus using load and displacement sensing indentation experiments. Journal of materials research 1992;7:1564-83.

[85] Cribb BW, Stewart A, Huang H, Truss R, Noller B, Rasch R, et al. Insect mandibles-comparative mechanical properties and links with metal incorporation. Naturwissenschaften 2008;95:17-23.

[86] Schofield R, Nesson M, Richardson K, Wyeth P. Zinc is incorporated into cuticular "tools" after ecdysis: The time course of the zinc distribution in "tools" and whole bodies of an ant and a scorpion. Journal of insect physiology 2003;49:31-44.

[87] Schofield RM, Nesson MH, Richardson KA. Tooth hardness increases with zinc-content in mandibles of young adult leaf-cutter ants. Naturwissenschaften 2002;89:579-83.

[88] Broomell C, Zok F, Waite J. Role of transition metals in sclerotization of biological tissue. Acta Biomater 2008;4:2045-51.

[89] Cribb BW, Lin CL, Rintoul L, Rasch R, Hasenpusch J, Huang H. Hardness in arthropod exoskeletons in the absence of transition metals. Acta Biomater 2010;6:3152-6.

[90] Israelachvili J, Pashley R. The hydrophobic interaction is long range, decaying exponentially with distance. 1982.

[91] Schnur J, Price R, Schoen P, Yager P, Calvert J, Georger J, et al. Lipid-based tubule microstructures. Thin Solid Films 1987;152:181-206.

[92] Ma PX. Biomimetic materials for tissue engineering. Advanced drug delivery reviews 2008;60:184-98.

[93] van Hest JC, Tirrell DA. Protein-based materials, toward a new level of structural control. Chemical Communications 2001:1897-904.

[94] Schnarr NA, Kennan AJ. Specific control of peptide assembly with combined hydrophilic and hydrophobic interfaces. J Am Chem Soc 2003;125:667-71.

[95] Rief M, Gautel M, Oesterhelt F, Fernandez JM, Gaub HE. Reversible unfolding of individual titin immunoglobulin domains by AFM. science 1997;276:1109-12.

[96] Mehta AD, Rief M, Spudich JA, Smith DA, Simmons RM. Single-molecule biomechanics with optical methods. Science 1999;283:1689-95.

[97] Gao H, Wang X, Yao H, Gorb S, Arzt E. Mechanics of hierarchical adhesion structures of geckos. Mechanics of Materials 2005;37:275-85.

[98] Autumn K, Sitti M, Liang YA, Peattie AM, Hansen WR, Sponberg S, et al. Evidence for van der Waals adhesion in gecko setae. Proceedings of the National Academy of Sciences 2002;99:12252-6.

[99] Duarte A, Coelho J, Bordado J, Cidade M, Gil M. Surgical adhesives: systematic review of the main types and development forecast. Progress in Polymer Science 2012;37:1031-50.

[100] Lee H, Lee BP, Messersmith PB. A reversible wet/dry adhesive inspired by mussels and geckos. Nature 2007;448:338-41.

[101] Riekel C, Müller M, Vollrath F. In situ X-ray diffraction during forced silking of spider silk. Macromolecules 1999;32:4464-6.

[102] Asakura T, Ito T, Okudaira M, Kameda T. Structure of Alanine and Glycine Residues of Samia c ynthia r icini Silk Fibers Studied with Solid-State 15N and 13C NMR. Macromolecules 1999;32:4940-6.

[103] Simmons AH, Michal CA, Jelinski LW. Molecular orientation and two-component nature of the crystalline fraction of spider dragline silk. Science 1996;271:84-7.

[104] Shao Z, Vollrath F, Sirichaisit J, Young R. Analysis of spider silk in native and supercontracted states using Raman spectroscopy. Polymer 1999;40:2493-500.

[105] MacKintosh F, Schmidt C. Microrheology. Current opinion in colloid & interface science 1999;4:300-7.

[106] Crick F, Hughes A. The physical properties of cytoplasm: A study by means of the magnetic particle method Part I. Experimental. Experimental Cell Research 1950;1:37-80.

[107] King M, Macklem PT. Rheological properties of microliter quantities of normal mucus. Journal of Applied Physiology 1977;42:797-802.

[108] Breedveld V, Pine D. Microrheology as a tool for high-throughput screening. Journal of Materials Science 2003;38:4461-70.

[109] Abou B, Gay C, Laurent B, Cardoso O, Voigt D, Peisker H, et al. Extensive collection of femtolitre pad secretion droplets in the beetle Leptinotarsa decemlineata allows nanolitre microrheology. Journal of The Royal Society Interface 2010;7:1745-52.

[110] Weihs D, Mason TG, Teitell MA. Bio-microrheology: a frontier in microrheology. Biophys J 2006;91:4296-305.

[111] Gambini C, Abou B, Ponton A, Cornelissen AJ. Micro-and macrorheology of jellyfish extracellular matrix. Biophys J 2012;102:1-9.

[112] Li Y, Ortiz C, Boyce MC. Bioinspired, mechanical, deterministic fractal model for hierarchical suture joints. Phys Rev E 2012;85:031901.

[113] Xia J, Gaynor SG, Matyjaszewski K. Controlled/"living" radical polymerization. Atom transfer radical polymerization of acrylates at ambient temperature. Macromolecules 1998;31:5958-9.

[114] Petka WA, Harden JL, McGrath KP, Wirtz D, Tirrell DA. Reversible hydrogels from self-assembling artificial proteins. Science 1998;281:389-92.

[115] Dooley K, Kim YH, Lu HD, Tu R, Banta S. Engineering of an environmentally responsive beta roll peptide for use as a calcium-dependent cross-linking domain for peptide hydrogel formation. Biomacromolecules 2012;13:1758-64.

[116] Chenal A, Guijarro JI, Raynal B, Delepierre M, Ladant D. RTX calcium binding motifs are intrinsically disordered in the absence of calcium. Implication for protein secretion. Journal of Biological Chemistry 2009;284:1781-9.

[117] Bauche C, Chenal A, Knapp O, Bodenreider C, Benz R, Chaffotte A, et al. Structural and functional characterization of an essential RTX subdomain of Bordetella pertussis adenylate cyclase toxin. Journal of Biological Chemistry 2006;281:16914-26.

[118] Betre H, Setton LA, Meyer DE, Chilkoti A. Characterization of a genetically engineered elastin-like polypeptide for cartilaginous tissue repair. Biomacromolecules 2002;3:910-6.

[119] Panitch A, Yamaoka T, Fournier MJ, Mason TL, Tirrell DA. Design and biosynthesis of elastin-like artificial extracellular matrix proteins containing periodically spaced fibronectin CS5 domains. Macromolecules 1999;32:1701-3.

[120] Urry D, Hugel T, Seitz M, Gaub H, Sheiba L, Dea J, et al. Elastin: a representative ideal protein elastomer. Philosophical Transactions of the Royal Society of London Series B: Biological Sciences 2002;357:169-84.

[121] Wright ER, Conticello VP. Self-assembly of block copolymers derived from elastin-mimetic polypeptide sequences. Advanced Drug Delivery Reviews 2002;54:1057-73.

[122] Kim W, Chaikof EL. Recombinant elastin-mimetic biomaterials: emerging applications in medicine. Advanced drug delivery reviews 2010;62:1468-78.

[123] Charati MB, Ifkovits JL, Burdick JA, Linhardt JG, Kiick KL. Hydrophilic elastomeric biomaterials based on resilin-like polypeptides. Soft Matter 2009;5:3412-6.

[124] Kwon I, Kirshenbaum K, Tirrell DA. Breaking the degeneracy of the genetic code. J Am Chem Soc 2003;125:7512-3.

[125] Barrera DA, Zylstra E, Lansbury Jr PT, Langer R. Synthesis and RGD peptide modification of a new biodegradable copolymer: poly (lactic acid-co-lysine). J Am Chem Soc 1993;115:11010-1.

[126] Halstenberg S, Panitch A, Rizzi S, Hall H, Hubbell JA. Biologically engineered protein-graft-poly (ethylene glycol) hydrogels: a cell adhesive and plasmin-degradable biosynthetic material for tissue repair. Biomacromolecules 2002;3:710-23.

[127] Tamerler C, Sarikaya M. Molecular biomimetics: utilizing nature's molecular ways in practical engineering. Acta Biomater 2007;3:289-99.

[128] Hart DS, Gehrke SH. Thermally associating polypeptides designed for drug delivery produced by genetically engineered cells. Journal of pharmaceutical sciences 2007;96:484-516.

[129] Yu M, Deming TJ. Synthetic polypeptide mimics of marine adhesives. Macromolecules 1998;31:4739-45.

[130] Rinaudo M. Main properties and current applications of some polysaccharides as biomaterials. Polymer International 2008;57:397-430.

[131] Fernandez JG, Ingber DE. Unexpected Strength and Toughness in Chitosan-Fibroin Laminates Inspired by Insect Cuticle. Advanced Materials 2012;24:480-+.

[132] Jin J, Hassanzadeh P, Perotto G, Sun W, Brenckle MA, Kaplan D, et al. A Biomimetic Composite from Solution Self-Assembly of Chitin Nanofibers in a Silk Fibroin Matrix. Advanced Materials 2013;25:4482-7.

[133] Zhong C, Cooper A, Kapetanovic A, Fang Z, Zhang M, Rolandi M. A facile bottom-up route to self-assembled biogenic chitin nanofibers. Soft Matter 2010;6:5298-301.

[134] Kogan G, Šoltés L, Stern R, Gemeiner P. Hyaluronic acid: a natural biopolymer with a broad range of biomedical and industrial applications. Biotechnology letters 2007;29:17-25.

[135] Balazs EA. Therapeutic use of hyaluronan. Structural Chemistry 2009;20:341-9.

[136] Esposito E, Menegatti E, Cortesi R. Hyaluronan-based microspheres as tools for drug delivery: a comparative study. International journal of pharmaceutics 2005;288:35-49.

[137] Jia X, Yeo Y, Clifton RJ, Jiao T, Kohane DS, Kobler JB, et al. Hyaluronic acid-based microgels and microgel networks for vocal fold regeneration. Biomacromolecules 2006;7:3336-44.

[138] Rinaudo M. Polyelectrolyte properties of a plant and animal polysaccharide. Structural Chemistry 2009;20:277-89.

[139] Sedo J, Saiz-Poseu J, Busque F, Ruiz-Molina D. Catechol-Based Biomimetic Functional Materials. Advanced Materials 2013;25:653-701.

[140] Waite JH. Nature's underwater adhesive specialist. International Journal of Adhesion and Adhesives 1987;7:9-14.

[141] Lee H, Scherer NF, Messersmith PB. Single-molecule mechanics of mussel adhesion. Proceedings of the National Academy of Sciences 2006;103:12999-3003.

[142] Wang J, Tahir MN, Kappl M, Tremel W, Metz N, Barz M, et al. Influence of Binding-Site Density in Wet Bioadhesion. Advanced Materials 2008;20:3872-6.

[143] McBride MB, Wesselink LG. Chemisorption of catechol on gibbsite, boehmite, and noncrystalline alumina surfaces. Environmental science & technology 1988;22:703-8.

[144] Li S-C, Chu L-N, Gong X-Q, Diebold U. Hydrogen bonding controls the dynamics of catechol adsorbed on a TiO2 (110) surface. Science 2010;328:882-4.

[145] Papov VV, Diamond TV, Biemann K, Waite JH. Hydroxyarginine-containing polyphenolic proteins in the adhesive plaques of the marine mussel *Mytilus edulis*. Journal of Biological Chemistry 1995;270:20183-92.

[146] Waite JH, Housley TJ, Tanzer ML. Peptide repeats in a mussel glue protein: theme and variations. Biochemistry 1985;24:5010-4.

[147] Waite JH. Adhesion a la moule. Integrative and comparative biology 2002;42:1172-80.

[148] Yu M, Hwang J, Deming TJ. Role of L-3, 4-dihydroxyphenylalanine in mussel adhesive proteins. J Am Chem Soc 1999;121:5825-6.

[149] Yamada K, Chen T, Kumar G, Vesnovsky O, Topoleski LT, Payne GF. Chitosan based water-resistant adhesive. Analogy to mussel glue. Biomacromolecules 2000;1:252-8.

[150] Lee BP, Messersmith PB, Israelachvili JN, Waite JH. Mussel-inspired adhesives and coatings. Annual review of materials research 2011;41:99.

[151] Brubaker CE, Kissler H, Wang L-J, Kaufman DB, Messersmith PB. Biological performance of mussel-inspired adhesive in extrahepatic islet transplantation. Biomaterials 2010;31:420-7.

[152] Murphy JL, Vollenweider L, Xu F, Lee BP. Adhesive performance of biomimetic adhesive-coated biologic scaffolds. Biomacromolecules 2010;11:2976-84.

[153] Ryu JH, Lee Y, Kong WH, Kim TG, Park TG, Lee H. Catechol-functionalized chitosan/pluronic hydrogels for tissue adhesives and hemostatic materials. Biomacromolecules 2011;12:2653-9.

[154] Holten-Andersen N, Harrington MJ, Birkedal H, Lee BP, Messersmith PB, Lee KYC, et al. pH-induced metal-ligand cross-links inspired by mussel yield self-healing polymer networks with near-covalent elastic moduli. Proceedings of the National Academy of Sciences 2011;108:2651-5.

[155] Watt AA, Bothma JP, Meredith P. The supramolecular structure of melanin. Soft Matter 2009;5:3754-60.

[156] Clancy CM, Simon JD. Ultrastructural organization of eumelanin from Sepia officinalis measured by atomic force microscopy. Biochemistry 2001;40:13353-60.

[157] Moses D, Mattoni M, Slack N, Waite J, Zok F. Role of melanin in mechanical properties *ofGlycera* jaws. Acta Biomater 2006;2:521-30.

[158] Lee H, Dellatore SM, Miller WM, Messersmith PB. Mussel-inspired surface chemistry for multifunctional coatings. science 2007;318:426-30.

[159] Tao C, Yang S, Zhang J, Wang J. Surface modification of diamond-like carbon films with protein via polydopamine inspired coatings. Applied Surface Science 2009;256:294-7.

[160] Shin M, Yoshimoto H, Vacanti JP. In vivo bone tissue engineering using mesenchymal stem cells on a novel electrospun nanofibrous scaffold. Tissue engineering 2004;10:33-41.

[161] Tao C, Zhang J, Yang S. Preparation and biocompatibility of BSA monolayer on silicon surface. Journal of nanoscience and nanotechnology 2011;11:5068-74.

[162] Poh CK, Shi Z, Lim TY, Neoh KG, Wang W. The effect of VEGF functionalization of titanium on endothelial cells in vitro. Biomaterials 2010;31:1578-85.

[163] Berglund JD, Nerem RM, Sambanis A. Incorporation of intact elastin scaffolds in tissue-engineered collagen-based vascular grafts. Tissue engineering 2004;10:1526-35.

[164] Weston MW, Rhee K, Tarbell JM. Compliance and diameter mismatch affect the wall shear rate distribution near an end-to-end anastomosis. Journal of biomechanics 1996;29:187-98.

[165] Kopeček J, Yang J. Peptide-directed self-assembly of hydrogels. Acta Biomater 2009;5:805-16.

[166] Kopeček J, Tang A, Wang C, Stewart RJ. De novo design of biomedical polymers: hybrids from synthetic macromolecules and genetically engineered protein domains. Macromolecular Symposia: Wiley Online Library; 2001. p. 31-42.

[167] Vandermeulen GW, Klok HA. Peptide/protein hybrid materials: enhanced control of structure and improved performance through conjugation of biological and synthetic polymers. Macromol Biosci 2004;4:383-98.

[168] Seal BL, Panitch A. Viscoelastic behavior of environmentally sensitive biomimetic polymer matrices. Macromolecules 2006;39:2268-74.

[169] Marsden HR, Korobko AV, van Leeuwen EN, Pouget EM, Veen SJ, Sommerdijk NA, et al. Noncovalent triblock copolymers based on a coiled-coil peptide motif. J Am Chem Soc 2008;130:9386-93.

[170] Zhao X. Multi-scale multi-mechanism design of tough hydrogels: building dissipation into stretchy networks. Soft Matter 2014;10:672.

[171] Berger J, Reist M, Mayer J, Felt O, Peppas N, Gurny R. Structure and interactions in covalently and ionically crosslinked chitosan hydrogels for biomedical applications. European Journal of Pharmaceutics and Biopharmaceutics 2004;57:19-34.

[172] Brown AE, Litvinov RI, Discher DE, Purohit PK, Weisel JW. Multiscale mechanics of fibrin polymer: gel stretching with protein unfolding and loss of water. Science 2009;325:741-4.

[173] DeKosky BJ, Dormer NH, Ingavle GC, Roatch CH, Lomakin J, Detamore MS, et al. Hierarchically designed agarose and poly (ethylene glycol) interpenetrating network hydrogels for cartilage tissue engineering. Tissue Engineering Part C: Methods 2010;16:1533-42.

[174] Gong JP, Katsuyama Y, Kurokawa T, Osada Y. Double-Network Hydrogels with Extremely High Mechanical Strength. Advanced Materials 2003;15:1155-8.

[175] Henderson KJ, Zhou TC, Otim KJ, Shull KR. Ionically Cross-Linked Triblock Copolymer Hydrogels with High Strength. Macromolecules 2010;43:6193-201.

[176] Kong HJ, Wong E, Mooney DJ. Independent control of rigidity and toughness of polymeric hydrogels. Macromolecules 2003;36:4582-8.

[177] Peppas NA, Merrill EW. Poly (vinyl alcohol) hydrogels: Reinforcement of radiation-crosslinked networks by crystallization. Journal of Polymer Science: Polymer Chemistry Edition 1976;14:441-57.

[178] Shin H, Olsen BD, Khademhosseini A. The mechanical properties and cytotoxicity of cell-laden double-network hydrogels based on photocrosslinkable gelatin and gellan gum biomacromolecules. Biomaterials 2012;33:3143-52.

[179] Shull KR. Materials science: A hard concept in soft matter. Nature 2012;489:36-7.

[180] Stauffer SR, Peppast NA. Poly (vinyl alcohol) hydrogels prepared by freezing-thawing cyclic processing. Polymer 1992;33:3932-6.

[181] Suekama TC, Hu J, Kurokawa T, Gong JP, Gehrke SH. Double-network strategy improves fracture properties of chondroitin sulfate networks. ACS Macro Letters 2013;2:137-40.

[182] Sun J-Y, Zhao X, Illeperuma WR, Chaudhuri O, Oh KH, Mooney DJ, et al. Highly stretchable and tough hydrogels. Nature 2012;489:133-6.

[183] Sun TL, Kurokawa T, Kuroda S, Ihsan AB, Akasaki T, Sato K, et al. Physical hydrogels composed of polyampholytes demonstrate high toughness and viscoelasticity. Nat Mater 2013;12:932-7.

[184] Wang Q, Mynar JL, Yoshida M, Lee E, Lee M, Okuro K, et al. High-water-content mouldable hydrogels by mixing clay and a dendritic molecular binder. Nature 2010;463:339-43.

[185] Yasuda K, Ping Gong J, Katsuyama Y, Nakayama A, Tanabe Y, Kondo E, et al. Biomechanical properties of high-toughness double network hydrogels. Biomaterials 2005;26:4468-75.

[186] Hu J, Kurokawa T, Nakajima T, Sun TL, Suekama T, Wu ZL, et al. High fracture efficiency and stress concentration phenomenon for microgel-reinforced hydrogels based on double-network principle. Macromolecules 2012;45:9445-51.

[187] Andersen SO. Insect cuticular sclerotization: a review. Insect biochemistry and molecular biology 2010;40:166-78.

[188] Vincent J, Hillerton J. The tanning of insect cuticle--A critical review and a revised mechanism. Journal of Insect Physiology 1979;25:653-8.

[189] Hopkins TL, Kramer KJ. Insect cuticle sclerotization. Annual review of entomology 1992;37:273-302.

[190] Sugumaran M. Unified mechanism for sclerotization of insect cuticle. Advances in Insect Physiology 1998;27:229-334.

[191] Kramer KJ, Kanost MR, Hopkins TL, Jiang H, Zhu YC, Xu R, et al. Oxidative conjugation of catechols with proteins in insect skeletal systems. Tetrahedron 2001;57:385-92.

[192] Hopkins TL, Morgan TD, Aso Y, Kramer KJ. N-β-Alanyldopamine: major role in insect cuticle tanning. Science 1982;217:364-6.

[193] Mendive F, Van Loy T, Claeysen S, Poels J, Williamson M, Hauser F, et al. *Drosophila* molting neurohormone bursicon is a heterodimer and the natural agonist of the orphan receptor DLGR2. FEBS letters 2005;579:2171-6.

[194] Luo C-W, Dewey EM, Sudo S, Ewer J, Hsu SY, Honegger H-W, et al. Bursicon, the insect cuticle-hardening hormone, is a heterodimeric cystine knot protein that activates G protein-coupled receptor LGR2. Proc Natl Acad Sci U S A 2005;102:2820-5.

[195] Arakane Y, Muthukrishnan S, Beeman RW, Kanost MR, Kramer KJ. Laccase 2 is the phenoloxidase gene required for beetle cuticle tanning. Proc Natl Acad Sci U S A 2005;102:11337-42.

[196] Niu BL, Shen WF, Liu Y, Weng HB, He LH, Mu JJ, et al. Cloning and RNAi-mediated functional characterization of MaLac2 of the pine sawyer, Monochamus alternatus. Insect molecular biology 2008;17:303-12.

[197] Hasson C, Sugumaran M. Protein cross-linking by peroxidase: Possible mechanism for sclerotization of insect cuticle. Archives of insect biochemistry and physiology 1987;5:13-28.

[198] Thomas B, Yonekura M, Morgan T, Czapla T, Hopkins T, Kramer K. A trypsin-solubilized laccase from pharate pupal integument of the tobacco hornworm, *Manduca sexta*. Insect Biochemistry 1989;19.

[199] Hori M, Hiruma K, Riddiford LM. Cuticular melanization in the tobacco hornworm larva. Insect biochemistry 1984;14:267-74.

[200] Kayser-Wegmann I, Kayser H. Black pigmentation of insect cuticles: a view based on microscopic and autoradiographic studies. The Larval Serum Proteins of Insects 1983:151-67.

[201] Hiruma K, Riddiford LM. Granular phenoloxidase involved in cuticular melanization in the tobacco hornworm: regulation of its synthesis in the epidermis by juvenile hormone. Developmental biology 1988;130:87-97.

[202] Hiruma K, Riddiford L. The molecular mechanisms of cuticular melanization: the ecdysone cascade leading to dopa decarboxylase expression in *Manduca sexta*. Insect Biochemistry and Molecular Biology 2009;39:245-53.

[203] Andersen SO, Jacobsen JP, Roepstorff P, Peter MG. Catecholamine-protein conjugates: Isolation of an adduct of N-acetylhistidine to the side chain of N-acetyldopamine from an insect-enzyme catalyzed reaction. Tetrahedron letters 1991;32:4287-90.

[204] Andersen SO, Perter MG, Roepstorff P. Cuticle-catalyzed coupling between N-acetylhistidine and N-acetyldopamine. Insect Biochemistry and Molecular Biology 1992;22:459-69.

[205] Andersen S, Jacobsen J, Roepstorff P. Coupling reactions between amino compounds and N-acetyldopamine catalyzed by cuticular enzymes. Insect biochemistry and molecular biology 1992.

[206] Okot-Kotber B, Morgan T, Hopkins T, Kramer K. Characterization of two high molecular weight catechol-containing glycoproteins from pharate pupal cuticle of the tobacco hornworm, *Manduca sexta*. Insect biochemistry and molecular biology 1994;24:787.

[207] Okot-Kotber B, Morgan T, Hopkins T, Kramer K. Catecholamine-containing proteins from the pharate pupal cuticle of the tobacco hornworm, *Manduca sexta*. Insect biochemistry and molecular biology 1996;26:475.

[208] Kramer K, Morgan T, Hopkins T, Christensen A, Schaefer J. Solid-state (13)-C-NMR and diphenol analyses of sclerotized cuticles from stored product Coleoptera. Insect Biochemistry 1989;19.

[209] Schaefer J, Kramer KJ, Garbow JR, Jacob GS, Stejskal EO, Hopkins TL, et al. Aromatic cross-links in insect cuticle: detection by solid-state 13C and 15N NMR. Science 1987;235:1200 -4.

[210] Kramer KJ, Hopkins TL, Schaefer J. Applications of solids NMR to the analysis of insect sclerotized structures. Insect biochemistry and molecular biology 1995;25:1067-80.

[211] Christensen AM, Schaefer J, Kramer KJ, Morgan TD, Hopkins TL. Detection of cross-links in insect cuticle by REDOR NMR spectroscopy. J Am Chem Soc 1991;113:6799-802.

[212] Merritt ME, Christensen AM, Kramer KJ, Hopkins TL, Schaefer J. Detection of intercatechol cross-links in insect cuticle by solid-state carbon-13 and nitrogen-15 NMR. J Am Chem Soc 1996;118:11278-82.

[213] Pryor M. On the hardening of the ootheca of *Blatta orientalis*. Proceedings of the Royal Society of London Series B, Biological Sciences 1940;128:378-93.

[214] Hopkins TL, Krchma LJ, Ahmad SA, Kramer KJ. Pupal cuticle proteins of *Manduca sexta*: characterization and profiles during sclerotization. Insect Biochemistry and Molecular Biology 2000;30:19-27.

[215] Vincent JFV. If it's tanned it must be dry: A Critique. The Journal of Adhesion 2009;85:755-69.

[216] Lomakin J, Huber PA, Eichler C, Arakane Y, Kramer KJ, Beeman RW, et al. Mechanical properties of the beetle elytron, a biological composite material. Biomacromolecules 2011.

[217] Dirks JH, Li MH, Kabla A, Federle W. In vivo dynamics of the internal fibrous structure in smooth adhesive pads of insects. Acta Biomater 2012;8:2730-6.

[218] Dirks JH, Taylor D. Fracture toughness of locust cuticle. The Journal of Experimental Biology 2012;215:1502-8.

[219] Sun JY, Bhushan B. Structure and mechanical properties of beetle wings: a review. Rsc Advances 2012;2:12606-23.

[220] Chen J, Wu G. Beetle forewings: Epitome of the optimal design for lightweight composite materials. Carbohydrate polymers 2013;91:659-65.

[221] Burstein AH, Wright TM. Fundamentals of orthopaedic biomechanics: Williams & Wilkins Baltimore, MD; 1994.

[222] Fernandez JG, Ingber DE. Unexpected strength and toughness in chitosan-fibroin laminates inspired by insect cuticle. Advanced Materials 2011;24:480-4.

[223] Rubin DJ, Miserez A, Waite JH. Diverse strategies of protein sclerotization in marine invertebrates:: structure-property relationships in natural biomaterials. Advances in Insect Physiology 2010;38:75-133.

[224] Oeffner J, Lauder GV. The hydrodynamic function of shark skin and two biomimetic applications. The Journal of Experimental Biology 2012;215:785-95.

[225] Chen J, Guo S, Wan C, Wang X, Gu C, Xie J, et al. Integrated honeycomb technology motivated by the structure of beetle forewings. Materials Science and Engineering: C 2012;32:1813-7.

[226] Waite JH, Broomell CC. Changing environments and structure–property relationships in marine biomaterials. The Journal of Experimental Biology 2012;215:873-83.

[227] Ito C, Goto SG, Shiga S, Tomioka K, Numata H. Peripheral circadian clock for the cuticle deposition rhythm in Drosophila melanogaster. Proc Natl Acad Sci U S A 2008;105:8446-51.

[228] Clark-Hachtel CM, Linz DM, Tomoyasu Y. Insights into insect wing origin provided by functional analysis of vestigial in the red flour beetle, *Tribolium castaneum*. Proceedings of the National Academy of Sciences 2013;110:16951-6.

[229] Ohde T, Yaginuma T, Niimi T. Insect morphological diversification through the modification of wing serial homologs. Science 2013;340:495-8.

[230] Doucet D, Retnakaran A. Insect Chitin: Metabolism, Genomics and Pest Management. Insect Growth Disruptors 2012;43:437.

[231] Locke M. Pore canals and related structures in insect cuticle. Journal of Biophysical and Biochemical Cytology 1961;10:589-618.

[232] Moussian B. Recent advances in understanding mechanisms of insect cuticle differentiation. Insect biochemistry and molecular biology 2010;40:363-75.

[233] Muller M, Olek M, Giersig M, Schmitz H. Micromechanical properties of consecutive layers in specialized insect cuticle: the gula of *Pachnoda marginata* (Coleoptera, Scarabaeidae) and the infrared sensilla of *Melanophila acuminata* (Coleoptera, Buprestidae). J Exp Biol 2008;211:2576-83.

[234] Caveney S. Juvenile hormone and wound modelling of *Tenebrio* cuticle architecture. Journal of Insect Physiology 1970;16:1087-95, 97-107.

[235] Delbecque JP, Hirn M, Delachamber J, De Reggi M. Cuticular cycle and molting hormone levels during the metamorphosis of *Tenebrio molitor* (Insecta Soleoptera). Developmental biology 1978;64:11-30.

[236] Wigglesworth V. The structure and deposition of the cuticle in the adult mealworm, *Tenebrio molitor* L.(Coleoptera). Quarterly journal of microscopical science 1948;3:197-216.

[237] Cheng L, Wang L, Karlsson AM. Mechanics-based analysis of selected features of the exoskeletal microstructure of *Popillia japonica*. Journal of Materials Research 2009;24:3253-67.

[238] Andersen SO. Cuticular sclerotization and tanning. In: Glibert LI, editor. Insect Molecular Biology and Biochemistry. San Diego: Academic Press; 2011. p. 167-92.

[239] Kerwin JL, Whitney DL, Sheikh A. Mass spectrometric profiling of glucosamine, glucosamine polymers and their catecholamine adducts: Model reactions and cuticular hydrolysates of *Toxorhynchites amboinensis* (Culicidae) pupae. Insect biochemistry and molecular biology 1999;29:599-607.

[240] Harrison DJP, Yates WR, Johnson JF. Techniques for the analysis of crosslinked polymers. Journal of Macromolecular Science-Reviews in Macromolecular Chemistry and Physics 1985;25:481-549.

[241] Yokozeki T, Takeda S, Ogasawara T, Ishikawa T. Mechanical properties of corrugated composites for candidate materials of flexible wing structures. Composites Part A: Applied Science and Manufacturing 2006;37:1578-86.

[242] Andersen S. Evidence for two mechanisms of sclerotisation in insect cuticle. Nature 1974;251:507-8.

[243] Morgan T, Hopkins T, Kramer K, Roseland C, Czapla T, Tomer K, et al. N-[beta]-alanylnorepinephrine: Biosynthesis in insect cuticle and possible role in sclerotization. Insect biochemistry 1987;17:255-63.

[244] Roseland CR, Kramer KJ, Hopkins TL. Cuticular strength and pigmentation of rust-red and black strains of *Tribolium castaneum*: Correlation with catecholamine and β-alanine content. Insect biochemistry 1987;17:21-8.

[245] Arakane Y, Lomakin J, Beeman RW, Muthukrishnan S, Gehrke SH, Kanost MR, et al. Molecular and functional analyses of amino acid decarboxylases involved in cuticle tanning in *Tribolium castaneum*. Journal of Biological Chemistry 2009;284:16584-94.

[246] Schachter J, Pérez M, Quesada-Allué L. The role of N-beta-alanyldopamine synthase in the innate immune response of two insects. Journal of insect physiology 2007;53:1188-97.

[247] Bode F, da Silva MA, Drake AF, Ross-Murphy SB, Dreiss CA. Enzymatically cross-linked tilapia gelatin hydrogels: physical, chemical and hybrid networks. Biomacromolecules 2011;12:3741-52.

[248] Kerwin JL, Turecek F, Xu RD, Kramer KJ, Hopkins TL, Gatlin CL, et al. Mass spectrometric analysis of catechol-histidine adducts from insect cuticle. Anal Biochem 1999;268:229-37.

[249] Suderman RJ, Dittmer NT, Kanost MR, Kramer KJ. Model reactions for insect cuticle sclerotization: Cross-linking of recombinant cuticular proteins upon their laccase-catalyzed oxidative conjugation with catechols. Insect Biochemistry and Molecular Biology 2006;36:353-65.

[250] Andersen SO. The stabilization of locust cuticle. Journal of Insect Physiology 1981;27:393-6.

[251] Hillerton J, Vincent J. The stabilisation of insect cuticles. Journal of Insect Physiology 1979;25:957-63.

[252] Ferry JD. Viscoelastic properties of polymers. 1980.

[253] Mani S, Winter H, Silverstein M, Narkis M. Power law relaxation in an interpenetrating polymer network. Colloid and Polymer Science 1989;267:1002-6.

[254] Ward IM, Sweeney J. An introduction to the mechanical properties of solid polymers: Wiley. com; 2005.

[255] Fried J. Polymer science and technology: Pearson Education; 2003.

[256] Um IC, Kweon HY, Lee KG, Park YH. The role of formic acid in solution stability and crystallization of silk protein polymer. International journal of biological macromolecules 2003;33:203-13.

[257] Mahoney WC, Hermodson MA. Separation of large denatured peptides by reverse phase high performance liquid chromatography. Trifluoroacetic acid as a peptide solvent. Journal of Biological Chemistry 1980;255:11199-203.

[258] Hirota N, Goto Y, Mizuno K. Cooperative α-helix formation of β-lactoglobulin and melittin induced by hexafluoroisopropanol. Protein science 1997;6:416-21.

[259] Gellynck K, Verdonk P, Almqvist K, Van Nimmen E, Gheysens T, Mertens J, et al. Chondrocyte growth in porous spider silk 3D-scaffolds. 2005.

[260] Greenstein JP. Sulfhydryl groups in proteins I. Egg albumin in solutions of urea, guanidine, and their derivatives. Journal of Biological Chemistry 1938;125:501-13.

[261] Cussler EL. Diffusion: mass transfer in fluid systems: Cambridge university press; 2009.

[262] Newman G, Jasani B, Williams E. The preservation of ultrastructure and antigenicity. Journal of Microscopy 1982;127:RP5-RP6.

[263] Sohn M, Ho C-T. Ammonia generation during thermal degradation of amino acids. Journal of agricultural and food chemistry 1995;43:3001-3.

[264] Köll P, Borchers G, Metzger J. Thermal degradation of chitin and cellulose. Journal of Analytical and Applied Pyrolysis 1991;19:119-29.

[265] Frushour B, Koenig J. Raman spectroscopy of proteins. Advances in infrared and Raman spectroscopy 1975;1:35-97.

[266] Yu N. Raman spectroscopy: a conformational probe in biochemistry. CRC critical reviews in biochemistry 1977;4:229.

[267] Spiro TG, Gaber BP. Laser Raman scattering as a probe of protein structure. Annual review of biochemistry 1977;46:553-70.

[268] Carey P. Biochemical applications of Raman and resonance Raman spectroscopes: Elsevier; 1982.

[269] Carey P, Salares V. Raman and resonance Raman studies of biological systems. Advances in infrared and Raman spectroscopy 1980;7:1-58.

[270] Cael S, Koenig J, Blackwell J. Infrared and raman spectroscopy of carbohydrates: Part III: raman spectra of the polymorphic forms of amylose. Carbohydrate research 1973;29:123-34.

[271] Mikkelsen A, Engelsen S, Skibsted L, Hansen H, Larsen O. Calcium carbonate crystallization in the alpha-chitin matrix of the shell of pink shrimp, Pandalus borealis, during frozen storage. Journal of Crystal Growth 1997;177:125-34.

[272] Yamada H, Nakao H, Takasu Y, Tsubouchi K. Preparation of undegraded native molecular fibroin solution from silkworm cocoons. Materials Science and Engineering: C 2001;14:41-6.

[273] Collins KD. Charge density-dependent strength of hydration and biological structure. Biophys J 1997;72:65-76.

[274] Holl SM, Schaefer J, Goldberg WM, Kramer KJ, Morgan TD, Hopkins TL. Comparison of black coral skeleton and insect cuticle by a combination of carbon-13 NMR and chemical analyses. Archives of biochemistry and biophysics 1992;292:107-11.

[275] Le XT, Turgeon SL. Rheological and structural study of electrostatic cross-linked xanthan gum hydrogels induced by beta-lactoglobulin. Soft Matter 2013;9:3063-73.

[276] Drury JL, Mooney DJ. Hydrogels for tissue engineering: scaffold design variables and applications. Biomaterials 2003;24:4337-51.

[277] Capadona JR, Shanmuganathan K, Tyler DJ, Rowan SJ, Weder C. Stimuli-responsive polymer nanocomposites inspired by the sea cucumber dermis. Science 2008;319:1370-4.

[278] Kim TG, Shin H, Lim DW. Biomimetic Scaffolds for Tissue Engineering. Advanced Functional Materials 2012;22:2446-68.

[279] MacEwan SR, Chilkoti A. Elastin-Like Polypeptides: Biomedical Applications of Tunable Biopolymers. Biopolymers 2010;94:60-77.

[280] Miessner M, Peter MG, Vincent JF. Preparation of insect-cuticle-like biomimetic materials. Biomacromolecules 2001;2:369-72.

[281] Qu Y, Payne SC, Apkarian RP, Conticello VP. Self-assembly of a polypeptide multi-block copolymer modeled on dragline silk proteins. J Am Chem Soc 2000;122:5014-5.

[282] Shanmuganathan K, Capadona JR, Rowan SJ, Weder C. Bio-inspired mechanically-adaptive nanocomposites derived from cotton cellulose whiskers. Journal of Materials Chemistry 2010;20:180-6.

[283] Vincent JFV. Biomimetics - a review. Proceedings of the Institution of Mechanical Engineers Part H-Journal of Engineering in Medicine 2009;223:919-39.

[284] Andersen SO. Biochemistry of insect cuticle. Annual review of entomology 1979;24:29-59.

[285] Arakane Y, Lomakin J, Beeman RW, Muthukrishnan S, Gehrke SH, Kanost MR, et al. Molecular and functional analyses of amino acid decarboxylases involved in cuticle tanning in *Tribolium castaneum*. Journal of Biological Chemistry 2009;284:16584-94.

[286] Khor E. Chitin: fulfilling a biomaterials promise: Elsevier Science; 2001.

[287] Pillai C, Paul W, Sharma CP. Chitin and chitosan polymers: Chemistry, solubility and fiber formation. Progress in Polymer Science 2009;34:641-78.

[288] Qin G, Lapidot S, Numata K, Hu X, Meirovitch S, Dekel M, et al. Expression, cross-linking, and characterization of recombinant chitin binding resilin. Biomacromolecules 2009;10:3227-34.

[289] Missios S, Carter DH, Linder D, Mortimer L, Okobi A, Doctor J. Characterization of cuticular proteins in the red flour beetle, *Tribolium castaneum*. Insect Biochemistry and Molecular Biology 2000;30:47-56.

[290] Arakane Y, Lomakin J, Gehrke SH, Hiromasa Y, Tomich JM, Muthukrishnan S, et al. Formation of rigid, non-flight forewings (elytra) of a beetle requires two major cuticular proteins. PLoS Genetics 2012;8:e1002682.

[291] Dittmer NT, Hiromasa Y, Tomich JM, Lu N, Beeman RW, Kramer KJ, et al. Proteomic and transcriptomic analyses of rigid and membranous cuticles and epidermis from the elytra and hindwings of the red flour beetle, *Tribolium castaneum*. Journal of Proteome Research 2011;11:269-78.

[292] Chen DTN, Wen Q, Janmey PA, Crocker JC, Yodh AG. Rheology of Soft Materials. Annual Review of Condensed Matter Physics. Palo Alto: Annual Reviews; 2010. p. 301-22.

[293] Crocker JC, Valentine MT, Weeks ER, Gisler T, Kaplan PD, Yodh AG, et al. Two-point microrheology of inhomogeneous soft materials. Phys Rev Lett 2000;85:888-91.

[294] Mason TG, Ganesan K, vanZanten JH, Wirtz D, Kuo SC. Particle tracking microrheology of complex fluids. Phys Rev Lett 1997;79:3282-5.

[295] Mizuno D, Head DA, MacKintosh FC, Schmidt CF. Active and Passive Microrheology in Equilibrium and Nonequilibrium Systems. Macromolecules 2008;41:7194-202.

[296] Dhar P, Cao Y, Fischer TM, Zasadzinski J. Active interfacial shear microrheology of aging protein films. Phys Rev Lett 2010;104:016001.

[297] Dhar P, Cao Y, Kline T, Pal P, Swayne C, Fischer TM, et al. Autonomously moving local nanoprobes in heterogeneous magnetic fields. The Journal of Physical Chemistry C 2007;111:3607-13.

[298] Dhar P, Fischer TM, Wang Y, Mallouk T, Paxton W, Sen A. Autonomously moving nanorods at a viscous interface. Nano letters 2006;6:66-72.

[299] Prasad V, Koehler S, Weeks ER. Two-particle microrheology of quasi-2D viscous systems. Phys Rev Lett 2006;97:176001.

[300] Dhar P, Cao Y, Fischer TM, Zasadzinski J. Active interfacial shear microrheology of aging protein films. Phys Rev Lett 2010;104:16001.

[301] Dobrynin AV, Colby RH, Rubinstein M. Scaling theory of polyelectrolyte solutions. Macromolecules 1995;28:1859-71.

[302] Edwards S. The statistical mechanics of polymerized material. Proceedings of the Physical Society 1967;92:9.

[303] De Gennes PG. Scaling concepts in polymer physics: Cornell university press; 1979.

[304] Larson RG. The structure and rheology of complex fluids: Oxford university press New York; 1999.

[305] Desbrieres J. Viscosity of semiflexible chitosan solutions: influence of concentration, temperature, and role of intermolecular interactions. Biomacromolecules 2002;3:342-9.

[306] Kasaai MR, Arul J, Charlet G. Intrinsic viscosity–molecular weight relationship for chitosan. Journal of Polymer Science Part B: Polymer Physics 2000;38:2591-8.

[307] Schmitt C, Sanchez C, Lamprecht A, Renard D, Lehr CM, de Kruif CG, et al. Study of beta-lactoglobulin/acacia gum complex coacervation by diffusing-wave spectroscopy and confocal scanning laser microscopy. Colloid Surf B-Biointerfaces 2001;20:267-80.

[308] Weinbreck F, Rollema HS, Tromp RH, de Kruif CG. Diffusivity of whey protein and gum arabic in their coacervates. Langmuir 2004;20:6389-95.

[309] Wang X, Li Y, Wang Y-W, Lal J, Huang Q. Microstructure of β-lactoglobulin/pectin coacervates studied by small-angle neutron scattering. The Journal of Physical Chemistry B 2007;111:515-20.

[310] Gupta AN, Bohidar HB, Aswal VK. Surface patch binding induced intermolecular complexation and phase separation in aqueous solutions of similarly charged gelatin-chitosan molecules. J Phys Chem B 2007;111:10137-45.

[311] Chen J, Xie J, Zhu H, Guan S, Wu G, Noori MN, et al. Integrated honeycomb structure of a beetle forewing and its imitation. Materials Science and Engineering: C 2012;32:613-8.

[312] Dittmer N, Suderman R, Jiang H, Zhu Y, Gorman M, Kramer K, et al. Characterization of cDNAs encoding putative laccase-like multicopper oxidases and developmental expression in the tobacco hornworm, *Manduca sexta*, and the malaria mosquito, *Anopheles gambiae*. Insect biochemistry and molecular biology 2004;34:29.

[313] Dittmer NT, Gorman MJ, Kanost MR. Characterization of endogenous and recombinant forms of laccase-2, a multicopper oxidase from the tobacco hornworm, *Manduca sexta*. Insect biochemistry and molecular biology 2009;39:596.

[314] Andersen SO. Involvement of tyrosine residues, N-terminal amino acids, and beta-alanine in insect cuticular sclerotization. Insect Biochemistry and Molecular Biology 2007;37:969-74.

[315] Andersen SO. Quantitative determination of catecholic degradation products from insect sclerotized cuticles. Insect Biochemistry and Molecular Biology 2008;38:877-82.

[316] Andersen SO, Roepstorff P. Aspects of cuticular sclerotization in the locust, *Scistocerca gregaria*, and the beetle, *Tenebrio molitor*. Insect Biochemistry and Molecular Biology 2007;37:223-34.

[317] Xu RD, Huang X, Hopkins TL, Kramer KJ. Catecholamine and histidyl protein cross-linked structures in sclerotized insect cuticle. Insect Biochemistry and Molecular Biology 1997;27:101-8.

[318] Pearson DS, Helfand E. Viscoelastic properties of star-shaped polymers. Macromolecules 1984;17:888-95.

[319] Larson RG. The structure and rheology of complex fluids. New York: Oxford University Press; 1999.

[320] Yamasaki N, Aso Y, Tsukamoto T. A convenient method for the preparation of N-beta-alanyldopamine as a substrate of phenoloxidase. Agricultural and biological chemistry 1990;54:833-.

[321] Waigh TA. Microrheology of complex fluids. Rep Prog Phys 2005;68:685-742.

[322] Gardel ML, Nakamura F, Hartwig JH, Crocker JC, Stossel TP, Weitz DA. Prestressed F-actin networks cross-linked by hinged filamins replicate mechanical properties of cells. Proc Natl Acad Sci U S A 2006;103:1762-7.

[323] Gardel ML, Shin JH, MacKintosh FC, Mahadevan L, Matsudaira P, Weitz DA. Elastic Behavior of cross-linked and bundled actin networks. Science 2004;304:1301-5.

[324] Gardel ML, Valentine MT, Crocker JC, Bausch AR, Weitz DA. Microrheology of entangled F-actin solutions. Phys Rev Lett 2003;91.

[325] Lee H, Ferrer JM, Nakamura F, Lang MJ, Kamm RD. Passive and active microrheology for cross-linked F-actin networks in vitro. Acta Biomater 2010;6:1207-18.

[326] Luan Y, Lieleg O, Wagner B, Bausch AR. Micro- and macrorheological properties of isotropically cross-linked actin networks. Biophys J 2008;94:688-93.

[327] Papagiannopoulos A, Waigh TA, Hardingham TE. The viscoelasticity of self-assembled proteoglycan combs. Faraday Discuss 2008;139:337-57.

[328] Schopferer M, Bar H, Hochstein B, Sharma S, Mucke N, Herrmann H, et al. Desmin and vimentin intermediate filament networks: Their viscoelastic properties investigated by mechanical rheometry. Journal of Molecular Biology 2009;388:133-43.

[329] Shin JH, Gardel ML, Mahadevan L, Matsudaira P, Weitz DA. Relating microstructure to rheology of a bundled and cross-linked F-actin network in vitro. Proc Natl Acad Sci U S A 2004;101:9636-41.

[330] Yang YL, Bai M, Klug WS, Levine AJ, Valentine MT. Microrheology of highly crosslinked microtubule networks is dominated by force-induced crosslinker unbinding. Soft Matter 2013;9:383-93.

[331] Dhar P, Prasad V, Weeks ER, Bohlein T, Fischer TM. Immersion of charged nanoparticles in a salt solution/air interface. The Journal of Physical Chemistry B 2008;112:9565-7.

[332] Mason TG. Estimating the viscoelastic moduli of complex fluids using the generalized Stokes–Einstein equation. Rheologica Acta 2000;39:371-8.

[333] Ju KY, Lee Y, Lee S, Park SB, Lee JK. Bioinspired Polymerization of Dopamine to Generate Melanin-Like Nanoparticles Having an Excellent Free-Radical-Scavenging Property. Biomacromolecules 2011.

[334] Dasgupta BR, Weitz D. Microrheology of cross-linked polyacrylamide networks. Phys Rev E 2005;71:021504.

[335] Ball R, McLeish T. Dynamic dilution and the viscosity of star-polymer melts. Macromolecules 1989;22:1911-3.

[336] Fetters LJ, Kiss AD, Pearson DS, Quack GF, Vitus FJ. Rheological behavior of star-shaped polymers. Macromolecules 1993;26:647-54.

[337] Milner S, McLeish T. Parameter-free theory for stress relaxation in star polymer melts. Macromolecules 1997;30:2159-66.

[338] Dasgupta BR, Weitz DA. Microrheology of cross-linked polyacrylamide networks. Phys Rev E 2005;71.

[339] Narita T, Knaebel A, Munch JP, Candau SJ. Microrheology of poly(vinyl alcohol) aqueous solutions and chemically cross-linked gels. Macromolecules 2001;34:8224-31.

[340] Kyle S, Aggeli A, Ingham E, McPherson MJ. Production of self-assembling biomaterials for tissue engineering. Trends in biotechnology 2009;27:423-33.

[341] Walshaw J, Woolfson DN. Socket: a program for identifying and analysing coiled-coil motifs within protein structures. Journal of molecular biology 2001;307:1427-50.

[342] Kopecek J, Yang JY. Smart Self-Assembled Hybrid Hydrogel Biomaterials. Angew Chem-Int Edit 2012;51:7396-417.

[343] Bracalello A, Santopietro V, Vassalli M, Marletta G, Del Gaudio R, Bochicchio B, et al. Design and Production of a Chimeric Resilin-, Elastin-, and Collagen-Like Engineered Polypeptide. Biomacromolecules 2011;12:2957-65.

[344] Anderson JP, Cappello J, Martin DC. Morphology and primary crystal-structure of a silk-like protein polymer synthesized by genetically-engineered *Escherichia-col*i bacteria Biopolymers 1994;34:1049-58.

[345] Prince JT, McGrath KP, Digirolamo CM, Kaplan DL. Construction, cloning, and expressino of synthetic genes encoding spider dragline silk. Biochemistry 1995;34:10879-85.

[346] McPherson DT, Morrow C, Minehan DS, Wu JG, Hunter E, Urry DW. Production and purification of a recombinant elastomeric polypeptide, G-(VPGVG)19-VPGV, from *Escherichia-coli* Biotechnol Prog 1992;8:347-52.

[347] Nagapudi K, Brinkman WT, Thomas BS, Park JO, Srinivasarao M, Wright E, et al. Viscoelastic and mechanical behavior of recombinant protein elastomers. Biomaterials 2005;26:4695-706.

[348] Lv S, Dudek DM, Cao Y, Balamurali MM, Gosline J, Li HB. Designed biomaterials to mimic the mechanical properties of muscles. Nature 2010;465:69-73.

[349] Elvin CM, Carr AG, Huson MG, Maxwell JM, Pearson RD, Vuocolo T, et al. Synthesis and properties of crosslinked recombinant pro-resilin. Nature 2005;437:999-1002.

[350] Dutta NK, Choudhury NR, Truong MY, Kim M, Elvin CM, Hill AJ. Physical approaches for fabrication of organized nanostructure of resilin-mimetic elastic protein rec1-resilin. Biomaterials 2009;30:4868-76.

[351] Tamburro AM, Panariello S, Santopietro V, Bracalello A, Bochicchio B, Pepe A. Molecular and Supramolecular Structural Studies on Significant Repetitive Sequences of Resilin. ChemBioChem 2010;11:83-93.

[352] Teng WB, Cappello J, Wu XY. Recombinant Silk-Elastinlike Protein Polymer Displays Elasticity Comparable to Elastin. Biomacromolecules 2009;10:3028-36.

[353] Saumonneau A, Rottier K, Conrad U, Popineau Y, Gueguen J, Francin-Allami M. Expression of a new chimeric protein with a highly repeated sequence in tobacco cells. Plant Cell Reports 2011;30:1289-302.

[354] Yao JM, Asakura T. Synthesis and structural characterization of silk-like materials incorporated with an elastic motif. Journal of Biochemistry 2003;133:147-54.

[355] Arakane Y, Dittmer NT, Tomoyasu Y, Kramer KJ, Muthukrishnan S, Beeman RW, et al. Identification, mRNA expression and functional analysis of several *yellow* family genes in *Tribolium castaneum*. Insect Biochemistry and Molecular Biology 2010;40:259e66.

[356] Arakane Y, Specht CA, Kramer KJ, Muthukrishnan S, Beeman RW. Chitin synthases are required for survival, fecundity and egg hatch in the red flour beetle,*Tribolium castaneum*. Insect biochemistry and molecular biology 2008;38:959-62.

[357] Tomoyasu Y, Denell RE. Larval RNAi in *Tribolium (Coleoptera)* for analyzing adult development. Development genes and evolution 2004;214:575-8.

[358] Tomoyasu Y, Miller SC, Tomita S, Schoppmeier M, Grossmann D, Bucher G. Exploring systemic RNA interference in insects: a genome-wide survey for RNAi genes in *Tribolium*. Genome Biol 2008;9:R10.

[359] Morgan TD, Baker P, Kramer KJ, Basibuyuk HH, Quicke DL. Metals in mandibles of stored product insects: do zinc and manganese enhance the ability of larvae to infest seeds? Journal of stored products research 2003;39:65-75.

[360] Vaccaro E, Waite JH. Yield and post-yield behavior of mussel byssal thread: a self-healing biomolecular material. Biomacromolecules 2001;2:906-11.

[361] Waite JH, Qin X-X, Coyne KJ. The peculiar collagens of mussel byssus. Matrix Biology 1998;17:93-106.

[362] Noble JE, Bailey MJ. Quantitation of protein. Methods in enzymology 2009;463:73-95.

[363] Smith P, Krohn RI, Hermanson G, Mallia A, Gartner F, Provenzano M, et al. Measurement of protein using bicinchoninic acid. Anal Biochem 1985;150:76-85.

[364] Van Holde KE, Johnson WC, Ho PS. Principles of physical biochemistry. 2006.

[365] Gill SC, Von Hippel PH. Calculation of protein extinction coefficients from amino acid sequence data. Anal Biochem 1989;182:319-26.

[366] Brown J. Structure of bovine serum albumin. Fed Proc1975. p. 591.

[367] Koppel DE. Analysis of macromolecular polydispersity in intensity correlation spectroscopy: the method of cumulants. The Journal of Chemical Physics 2003;57:4814-20.

[368] Lobanov MY, Bogatyreva N, Galzitskaya O. Radius of gyration as an indicator of protein structure compactness. Molecular Biology 2008;42:623-8.

[369] Katz J. Anisotropy of Young's modulus of bone. Nature 1980;283:106.

[370] Katz J. Hierarchical modeling of compact haversian bone as a fiber reinforced material. Advances in Bioengineering 1976:17-8.

[371] Katz JL, Yoon HS, Maharidge RL. The estimation of inter-osteonal mechanical properties from a composite model for haversian bone. Biomechanics: Current Interdisciplinary Research: Springer; 1985. p. 179-84.

[372] Lakes R. Materials with structural hierarchy Nature 1993;361:511-5.

[373] Narita T, Knaebel A, Munch J-P, Candau SJ. Microrheology of poly (vinyl alcohol) aqueous solutions and chemically cross-linked gels. Macromolecules 2001;34:8224-31.

[374] Pelletier V, Gal N, Fournier P, Kilfoil ML. Microrheology of microtubule solutions and actin-microtubule composite networks. Phys Rev Lett 2009;102:188303.

[375] Lee EC, Solomon MJ, Muller SJ. Molecular orientation and deformation of polymer solutions under shear: a flow light scattering study. Macromolecules 1997;30:7313-21.

[376] Sattler M, Schleucher J, Griesinger C. Heteronuclear multidimensional NMR experiments for the structure determination of proteins in solution employing pulsed field gradients. Progress in Nuclear Magnetic Resonance Spectroscopy 1999;34:93-158.

[377] Wider G. Structure determination of biological macromolecules in solution using nuclear magnetic resonance spectroscopy. BioTechniques 2000;29:1278-95.

APPENDIX FOR CHAPTER 5

Figure 5.3b from Chapter 5 is presented here on a linear scale to more clearly show the differences in viscosities of KITO with and without the protein.

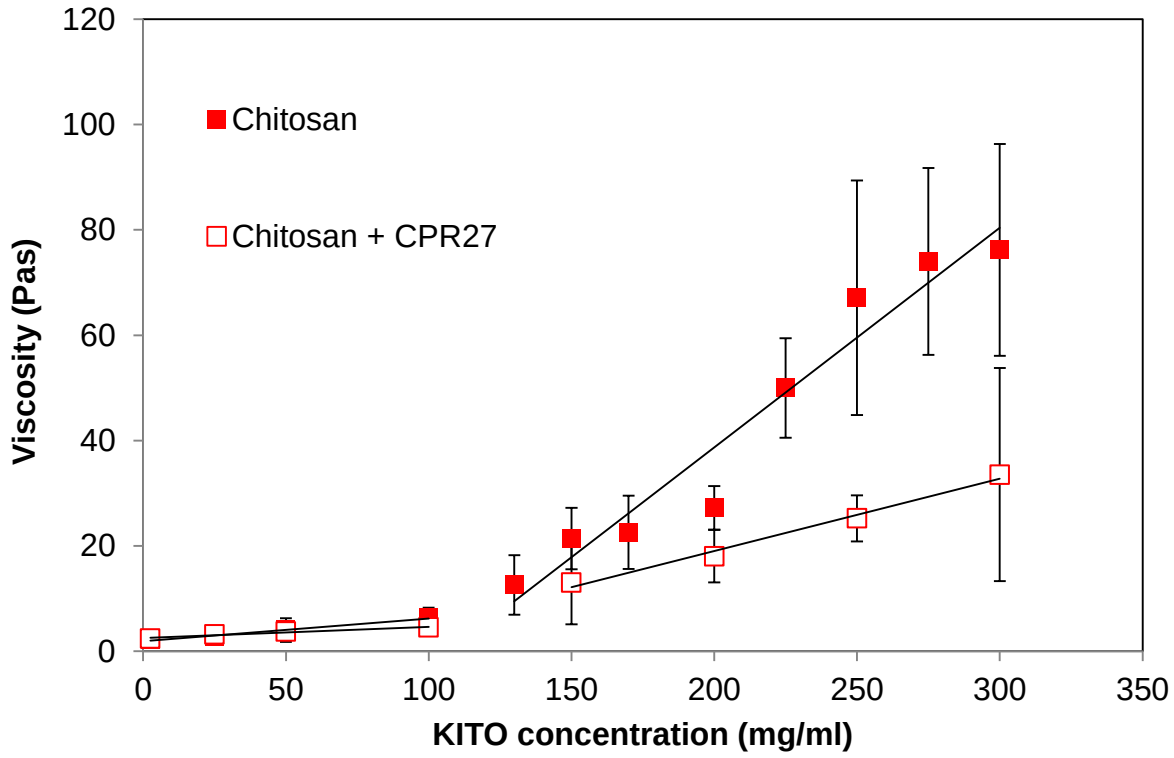

Figure 5.3b presented on a linear scale. Dependence of viscosity on concentration for KITO solutions with and without 3 mg/ml CPR27. The protein caused a drop in viscosity at the higher chitosan concentrations. The solvent was 0.2 M acetic acid/ 0.2 M sodium acetate (pH 5). The isoelectric point of chitosan and CPR27 are about 6.5 and 6.72, respectively. Error bars are standard deviations with $n \geq 4$.

APPENDIX FOR CHAPTER 6

Counting particles using Image J software. Image J, version 1.47v, can be downloaded from the NIH website, http://rsb.info.nih.gov/ij/. Open the brightfield image in Image J. Select the Image Tab and choose Adjust… and Threshold from the dropdown menus. Manually adjust the threshold until the color has filled as much of the particle areas as possible with minimal background coloring. Choose apply. A black and white image of the particles will

appear. Next, choose the Analyze tab and Analyze Particles from the dropdown menu. Set the pixel size range such that it will count particles, but not background small background specs or large dust particles on the lens. Also set the circularity so that non-particle artifacts are not counted. Choose Show: Outlines and select the results to be displayed; push OK. Double check against the original image to ensure that the outlines are, in fact, marking particles.